Molecular and Cellular Analysis of Zinc Homeostasis and its Interaction with Auxin in *Arabidopsis thaliana*

Thomas Gate

University of East Anglia

John Innes Centre

Thesis submitted for Doctor of Philosophy

December 2022

Abstract

Zinc (Zn) is an essential micronutrient in all organisms. Auxin (IAA) is a major plant hormone, co-ordinating growth and development. Transport of Zn between the endoplasmic reticulum (ER) and cytosol in plant cells is proposed to be important for the systemic Zn deficiency response and the activation of auxin amino acid conjugates. This thesis aims to increase understanding of how ER Zn transport is controlled and how it impacts wider Zn and auxin homeostasis.

Metal tolerance protein 2 (AtMTP2) was shown to transport Zn into the ER in Zn deficient conditions. Reporter plants expressing *AtMTP2* promotor-controlled luciferase were generated and *AtMTP2* was shown to be specifically induced in Zn deficiency. These reporter plants will be used in future forward genetic screens to find regulatory elements that control Zn ER import in Zn deficiency.

IAA-Alanine resistant 1 (*AtIAR1*) has previously been identified as a likely ER metal transporter that when mutated led to insensitivity to IAA-Alanine as a result of a hypothesised build-up of metal ions in the ER. In this work, AtIAR1 was shown to transport Zn, likely not only out of the ER, but also Golgi. One mutant found in the screen, *Atiar1-3*, still showed Zn transport, but reduced trafficking in yeast assays.

Both the *Atiar1-3* mutant and a suspected knockout *Atiar1-t* mutant were tested for disrupted response to Zn deficiency and excess conditions but showed mostly developmental phenotypes. Testing of auxin-related developmental phenotypes in these two *Atiar1* mutants enabled the discovery of an excess Zn - exogenous auxin interaction that was partially *AtIAR1* dependant. In addition, the two *Atiar1* mutants were found to differ in severity and time dependence of their phenotypes. Both mutants showed altered IAA conjugation and enhanced skotomorphogenesis. Overall, this work demonstrates a role for ER/Golgi Zn homeostasis in wider auxin-related development.

List of Contents

Abstract……...…2

List of Contents……...……3

List of Figures……...…13

List of Tables……..…17

List of Abbreviations……...…18

Acknowledgements……...……21

Chapter 1: Introduction……..……23

1.1 Understanding Zn homeostasis in plants is important for global crop productivity……..……24

1.1.1 Zn deficiency……..…24

1.1.2 Tackling Zn deficiency……..…25

1.1.3 Zn excess in soils……...……26

1.1.4 Utility of understanding Zn homeostasis in plants……26

1.2 Zn homeostasis in *Arabidopsis thaliana*……27

1.2.1 Zn chelators……...…27

1.2.2 Zn transporters……..……28

1.2.3 Zn deficiency response in plants……..……33

1.2.4 Regulation of the Zn deficiency response in *Arabidopsis thaliana*……...…35

1.2.5 Zn excess response in plants……38

1.2.6 Gene expression regulation in Zn excess is mostly that of the Fe deficiency response.……40

1.3 Auxin homeostasis in *Arabidopsis thaliana*……..42

1.3.1 Auxin transport is important to many aspects of plant development……...43

1.3.2 Auxin signalling……44

1.3.3 Auxin synthesis.……46

1.3.4 Auxin conjugation and oxidation.……47

1.3.5 Auxin induced changes in auxin signalling, metabolism and transport.……51

1.4 Auxin and Zn interactions.……52

1.4.1 Control of auxin conjugate hydrolysis.……53

1.5 Aims of the thesis.……..57

Chapter 2: Materials and Methods.……58

2.1 *Saccharomyces cerevisiae* growth, transformation, and phenotyping.……..59

2.1.1 *Saccharomyces cerevisiae* strains.……59

2.1.2 Constructs for *Saccharomyces cerevisiae* expression.……60

2.1.3 *Saccharomyces cerevisiae* media.……..…63

2.1.4 *Saccharomyces cerevisiae* growth conditions and transformation.……...64

2.1.5 *Saccharomyces cerevisiae* drop assay.……..64

2.2 *Arabidopsis* growth and transformation……..66

2.2.1 Plant materials……..66

2.2.2 Generating constructs for *Arabidopsis* transformation…..67

2.2.2.1 DNA extraction using the CTAB methodology……67

2.2.2.2 Cloning fragments and golden gate cloning of *AtMTP2*::*LUC* plasmid……...……68

2.2.2.3 Cloning fragments and golden gate cloning of *AtIAR1*::*GUS* and *GFP* plasmids……..……72

2.2.3 *Agrobacterium tumefaciens* transformation by electroporation……..……..82

2.2.4 *Arabidopsis* growth media and conditions..…….83

2.2.4.1 Seed sterilisation and vernalisation.……..…..83

2.2.4.2 MS-based media.…….…..83

2.2.4.3 Zn deficient media.……..…….84

2.2.4.4 Growth in soil……..85

2.2.4.5 *Arabidopsis* growth conditions.…….……..85

2.2.5 *Arabidopsis* transformation.……..86

2.3 *Arabidopsis* phenotyping……87

2.3.1 Luciferase expression.…….……..87

2.3.2 Root and shoot growth phenotyping.……...87

2.3.3 Chlorophyll content measurement.……..89

2.3.4 Inductively coupled plasma-optical emission spectrometry (ICP-OES).……..89

2.3.5 Reverse transcriptase quantitative PCR (RT-qPCR).…...90

2.3.6 Microscopy methods.……93

2.3.6.1 *GUS* expression.……...93

2.3.6.2 Root meristem size…….……93

2.3.7 Metabolite analysis……...94

2.3.7.1 Metabolites of interest……94

2.3.7.2 Metabolite extraction.……96

2.3.7.3 Liquid chromatography mass spectrometry (LC-MS)……..……..96

2.3.7.4 Calculation of metabolite content.……98

2.4 Bioinformatic methods.……100

2.4.1 Phylogenetic analysis of the ZIP transporter family…...100

2.4.2 Bioinformatic analysis on amino acid composition in AtIAR1 homologues.……100

2.4.3 Subcellular localisation predictions of AtIAR1 homologues……101

2.4.4 Promotor region annotation.……...…….…..102

Chapter 3: Control of *AtMTP2* Expression……...103

3.1 Introduction.……...…….104

3.1.1 Role of *AtMTP2* in ER Zn homeostasis.……104

3.2 Results.……..…….105

3.2.1 Identifying components in a systemic Zn deficiency response.……..…..105

3.2.2 *AtMTP2*::*LUC* lines respond to Zn deficiency.……106

3.2.3 *AtMTP2*::*LUC* B4 line responds to Zn deficiency specifically.……...…….107

3.2.4 Promotor analysis of *AtMTP2* showed multiple potential regulators of expression.…….…….109

3.2.5 *AtMTP2*::*LUC* expression in Zn deficiency is reduced by exogenous auxins…….110

3.3 Discussion…….…….113

Chapter 4: IAR1 fundamentals: Transport, Localisation and Expression……..114

4.1 Introduction…….…….115

4.1.1 *AtIAR1* was found to influence auxin conjugate hydrolysis……...115

4.1.2 AtIAR1 is likely an ER and/or Golgi-based Zn transporter…….……..116

4.2 Results…….……..118

4.2.1 *AtIAR1* is a LIV-1 subfamily member of the ZIP family ……..…….118

4.2.2 Transport…….…120

4.2.2.1 *AtIAR1* and *Atiar1-3* expression complements *yke4*Δ phenotype……..120

4.2.2.2 AtIAR1 can transport Zn but not Fe or Mn..……122

4.2.2.3 AtIAR1 plant homologues show similar transport-related structural features……125

4.2.3 Localisation…….129

4.2.3.1 *AtIAR1*::*GFP* complementation lines did not yield observable GFP fluorescence……...130

4.2.3.2 AtIAR1 and the majority of the plant AtIAR1 homologues are predicted to have ER or Golgi localisation…….132

4.2.4 Expression……..…..135

4.2.4.1 Promotor analysis of *AtIAR1* illustrates multiple potential inducers of expression……...…136

4.2.4.2 *AtIAR1* expression is dependent on Zn, IAA and IAA-Ala…….……...…137

4.3 Discussion…….……..…142

4.3.1 AtIAR1 and plant homologues transport Zn……..…..142

4.3.2 AtIAR1 and plant homologues predominantly localise to the secretory pathway……..…143

4.3.3 *AtIAR1* is expressed in the vasculature of above ground tissues in a Zn and auxin dependant manner…….……...…143

4.3.4 Atiar1-3 may have improper dimerization and localisation…….144

Chapter 5: *AtIAR1* and Zn homeostasis……..….147

5.1 Introduction……...148

5.1.1 Zn deficiency in *Arabidopsis thaliana*……148

5.1.1.1 Zn homeostasis in *Arabidopsis thaliana* in Zn deficient conditions……...…….148

5.1.1.2 Zn deficiency sensitive mutants give insights into the Zn deficiency response…….....…..149

5.1.2 Zn excess in *Arabidopsis thaliana*……..……..…150

5.1.2.1 Zn and Fe homeostasis within *Arabidopsis thaliana* in Zn excess conditions…….……150

5.1.2.2 Zn excess sensitive mutants show common phenotypes associated with Fe deficiency…….…….…….152

5.1.3 ER stress is regulated by ER Zn levels…….....153

5.1.4 Measurements of Zn content in plants…….…….154

5.2 Results……156

5.2.1 *Atiar1-3* and *Atiar1-t* mutants are predicted to have differing severity of phenotype…….…..156

5.2.2 Root and shoot phenotypes vary across Zn conditions and genotypes…….…….…….…159

5.2.2.1 *Atiar1-3* and *Atiar1-t* show different primary root growth responses to altered Zn……159

5.2.2.2 *Atiar1-3* and *Atiar1-t* show altered shoot development…….……...161

5.2.3 Expression analysis reveals altered Zn deficiency and excess response in *Atiar1-3* and *Atiar1-t* plants……..…164

5.2.3.1 Parts of the local Zn deficiency response may be reduced in *Atiar1-t* mutants…….……..164

5.2.3.2 *Atiar1-3* mutants show an enhanced Fe deficiency response …….168

5.2.4 ICP-OES analysis show no change in Mn, Zn and Fe levels in *Atiar1-3* plants……..….171

5.2.5 Hydroponic long-term growth showed little difference between Col-0 and *Atiar1-3* plants…….….176

5.3 Discussion…….…..177

5.3.1 *Atiar1* mutants show mostly developmental phenotypes in Zn deficiency and control Zn conditions……...….177

5.3.2 Slight Zn excess sensitivity is seen in *Atiar1-3*……...…178

5.3.3 *Atiar1-3* and *Atiar1-t* mutants differ in their Zn related phenotypes…….……178

Chapter 6: *AtIAR1* and auxin homeostasis……...180

6.1 Introduction……..….181

6.1.1 Auxin signalling, metabolism and transport……...…..181

6.1.2 Auxin in development……..184

6.1.2.1 Auxin homeostasis and primary root growth…….184

6.1.2.2 Auxin homeostasis and lateral root formation……187

6.1.2.3 Auxin homeostasis and hypocotyl length…….188

6.1.2.4 Mutants in auxin related genes show characteristic phenotypes……..191

6.1.3 Auxin and Zn interactions can be probed using *Atiar1* mutants……..……192

6.2 Results……..……..193

6.2.1 Auxin related root phenotypes……..…….193

6.2.1.1 Primary root length and meristem size after 5 days depends on Zn and *AtIAR1*……..…….193

6.2.1.2 *Atiar1* mutants show different levels of IAA-Ala insensitivity depending on Zn status……..……..195

6.2.1.3 *Atiar1-t* mutant shows increased lateral root density……...……. 199

6.2.2 Auxin related shoot phenotypes…….203

6.2.2.1 Hypocotyl length after 10 days is reduced in *Atiar1-t* plants in Zn deficient and control conditions…….……203

6.2.2.2 Hypocotyl length is increased in *Atiar1-t* plants after 5 days in light and dark conditions……...…..207

6.2.3 Auxin-related metabolite analysis…….…209

6.2.3.1 Generation of a method to simultaneously measure IAA and IAA-related metabolites…….209

6.2.3.2 IAA-Glc levels are decreased in *Atiar1* mutants under Zn deficiency and excess conditions…….210

6.3 Discussion……...216

6.3.1 IAA glucose and amino acid conjugates appear to show crosstalk…….……216

6.3.2 *Atiar1-t* mutants show time dependence in their phenotypes…….217

6.3.3 Both *Atiar1* mutants are less sensitive to exogenous IAA-Ala than IAA……..…218

6.3.4 Zn excess and exogenous IAA-Ala and IAA interact in Col-0……..……218

6.3.5 Potential confounding factors include cell wall integrity…….……219

Chapter 7: Conclusion……222

7.1 This study has advanced understanding in how ER Zn control plays a role in Zn and auxin homeostasis……..223

7.2 *Atiar1-t* phenotypes show time dependence……...228

7.2.1 AtIAR1 may influence light-related auxin signalling in early development up to 5 days……..228

7.2.2 After 5 days a developmental switch leads to a change in *Atiar1-t* phenotypes……..230

7.3 The Zn excess response may involve auxin transport from shoots…….……..234

7.3.1 Zn excess response in conditions with no exogenous auxin involves AtIAR1-mediated auxin transport from shoots…….234

7.3.2 The excess Zn–exogenous auxin interaction requires this AtIAR1-mediated auxin transport……236

7.4 The *Atiar1-t* and *Atiar1-3* mutants show different phenotypes……..239

7.5 The ER and Golgi are differently regulated Zn stores……241

7.6 Studies on hormone-nutrient interaction require high spatial and temporal resolution…….243

Bibliography…...…….244

List of Figures

Figure 1.1 Schematic of Zn movement in a single *Arabidopsis thaliana* Col-0 cell……...…….33

Figure 1.2 Zn deficiency response in *Arabidopsis thaliana*…….37

Figure 1.3 Fe deficiency response induced by Zn excess…….42

Figure 1.4 Auxin synthesis, conjugation and degradation pathways……..…50

Figure 1.5 Adapted Rampey et al, 2013[1] model on metal transport in the ER and IAA-Ala hydrolysis in wildtype and *AtIAR1* mutant plants…….56

Figure 2.1 Plasmid maps of different *AtIAR1* constructs for *Saccharomyces cerevisiae* transformation……...……..63

Figure 2.2 *Atiar1* mutants used in this study……...…….66

Figure 2.3 *AtMTP2*::*LUC* plasmid map for *Arabidopsis* transformation……..…..72

Figure 2.4 Synthesised *AtIAR1* part 3……..……...…..76

Figure 2.5 *AtIAR1*::*GUS* and *GFP* plasmid maps for *Arabidopsis* transformation……..……..…..82

Figure 2.6 Picture of a typical agar plate containing vertically grown *Arabidopsis thaliana* used for image analysis…….…….88

Figure 2.7 Root meristem cortex cell counting……...…….94

Figure 2.8 Structures of metabolites measured in this study……..……..95

Figure 3.1 *AtMTP2*::*LUC* transformants respond differently to Zn deficiency……..…...106

Figure 3.2 Metal specificity of the *AtMTP2*-driven luciferase expression…..…...108

Figure 3.3. Promotor elements present in *AtMTP2* promotor……...…..…109

Figure 3.4 Auxin responsiveness of *AtMTP2* driven luciferase expression……...111

Figure 4.1 Adapted Rampey et al, 2013[1] model on metal transport in the ER and IAA-Ala hydrolysis in wildtype and *AtIAR1* mutant plants……..…..117

Figure 4.2 Phylogenetic analysis of the ZIP family……...……119

Figure 4.3 *AtIAR1* and *Atiar1-3* expression complements *yke4*Δ strain……..…..121

Figure 4.4 Complementation of metal import mutants by *AtIAR1* constructs……124

Figure 4.5 AtIAR1 protein topology and predicted structure…….……125

Figure 4.6 Conservation of equivalent metal-contacting residues present in BbZIP crystal structure……..…….126

Figure 4.7 Histidine density of loops is similar in AtIAR1 homologues in plants and animals……128

Figure 4.8 GFP complementation lines show a range of complementation…….…..131

Figure 4.9 Most plant AtIAR1 homologues are predicted to localise to the secretory pathway…….…..133

Figure 4.10 AtIAR1 homologues in many *Solanaceae* species are predicted to localise outside the secretory pathway……...134

Figure 4.11 Promotor elements present in *AtIAR1* promotor…….137

Figure 4.12 *AtIAR1*::*GUS* reporter plants show increased *GUS* expression in the hypocotyl and leaf under excess Zn……..…….138

Figure 4.13 *AtIAR1*::*GUS* reporter plants show *GUS* expression in Zn deficient and control conditions with exogenous auxin…….…..139

Figure 4.14 *AtIAR1* expression under different Zn conditions……..….140

Figure 4.15 *Atiar1-3* mutations cause substitutions within the highly conserved C-terminus……..145

Figure 5.1 Zn deficiency response in *Arabidopsis thaliana*…….…….149

Figure 5.2 Fe deficiency response induced by Zn excess……..…….152

Figure 5.3 *Atiar1* mutants used in this study……..157

Figure 5.4 *AtIAR1* expression in *Atiar1-3* and *Atiar1-t* plants……..…..158

Figure 5.5 Primary root length of *Atiar1* mutants grown on different Zn levels…….……..160

Figure 5.6 Shoot phenotypes of *Atiar1* mutants grown on different Zn levels……..…….162

Figure 5.7 Expression of genes involved in *AtbZIP19/23* dependant regulation…….…….……...166

Figure 5.8 Expression of *AtMTP2* in *Atiar1* mutants…….168

Figure 5.9 Expression of Fe-deficiency genes in *Atiar1* mutants……...……169

Figure 5.10 Expression of *AtBiP* genes in *Atiar1* mutants……..…170

Figure 5.11 Zn content in root and shoot of Col-0 and *Atiar1-3* plants…….172

Figure 5.12 Mn content in root and shoot of Col-0 and *Atiar1-3* plants……173

Figure 5.13 Fe content in root and shoot of Col-0 and *Atiar1-3* plants……..…175

Figure 6.1 Auxin synthesis, conjugation, and degradation pathways……182

Figure 6.2 Auxin transport in the root tip…….…..186

Figure 6.3 Lateral root formation……..…….188

Figure 6.4 Role of auxin in hypocotyl elongation……..190

Figure 6.5 Primary root length and meristem size…….…..……194

Figure 6.6 Primary root length of *Atiar1* mutants grown at different Zn concentrations…….196

Figure 6.7 Primary root length percentage change in IAA-Ala media……..….197

Figure 6.8 Primary root length percentage change in IAA media……..……198

Figure 6.9 Lateral root density across Zn conditions…….……200

Figure 6.10 Lateral root density percentage change in IAA-Ala media……...…..201

Figure 6.11 Lateral root density percentage change in IAA media……202

Figure 6.12 Shoot hypocotyl length across Zn conditions…….204

Figure 6.13 Shoot hypocotyl length percentage change in IAA-Ala media……..205

Figure 6.14 Shoot hypocotyl length percentage change in IAA media……..206

Figure 6.15 Shoot hypocotyl length in light and dark conditions……..207

Figure 6.16 Apical hook angle across Zn conditions……..…208

Figure 6.17 IAA precursor content…….....211

Figure 6.18 IAA and IAA-Glc content…….…..212

Figure 6.19 IAA-Asp and oxIAA content……..…213

Figure 6.20 Summary of IAA-related metabolite changes…….215

Figure 6.21 Interaction of AtIAR1, Zn and exogenous auxins……..…219

Figure 7.1 Adapted Rampey et al, 2013[1] model of metal transport in the ER and IAA-Ala hydrolysis in wildtype and *Atiar1* mutant plants…….…….223

Figure 7.2 Updated model of auxin conjugation and Zn homeostasis within the secretory pathway…….……..224

Figure 7.3 Potential involvement of AtIAR1 in light-induced changes during early development……229

Figure 7.4 Auxin metabolism pools predicted and measured across Zn and *AtIAR1* genotypes……..…..231

Figure 7.5 Model for Zn dependant auxin mobilisation in 5-day-old Col-0 and *Atiar1-t* plants……..……..236

List of Tables

Table 1.1 Zn-transporting AtZIPs: transport capabilities, subcellular localisation, and expression…….…….30

Table 2.1 List of *Saccharomyces cerevisiae* strains used in this study……60

Table 2.2 Primers used to amplify *AtMTP2* parts for golden gate assembly……..…….69

Table 2.3 Synthesised *AtMPT2* part 4……..…70

Table 2.4 Domestication sites created during golden gate cloning of *AtMTP2*……70

Table 2.5 Synthesised linker fragments and amino acid composition when translated in-frame…….……...73

Table 2.6 Primers used to amplify *AtIAR1* parts for golden gate assembly…….75

Table 2.7 Domestication sites created during golden gate cloning of *AtIAR1*.……77

Table 2.8 Primers used to amplify domesticated *AtIAR1* parts for golden gate assembly…….……..78

Table 2.9 Components of modified Hoagland solution……85

Table 2.10 Primers used in RT-qPCR for gene expression analysis……92

Table 2.11 Metabolites measured in this study and sources…….95

Table 2.12 Properties of LC column used in this study……....97

Table 2.13 LC conditions used in this study.……..97

Table 2.14 Inlet method for LC used in this study……..….98

Table 2.15 MS conditions used in this study……..…..98

Table 6.1 LC-MS detection parameters for IAA-related metabolites……...….210

List of Abbreviations

ANOVA – Analysis of variance

BPDS – Bathophenanthroline disulfonate

BSA – Bovine serum albumin

Cd – Cadmium

Col-0 – Columbia ecotype of *Arabidopsis thaliana*

Ct – C-terminal

CTAB – Hexadecyltrimethylammonium bromide

Cu – Copper

D_2-IAA – Indole-3-acetic-2,2-d_2 acid

dH_2O – Distilled water

EDTA – Ethylenediaminetetraacetic acid

EGTA – Ethylene glycol-bis(β-aminoethyl ether)-N,N,N′,N′-tetraacetic acid

ER – Endoplasmic reticulum

Fe – Iron

FOR – Forward primer

FRET – Förster resonance energy transfer

g – Gravity

GFP – Green fluorescent protein

GUS – β-glucuronidase

HBED – N,N'-bis(2-hydroxybenzyl)ethylenediamine-N,N'-diacetate

IAA – 3-Indoleacetic acid

IAA-aa – IAA amino acid conjugates

IAA-Ala – N-(3-Indolylacetyl)- L -alanine

IAA-Asp – (2S)-2-[[2-(1H-Indol-3-yl)acetyl]amino]butanedioic acid

IAA-Glc – Indole-3-acetyl b-D-Glucopyranose

IAM – Indole-3-acetamide

IAN – 3-Indoleacetonitrile

ICP-OES – Inductively coupled plasma-optical emission spectrometry

IPTG – Isopropyl β-D-1-thiogalactopyranoside

JTT – Jones-Taylor-Thornton

kbp – Kilobase pairs

LB – Luria Broth

LC-MS – Liquid chromatography mass spectrometry

LLE – Liquid-liquid extraction

LR – Lateral rots

LRC – Lateral root cap

MES – 2-Ethanesulfonic acid

Mn – Manganese

MS – Murashige and Skoog medium

NA – Nicotianamine

NAA - 1-naphthalene acetic acid

Nt – N-terminal

NTC – No template control

NRT – No reverse transcriptase control

OD600 – Optical density measured at a wavelength of 600 nm

oxIAA – 2-Oxo-2,3-dihydro-1H-indol-3-yl)acetic acid

PC – Phytochelatin

PCR – Polymerase chain reaction

QC – Quiescent centre

RAM – Root apical meristem

REV – Reverse primer

ROS – Reactive oxygen species

RT-qPCR – Reverse transcriptase quantitative PCR

rpm – Revolutions per minute

SCN – Stem cell niche

SP – Signal peptide

TF – Transcription factor

TQ-S – Triple quadrupole mass spectrometry

Tris – Tris(hydroxymethyl)aminomethane

Trp – L-Tryptophan

v/v – Volume per volume

WT – Wildtype

w/v – Weight per volume

X-Gal – 5-Bromo-4-chloro-3-indolyl β-D-galactopyranoside

X-Glc – 5-Bromo-4-chloro-3-indolyl-β-D-glucuronic acid

XPP – Xylem pole pericycle

ZDRE – Zinc Deficiency Response Element

Zn – Zinc

Acknowledgements

I would like to firstly thank my primary supervisors, Dale Sanders and Tony Miller, for their advice and support over the 4 years which has been fantastic. Your dedication to scientific discovery has been and will continue to be an inspiration to me. I want to also thank my secondary supervisors Laila Moubayidin and Myriam Charpentier who have been incredibly insightful throughout the project, helping critique experimental design and suggesting ways forward throughout the PhD.

The Miller/Sanders lab has been a lovely environment in which to do my PhD. My lab colleagues Millie, Sigi, Yi, Josh, Marco and Ben have been friendly and exceptionally helpful, helping me learn quickly and carry out complex protocols. In addition, members of the Bioimaging and Metabolomics department have been incredibly helpful and forgiving whilst helping me conduct various experiments. I would like to also thank my supervisors of my first two rotations, Jake Malone and Andy Truman, for starting out my PhD journey in such a welcoming atmosphere and the John Innes Foundation for funding the research I have conducted.

I want to thank my university tutors Jason Schnell and Natalia Gromak for pushing me further and harder than I thought possible, helping me get where I am today and establish a strong internal drive which I have no doubt required to finish this PhD. I would like to thank my old teachers, in particular Sarah Thwaites whose science-based humour I have carried with me and Marion Page whose words of wisdom keep me focussed on what is important.

My friends and family have been my grounding rock during a turbulent 4 years. I want to thank my Mum, Dad, Luke, and Abi from the bottom of my heart for supporting me through every part of this journey, always there to chat and argue about a vast array of unrelated topics and keep my head on straight. I am extremely thankful to have such funny and caring friends to surround me. This includes Chay, Michael, Patch, Em, Crudge, Ollie, Kalinna, Charlie, both Annas, Jiawen, Lauren and Jenny whose company both in person and virtually brightened my days and

kept me going. I would also like to thank Steph Bornemann for being someone to talk to during difficult times and who always had time to listen to any goings on.

Finally, I would like to thank my wonderful partner Michelle Ko, who supported me every step of the way and was there for every rant, every failed experiment and every significant result. Your unwavering support has been a constant during a time of large changes and contributed a huge amount to my ability to carry out the work in the way I did. For this and everything else, I am incredibly grateful.

My vocabulary is not advanced enough to properly express the depth of gratitude I have to all these people and more that I have not mentioned by name, but suffice to say I am partially a product of my environment, and my environment has been good.

Chapter 1: Introduction

1.1 Understanding Zn homeostasis in plants is important for global crop productivity

1.1.1 Zn deficiency

Zinc (Zn) is a redox-stable transition metal that has strong Lewis acid properties, flexible co-ordination geometry and exists in nature only in the +2 oxidation state. This, in addition to its high abundance and bioavailability on land, has led to Zn use as a cofactor ubiquitously in nature where it binds to around 9% of the eukaryotic proteome[2]. Its roles include acting as catalytic centres in enzymes such as carbonic anhydrase[3], structural components in some transcription factors[4], stabilisation of membranes[5], an intracellular second messenger in mammals[6,7], and reactive oxygen species (ROS) protection[8].

Zn deficiency ranks as one of the commonest micronutrient deficiency in plants and affects around half of the world's agricultural soils[9,10]. Zn deficiency of crops is dependent on the availability of Zn in the soil, with soil Zn existing either as a soluble form which can be taken up by plant roots, in an insoluble complex, or in an adsorbed and exchangeable form[11]. Soil factors can influence how soluble and mobile the Zn is. Soils with high pH[12] and calcareous makeup[13] are good predictors of soil Zn deficiency.

Plants can show Zn deficiency symptoms when Zn levels in the shoot are below 15-20 mg Zn kg^{-1} dry biomass. Plants with Zn deficiency show increased susceptibility to both abiotic and biotic stresses, stunted growth, leaf chlorosis, increased shoot branching, early senescence of leaves and reduced floral fertility[14,15] and therefore this represents a substantial yield loss.

Some of the symptoms of Zn deficiency are due to increased ROS levels[16] which leads to oxidative cell damage, observed by the accumulation of malondialdehyde, a product of lipid peroxidation[17]. This increased ROS results from the upregulation of non-specific transporters which leads to an excess of redox active metals such as iron (Fe)[18] which through the Fenton reaction[19] generates superoxide. The activity

of Copper-Zn superoxide dismutase (Cu-Zn SOD) required to catalyse the detoxification of superoxide is also lowered by Zn deficiency, further increasing oxidative stress.

Crops grown on Zn-deficient soil provide poor levels of Zn to consumers. In addition, modern varieties of wheat show a reduced bioavailable micronutrient content relative to their wild ancestors[20]. In places where cereals provide the majority of the calories for the population, this Zn deficiency is compounded by the Zn-chelating compounds within the plant such as phytate[21], tannins and lignin. Therefore, Zn deficiency in the human population is a major concern, particularly in poorly developed areas. It is thought that 2 billion people are Zn-deficient[22] and this deficiency leads to around 450,000 deaths of children under five annually[23]. In humans, Zn deficiency manifests as appetite loss, stunted growth and poor immune system functionality[24-28]. Zn deficiency is therefore a major issue and many tactics have been employed to reduce its prevalence.

1.1.2 Tackling Zn deficiency

Currently the leading strategy to fight soil Zn deficiency is adding Zn to fertilisers, most commonly Zn sulphate which has proved successful in Zn deficient soils in India where increases in yield of rice and Zn content in grain of three-fold were recorded when soils were treated with Zn mixed with urea[29]. However, this may be difficult to achieve in developing countries with poorer infrastructure where Zn-deficiency is a widespread problem. A possible solution that bypasses any infrastructure development issues is the production of biofortified crops[30], where beneficial traits are bred into crops and are chosen based on enhanced micronutrient uptake and efficiency in concentrating the Zn into edible regions of the plant. In addition to breeding of beneficial traits, genetically engineering components of the Zn homeostasis network to improve Zn grain content could also be a solution, as evidenced by the recent Zn biofortification achieved through manipulation of expression of genes encoding Zn transporters and enzymes which catalyse the synthesis of nicotianamine (NA), a Zn-chelator[31,32].

1.1.3 Zn excess in soils

Zn can also be present in excess within soils, with the main causal factor being proximity to industrial activity[33]. Plants can show symptoms of Zn excess when Zn concentration in the leaf is above 300 µg Zn g^{-1} dry biomass[14]. Non-adapted crop species grown with toxic high levels of Zn, show reduced biomass and chlorosis[34], both of which are symptoms associated with Fe deficiency, as Zn outcompetes Fe for transporters capable of transporting Zn and Fe[35]. Characteristics of Fe-deficient soils are similar to those of Zn-deficient soils (including high pH which reduces Fe solubility and so uptake), and represents 30% of arable land[14].

Metal hyperaccumulators are specially adapted plants that can survive on metal rich soils. Zn hyperaccumulators, store large amounts of Zn (above 3000 µg Zn g^{-1} dry biomass) within Zn sinks such as vacuoles in leaves. These Zn hyperaccumulator species[36] are mostly in the order *Brassicales*, with the hyperaccumulation seeming to have evolved many times independently[37]. Two model species which have been extensively investigated for Zn hyperaccumulation and increased tolerance to high soil Zn, *Arabidopsis halleri* and *Noccaea caerulescens*, employ a wide range of strategies to adapt to high Zn soils even between populations in a species[38-41].

1.1.4 Utility of understanding Zn homeostasis in plants

Understanding the mechanisms behind Zn uptake, transport and storage in deficient and excess conditions is vital to genome-assisted breeding or genetic engineering of future crops. For example, understanding what factors are involved in the Zn deficiency response may aid creation of plants with greater productivity on poor Zn soils. Another example may include understanding the factors involved in the Zn excess response to enable breeding of increased Zn tolerance for growth on contaminated soil for agriculture, phytomining or phytoremediation purposes[42]. As land plants share the principles involved in metal homeostasis and many of the

same network components[43], the Zn excess response in model species such as *Arabidopsis thaliana* can also be used to further understand transition metal homeostasis in crop plants, thus contributing to crop biofortification research[44]. It should be noted however, that although a large number of the components are shared across land plants, there is still a large amount of intraspecific and interspecific variation in Zn requirement, efficiency and tolerance[45]. In addition, as Zn homeostasis is related to Fe homeostasis, any traits beneficial in tolerance to Zn excess could potentially be useful traits for crop production in low Fe soils.

Therefore, the more knowledge we have on the components of the Zn homeostatic network in plants, the easier it will be to breed crops capable of growing on Zn-deficient soils or Zn-toxic soils.

1.2 Zn homeostasis in *Arabidopsis thaliana*

As most living systems depend on maintaining Zn within a specific range, they have evolved different strategies to maintain homeostasis. Firstly, within the cell, Zn is mostly chelated by being tightly bound to proteins and low molecular weight ligands to keep the level of free Zn in the cytosol buffered in the sub-nM range[46]. Secondly, the influx and efflux of Zn into and between cells and subcellular compartments is controlled by the activity of membrane transporter proteins, phytosiderophores and nicotianamine (NA) each with differing affinities for Zn.

1.2.1 Zn chelators

Chelation within the cell by high and low molecular weight ligands buffer the cytosolic free Zn concentration from external changes in Zn availability. These can be metal binding proteins such as metallothioneins (MTs)[47] and phytochelatins (PCs)[48] which together act to sequester transition metals including Zn in response to Zn excess. MTs[49,50] are cysteine rich small proteins that bind transition metals,

implicated in increasing resistance to high cadmium (Cd)[51], Cu[52] and Zn levels[47] through binding of the metals with cysteine-rich sequence motifs. PCs are small peptides synthesised by PC synthase from glutathione[53], and represent a major detoxification mechanism for arsenic and Cd. In plants PC synthesis has also been shown to be increased in response to Zn[54] and is essential for the detoxification of Zn[48]. Interestingly, PCs have also been shown to be transported in the phloem opening up possibilities for them to be involved in long distance Zn transport[55]. In addition to these higher molecular weight ligands, lower molecular weight ligands for Zn are known to be utilised including NA[56] and to a lesser extent histidine[57]. NA is a non-proteinogenic amino acid synthesised from condensation of three S-adenosyl methionine molecules in a process catalysed by NA synthases. Overexpression of NA synthase genes in *Arabidopsis thaliana* leads to increased leaf Zn and NA and has also been implicated in the root-to-shoot transport of several transition metals including Zn, Fe and Cu[58-60]. This long distance transport of metal-bound NA is likely facilitated through the activity of YSL proteins[61] and double *Atysl1 Atysl3* mutants show disrupted Zn and Cu mobilisation into seeds illustrating the importance of transport of Zn-NA complexes across the plasma membrane in the vasculature[62]. In addition, NA synthesis was shown to be essential to metal hyperaccumulation in *Arabidopsis halleri*[63].

1.2.2 Zn transporters

As Zn is a charged species within the cell, a series of membrane transport protein families are responsible for controlling the movement of the Zn across membranes between cells and subcellular compartments. The import of Zn into the cytoplasm mostly occurs through Zinc-Regulated Transporter, Iron-Regulated Transporter (ZRT-IRT)-like proteins[64] (ZIPs). ZIPs are present in all domains of life[65] and in *Arabidopsis* 18 *ZIP* genes have been identified.

As a family these transporters transport Zn, Fe, and manganese (Mn), are often non-specific, and where specific, metal specificity can be altered by amino acid mutations[66]. For example, AtIRT1 transports Fe as well as Zn and Cd into the plant

cell[67], and AtZIP2 is capable of transporting Mn and Zn[68]. Many different ZIPs are capable of transporting Zn and are involved in Zn deficiency and Zn excess, with a summary of all Zn transporting ZIPs in *Arabidopsis* including *AtIAR1* which is investigated in this study, shown below in **Table 1.1**.

Gene Name	Metal Transported	Subcellular Localisation	Tissue Expression	References
AtZIP1	Zn, Mn	Vac	Root stele and vasculature	68
AtZIP2	Zn, Mn, Cu	PM	Root stele	56,68
AtZIP3	Zn		Root epidermis, vasculature	68,69
AtZIP4	Zn, Cu	PM	Root endodermis, pericycle, leaf, trichromes	70-72
AtZIP5	Zn, Mn, Fe		Root epidermis, leaf veins	68,69,73-75
AtZIP6	Zn, Mn	PM	Roots, anthers, leaf veins	68,72,74
AtZIP9	Zn, Mn	PM	Root vasculature, first Silique	68,69,74 72
AtZIP10	Zn, Mn		Root	68,74
AtZIP11	Zn, Mn		Seeds, leaves, root vasculature	68,69

AtZIP12	Zn		Senescent leaf vein	[68,74]
AtZIP13	Zn	Golgi	Ubiquitous	[74,76]
AtIRT1	Zn, Mn, Fe, Cd	PM	Root epidermis	[67,77]
AtIRT2	Zn, Fe	Intracellular	Root epidermis	[76,78]
AtIRT3	Zn, Fe	PM	Germinating seeds, anthers, phloem	[69,72,74,79]
AtIAR1			Ubiquitous	[74]
AtZTP29	Zn	ER	Ubiquitous	[74,80]

Table 1.1 Zn-transporting AtZIPs: transport capabilities, subcellular localisation, and expression. Vac = Vacuole, PM = plasma membrane, ER = endoplasmic reticulum. Note *AtZTP29* is also referred to as *AtGUFA* in the literature and *AtZIP13* is also referred to as *AtZNE1*. Metal transport assays were all conducted through yeast complementation studies, subcellular localisation by GFP tagging, and tissue expression derived from *GUS* expression and staining or the developmental expression atlas generated by Klepikova et al.[74]. Those left blank are unknown or in the case of AtIAR1 under investigation in this study.

Reversing this influx of Zn into the cytosol, export of Zn from the cytoplasm to the extracellular space in *Arabidopsis thaliana* occurs through AtPCR2, a homodimeric transporter with two transmembrane helices per sub-unit[81]. *AtPCR2* is expressed in the shoot, the root epidermis, the xylem of the root elongation zone and the root tip[81]. *Atpcr2* knockout mutants suggest that AtPCR2 is involved in long distance transport of Zn through export of Zn from the cytosol[81].

Transport from the cytosol into storage organelles such as the vacuole is a common mechanism to adapt to high Zn levels. The protein families involved in this sequestration are Heavy Metal ATPases (HMAs), Metal Tolerance Proteins (MTPs), Natural Resistance-Associated Macrophage Proteins (NRAMPs) and ZIFL (ZIF1-like) proteins. HMAs are P_{1B}-type ATPases capable of actively transporting a wide range of metals using ATP hydrolysis and are subdivided based on substrate specificity (monovalent copper and silver or divalent Zn, cobalt, lead and cadmium ions)[82,83]. Although non-functional due to a nonsense mutation in the Columbia (Col-0) accession of *A. thaliana*, AtHMA3 is a vacuolar transporter in closely related accessions and is responsible for vacuolar sequestration of Zn[84,85]. MTPs operate through antiport of a divalent metal ion with a proton[86,87]. In *Arabidopsis* there are 12 MTP proteins with different metal specificities[88], with AtMTP1, AtMTP2, AtMTP3, AtMTP4 possessing Zn transport capability when expressed alone and AtMTP5 only when in complex with AtMTP12[89-92]. AtMTP1 and AtMTP3 transport Zn into the vacuole and mutations in these *AtMTP* genes lead to hypersensitivity to Zn[91,93], as Zn is unable to be appropriately sequestered into the vacuole. *AtMTP1* is expressed in both root and leaf cells in subpopulations of dividing, expanding and differentiating cells[93], whilst *AtMTP3* is expressed in the root epidermis and cortex[91]. NRAMPs are capable of both metal-proton cotransport and antiport of transition metal ions with protons[94-96]. In *Arabidopsis* the only known Zn-transporting NRAMP is AtNRAMP4[97], which it is capable of vacuolar Zn export but also has been shown to transport Fe and Mn out of vacuoles in plants[98,99]. ZIFL (ZIF1-like) proteins are members of the Major Facilitator Superfamily. *AtZIF1*, identified by screening for mutants hypersensitive to Zn[100], is responsible for NA transport into the vacuole from the cytoplasm[101]. This vacuolar NA accumulation is then correlated with increased Zn storage in the vacuole. Another vacuolar ZIF protein involved in Zn homeostasis is AtZIF2, which directly transports Zn into the vacuole[102].

Transport of Zn to endoplasmic reticulum (ER) has been shown to occur through AtMTP2. *AtMTP2* codes for an ER-localised Zn transporter in the outer cell layers of the elongation zone in roots[92] that is upregulated in Zn deficiency. It is therefore hypothesised that AtMTP2 functions to transport Zn symplastically through the ER-luminal continuum in the root cortex[103]. AtMTP5 is also capable of transporting Zn

into the secretory system, however only when in a *cis*-Golgi-localised complex with AtMTP12[1,89]. AtZIP13, an unusual ZIP protein, also appears to show transport of Zn into the Golgi[76], transporting Zn in the opposite direction to that of other plant ZIPs thus far investigated.

HMAs also contribute to Zn transport in *Arabidopsis thaliana* through aiding xylem loading of Zn. *AtHMA2* and *AtHMA4* contribute redundantly to Zn homeostasis by aiding the root-to-shoot translocation of Zn with double *Athma2 Athma4* mutants showing a severe Zn-deficiency phenotype in the shoot, along with seed infertility and stunted growth[84]. These transporters localise to the plasma membrane of pericycle cells in the vasculature[104] and so are thought to help load Zn into the phloem for root to shoot transport.

The combined action of the various components listed above leads to a spatially controlled and dynamic movement of Zn between subcellular compartments as shown in **Figure 1.1**. As these different components are expressed in different tissues at different times in different conditions, it is also important to understand how these components of Zn homeostasis act together in Zn deficiency and excess conditions.

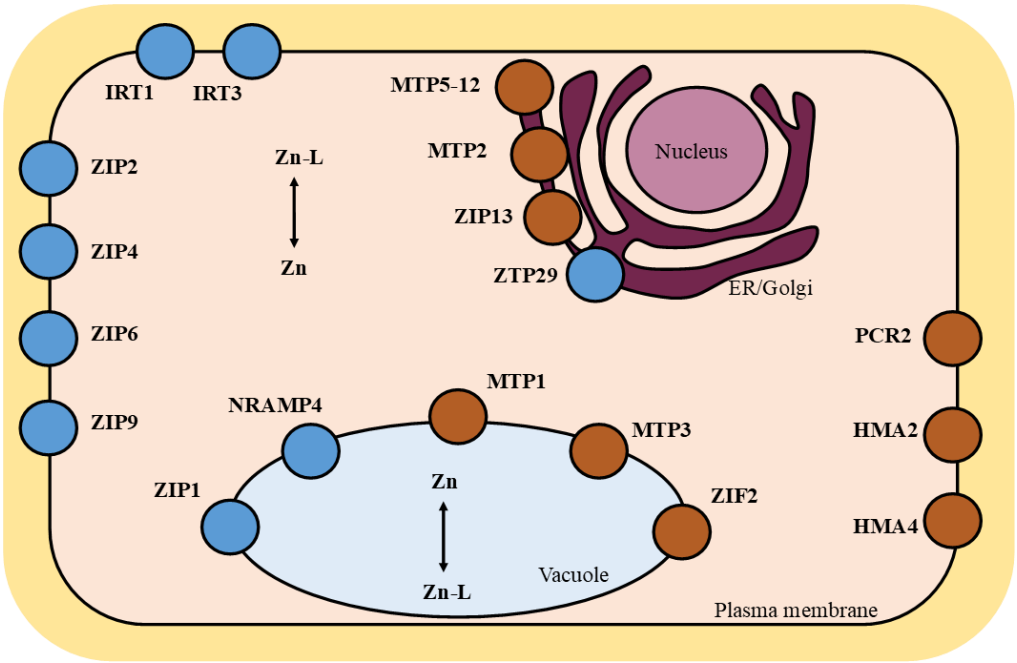

Figure 1.1. Schematic of Zn movement in a single *Arabidopsis thaliana* Col-0 cell. Transporters are shown in circles responsible for increasing (blue) or decreasing (brown) cytosolic Zn levels**.** Within each subcellular compartment Zn is then reversibly bound to ligands (L). It should be noted that tissue and cell-specific expression of these transporters has been ignored for clarity.

1.2.3 Zn deficiency response in plants

In conditions of Zn deficiency, plants maximize Zn uptake from the soil, Zn use efficiency and mobilisation from stores to sinks such as young leaves or developing seeds. To maximize Zn uptake from the soil, two different strategies are employed by plants. In strategy I, plants including *Arabidopsis thaliana* exude acidic compounds and reductants into the soil which lead to Zn ion release from complexes such as Zn phosphates for uptake by the plant root[105]. The profile of these root exudates is a greater predictor for tolerance to Zn deficiency than Zn transport activity[106]. Strategy II is used only by plants from the *Poaceae* family which include cereal grasses, and involves the exudation of Zn phytosiderophores

which bind strongly to Zn, creating a Zn-phytosiderophore complex which can be transported into plant roots[107].

To increase influx of soluble Zn^{2+} from the soil into the cytosol, ZIP transporters are transcriptionally upregulated[71] which act to increase free Zn in the cytosol of root cells. In addition to increasing Zn availability in Zn-deficient conditions, Fe and Mn levels must be balanced through modulating Fe and Mn transporters to ensure ROS levels are kept within limits. Due to the non-specific nature of metal transporters upregulated in Zn deficiency, Zn deficiency leads to increased Fe levels in the roots and increased ROS production[8,14]. Free Fe ions act to increase ROS levels through the Fenton reaction[19]. In addition, long-term Zn deficiency and low Zn efficiency rice cultivars show a reduction in Cu-Zn SOD activity, further increasing ROS levels[108,109]. Mn treatment, however, can be used to rescue Zn deficiency symptoms in short term growth (two weeks) through the reduction of ROS levels[110]. Therefore, to combat increased ROS levels in the root during Zn deficiency, ZIP transporters capable of transporting Mn into the cytosol (*AtZIP1, 5,* and *9*) are upregulated[68,71]. *AtIRT1*, which is responsible for the majority of Fe uptake in roots, is also downregulated in Zn deficiency and upregulated only in Fe deficiency[111].

To increase the transport of Zn to the xylem for long distant transport to the shoot, Zn deficiency also enhances transcription of *AtMTP2* and *AtHMA2*[92] which increases symplastic Zn flow and Zn loading to the xylem respectively. To increase Zn-NA mediated long distance transport of Zn two NA synthases, *AtNAS2* and *AtNAS4*[112] are upregulated transcriptionally as well as putative Zn-NA transporters *AtYSL1* and *AtYSL3*[62]. In addition, AtPCR2-mediated extrusion of Zn from the cytosol may also play a role in root-to-shoot transport of Zn[81].

Mobilisation of above ground Zn also occurs to move the Zn from senescing tissue to sink tissue such as developing seeds and meristems. For example, trichromes and cell vacuoles are major stores of Zn when Zn is in adequate supply[113], and these reservoirs can release Zn which then can be transported to the phloem for redistribution to sink tissue[114], most likely in the form Zn-NA.

Furthermore, autophagy genes are upregulated in Zn deficiency conditions and mutants in autophagy-related genes show an enhanced Zn deficiency transcriptional

response[115]. Although autophagy mutants show similar total Zn levels to wildtype in most tissues, they show increased chlorosis associated with increased ROS stress in the chloroplast[116].

How these components work together has only recently begun to be elucidated. Each of the components involved in Zn homeostasis is part of a plastic network[117]. The network utilises the redundancies of many of the transporters to adapt to differing conditions for example through differing expression levels of *AtHMA3*[117]. This network of redundancy is likely to be present in crop species and further understanding of this network could help develop crops with beneficial characteristics to withstand Zn deficiency or excess.

1.2.4 Regulation of the Zn deficiency response in *Arabidopsis thaliana*

In the search for mechanisms of Zn homeostasis, a yeast one-hybrid screen was set up to identify transcription factors able to bind the *AtZIP4* promotor. Here, the transcription factors AtbZIP19/23 have been shown to modulate the activity of different metal transporters in conditions of low Zn[71]. The target genes of AtbZIP19/23 contain one or more copies of the Zinc Deficiency Response Element (ZDRE) which is a 10-bp palindrome (RTGTCGACAY). In *Arabidopsis* in Zn deficient conditions, this pair of transcription factors was found to be responsible for an increase in transcription of several ZIPs including *AtZIP4, 1, 3, 5, 9, 12* and *AtIRT3*[71]. In addition to ZIPs, the *Atbzip19 Atbzip23* double mutant also showed downregulation of lipid signalling and NA synthase genes, representing the multi-faceted response to Zn deficiency that AtbZIP19/23 is responsible for[71]. It was later shown that this pair of transcription factors is located in the nucleus[118] and in single mutants slightly different subsets of genes are activated suggesting they do not function entirely redundantly[119]. It has recently been found that the AtbZIP19/23 transcription factor pair harbour a Zn binding site that when disrupted causes a constitutive Zn deficiency response, creating a model whereby lower cellular Zn allows conformational changes which enable AtbZIP19/23 transcriptional

activity[120]. It is important to note that Zn homeostasis in *Arabidopsis* shares key regulatory features to that of crop plants including regulation by *bZIP* genes which are responsible for a similar transcriptional response to Zn deficiency in a variety of cereals including rice[121,122].

There appears to be an additional AtbZIP19/23-independent mechanism to regulate Zn deficiency, as some genes, including *AtMTP2* and *AtHMA4,* that are upregulated in Zn deficiency lack any upstream ZDREs. Through experiments in *Athma2 Athma4* double mutant plants which have Zn deficiency in the shoots only, it was identified that one component of the *AtMTP2* regulation machinery was a shoot-derived signal that could override local signals of Zn sufficiency in the root to upregulate *AtMTP2*[92]. Both the local and systemic Zn deficiency responses are outlined below in **Figure 1.2**.

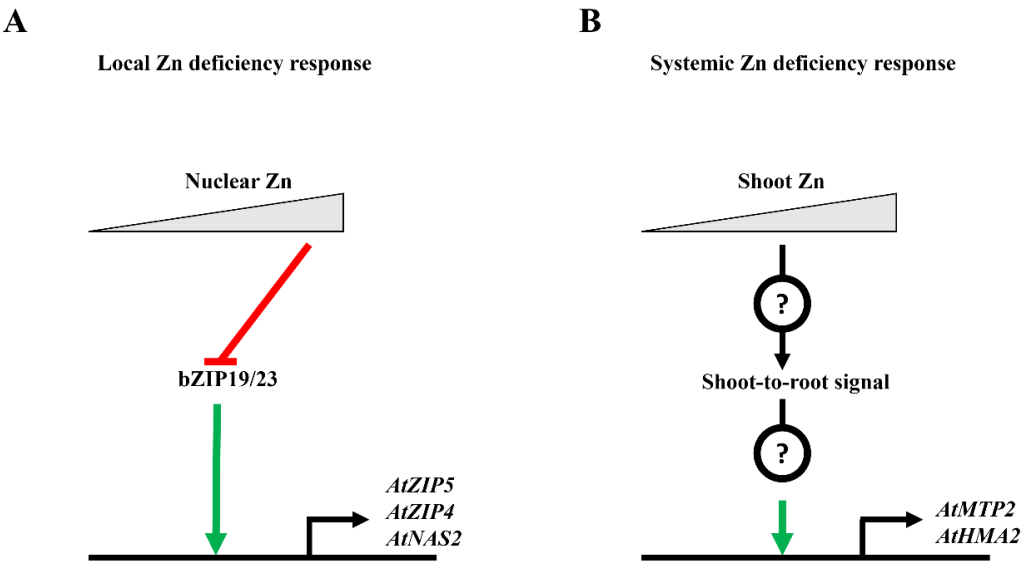

Figure 1.2 Zn deficiency response in *Arabidopsis thaliana*. (A) Local Zn deficiency response. AtbZIP19/23 transcription factor activity is inhibited by direct binding of Zn. In low Zn conditions, the active transcription factor pair activate the transcription of many genes including those for Zn and Mn transport (*AtZIP5*, *AtZIP4*) as well as for NA synthesis (*AtNAS2*). (B) Systemic Zn deficiency response. Low Zn status in the shoot is transmitted through unknown components to the root leading to induction of genes involved in ER Zn import (*AtMTP2*) and xylem loading (*AtHMA2*). See text for further details.

As well as transcriptional changes, plants have been shown to regulate metal transporters in other ways. For example, AtZIF2, a transporter that is responsible for increasing Zn tolerance and upregulated transcriptionally by Zn, is also regulated by Zn through intron retention. In the presence of Zn the intron is retained and this increases translation[102]. In addition, post-translational modifications play a role in ZIP activity. AtIRT1 exhibits monoubiquitin-dependent reversible endocytosis in low Fe high Zn conditions[123]. In a scenario where Fe is low and non-iron metals such as Zn are high, these metals bind to a histidine rich cytoplasmic loop of AtIRT1 and facilitate AtIRT1 phosphorylation by recruitment of AtCIPK23 which then allows AtIRT1 to be trafficked to late endosomes and degraded[124]. It is

currently unknown whether similar mechanisms are used in the regulation of the other ZIPs.

Therefore, more knowledge of any component of this homeostatic network is vital to understand Zn homeostasis in model and crop plant species enabling design of crops with improved Zn uptake in Zn poor soils or Zn allocation to grains for human consumption.

1.2.5 Zn excess response in plants

Under Zn excess, Zn^{2+} outcompetes other divalent cations, including Mg^{2+} and Fe^{2+}, for binding sites according to the Irving-Williams series[125]. The competition leads to the inhibition of photosynthetic enzymes[126,127]. In addition excess Zn leads to increased oxidative stress as shown by an increased ratio of oxidised glutathione and lipid peroxidation[128,129].

Chelation within the cell by high and low molecular weight ligands buffer the cytosolic free Zn concentration from external changes in Zn availability. Of these, in *Arabidopsis thaliana*, only phytochelatins so far have been shown to be essential to buffer Zn concentrations in Zn excess conditions[48].

Transport of Zn out of the cytosol is another mechanism by which *Arabidopsis thaliana* detoxifies Zn. Export of Zn from the cytoplasm to the extracellular space occurs through AtPCR2[81]. *AtPCR2* is expressed in the shoot, the root epidermis, the xylem of the root elongation zone and root tip[81] with knock-out studies suggest that PCR2, in addition to the role in Zn deficiency outlined previously, is also part of the Zn excess response[81]. Cell wall components, particularly pectin, have been shown to bind and immobilise a large range of divalent cations including Zn[130,131], with mutants in pectin synthesis or modification particularly sensitive to high Zn levels[132,133].

Transport from the cytosol into storage organelles such as the vacuole is a common mechanism of adaptation to high Zn levels either directly through Zn transport in the case of AtMTP1[93], AtMTP3[91] and ZIF2[102] or indirectly through vacuolar

loading of NA in the case of AtZIF1[101]. Of these, *AtMTP3* is transcriptionally upregulated in Zn excess conditions[134].

In addition to the vacuole, the Golgi has been identified as another organelle used to store Zn in Zn excess conditions. AtZIP13 (also known as AtZNE-1) has been identified as a Zn transporter capable of transporting Zn into the Golgi[76]. *Atzip13* mutants show increased sensitivity to both high Zn and low Fe conditions, implying the importance of Zn storage in the Golgi in these conditions.

One of the major features of Zn excess is Fe deficiency. Zn in excess will outcompete Fe for binding sites on proteins including transporters, thus creating Fe deficiency. Zn and Fe intersect along many parts of the Fe uptake and redistribution system. For example, the Fe import machinery involves the ZIP transporter AtIRT1 that in addition to Fe can also transport Zn[77] which when in excess will outcompete the Fe. In conditions of excess Zn *AtFRO2*, which is responsible for reduction of Fe^{3+} to Fe^{2+}, and *AtIRT1*, which is the major importer of Fe^{2+} in the roots, are upregulated[35,135-138]. In addition, *AtIRT2* is upregulated in epidermal root cells, and probably functions to release Fe into the cytosol from intracellular compartments[78,139].

Fe root-to-shoot translocation is decreased in Zn excess and the resulting chlorosis can be complemented by Fe addition[135]. This Fe deficiency in the shoot under Zn excess is exacerbated within *Arabidopsis thaliana* accessions with alleles of *AtFRD3* that encode a non-functional protein. AtFRD3 is a member of the multidrug and toxic compound extrusion (MATE) protein family[140], and is a crucial component of the Fe deficiency response[140] through its action in exporting citrate into the xylem[141] for root-to-shoot Fe translocation. Natural variation within *Arabidopsis thaliana* accessions has shown that some alleles of *AtFRD3* exhibit no citrate transport activity and increased sensitivity to Zn excess[142] due to this reduced Fe translocation.

Fe release from vacuoles is an essential part of the Fe deficiency response and is also important in Zn excess tolerance. Mutants in genes coding for the tonoplast-localised AtNRAMP3 and 4 are unable to germinate on low Fe media[98,99]. Whereas AtNRAMP3 can transport Fe and Mn, AtNRAMP4 has additionally been shown to transport Zn in yeast complementation studies[97,143]. Double *Atnramp3 Atnramp4*

mutants show Zn hypersensitivity which is thought to be due to lack of appropriate mobilisation of metals including Fe from vacuoles in Zn excess conditions.

Similar to Zn deficiency, autophagy has also been shown to play a role in Zn excess, as mutants in autophagy-related genes show sensitivity to excess Zn conditions that can be complemented by addition of Fe and exacerbated by removal of cotyledons[144]. This together suggests the role of autophagy in Zn excess is to help mobilise Fe from cotyledons to other tissue such as true leaves.

Overall, *Arabidopsis thaliana* must respond to Zn excess by sequestering Zn and increasing Fe uptake to combat Fe deficiency.

1.2.6 Gene expression regulation in Zn excess is mostly that of the Fe deficiency response

Although no Zn-specific Zn excess response has been demonstrated to date, *Arabidopsis thaliana* in Zn excess does have a characteristic change of redox homeostasis[128] compared to that generated by excess Cd[145] and Cu[146]. Recent work in *Populus ussuriensis*[147] has identified a heat shock transcription factor (PuHSF4a) responsible for Zn excess-specific induction of *GLUTATIONE-S-TRANSFERASE U17* and *PHOSPHOLIPASE A2* genes, which together improved the tolerance of plants to Zn excess generated oxidative stress. Whether this mechanism operates in *Arabidopsis* species is currently unknown. In addition to potential Zn excess-specific redox state regulation, Zn excess has been shown to increase phytochelatin synthesis and alter the expression of miRNAs in plants[128], although the mechanisms behind this regulation is still unknown.

Although in *Arabidopsis* no Zn excess specific signalling pathways are known, the Fe deficiency response which is activated under Zn excess is well characterised. In the Zn hyperaccumulator *Arabidopsis halleri* spp *gemmifera*, one of the differences compared to *Arabidopsis thaliana* is improvement of Fe uptake in Zn excess conditions[35], illustrating the importance of Fe regulation in the Zn excess response. Fe-deficiency genes are upregulated through a cascade of basic helix-loop-helix (bHLH) transcription factors. At the top of the cascade is AtURI, a IVb subfamily

bHLH member which dimerises with members of the IVc subfamily[148]. The IVc subfamily genes includes *AtILR3*[149], *AtbHLH34*, *AtbHLH104* and *AtbHLH115*[150,151] which are active in conditions of Fe deficiency. The IVc bHLHs then go onto induce members of the Ib bHLH subfamily including *AtFIT*, *AtbHLH38* and others, which dimerise and function redundantly[152,153]. FIT in dimerization with other Ib bHLHs then induces the transcription of Fe deficiency machinery including *AtFRO2* which is responsible for reduction of Fe^{3+} to Fe^{2+}, and *AtIRT1* which as mentioned previously is the major importer of Fe^{2+} in the roots[136-138]. In addition to increasing Fe deficiency genes such as *AtIRT1*, through interactions with AtPYE in pericycle cells, AtILR3 mediates the repression of Fe transport and storage genes such as those controlling the synthesis of NA synthesis and ferritin synthesis[149,154,155].

It has recently become elucidated how Fe levels co-ordinate this cascade. Fe-dependant degradation of bHLHs within the cascade occur by BRUTUS (BTS) and BRUTUS-LIKE (BTSL) E3 ligases which target AtFIT and IVc bHLHs for degradation in Fe sufficient conditions[156-158]. This interaction and degradation is thought to be attenuated by IRON MAN (IMA) peptides through binding to BTS and BTSL proteins[159,160]. Therefore, IMAs which are transcriptionally induced in Fe deficiency promote the Fe deficiency response[161]. The main components of this regulatory cascade are shown below in **Figure 1.3**.

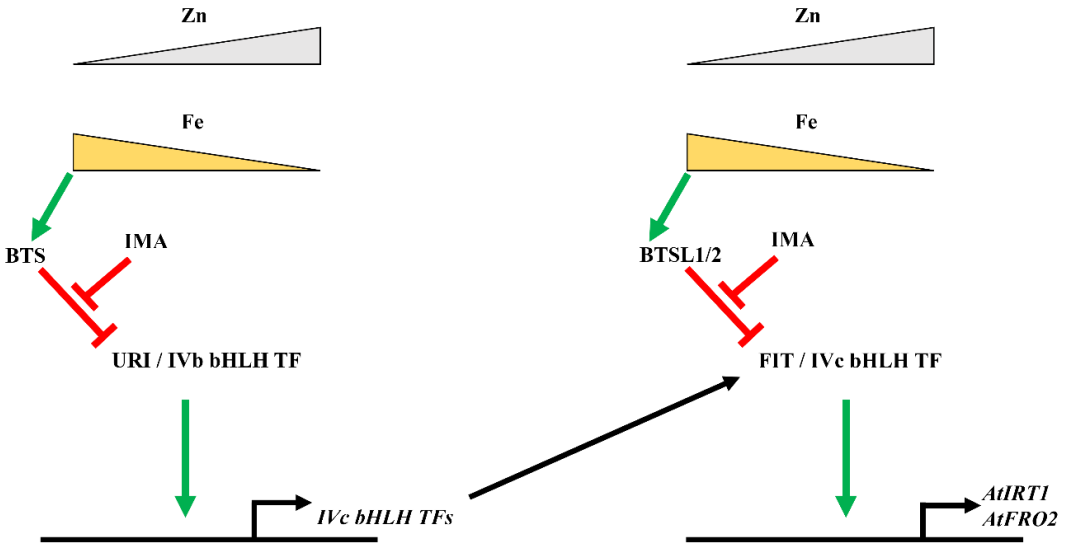

Figure 1.3 Fe deficiency response induced by Zn excess. In Fe replete conditions, BTS and BTSL proteins are active and degrade members of the bHLH transcription factor (TF) cascade reducing expression of Fe deficiency genes. In low Fe conditions, BTS and BTSL proteins are inactive thus stabilising URI and IVb bHLH TFs. URI IVb bHLH TFs then induce expression of *AtFIT* and IVc *bHLH* TF genes which then induce genes including those involved in Fe uptake (*AtIRT1* and *AtFRO2*).

1.3 Auxin homeostasis in *Arabidopsis thaliana*

Plants are sessile organisms that adapt to changing conditions through growth and development mediated through a variety of plant hormones. Some of the earliest plant growth responses to be analysed were gravitropism and phototropism, which were discovered to rely on a transported signal from the root or coleoptile tip[162,163]. The transported molecule was later isolated and identified as indole-3-acetic acid (IAA, auxin)[164,165]. In addition to the role of auxin in tropisms, application of auxin inhibitors and antagonists showed auxin to be a major player in embryonic development of plants[166-169]. Furthermore, post-embryonic development through maintenance of the root apical meristem[170-172] and the shoot apical meristem[173-176] is

also regulated through auxin in conjunction with other plant hormones such as cytokinin[177-180].

1.3.1 Auxin transport is important to many aspects of plant development

Auxin transport is key to many aspects of auxin regulation of development. Key to understanding auxin transport was the generation of the chemiosmotic model where protonation of auxin at extracellular acidic pH, electrochemical gradients of deprotonated auxin and protons, and polarly localised auxin transporters drive auxin movement between and within cells and tissues[181,182]. Studies on auxin transport found *Arabidopsis* mutants such as *Atpin-formed 1* which shared a growth phenotype with plants treated with inhibitors of polar auxin transport[183]. The phenotypes of these reduced auxin transport mutant plants included a long inflorescence with no or few flowers, from which the causal gene (*AtPIN1*) was isolated and characterised[184]. *AtPIN1* is one of a number of PIN family members that since have been characterised to facilitate polar auxin transport[183-188]. Mutations in other *PIN* genes responsible for polar auxin transport show distinct phenotypes, implying that they function non-redundantly, such as *Atpin2* which displayed reduction in root gravitropism and root growth[185]. Present in all land plants, with *Arabidopsis* containing 8[189], PINs can be split into two groups based on the length of a loop between two central transmembrane helices. In *Arabidopsis*, AtPIN1,2,3,4,7 are so called long PINs, AtPIN5 and 8 are short PINs and AtPIN6 shows an intermediate length of loop[189]. Long PINs have been shown to take part in polar transport of auxin through cell efflux[183-188], with the long hydrophilic loop playing a role in the intracellular trafficking of PINs to their polar location[190]. Short PINs on the other hand, have been found to be localised to the ER membrane with AtPIN5 transporting auxin into the ER lumen and AtPIN8 exporting auxin from the ER lumen[191-193]. AtPIN6 appears to show dual localisation to the ER and plasma membrane and so plays a role in intracellular auxin homeostasis as well as polar auxin transport[194]. ER accumulation of auxin also occurs through members of the PIN-LIKES (PILS) family, with the ER accumulation associated with an increase in

auxin inactivation through conjugation[195], a process which will be explored later. Further subcellular transport machinery for auxin includes WALLS ARE THIN1 (AtWAT1) which was shown to be important for release of vacuolar stores of auxin to aid secondary wall formation in the developing vasculature[196,197].

Mutants showing resistance to the root growth effects mediated by auxin and ethylene treatment led to the identification and later characterisation of AUX1 as a facilitator of auxin uptake into cells that requires a proton gradient[198-202]. *AtAUX1* and its homologues in *Arabidopsis*, *LIKE-AUX1* (*AtLAX*)*1*, *AtLAX2* and *AtLAX3* are members of the amino acid/auxin permease super family[203]. Mutations in different *AUX/LAX* genes show different phenotypes. For example *Atlax3* mutants show reduced lateral root density due to a role in auxin-induced auxin accumulation in cortical cells[204], whereas *Atlax2* mutants show disruption of auxin induced vasculature formation in cotyledons[205].

Other less well characterised auxin transporters include members of the P-GLYCOPROTEIN class of the ATP BINDING CASSETTE (ABC) transporter family that have also been implicated in auxin import and export, both through direct transport activity and also through interactions with AtPIN proteins[206-208]. Finally, AtNRT1.1 has also been shown to catalyse the influx of auxin into cells in addition to its role in nitrogen homeostasis[209].

In summary, auxin import and polar export can be used to create gradients in auxin concentration between and within cells and tissues to mediate growth responses through activating concentration-dependant signalling events.

1.3.2 Auxin signalling

To initiate auxin signalling, auxin needs to bind to receptors. Several auxin receptors have been identified, including components of the Skp-Cullin-F-box (SCF) E3 ubiquitin ligase complex. The SCF ubiquitin ligase complex ubiquitinates proteins for subsequent degradation by the proteasome[210,211]. The F-box protein within the SCF complex acts as a receptor determining the specificity of the targeted ubiquitination[212]. Using a combination of work including mutants and use

of proteasome inhibitors it was demonstrated that the SCF^{TIR1} complex (SCF complex with TIR1 as the F-box protein) mediates the degradation of Aux/IAA proteins[213-215]. Auxin binds to the nuclear-localised coreceptor AtTIR1, a state which is made more stable by the further binding of coreceptor Aux/IAA proteins and thus promoting their ubiquitination and degradation in an auxin dependant manner[216-218]. AtTIR1 is part of the 6 member TIR1/AFB family of F-box proteins with other members of this family that show different auxin affinities[219] playing similar roles to AtTIR1, with some overlapping function, although AtTIR1 and AtAFB2 constitute the majority of physiological auxin binding in this family[220-222]. A similar degradation-dependant mechanism for auxin signalling has also been found within cell cycle control. In *Arabidopsis*, auxin promotes the degradation of a cell division related transcription factor AtDPB through binding to an F-box protein AtSKP2A[223,224].

The Aux/IAA proteins are nuclear localised proteins whose expression is rapidly induced[225] and whose protein stability is reduced after exogenous auxin application[226] through the aforementioned ubiquitination. Aux/IAA proteins act as transcriptional repressors of auxin responsive genes through recruiting TOPLESS/TOPLESS-RELATED corepressors and binding with AUXIN RESPONSE FACTORS (ARFs)[226-228]. ARFs, unlike Aux/IAA proteins, bind DNA directly to auxin response elements[225,229]. Therefore, when Aux/IAA is degraded, auxin-responsive genes are released from repression and are transcribed. Both Aux/IAA proteins and ARFs are part of large families, with differing activities which enable precise control of auxin signalling[230-232]. Interestingly an atypical ARF (ETTIN) has also been found to bind directly to auxin, which leads to dissociation of corepressors and so enables rapid gene induction[233,234].

Auxin binding has also been demonstrated for AUXIN BINDING PROTEIN1 (AtABP1)[235] which localises to the ER and plasma membrane[236] and was thought to be responsible for signalling from extracellular IAA. Work on the physiological role of *AtABP1* in auxin biology has been hindered by apparent off-site mutations within knockdown lines, as null *Atabp1* alleles show none of the major auxin response defects previously ascribed to it[237]. However, more recent work has shown that AtABP1 binds auxin in the apoplast and through TRANSMEMBRANE KINASE 1 (AtTMK1) orchestrates a series of phosphorylations that contribute to

auxin-promoted vasculature formation and regeneration after wounding[238]. Null mutants in *Atabp1* and *Attmk1* cannot establish the auxin-induced vasculature formation and *Atabp1* plants are not complemented by mutated AtABP1 which lacks auxin binding[238]. AtTMK1 activation leads to altered expression of auxin response genes in formation of the apical hook during seedling growth in the dark through cleavage of the C-terminus of AtTMK1. This enables the cytosolic fragment to phosphorylate and stabilise non-canonical Aux/IAA family members, the reverse of that occurring in the canonical TIR1/AFB auxin signalling pathway[239]. Auxin induced AtTMK1 activation also leads to rapid changes in phosphorylation status of many proteins[238]. This fast change in phosphorylation status may also explain part of the rapid auxin-induced reduction in root cell elongation in high exogenous auxin conditions that requires TIR/AFB[240]. However, exactly how ABP1/TMK1 signalling may relate with this is currently unclear.

Within plants the total concentration of active auxin which can be transported and initiate signalling events is mediated through a combination of synthesis, conjugation and catabolism.

1.3.3 Auxin synthesis

In young seedlings, the majority of IAA synthesis occurs in above-ground tissue particularly cotyledons, but all tissues do show localised *de novo* synthesis[241,242]. IAA can be synthesised from tryptophan (Trp) and Trp-independent sources. Trp-independent IAA synthesis is hypothesised to operate through indole synthase action on indole-3-glycerol phosphate to generate indole[243-245], however evidence of the following steps to generate IAA is lacking[246].

The pathway of synthesis from Trp to IAA can take two routes: via indole-3-acetaldoxime (IAOx) or via indole-3-pyruvic acid (IPA). Trp can be converted to IPA by Trp aminotransferases (TAA/TARs)[247-249], which is then converted to IAA through the activity of cytosolically active YUCCA (YUC) flavin monooxygenases[247-249]. All TAA/TAR and YUC steps are catalysed within the cytosol, with some enzymes showing tethering to the ER membrane[250]. There are

three *TAA*/*TAR* genes and 11 *YUC* genes in *Arabidopsis*, with single mutants showing only minor phenotypes, although higher order mutants show stronger phenotypes indicative of some redundancy in this important pathway of auxin synthesis[251-253]. *AtYUC*s are differentially expressed throughout the plant in root and shoot[253,254]. Shoot overproduction of auxin cannot complement lack of root-synthesised auxin through the YUC containing pathway, further underlining that local auxin synthesis occurs in all tissues and plays vital roles in plant development[251]. Control of auxin synthesis through *AtYUCCA* expression is seen in the shade avoidance response, whereby detection of shade induces *AtYUCCA* expression and leads to auxin induced hypocotyl elongation and increased leaf angle[255,256].

The second route to IAA from Trp is a pathway first involving conversion of Trp to IAOx which is catalysed by the cytochrome P450 monooxygenase AtCYP79B2/B3[257,258] within the chloroplast[257]. IAOx can then be used for synthesis of IAA or the synthesis of glucosinolates[259]. This IAOx pathway and glucosinolates are only present in *Brassicaceae*[260], and act with increased importance for IAA synthesis at elevated temperatures[261] in root meristems and lateral root primordia[242]. IAOx is converted to indole-3-acetonitrile (IAN) by AtCYP71A13[262]. The subsequent conversion of IAN to IAA is thought to occur through the activity of AtNITRILASE1[263,264], an enzyme localised in the cytosol[265]. Another route to IAA appears to be from IAOx-generated indole-3-acetamide (IAM)[260,266], although loss of function mutants in IAM hydrolases did not yield changes in IAA content nor a strong phenotype implying this route to IAA is a minor one[267]. A further minor route to IAA is from indole-3-butyric acid (IBA) which occurs in the peroxisome through a putative peroxisomal acyl-CoA oxidase/dehydrogenase[268,269].

1.3.4 Auxin conjugation and oxidation

The concentration of active IAA can be regulated by conjugation into inactive storage forms and degradation via oxidation.

Amide-linked IAAs include amino acid-linked IAAs (IAA-aas), peptide-linked IAAs and protein-linked IAAs. IAA-aas are formed from IAA through the action of enzymes in the Gretchen Hagen 3 (GH3) family[270], which have three subgroups, of which only those in group II (containing nine members in *Arabidopsis*) show conjugation activity with IAA as a substrate[270]. Few of the group II GH3 enzymes have been characterised *in vivo*, with those characterised so far in *Arabidopsis* and *Physcomitrella patens* showing cytosolic localisation[271,272]. *In vitro* data have shown different group II GH3 enzymes show a wide range of amino acid selectivity for IAA conjugation[270,273]. This has been supported by *in vivo* data from *Arabidopsis*, with either single or higher order *Atgh3* mutants showing reduced levels of specific IAA-aa[274,275].

In some cases (IAA-Asp and IAA-Glu), this conjugation is irreversible[276] and the conjugate is then catabolised. The concentration of these irreversibly synthesised conjugates is higher than those for reversibly synthesised conjugates[277,278]. Other IAA-aa conjugates however (IAA-Ala, IAA-Leu, IAA-Phe among others) are hydrolysed back into IAA through IAA-aa amidohydrolases in the ER[279-282]. It is interesting to note that IAA-aa synthesis in all reported cases so far occurs in the cytosol[271,272], while IAA-aa hydrolysis occurs in the ER[279-282], with no IAA-aa transporters found thus far. Furthermore, transport of IAA into the ER is associated with increased conjugation[195,271], hypothesised to be due to ER-nuclear migration of auxin increasing auxin signalling which promotes conjugation[283]. Further work on the subcellular compartmentalisation of auxin and its conjugates is therefore required to understand these features of auxin.

Larger molecular weight amide-linked IAAs were found in seeds of *Phaseolus vulgaris*[284,285], with similar results seen in *Arabidopsis*[286] suggesting a role for these different larger protein-IAA conjugates in seed IAA storage. Activation of IAA in germination in *Arabidopsis* is hypothesised to involve hydrolysis of IAA-aa[287]. IAA-aa hydrolase enzymes were expressed during in the first 3 days after germination and triple mutants in those hydrolases led to reduced seed and early seedling IAA levels indicating a role of IAA-aa hydrolysis in seed storage and germination[287].

The major ester linked IAA conjugate observed in *Arabidopsis* is IAA-glucose (IAA-Glc). This conjugation to glucose occurs through the activity of a UDP-glucosyltransferase (UGT), AtUGT84B1[288] with lower activity levels also noted for AtUGT84B2, AtUGT75B1, AtUGT75B2, AtUGT74D1, AtUGT76F1 and a group of auxin-induced AtUGT76E enzymes[288-293]. This glucosylation of IAA is reversible in rice[294] and maize[295], and although the hydrolysis step has not been demonstrated in *Arabidopsis*, it is suspected[296]. In addition to glucosylation of IAA, glucosylation of IPA and oxIAA has been shown to take place through these same glucosylation enzymes as they show activity across a broad range of substrates[288-290,293,297]. These different enzymes show different expression profiles, substrate specificity and phenotypes in mutants illustrating that these enzymes do not function redundantly, although compensatory upregulation in single *Atugt* mutants is observed[290].

Glycosylation of IAA to form IAA-*myo*-inositol takes place in *Zea mays*[298,299]. Interestingly, *Arabidopsis* mutants with low *myo*-inositol concentrations show embryo developmental defects that are made more severe by overexpression of *AtUGT84B1*, implying that IAA is stored as IAA-*myo*-inositol and its hydrolysis to IAA is important in early development[300].

Methylated IAA is formed through IAA CARBOXYMETHYLTRANSFERASE 1 (IAMT1)[301] and this process is reversed via esterases including AtMES17[302]. The importance of this storage of IAA as methylated IAA has so far only been demonstrated in hypocotyl gravitropism where *Atiamt1* mutants exhibit altered PIN distribution and so gravitropic reponse[303].

Oxidation is the main pathway by which IAA is catabolised at physiological auxin levels[304]. DIOXYGENASE FOR AUXIN OXIDATION enzymes (AtDAO1/2)[304-306] catalyse the oxidation of IAA to oxIAA, which can then become glucosylated to oxIAA-Glc mostly through the action of AtUGT74D1[297]. A summary of these auxin related metabolic pathways is shown in **Figure 1.4**.

Metabolism, transport and signalling of auxin is then tightly controlled by many factors including auxin itself.

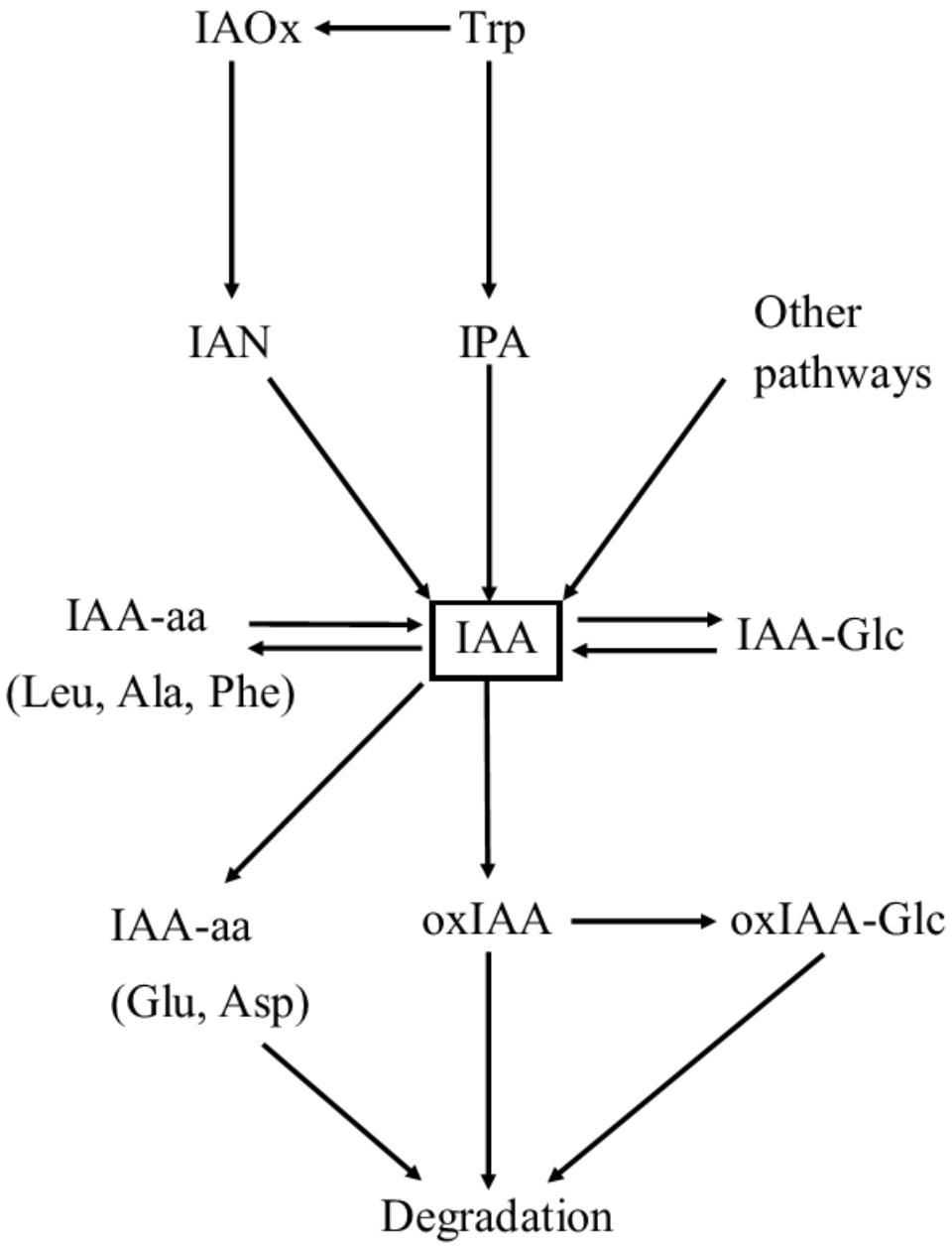

Figure 1.4 Auxin synthesis, conjugation and degradation pathways. Other pathways for IAA synthesis include from methylated IAA, the Trp-independent pathway via indole and that from IBA. For details of metabolic conversions see text.

1.3.5 Auxin-induced changes in auxin signalling, metabolism and transport

Auxin induces both transcriptional and non-transcriptional changes to regulate developmental output in addition to regulating its own levels. Meta-analysis of separate transcript profiling experiments for gene regulation changes under different auxin treatments[283] has shown increases in expression of many but not all *AtAUX/IAA* genes, along with some *AtGH3* and *AtPIN* genes. Increased expression of *AUX/IAA* genes[283] provides a negative feedback to inhibit auxin responsive gene expression[226-228].

Metabolic changes also show a negative feedback loop in auxin induction. Increased auxin level leads to a decrease of expression of *AtYUCCA* genes, thus reducing IAA synthesis through the TAA-YUCCA pathways[307,308]. Expression of *AtCYP79B2 AtCYP79B3* as well as *AtSUR1* and *AtSUR2* genes involved in IAOx utilisation in glucosinolate synthesis is also decreased by exogenous auxin together reducing IAA synthesis through the IAOx pathway[283].

Auxin levels also can alter the rate of auxin conjugation and oxidation through a different negative feedback loop. This feedback mechanism within IAA conjugation and oxidation is hypothesised to operate through the auxin mediated induction of *AtGH3*[283] and *AtDAO1* genes[304] which are coregulated with genes for auxin glucosylation[290]. Disruption of IAA oxidation in *Atdao1* mutants leads to increased *AtGH3* induction resulting in dramatically increased IAA-Glu and IAA-Asp levels whilst IAA itself remains at wildtype levels[309]. Additionally, overexpression of *AtUGT84B1* led to increased IAA-Glc with reduction in IAA-aas[288]. This overexpression of *AtUGT84B1* also led to increased IAA levels suggesting compensatory mechanisms to control IAA levels are not fully complementary. On the opposite side of this feedback loop, disruption of activation of IBA, methylated IAA and IAA-aas leads to increases in IAA synthesis through *TAA/YUCCA* gene induction[310]. Overall IAA metabolism appears to be regulated through a series of complex negative feedback loops with many partially redundant pools of inactive auxin compounds.

The expression of certain *PIN* genes (particularly *AtPIN1*, *AtPIN3* and *AtPIN7*) can be induced by exogenous auxin treatment[283,311], with change of activity of one PIN influencing the expression and localisation of another PIN in an auxin-dependant manner[311]. These auxin-dependant PIN changes have been demonstrated in the root, in vasculature formation, in the stem wounding response and in lateral root formation[312]. Auxin-induced changes in auxin transport had been theorised previously[313-315] and lead to the creation and narrowing of auxin transport pathways in a process referred to as canalization. Both intracellular[311,316] and extracellular auxin sensing[238] is required for this canalisation response, involving changing activity of *AtWRKY23*[317] and receptor kinases CANALIZATION-RELATED AUXIN-REGULATED MALECTIN-TYPE RECEPTOR-LIKE KINASE (AtCAMEL) and CANALIZATION-RELATED RECEPTOR-LIKE KINASE (AtCANAR)[318]. The mechanistic link between these components and altered PIN distribution is currently unknown, but probably involves regulation of cytoskeletal components[319]. How all these auxin related components work together to regulate parts of a developmental response to different conditions such as altered Zn nutrition is only recently becoming elucidated.

1.4 Auxin and Zn interactions

Currently the intersection of auxin action with Zn status is not well understood. Under Zn deficiency in *Solanum lycopersicum*, IAA levels were decreased and IAA inactivation rates were increased relative to controls[320]. In addition, in *Glycine max* and *Zea mays* Zn deficiency is correlated with a change in expression of auxin signalling related genes[321,322], although how this relates to wider auxin activity and development remains to be determined. Early experiments have also determined that biosynthesis of Trp requires Zn[323], but the *in vivo* relevance of this Zn dependency is unknown.

Comparatively more is known about the interaction of auxin and Zn excess. Transient Zn excess has been shown in *Arabidopsis* to increase IAA levels through *AtYUCCA* gene induction[324], but *AtYUCCA* gene expression and IAA levels are

both reduced after continual Zn excess[325]. It is suggested that auxin transport also has a role in the Zn excess response with inhibition of auxin transporters causing hypersensitivity to Zn excess[325], and *AtPIN4* expression was shown to be down regulated after transient Zn excess[324]. A reduction of the division rates in the meristem[324] was detected after transient Zn excess with this feature showing consistency with previous work investigating the effect of continual Zn excess in *Festuca rubra*[326] and *Arabidopsis*[325,327], suggesting a reliable auxin-related feature of Zn excess is reduced root length and meristem size. Transient exposure to Zn levels up to 200 µM was also shown to increase LR formation whereas Zn concentrations above this point were inhibitory to LR formation[324]. Continuous exposure to high levels of Zn however was shown to be inhibitory to LR formation[325].

The molecular underpinnings of these responses remain unknown, and in some cases may relate to a general nutrient stress response rather than a Zn specific response. One of the hypothesised molecular links between auxin homeostasis and Zn is through IAA-aa hydrolysis.

1.4.1 Control of auxin conjugate hydrolysis

In *Arabidopsis* IAA-aa hydrolysis to IAA is governed by four of a seven-member Ilr1-like amidohydrolase family[281]. Enzymes shown to have IAA-aa hydrolysis activity include IAA-LEUCINE RESISTANT 1 (ILR1)[279], ILR-LIKE 1 (ILL1), ILL2 and IAA-ALANINE RESISTANT 3 (IAR3)[280] which show differing substrate specificity including some redundancy but all show enhanced *in vitro* activity with increased Mn and Co and are repressed by Zn, Ca and Mg ions[281]. Zn however was the strongest inhibitor of Ilr1-like amidohydrolases tested and no Ca or Mg transporters have been identified in screens for genes that regulate sensitivity to IAA-aas. This together indicates Zn is the most physiologically relevant metal ion that regulates the Ilr1-like amidohydrolase family and so will be examined further in this study.

The activity of the enzymes has also been tested *in vivo*, through use of an auxin sensor, and it has been determined that IAA-Phe is preferentially hydrolysed by AtILR1 and AtILL2, IAA-Leu by AtILR1 and to a lesser extent AtILL2 and AtIAR3, and IAA-Ala hydrolysed preferentially by AtIAR3 and to a lesser extent AtILL2 and AtILR1[282]. The IAA-aa hydrolysing enzymes were all determined to be localised to the ER through bioinformatic, proteomic and GFP-tagging experiments[279-282]. To identify genes responsible for controlling auxin conjugation, screening conditions were established with high concentrations of auxin conjugates to find mutants that did not show the characteristic root or hypocotyl shortening elicited by high concentrations of IAA-aa conjugates[279,328].

Isolation of mutants insensitive to certain IAA-aa conjugates further emphasised a potential link between auxin conjugation and metal homeostasis. Firstly, *Atilr2* mutants, specifically resistant to IAA-Leu and IAA-Phe but not IAA-Ala, show reduced lateral root number similar to *Atiar1 Atilr2* and *Atiar3 ilr2* double mutants, but in addition showed resistance to low and high Mn induced changes to root length[329]. Furthermore, microsomal vesicles from *Atilr2* plants showed increased ATPase-dependant Mn transport activity into vesicles without changes in whole plant metal content. Sequence analysis of AtILR2 protein shows no transmembrane domains and high similarity (54% amino acid identity) to *Arabidopsis halleri partitivirus 1*[330,331]. Although currently unclear, it is hypothesised that activation of the Mn transport system would sequester Mn away from IAA-aa hydrolases and thus lead to reduced hydrolytic rates. It is interesting that *Atilr2* remains sensitive to IAA-Ala which is hydrolysed preferentially by AtIAR3[282] *in vivo* and may point to differing metal requirements or affinities of the IAA-aa hydrolases.

A further *Atilr* mutant was found to be connected with metal homeostasis, in this case *Atilr3*. Interestingly, *AtILR3* is involved in upregulating the Fe deficiency response[150], but additionally functions to suppress the Fe excess response in conjunction with AtPYE[149,154,155]. Gain of function *Atilr3* mutants showed slightly increased resistance to IAA-Leu in addition to insensitivity to excess Mn, whilst loss-of-function *Atilr3* mutants show enhanced sensitivity to IAA-Leu[332]. Although the influence of Fe on *in vitro* IAA-aa hydrolase activity was not assayed[281], it could be hypothesised that increasing Fe availability relative to Mn availability reduces hydrolytic rates. However, further work is required on Fe subcellular

homeostasis in the ER to understand this, particularly because AtILR3 regulates a vast array of genes. Therefore, together the *Atilr2* and *Atilr3* mutants illustrate that activities of IAA-aa hydrolases are influenced *in vivo* by metal homeostasis disruptions.

In a screen for mutants insensitive to IAA-Ala or enhancers of IAA-Leu or Phe insensitivity in *Atilr1* mutants, the *IAA-Ala resistance1* (*AtIAR1*) gene was found[328]. Seven mutants were generated with five in a Ws background and two in a Col-0 background with a range of phenotypic severity. In the Col-0 background *Atiar1-3* and *Atiar1-4* were generated showing a frame shift near the 3' end of the coding sequence and a 65-80 kbp deletion of the *AtIAR1* coding region and a neighbouring gene respectively. The *Atiar1* mutants were all shown to be less sensitive to all IAA-aa conjugates tested including IAA-Ala, IAA-Leu and IAA-Phe among others, although weaker mutants such as *Atiar1-3* were less resistant to IAA-Leu. High auxin *Atsuperroot1* plants[333,334] had their high auxin phenotype of reduced root growth after 10 days partially suppressed in *Atsuperroot1 Atiar1* double mutants suggesting *Atiar1* mutants were low in auxin.

Evidence available at that time and since has indicated a role in ion homeostasis in the phenotypes of *Atiar1* mutants. Increasing the Mn content of the media gradually suppressed this IAA-aa insensitivity in *Atiar1-1* and *Atiar1-2* plants[328]. *AtIAR1* was identified as a ZIP transporter with expression of its mouse homologue *MmKE4* (*MmZIP7*) complementing the *Atiar1* phenotype, suggesting that the phenotype was metal-transport related. Further work has shown that MmZIP7 functions as a Golgi-localised Zn transporter in mice[335], and also complements the yeast strains lacking the *AtIAR1* homologue (*yke4*Δ), which is hypothesised to conduct bidirectional transport of Zn on the ER membrane[336].

In addition, the *Atiar1* phenotype was partially compensated by additional mutations in *AtMTP5*[1]. These mutants showed defective or absent transcripts of the full length *AtMTP5* splice variant (referred to as *AtMTP5A*). Single *Atmtp5-2* mutants with no detectable full-length transcript showed similar IAA conjugate sensitivity to wildtype, although *Atmtp5-1* mutants with altered splice positioning showed increased sensitivity to IAA conjugates compared with wildtype. These *Atmtp5-1* splice mutants were crossed with *Atiar3* and *Atilr1* mutants and did not

complement their respective IAA-Ala and IAA-Leu insensitivities, although the *Atiar3 Atmtp5* double mutant now showed enhanced sensitivity to IAA-Leu compared to wildtype. As AtMTP5 at the time was predicted to be a Zn cytoplasmic exporter similar to AtMTP1, the following model was established for the antagonistic transport of inhibitory metals by AtIAR1 and AtMTP5 in the ER as shown below in **Figure 1.5.**

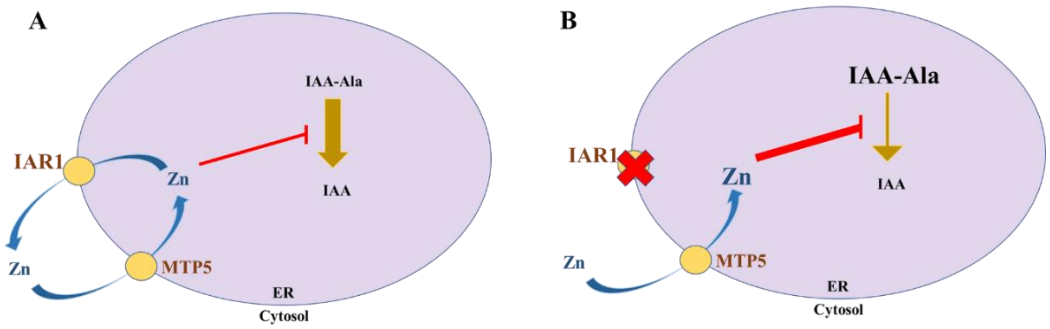

Figure 1.5 Adapted Rampey et al, 2013[1] model on metal transport in the ER and IAA-Ala hydrolysis in wildtype and *Atiar1* mutant plants. (A) *AtMTP5* and *AtIAR1* antagonistically control levels of metals including Zn in the ER which then controls the activity of IAA-Ala hydrolases. (B) *Atiar1* mutants lose Zn transport activity, causing ER Zn levels to increase which inhibits IAA-Ala hydrolases. Model adapted with permission to focus on Zn as the inhibitory cation.

Although IAA-aa hydrolases have been determined to be localised to the ER through bioinformatic, proteomic and GFP-tagging experiments[279-282], *AtMTP5A* was found to encode a *cis*-Golgi localised protein that interacts with AtMTP12 to facilitate transport of Zn into the Golgi[89]. Neither expression of AtMTP12 or AtMTP5A alone was seen to complement yeast transporter mutants, indicating neither of these proteins alone shows Zn import activity. This could suggest that the *Atmtp5* compensatory mutations observed is mediated through disrupting of the AtMTP5-AtMTP12 Golgi-located Zn transporting complex rather than AtMTP5 transport activity alone in the ER.

1.5 Aims of the thesis

With the complexities of auxin and Zn homeostasis in mind, this thesis aims to investigate the Zn-auxin interaction mediated through Zn transporters in the secretory system. These aims will be addressed through chapters focussing on different aspects of the ER/Golgi focussed Zn-auxin interaction as shown below.

- How is Zn transport into the ER through AtMTP2 transcriptionally controlled?
- What is the transport activity, localisation, and expression pattern of *AtIAR1*?
- What are the effects of *Atiar1* mutations on wider Zn homeostasis?
- What are the effects of *Atiar1* mutations on wider auxin homeostasis?

Through answering these questions, this thesis will further understanding of auxin conjugate utilisation and ER/Golgi Zn homeostasis in different Zn conditions.

Chapter 2: Materials and Methods

2.1 *Saccharomyces cerevisiae* growth, transformation, and phenotyping

2.1.1 *Saccharomyces cerevisiae* strains

AtIAR1 (*Arabidopsis thaliana* IAA-Ala resistant 1) functionality including transport capabilities was assessed by transforming *AtIAR1*-based constructs into *Saccharomyces cerevisiae* transporter mutants using BY4741 and DY1457 strains as controls where relevant. Details of these mutants are shown in **Table 2.1**

Strain	Description	Genotype	Source
BY4741	Background for *yke4*Δ and *smf1*Δ	*MATa*; *his3*Δ1; *leu2*Δ0; *met15*Δ0; *ura3*Δ0	Podar et al.[337]
*yke4*Δ	*AtIAR1* yeast homologue mutant	BY4741; *MATa*; *his3*Δ1; *leu2*Δ0; *met15*Δ0; *ura3*Δ0; *YIL023c*::*kanMX4*	Euroscarf
*smf1*Δ	Mn import mutant	BY4741; *MATa*; *his3*Δ1; *leu2*Δ0; *met15*Δ0; *ura3*Δ0; *YOL122c*::*kanMX4*	Euroscarf
DY1457	Background for *zrt1*Δ *zrt2*Δ and *fet3*Δ *fet4*Δ	DY1457; *MATa*; *ade1*/+; *can1*; *his3*; *leu2*; *trp1*; *ura3*	Evens et al.[338]
*zrt1*Δ *zrt2*Δ	Zn import mutant	DY1457; *MATa*; *ade1*/+; *can1*; *his3*; *leu2*; *trp1*; *ura3*; *zrt1*::*LEU2*,	Evens et al.[338]

		zrt2::*HIS3*	
*fet3*Δ *fet4*Δ	Fe import mutant	DY1457; *MATa*; *ade1*/+; *can1*; *his3*; *leu2*; *trp1*; *ura3*; *fet3-2*::*HIS3*, *fet3-1*::*LEU2*	Evens et al.[338]

Table 2.1 List of *Saccharomyces cerevisiae* strains used in this study

2.1.2 Constructs for *Saccharomyces cerevisiae* expression

To assess the function of AtIAR1, constructs for heterologous expression of *AtIAR1* in *Saccharomyces cerevisiae* were assembled into a pYES2 (lab stock) vector, allowing for selection in bacterial and yeast hosts with ampicillin resistance and uracil autotrophy respectively. Constructs were synthesised (Integrated DNA Technologies) to represent codon-optimised *AtIAR1* cDNA from *Arabidopsis thaliana* Col-0 ecotype as well as for the *Atiar1-3* mutant identified in Lasswell et al.[328]. For each of these constructs, the signal peptide (SP) sequence was either kept as *AtIAR1* or swapped with that of *AtIRT1*, using the signal peptide cleavage site for AtIAR1 predicted by SignalP-5.0[339]. This method had previously been utilised to traffic the endoplasmic reticulum (ER) bound transporter AtZTP29, a member of the ZIP (Zinc-regulated transporters, Iron-regulated transporter-like Proteins) family to the plasma membrane for similar *Saccharomyces cerevisiae* complementation studies[80]. Detailed diagrams of these plasmids are shown as plasmid maps in **Figure 2.1.**

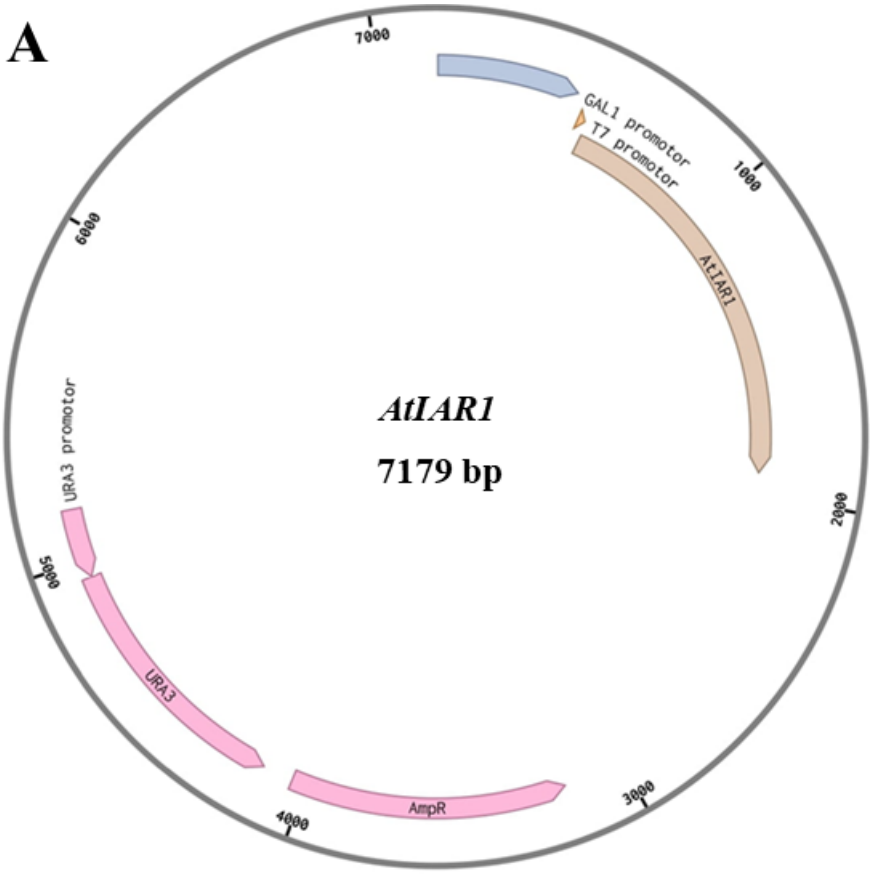
A
7000
1000
2000
3000
4000
5000
6000
GAL1 promotor
T7 promotor
AtIAR1
URA3 promotor
URA3
AmpR
AtIAR1
7179 bp

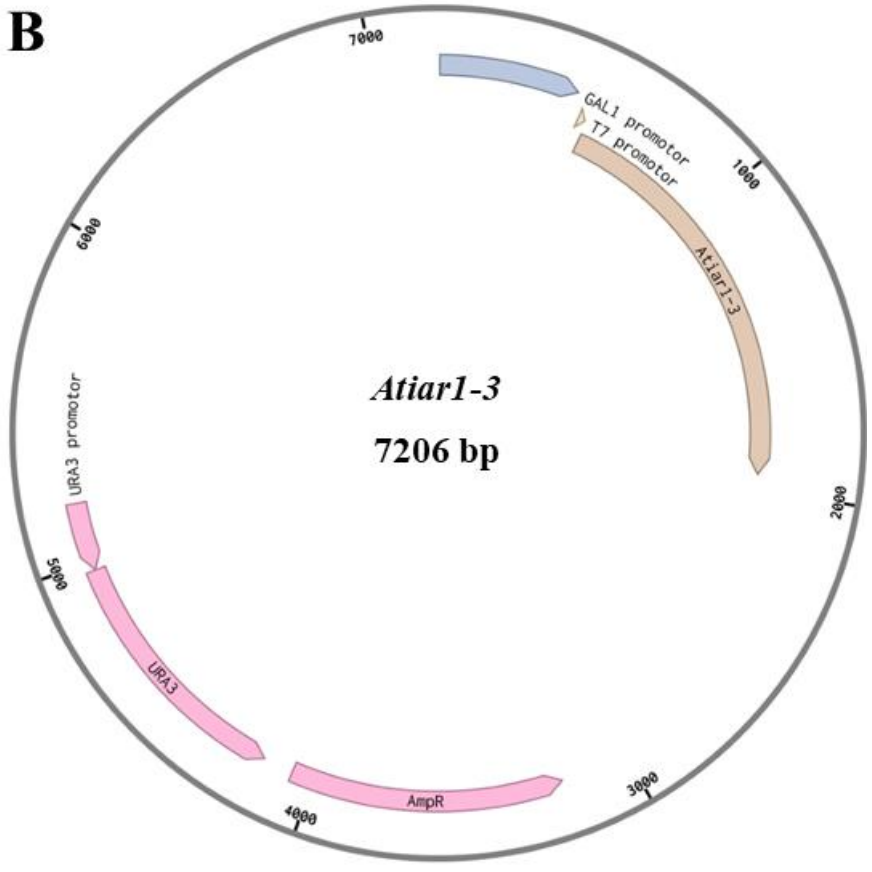
B
7000
1000
2000
3000
4000
5000
6000
GAL1 promotor
T7 promotor
Atiar1-3
URA3 promotor
URA3
AmpR
Atiar1-3
7206 bp

C

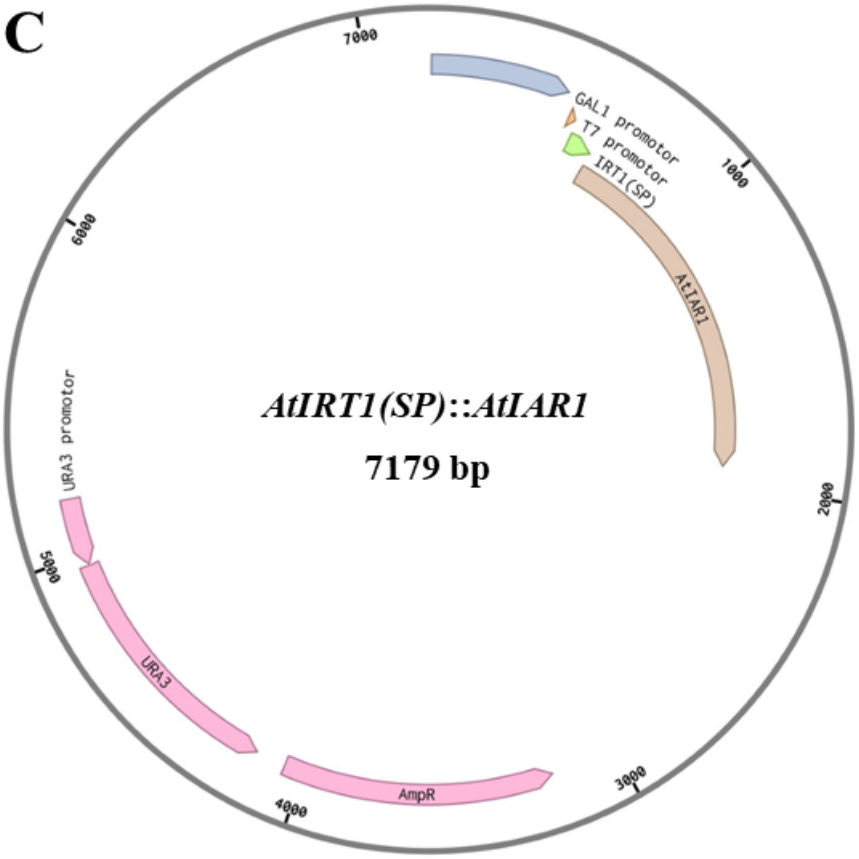
7000
1000
2000
3000
4000
5000
6000
GAL1 promotor
T7 promotor
IRT1(SP)
AtIAR1
URA3 promotor
URA3
AmpR
AtIRT1(SP)::AtIAR1
7179 bp

D

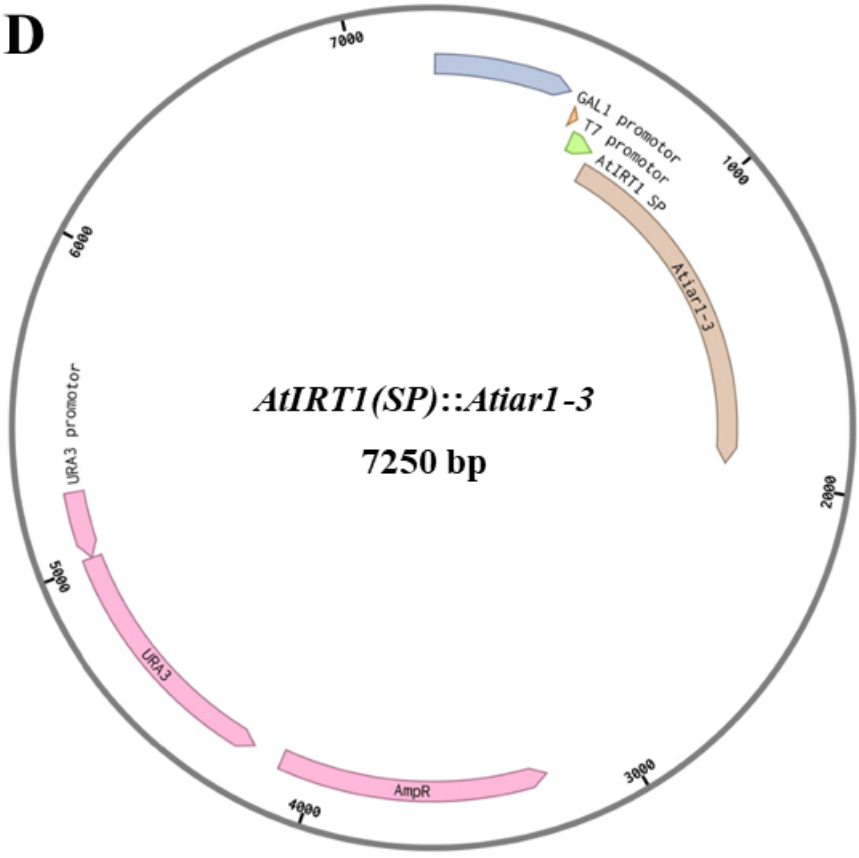
7000
1000
2000
3000
4000
5000
6000
GAL1 promotor
T7 promotor
AtIRT1 SP
Atiar1-3
URA3 promotor
URA3
AmpR
AtIRT1(SP)::Atiar1-3
7250 bp

Figure 2.1 Plasmid maps of different *AtIAR1* constructs for *Saccharomyces cerevisiae* transformation. (A) *AtIAR1* – for expression of *AtIAR1* gene with no adjustments. (B) *Atiar1-3*– for expression of *AtIAR1* gene with changes caused in the *Atiar1-3* mutation from Lasswell et al.[328]. (C) *AtIRT1(SP)*::*AtIAR1* – for expression of *AtIAR1* with the signal peptide (SP) sequence swapped for that of *AtIRT1*. (D) *AtIRT1(SP)*::*Atiar1-3* – for expression of *AtIAR1* with the signal peptide (SP) sequence swapped for that of *AtIRT1* with changes caused in the *Atiar1-3* mutation. URA3 – uracil autotrophy, AmpR – ampicillin resistance, GAL1 promotor – galactose mediated expression in yeast, T7 promotor – strong promotor for expression.

2.1.3 *Saccharomyces cerevisiae* media

Growth of non-transformed *Saccharomyces cerevisiae* strains was conducted in YPAD media with or without agar. YPAD media consisted of 1% (w/v) yeast extract (Millipore, 70161), 2% (w/v) peptone (Formedium, PEP02), 2% glucose (Fisher Scientific, G/0500/53), 0.002% (w/v) Adenine (Sigma-Aldrich, A2786) and 2% (w/v) agar (Formedium, AGA03) if required.

Once transformed with recombinant plasmids, transformed *Saccharomyces cerevisiae* gained uracil autotrophy and were grown on synthetic complete media lacking uracil (SC-U). In addition, expression of the *AtIAR1* based construct was controlled by glucose or galactose addition. Unless otherwise stated SC-U was made using glucose to repress expression of the *AtIAR1* based construct. SC-U media consisted of 0.69% (w/v) yeast nitrogen base (Formedium, CYN0405), 2% (w/v) glucose or galactose (Formedium, GAL03), 0.19% (w/v) Kaiser mixture synthetic complete uracil drop-out (Formedium, DSCK102) and 2% (w/v) agar if required. Due to slow growth, for *fet3*Δ *fet4*Δ transformants the pH of SC-U liquid and solid media was set to 4.5, whilst all other strains were grown at pH 5.3.

2.1.4 *Saccharomyces cerevisiae* growth conditions and transformation

Non-transformed *Saccharomyces cerevisiae* strains were streaked onto solid YPAD plates at 28°C for 2-4 days until individual colonies were visible. These strains were then transformed using the lithium acetate method[340]. In this method individual colonies were picked and grown in 50 ml YPAD media for 12-20 hours at 30°C and 210 rpm until the optical density at 600 nm (OD600) reached between 1 and 2. After diluting these cultures in YPAD to OD600 of 0.3 they were then returned to 30°C, shaking at 210 rpm until the OD600 reached 1.

The cells were then harvested by centrifugation at 3000 x *g* for 5 minutes and resuspended in distilled water (dH2O). The centrifugation and dH_2O resuspension steps were repeated to remove all YPAD media. After a final centrifugation step the cells were then resuspended in a solution of 10 mM lithium acetate (Sigma-Aldrich, 517992), 1 mM ethylenediaminetetraacetic acid (EDTA, Sigma-Aldrich, E9884) and 10 mM tris(hydroxymethyl)aminomethane (Tris, Melford Biolaboratories Ltd T60040) pH 7.6 for transformation.

Resuspended cells were then vortexed with single stranded salmon sperm DNA (D9156, Invitrogen), plasmid DNA, and a solution of 40% (w/v) polyethylene glycol 3350 (Sigma-Aldrich, P4338), 10 mM lithium acetate, 1 mM EDTA and 10 mM Tris pH 7.6. The vortexed mixture was then incubated at 30°C for 30 minutes before being transferred to a 42°C water bath for 15 minutes to allow heat shock mediated transformation. Transformed cells were then grown on SC-U selective plates for 2-4 days at 30°C, with colonies replated and confirmed by PCR.

2.1.5 *Saccharomyces cerevisiae* drop assay

To assay complementation of mutant strains on restrictive media, a drop assay was performed with the transformed *Saccharomyces cerevisiae* strains. Individual colonies of the transformed *Saccharomyces cerevisiae* were grown in 10 mL liquid

SC-U overnight at 30°C, shaking at 210 rpm. These cultures were pelleted by centrifugation at 1,500 x *g* for 10 minutes at room temperature, with the supernatant discarded and the pellet resuspended in dH_2O. After repeating the centrifugation step and discarding the supernatant, the pellet was then resuspended in dH_2O to an OD600 of 1.0. 10 µL of this diluted culture and serial dilutions up until 10^5 were then pipetted onto SC-U agar plates containing 2% (w/v) galactose to induce expression of the *AtIAR1*-based construct.

Restrictive media for transformants were based on those from previous publications [68,336,337] with some minor alterations. The *yke4*Δ strain was sensitive to cell wall binding cell wall disruption so was complementation was assayed in media with 20 µg/ml calcofluor white and 10 µg/ml evans blue dye (Sigma-Aldrich, 18909). The *smf1*Δ strain was sensitive to Mn deficiency and so complementation was assayed in media with 20 mM ethylene glycol-bis(β-aminoethyl ether)-N,N,N′,N′-tetraacetic acid (EGTA, Millipore, 324626) and 50 mM 2-ethanesulfonic acid (MES, Sigma-Aldrich, M8250) at pH 5.5. The *zrt1*Δ *zrt2*Δ strain was sensitive to Zn deficiency and so complementation was assayed in media with 500 µM $ZnSO_4$ (Sigma-Aldrich, Z1001) and 1 mM EDTA. The *fet3*Δ *fet4*Δ strain was sensitive to Fe deficiency and so complementation was assayed in media with 25 µM bathophenanthroline disulphonate (BPDS, Sigma-Aldrich, 146617) and 20 mM MES.

2.2 *Arabidopsis* growth and transformation

2.2.1 Plant materials

To assess the impact of loss of AtIAR1 activity in *Arabidopsis thaliana*, two different mutant lines were sourced. The *Atiar1-3* mutant was obtained from Lasswell et al.[328]. This mutant was generated through neutron–mutagenized Columbia (Col-0) seeds and contains a frame shift mutation resulting in a change in C-terminal (Ct) residues. The second mutant was a T-DNA insertion mutant[341] (SALK_ 047876C, obtained through the Nottingham Arabidopsis Stock Centre), in a Col-0 background, hereafter referred to as *Atiar1-t*. *Atiar1-t* plants are homozygous for a T-DNA insertion within the coding region corresponding to one of the central metal transporting helices in AtIAR1. The position of mutations for the AtIAR1 mutants is shown below in **Figure 2.2**. *Arabidopsis thaliana* Col-0 ecotype was therefore used as a wildtype (WT) reference for both these mutants.

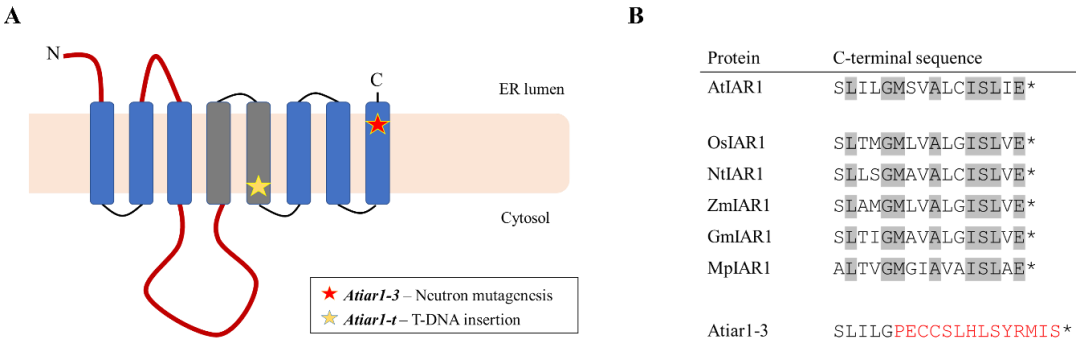

Figure 2.2 *Atiar1* mutants used in this study. (A) Schematic of AtIAR1 topology with the yellow and red asterisks representing the amino acid positions corresponding to the site of T-DNA insertion or neutron mutagenesis in *Atiar1-t* and *Atiar1-3* plants respectively. Transmembrane helices containing conserved transport-associated residues are in grey and histidine rich loops shown in red. (B) Amino acid sequences at the C-terminus in AtIAR1, AtIAR1 plant homologues and

Atiar1-3. Asterisks indicate STOP codons while the sequences in red are those altered through a frame shift mutation in the *Atiar1-3* gene. Residues highlighted in grey are those showing 100% conservation in the sample of plant AtIAR1 homologues shown (*Oryza sativa*, *Nicotiana tabacum*, *Zea mays*, *Glycine max* and *Marchantia polymorpha*).

Genotyping of the *Atiar1-3* plants were conducted as described in Lasswell et al.[328] whilst genotyping of the *Atiar1-t* plants were conducted using left border primer GTCTCTTGCGTGAATGAGAGG, right border primer CATTTCTGCAAGAACTCCAGC and T-DNA border primer ATTTTGCCGATTTCGGAAC.

2.2.2 Generating constructs for *Arabidopsis* transformation

2.2.2.1 DNA extraction using the CTAB methodology

For cloning of *AtIAR1*, genomic DNA was extracted from *Arabidopsis thaliana* Col-0 ecotype leaves using the Hexadecyltrimethylammonium bromide (CTAB) methodology[342]. Briefly, 200 mg leaf tissue was snap frozen and homogenized by 3 mm tungsten carbide beads (QIAGEN, 69997) using the TissueLyser LT homogeniser (85600, QIAGEN). Homogenised tissue was then vortexed with CTAB buffer containing 2% (w/v) CTAB (Sigma-Aldrich, H5882), 20 mM EDTA, 2.5 M NaCl (Sigma-Aldrich, S7653) and 0.1 M Tris. After incubation at 55°C for 15 minutes, the suspension was pelleted by centrifugation at 10,000 x *g* for 5 minutes. The resulting supernatant was extracted and added to 250 µL 24:1 chloroform:isoamyl alcohol (Sigma-Aldrich, C0549) to undergo liquid-liquid extraction (LLE) via inversion and centrifugation at 15,800 x *g* for 1 minute. The upper aqueous phase was extracted and then subject to another LLE step before 500 µL ethanol (Sigma-Aldrich, 51976) kept on ice and 50 µL 7.5 M ammonium acetate (Sigma-Aldrich, A1542) was added to precipitate the DNA. This mixture was then inverted several times and stored at -20°C for at least 2 hours before pelleting the DNA by centrifugation at 15,800 x *g* for 1 minute. The DNA pellet

was washed by removing the supernatant, adding 70% (v/v) ethanol kept on ice to the pellet and centrifuging again. After a further wash step with 70% (v/v) ethanol the pellet was air-dried for 15 minutes before resuspending the DNA in dH_2O and its quality assessed by spectrophotometry using a NanoDrop™ 2000 spectrophotometer (ND-2000, ThermoFisher Scientific).

2.2.2.2 Cloning fragments and golden gate cloning of *AtMTP2*::*LUC* plasmid

To investigate the control of *AtMTP2* expression a recombinant plasmid (*AtMTP2*::*LUC*) was generated, with luciferase expression controlled with the native *AtMTP2* promotor and terminator. Genomic DNA was extracted as in **2.2.2.1** and was used as a template for polymerase chain reaction (PCR) to amplify *AtMTP2* promotor and terminator sequences in several parts of the genome using primers with overhangs that would be compatible with golden gate cloning[343]. The primers used are shown below in **Table 2.2** and cause changes in single base pairs to accommodate the BsaI/BbsI-based cloning used in golden gate cloning. In addition to these PCR-amplified parts, due to the positioning of BbsI and BsaI sites, a section of *AtMPT2* (part 4, **Table 2.3**) was synthesised (Integrated DNA Technologies). These changes are referred to as domestication and are shown in **Table 2.4**.

Primer name	Sequence
AtMTP2 domestication part 1 FOR	GATGAAGACATCTCAGGAGGCTAAACTTCACTGAATGGAACTACATAATG
AtMTP2 domestication part 1 REV	GATGAAGACATCTCGCCACGTGTCATCCTCTTCCTCCG
AtMTP2 domestication part 2 FOR	GATGAAGACATCTCAGTGGACGAGCCGCCGC
AtMTP2 domestication part 2 REV	GATGAAGACATCTCGCATTTGCAGCAAAAAAGATTGTAACTTTAGAGCATGAATC
AtMTP2 domestication part 3 FOR	GATGAAGACATCTCATTCGTAAAACAACAAAAGGGTTCATTTCTCTGG
AtMTP2 domestication part 3 REV	GATGAAGACATCTCGTAGAAACCTTATCAACACATCAAAACTCCAAAG
AtMTP2 domestication part 5 FOR	GATGAAGACATCTCACGGATATGAAGTTACCCGTTTGGATTG
AtMTP2 domestication part 5 REV	GATGAAGACATCTCGAGCGTTCACTTTGCAGCATCTGTAGAAATGG

Table 2.2 Primers used to amplify *AtMTP2* parts for golden gate assembly. Red sequences denote overhang with BbsI recognition and cleavage site. Purple sequences denote the overhangs left after BsaI digestion from a pUAP1 backbone for level 1 assembly. Source: T.Gate

Part name	Sequence
AtMTP2 part 4	GATGAAGACATCTCATCTAAGGT CTTGGTTAACCAATAACCATGCA AAGCACGAATGTTTTGTTTCTTT GCTCAAATTTTGTGTGACCGGAC GAGATGTCTTCTTG

Table 2.3 Synthesised *AtMPT2* part 4. Red sequences denote overhang with BbsI recognition and cleavage site. Purple sequences denote the overhangs left after BsaI digestion from a pUAP1 backbone for level 1 assembly. Designed by T.Gate.

Wildtype base	Domesticated base	Region (position)	Reason for change	Amino acid change
A	T	promotor (-1784)	BbsI site	N/A
C	G	terminator (1404)	BbsI site	N/A
A	T	terminator (1404)	BsaI site	N/A

Table 2.4 Domestication sites created during golden gate cloning of *AtMTP2*.

The product of amplification was then assembled into a level 0 pUAP1 plasmid containing LacZ gene (SynBio) to allow blue-white screening, and chloramphenicol resistance testing. The golden-gate assembly for a level 0 plasmid required 100 ng of pUAP1 acceptor plasmid, PCR amplified insert in 2:1 molar ratio to pUAP1, 10 units BbsI-HF (NEB, R3539), 1.5 µL T4 ligase buffer (NEB, B0202), 200 units T4 DNA ligase (NEB, M0202), 1.5 µL 10x bovine serum albumin (BSA) and dH2O to a reaction volume of 15 µL. This mixture was incubated for 20 seconds at 37°C, then 26 cycles of 3 minutes at 37°C followed by 4 minutes at 16°C, 5 minutes at

50°C, 5 minutes at 80°C to denature the restriction enzyme and then 5 minutes at 16°C for a final ligation step.

After the digestion-ligation golden gate reaction, 1 µL the reaction mixture was transformed into chemically competent *E.coli* strain DH5α (NEB, C2987) using a heat shock protocol. After incubating 100 ng of plasmid with 25 µL of competent cells on ice for 30 minutes, the mixture was placed in a water bath set to 42°C for 15 seconds. The mixture was then cooled on ice for a further 5 minutes before adding 600 µL super optimal broth medium (Sigma-Aldrich, S1797) and incubating at 37°C for 1 hour while shaking at 220 rpm. This resulting mixture was plated onto solid Luria broth (LB) plates containing Isopropyl β-D-1-thiogalactopyranoside (IPTG, Formedium, IPTG025S), 5-Bromo-4-chloro-3-indolyl β-D-galactopyranoside (X-Gal, Sigma-Aldrich, B4252) and chloramphenicol (Sigma-Aldrich, C0378) at a final concentration of 25 µg/mL. Successful white colonies were picked and grown overnight in liquid LB media containing chloramphenicol for extraction of the recombinant plasmids using a miniprep kit (QIAGEN, 27106), checked for insert length and then sent to be confirmed by sequencing (Genewiz).

After the sequence of the insert was verified, another digestion-ligation reaction was used with the donors being the pUAP1 *AtMTP2* plasmids and a luciferase donor plasmid (pICSL80001, SynBio) with the acceptor being a level 1 plasmid (pICSL86955OD, SynBio) with LacZ for blue-white screening, a kanamycin resistance gene and a nos:bar:nos cassette for L-Phosphinothricin selection once transformed into plants. The digestion ligation reaction was performed identically to a level 0 assembly except BsaI-HFv2 (NEB, R3733) was used as the restriction enzyme in place of BbsI-HF. After transformation into the chemically competent *E.coli* strain DH5α, the cells were plated onto LB agar plates containing IPTG, X-Gal and kanamycin (Sigma-Aldrich, K1377) at a final concentration of 50 µg/mL for a round of blue-white screening. Successful colonies were picked and the extracted plasmid, checked for insert length and then sent to be confirmed by sequencing (Genewiz). The final *AtMTP2*::*LUC* plasmid map is detailed below in **Figure 2.3.**

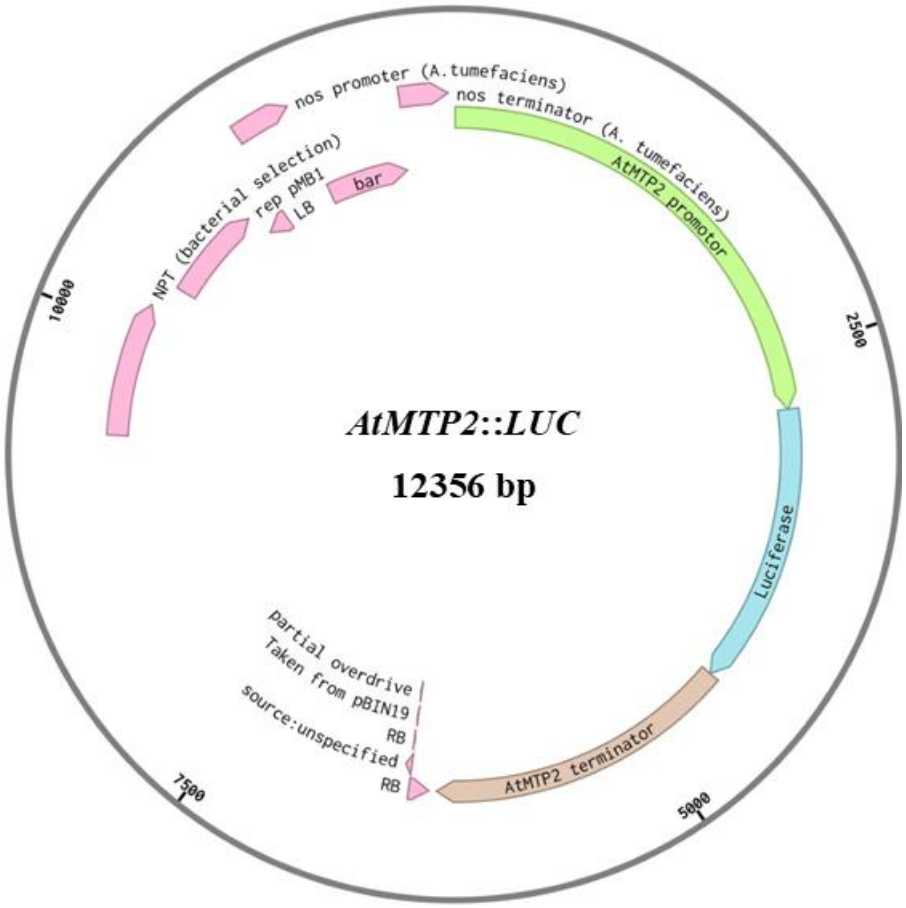

Figure 2.3 *AtMTP2*::*LUC* plasmid map for *Arabidopsis* transformation.
AtMTP2 native promotor (3 kb) and terminator (1 kb) control luciferase expression. NPT (Neomycin phosphotransferase II) generates kanamycin resistance and nos:bar:nos generates L-Phosphinothricin resistance. See text for further details.

2.2.2.3 Cloning fragments and golden gate cloning of *AtIAR1*::*GUS* and *GFP* plasmids

To investigate the control of *AtIAR1* expression, a recombinant plasmid (*AtIAR1*::*GUS*) was generated, with β-glucuronidase (*GUS*) expression controlled by the native *AtIAR1* promotor and terminator. To investigate subcellular localisation, recombinant plasmids were synthesised with *GFP* modules within the *AtIAR1* coding regions. In the cloning of Green fluorescent protein (GFP) tagged

membrane proteins, GFP presence can result in non-functional proteins due to misfolding or interruption of functional sites. To reduce the likelihood of interruption, monomeric enhanced GFP (mEGFP) were engineered to be cloned with surrounding loop regions (see **Table 2.5**) and then inserted separately into three areas. The GFP sites are the N-terminus (Nt) after a predicted signal peptide cleavage event, C-terminus (Ct) and in the intracellular loop 3 (ICL3) avoiding the putative metal binding sequences in other loop regions such as the first extracellular loop (ECL1) that proved successful with AtIRT1[123].

Part name	DNA Sequence	Amino acid sequence
Pre-mEGFP linker	GGCATAGGTCTCATA CTGGAAGTGCAGGCT CAGCTGCCGGGTCTG GTGGAAGTGCAGGC TCAGCTGCCGGGTCT GGTGGAGCCATTGA GACCATTGGC	GSAGSAAGSGGSAGS AAGSGGA
Post-mEGFP linker	CGGATAGGTCTCAAA TGGGAAGTGCAGGC TCAGCTGCCGGGTCT GGTGGAAGTGCAGG CTCAGCTGCCGGGTC TGGTGGAGCTTCGTG AGACCTTACCG	GSAGSAAGSGGSAGS AAGSGGAS

Table 2.5 Synthesised linker fragments and amino acid composition when translated in-frame. Red sequences denote overhang with the BbsI recognition and cleavage site. Purple sequences denote the overhangs remaining after BsaI digestion from a pUAP1 backbone for level 1 assembly. Source: T.Gate.

Genomic DNA was extracted as in **2.2.2.1** and was used as a template for PCR to amplify *AtIAR1* sequences in the genome using primers with overhangs that would be compatible with golden gate cloning[343]. Due to the number and positions of already existing BsaI and BbsI sites within *AtIAR1* it was necessary to create a *AtIAR1* fully domesticated level 1 plasmid which could then be used as a template for the level 0 parts required for the GUS and GFP plasmids. In addition, a synthesised fragment (Integrated DNA Technologies) was used. These first level 0 and level 1 assemblies were carried out as in **2.2.2.2** with primers, synthesised parts and resulting domestication sites shown in **Table 2.6**, **Figure 2.4** and **Table 2.7** respectively.

Primer name	Sequence
AtIAR1 domestication part 1 FOR	GATGAAGACATCTCAGGAGAAA GGATTCACTCGACTTGAC
AtIAR1 domestication part 1 REV	GATGAAGACATCTCGACAACAA GACTTTGTACAATGCTG
AtIAR1 domestication part 2 FOR	GATGAAGACATCTCATTGTATCT CTTACGGTATTCTGTGATG
AtIAR1 domestication part 2 REV	GATGAAGACATCTCGGTCATGAG AATGACTACACCC
AtIAR1 domestication part 4 FOR	GATGAAGACATCTCACTTCTTGT GGAGAAGTTGG
AtIAR1 domestication part 4 REV	GATGAAGACATCTCGAGTAAAG ACCTCTTGGGG
AtIAR1 domestication part 5 FOR	GATGAAGACATCTCATACTCTAT TTCCTAAACAAACCTAAAAATG
AtIAR1 domestication part 5 REV	GATGAAGACATCTCGAGCGATTT AAGAGCAACGATCCAGC

Table 2.6 Primers used to amplify *AtIAR1* parts for golden gate assembly. Red sequences denote overhang with BbsI recognition and cleavage site. Purple sequences denote the overhangs left after BsaI digestion from a pUAP1 backbone for level 1 assembly. Source: T.Gate.

GATGAAGACATCTCATGACCACGACCACGACCACGATCATGATCATCAT
GTGAAGAAAACGACGGCGAAGGTGGAGATGAAGTTGCCGGAGGAGCTT
GCTGAAGAGGAGGATATGAGATTATGTGGGTTTGGGCCTTGTCTCCATG
ATCACGATCACGAATCAAGTTCCACTCTTACGGGGTTTGGTAAATTTGG
TTCCTTTAGCTACATTCTTCATTGGGTTTTACAAATCATTACTTGATGATT
AGAATCTCTTCTTCTTGTTGGTTTTTGTAGCTCTGTGGCTTAATGCATTG
GGATGCTCTCTTTTAGTTAGCTTGGCCTCACTCATCTGCCTTGTTTTGCTT
CCCATTATGTTTGGTAAGCAATTTTTTGTATACCTATGAAAACCAAAAA
GCATTGCTTTTAATTGTCCTGGAGAAAATGCTCTCTTTCGTTTATTCATG
TGCTATAATGTGTTCATGAGAGTAACTGTTTCAAGTCTTATGTTGCAACT
AACAGTTCAAGGGAAGCCATCAAAATGGTTCGTTGATTCTTTGGCTCTC
TTTGGGGTAAGTCATTAGACTGACTACAGTAGCTTTTTCTTTGGCGGTGG
TGGTTCTGAATGCAAGAAAAATATTTTAGCAATATCTATACACTGTGTTT
CGTCGCAACTTTATCACTTGGATGAGTTGGAAATGTTAATAATATATGA
TCTGTTGATTCAGTTAATTTGTTTACCAGGCAGGAGCTATGTTGGGAGAT
GCTTTTCTTCACCAACTGCCCCATGCTTTTGGTACAGTAATGGACACAAG
TTTCTGATCTCTTTTTTAGTATCTGCATTGTTTCATAATTTGGCTTTTATG
CCTTCTCATTTTGTTTGCTTTTATATCTTCCTGAAGTGCAAAATATATTTA
TGGTTTGGCAGGTGGTGGCCACTCTCACTCTAATGATCACCATGAGAAC
CATGACCATCATGATCATTCTCATTCGGATTCGCCTTCACACTCACATTC
TATACAAGATTTGTCTGTTGGATTGTCTGTTCTTGGTAAGTATCATAACA
CTTCCTCTTGTGTTTATTGAACAAAATATTTTGACAGAATTGACACTTTC
AATCATCATTCTTAATTATCCAGCTGGGATTGTGGTGTTCCTTCCGAGAT
GTCTTCATC

Figure 2.4 Synthesised *AtIAR1* part 3. Red sequences denote overhang with the BbsI recognition and cleavage site. Purple sequences denote the overhangs remaining after BsaI digestion from a pUAP1 backbone for level 1 assembly. Source: T.Gate.

Wildtype base	Domesticated base	Region (position)	Reason for change	Amino acid change
C	G	Promotor (-1673)	BbsI site	N/A
G	A	Exon 1 (189)	BbsI site	none
T	C	Exon 1 (273)	BbsI site	none
C	G	Exon 7 (1263)	BbsI site	none
C	T	Intron 9 (2145)	BsaI site	N/A

Table 2.7 Domestication sites created during golden gate cloning of *AtIAR1*.

Using the domesticated *AtIAR1* plasmid as a template it was then possible to create level 0 and subsequently level 1 *AtIAR1*::*GUS* and *GFP* plasmids, using *GUS* donor plasmids (pICH75111, SynBio), *mEGFP* donor plasmids (pICSL30032, SynBio) and the same acceptor plasmid as in **2.2.2.2**. Primers used for this second round of golden gate cloning are shown below in **Table 2.8.** All final plasmids were then verified by sequencing (Genwiz) and with plasmid maps shown below in **Figure 2.5**.

Primer name	Sequence
AtIAR1::*GUS*	
AtIAR1 domestication part 1 FOR	GATGAAGACATCTCAGGAGAAA GGATTCACTCGACTTGAC
AtIAR1::*GUS* part1 REV	GATGAAGACATCTCGCATTTCTG AGTGAGCTAAGAAGAGCG
AtIAR1::*GUS* part2 FOR	GATGAAGACATCTCATTCGTGAT CTCATAACAATTGTTTTTGTAAC CGATATAGAAATCCCAAG
AtIAR1 domestication part 5 REV	GATGAAGACATCTCGAGCGATTT AAGAGCAACGATCCAGC
AtIAR1::*(i)GFP*	
AtIAR1 domestication part 1 FOR	GATGAAGACATCTCAGGAGAAA GGATTCACTCGACTTGAC
AtIAR1::*(i)GFP* part1 REV	GATGAAGACATCTCGAGTACCAA CTGATCCATAGATGAGAAACGC
AtIAR1::*(i)GFP* part2 FOR	GATGAAGACATCTCATTCGGGTT GGTCAAGAACTATGTTTTTACTT GCCC
AtIAR1 domestication part 5 REV	GATGAAGACATCTCGAGCGATTT AAGAGCAACGATCCAGC
AtIAR1::*(Nt)GFP*	
AtIAR1 domestication part 1 FOR	GATGAAGACATCTCAGGAGAAA GGATTCACTCGACTTGAC
AtIAR1::*(Nt)GFP* part1 REV	GATGAAGACATCTCGAGTAGCCG GCGTTGACTGAG

AtIAR1::*(Nt)GFP* part2 FOR	GATGAAGACATCTCATTCGCGTG ACGATCACGTGCATC
AtIAR1 domestication part 5 REV	GATGAAGACATCTCGAGCGATTT AAGAGCAACGATCCAGC
AtIAR1::*(Ct)GFP*	
AtIAR1 domestication part 1 FOR	GATGAAGACATCTCAGGAGAAA GGATTCACTCGACTTGAC
AtIAR1::*(Ct)GFP* part1 REV	GATGAAGACATCTCGAGTAGCTT CTATAAGAGAGATGCAAAGAGC
AtIAR1::*GUS* part2 FOR	GATGAAGACATCTCATTCGTGAT CTCATAACAATTGTTTTTGTAAC CGATATAGAAATCCCAAG
AtIAR1 domestication part 5 REV	GATGAAGACATCTCGAGCGATTT AAGAGCAACGATCCAGC

Table 2.8 Primers used to amplify domesticated *AtIAR1* parts for golden gate assembly. Red sequences denote overhang with BbsI recognition and cleavage site. Purple sequences denote the overhangs remaining after BsaI digestion from a pUAP1 backbone for level 1 assembly. Source: T.Gate.

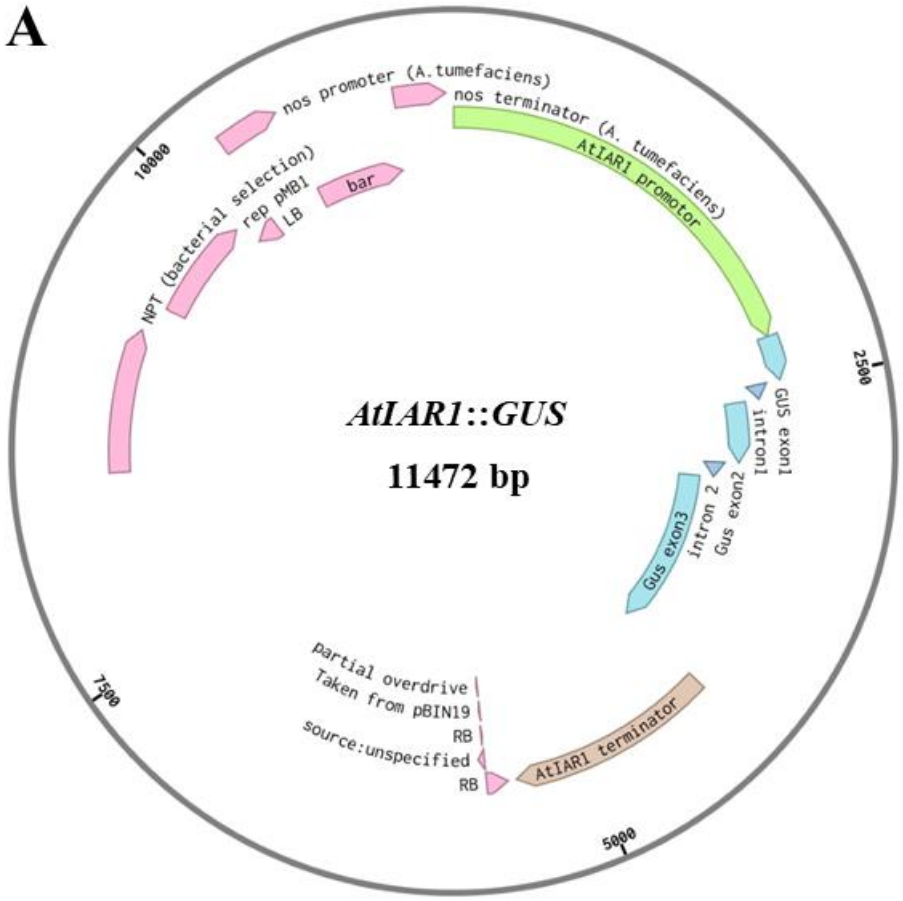
A
nos promoter (A.tumefaciens)
nos terminator (A. tumefaciens)
AtIAR1 promotor
GUS exon1
intron1
Gus exon2
intron 2
Gus exon3
AtIAR1 terminator
partial overdrive
Taken from pBIN19
RB
source:unspecified
RB
NPT (bacterial selection)
rep pMB1
LB
bar
AtIAR1::GUS
11472 bp
2500
5000
7500
10000

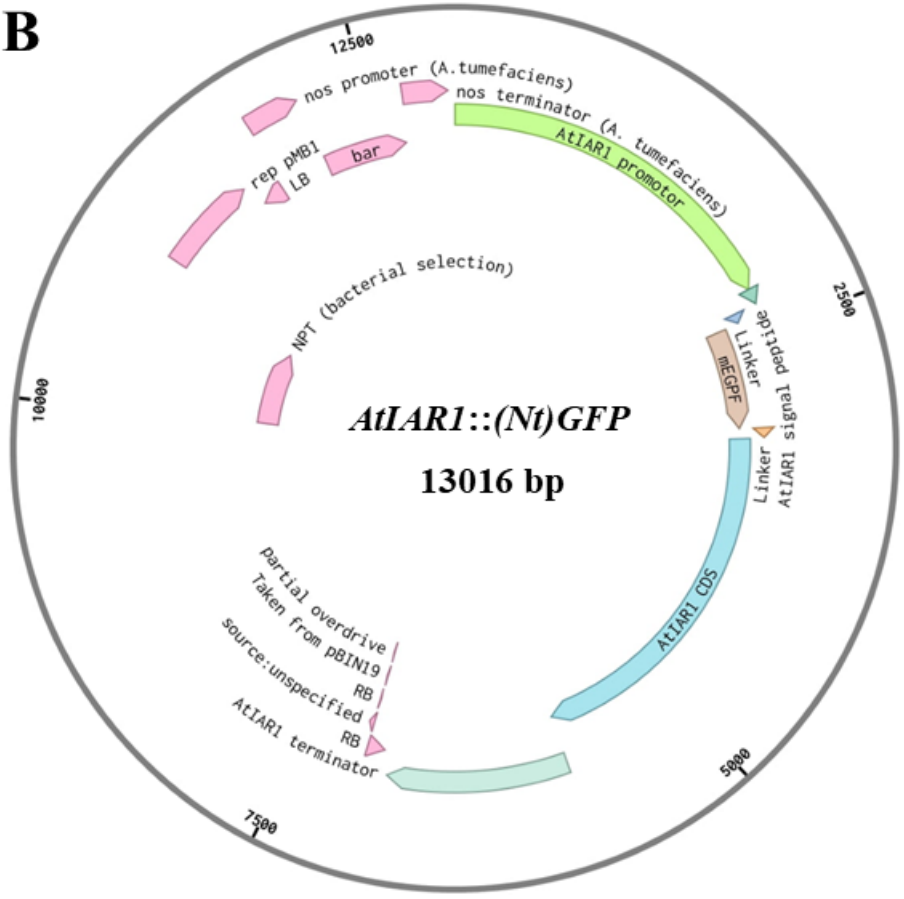
B
12500
nos promoter (A.tumefaciens)
nos terminator (A. tumefaciens)
AtIAR1 promotor
AtIAR1 signal peptide
Linker
mEGFP
Linker
AtIAR1 CDS
AtIAR1 terminator
partial overdrive
Taken from pBIN19
RB
source:unspecified
RB
NPT (bacterial selection)
rep pMB1
LB
bar
AtIAR1::(Nt)GFP
13016 bp
2500
5000
7500
10000

C

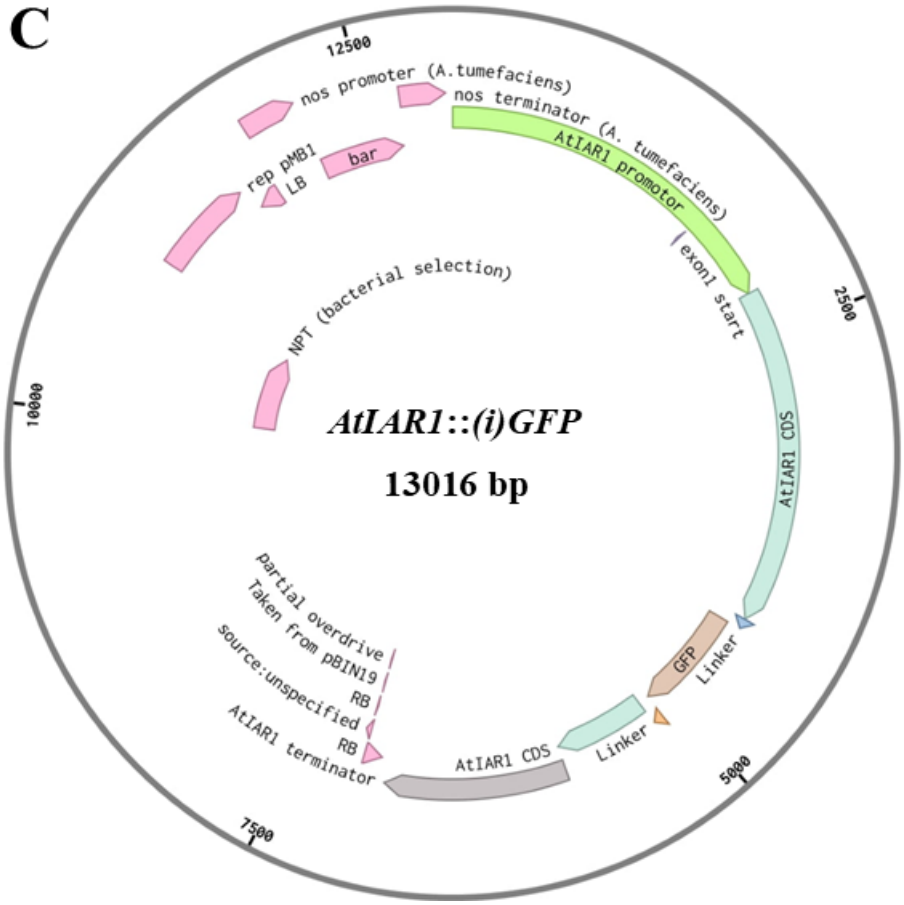
12500
nos promoter (A.tumefaciens)
nos terminator (A. tumefaciens)
AtIAR1 promotor
exon1 start
2500
AtIAR1 CDS
GFP
Linker
5000
AtIAR1 CDS
Linker
AtIAR1 terminator
RB
source:unspecified
RB
Taken from pBIN19
partial overdrive
7500
10000
NPT (bacterial selection)
rep pMB1
LB
bar
AtIAR1::(i)GFP
13016 bp

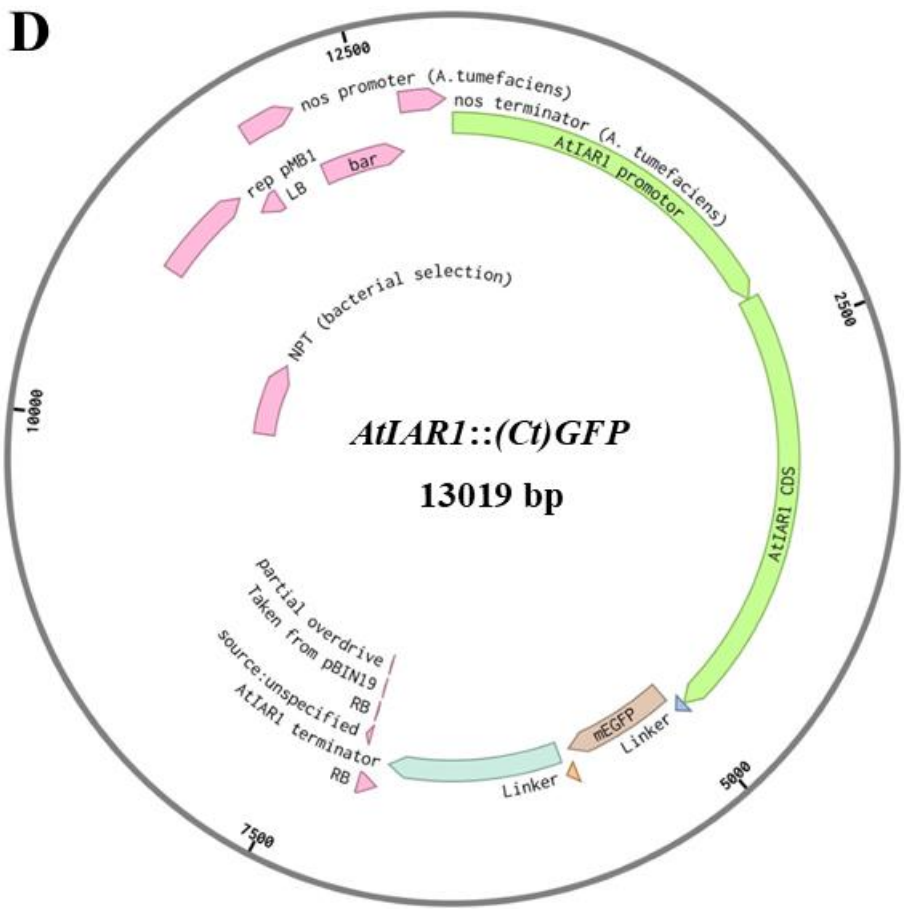

Figure 2.5 *AtIAR1*::*GUS* and *GFP* plasmid maps for *Arabidopsis* transformation. (A) *AtIAR1*::*GUS*: *GUS* expression controlled by *AtIAR1* promotor (2 kb) and terminator (1 kb). (B) *AtIAR1*::(*Nt)GFP*: mEGFP integrated into the N-terminus of AtIAR1 whose expression was controlled by the native *AtIAR1* promotor and terminator. (C) *AtIAR1*::*(i)GFP*: mEGFP integrated within ICL3 of AtIAR1 whose expression was controlled by the native *AtIAR1* promotor and terminator. (D) *AtIAR1*::(*Ct)GFP*: mEGFP integrated into the C-terminus of AtIAR1 whose expression was controlled by the native *AtIAR1* promotor and terminator. NPT (Neomycin phosphotransferase II) for kanamycin resistance, with nos:bar:nos for L-Phosphinothricin resistance. See text for further details.

2.2.3 *Agrobacterium tumefaciens* transformation by electroporation

Transformation of *Agrobacterium tumefaciens* strain GV3101 (lab stock) was conducted through electroporation, using the Gene Pulser (BioRad). 50 µL of

electrocompetent agrobacterium culture was added to 100 ng plasmid in an electroporation cuvette (1652083, BioRad). Electroporation conditions were 2.4 kV voltage and 400 ohm resistance. After electroporation, cells were recovered in 10 mL LB for 3 hours at 28°C, shaking at 210 rpm, then plated onto LB agar plates containing rifampicin (Sigma-Aldrich, 13292-46-1) final concentration of 50 µg/mL, Gentamycin (Sigma-Aldrich, G3632) final concentration of 10 µg/mL, and kanamycin. A colony from the LB plate was picked and grown in 10 mL LB with the appropriate antibiotics and incubated at 28°C to create a starter culture. The starter culture was then checked for the correctly sized insert by PCR and then used for *Arabidopsis* transformation by floral dipping[344].

2.2.4 *Arabidopsis* growth media and conditions

2.2.4.1 Seed sterilisation and vernalisation

Arabidopsis thaliana seeds were surface sterilised using 70% (v/v) ethanol followed by treatment with 5% (v/v) bleach and 0.05% (v/v) tween 20 (Sigma-Aldrich, P2287) solution for 10 minutes. After three 10-minute washes with dH_2O, the seeds were then placed into sterile 0.1% (w/v) agarose (Melford Biolaboratories Ltd, A20080) solutions. Sterilised seeds were then vernalised for 48 hours at 4°C in darkness, before being placed into the relevant media.

2.2.4.2 MS-based media

When control of Zn deficiency was not needed, plants were grown on ¼ strength MS (Murashige and Skoog) media consisting of 0.1% (v/v) Murashige and Skoog medium (Duchefa, M0222), 0.75% (w/v) sucrose (Formedium S/8600/60) and 1% (w/v) agar if required.

2.2.4.3 Zn deficient media

If Zn deficiency on solid media was required, agar was washed with EDTA as shown in Sinclair et al.[92]. Contaminating cations bound to agar were removed through chelator washing. For this process, 30 g agar was washed three times with 1 L 50 mM EDTA pH 8.0, twice for 5 hours then once for 14 hours. The agar was then washed again with 1 L dH2O four times for 4 hours then once for 14 hours. To maintain suspension of agar during washes, the agar solution was placed in a shaker shaking at 130 rpm. To exchange media, the agar suspension was filtered through Miracloth (475855, Merck Millipore Ltd., Watford, UK). After the water washes, the agar was air-dried on filter paper (185 mm diameter, FT3205185, Sartorius Ltd., UK) for 1 day at room temperature, before adding the modified Hoagland growth media[345] shown below (**Table 2.9**) with 0, 1 or 150 µM Zn and sucrose to 1% (w/v) to yield media with 1.5% (w/v) agar.

Stock solution	Source	Final Concentration
$Ca(NO_3)_2$	Sigma-Aldrich, C1396	1.5 mM
KH_2PO_4	Sigma-Aldrich, P3786	0.28 mM
$MgSO_4$	Sigma-Aldrich, M2643	0.75 mM
KNO_3	Sigma-Aldrich, 221295	1.25 mM
$CuSO_4$	Sigma-Aldrich, C1297	0.5 µM
$ZnSO_4$	Sigma-Aldrich, Z1001	1 µM
$MnSO_4$	Sigma-Aldrich, M7634	5 µM
H_3BO_3	Sigma-Aldrich, B6768	25 µM
Na_2MoO_4	Sigma-Aldrich, 243655	0.1 µM
KCl	Sigma-Aldrich, 31248	50 µM
MES pH 5.7	Sigma-Aldrich, M8250	3 mM
10 mM FeHBED (10 mM $Fe(NO_3)_3$ + 10.5 mM HBED	Sigma-Aldrich, 216828 and Strem Chemicals, 35369-53-0	5 µM

Table 2.9 Components of modified Hoagland solution.

2.2.4.4 Growth in soil

After vertical growth on ¼ MS agar plates for 10 days, seedlings were transplanted onto soil containing peat mix with 600 L Levington F2 peat (Scotts, Ipswich, UK), 196 g Exemptor® (chloronicotinyl insecticide, GB84080896A, Bayer CropScience Ltd., UK) and 100 L 4 mm grit.

2.2.4.5 *Arabidopsis* growth conditions

Unless otherwise specified, *Arabidopsis* was grown vertically at 21°C in long day conditions (16-hour light, 8-hour dark) under 90 µmol m^{-2} s^{-1} light.

2.2.5 *Arabidopsis* transformation

Arabidopsis thaliana was grown on ¼ MS agar plates then transferred to soil and grown until the plants had bolted and had stems approximately 10cm high. For transformation with *AtIAR1*::*GUS* and *AtIAR1*::*LUC* plasmids, Col-0 plants were grown for transformation, whilst for transformation with *AtIAR1*::*GFP* plasmids, *Atiar1-3* plants were grown, to allow possible phenotype complementation.

To prepare the transformed *Agrobacterium* strains, 100 mL of LB with appropriate antibiotics was inoculated with starter culture prepared as in **2.2.3**, and then incubated at 28°C for 16 hours. The cultures were then centrifuged at 4000 x *g* for 10 minutes at room temperature to collect the cells and resuspended the pellet in 5% (w/v) sucrose (Formedium S/8600/60) to an OD600 of 0.8. Silwet L-77 (Fisher Scientific, 306302161) was added to the suspension to a final concentration of 0.02% (v/v) and mixed well. To undertake floral dipping, plants were inverted and dipped in the *Agrobacterium* suspension and mixed lightly for around 10 seconds before being removed, drained for 5 seconds and then covered for 24 hours before resuming regular growth conditions.

Seeds produced from transformed plants were sown onto selective ¼ MS agar plates containing 5 µg/mL L-Phosphinothricin (Gold Biotechnology, P-165-250). After 2 weeks, seedlings showing resistance to L-Phosphinothricin by root growth and green leaves were transplanted to soil for further growth and seed collection. After a further round of L-Phosphinothricin selection, transplanting and seed collection, homozygosity was tested by assessing the ratio of seeds still resistant to L-Phosphinothricin, and lines showing 100% resistance were continued. After transplanting to soil these lines were subject to DNA extraction as in **2.2.2.1** and had the presence of the desired construct checked by PCR using primers from the cloning stages in **2.2.2**.

2.3 *Arabidopsis* phenotyping

2.3.1 Luciferase expression

Seeds containing the *AtMTP2*::*LUC* construct were surface sterilised, vernalised and then grown in 96-well plates (655073, Greiner Bio-one ltd) with liquid MS media for 14 days. These MS media, depending on the condition, had variable Zn (0, 30, 100 µM $ZnSO_4$), Mn (0, 80, 500 µM $MnSO_4$), and Fe (0, 100, 250 µM NaFe-EDTA (Sigma-Aldrich, E6760)). Additionally, to assess the potential impact of auxin and auxin conjugates on *AtMTP2* expression, indole acetic acid (IAA, Sigma-Aldrich, 45533) to a final concentration of 100 nM and N-(3-indolylacetyl)-L-alanine (IAA-Ala, Sigma-Aldrich, 345911) to a final concentration of 20 µM were added across the different Zn conditions.

On day 14, media were exchanged with fresh media containing 5 mM luciferin (FA141819, Biosynth) and incubated in the dark for 4 hours at room temperature. After incubation the plants were then imaged for luciferase activity with NightOWL II LB 983 (Berthold Technologies). Images were taken at 560 nm, with luminescence exposure time set to 120 seconds. Using indiGo software (Berthold Technologies), regions of interest were drawn around each well and data on total counts were gathered for each well and exported for analysis.

2.3.2 Root and shoot growth phenotyping

To assess root architecture phenotypes, sterilised and vernalised seeds were sown onto Hoagland solution-based EDTA-washed agar media with 0, 1 or 150 µM $ZnSO_4$ and with either no auxin, 100 nM IAA or 20 µM IAA-Ala added. As even EDTA-washed agar contains residual Zn ions, the '0 µM' Zn conditions contain sufficient Zn for plant growth whilst causing a Zn deficiency response. After 10 days of growth, images of plants were taken for measurement of lateral root density

and primary root length (see **Figure 2.6**). For calculating the percentage primary root growth in auxin-containing media, the length of the primary root was compared to the mean primary root length of the same biological repetition grown on media without any auxin added.

Figure 2.6. Picture of a typical agar plate containing vertically grown *Arabidopsis thaliana* used for image analysis.

To assess hypocotyl growth phenotypes, sterilised and vernalised seeds were sown onto Hoagland solution-based EDTA-washed agar media with 0, 1 or 150 µM $ZnSO_4$. For hypocotyl length and apical hook angle experiments, skotomorphogenesis was induced as previously carried out in Mateo-Bonmatí et al.[290] by transferring vernalised seeds to light conditions at 21°C for 8 hours to allow germination before transferring to darkness for four more days at 21°C.

All images were then analysed with Fiji (ImageJ) software.

2.3.3 Chlorophyll content measurement

Sterilised and vernalised seeds were sown onto Hoagland solution-based EDTA-washed agar media with 0, 1 or 150 µM $ZnSO_4$ and grown for 16 days before having the shoot fresh weight measured and then snap frozen in 50 mg pools. These pools were homogenized using 3 mm tungsten carbide beads and the TissueLyser LT homogeniser. Samples were dissolved in 100% methanol (Fisher Scientific, 10674922) for 30 minutes at 40°C, before being clarified by centrifugation at 10,000 x *g* for 1 minute. The resulting supernatant was then diluted as appropriate and absorbances at 650 nm (A650) and 665 nm (A665) were measured using a spectrophotometer to calculate chlorophyll concentration based on the equation below[346]. Chlorophyl content was then reported as µg/mg of fresh weight.

$$\text{Chl } (\mu g/mL) = 22.5 \text{ x A650} + 4 \text{ x A665}$$

2.3.4 Inductively coupled plasma-optical emission spectrometry (ICP-OES)

Sterilised and vernalised seeds were sown onto Hoagland solution-based EDTA-washed agar media with 0, 1 or 150 µM $ZnSO_4$ and grown for 16 days. Shoots and roots were separated. To remove apoplastic cations from the roots, roots were washed in a solution of 2 mM $CaSO_4$ (Sigma-Aldrich, C3771) and 10 mM EDTA for 10 minutes with shaking at 4°C. To remove Fe ions, the roots were further washed with shaking for 3 minutes in a solution of 5.7 mM sodium dithionite (Supelco, 1.06505) and 0.3 mM BPDS. The roots were then washed twice further with dH_2O while shaking.

After air drying for 15 min, roots and shoots were dried for 48 hours at 65°C and subsequently weighed. Dried roots and shoots were separately digested at 95°C for 4 hours in a solution of 2 mL 65% v/v HNO_3 (Sigma-Aldrich, 1004410250) and 0.5 mL H_2O_2 (Sigma-Aldrich, 95321). After digestion, Milli-Q ultrapure water was

added to 15 mL. Diluted samples were then transferred to the Balk lab, Department of Biochemistry and Metabolism, John Innes Centre for ICP-OES.

2.3.5 Reverse transcriptase quantitative PCR (RT-qPCR)

Sterilised and vernalised seeds were sown onto Hoagland solution-based EDTA-washed agar media with 0, 1 or 150 µM $ZnSO_4$ and grown for 16 days. Whole 16-day-old seedlings were pooled into 100 mg samples which were snap frozen in liquid nitrogen. The samples were then homogenised using 3 mm tungsten carbide beads and the TissueLyser LT homogeniser. RNA was then extracted using the RNeasy Plant Mini Kit (74904, QIAGEN, Hilden, Germany) as instructed with RNA concentration measured with the NanoDrop™ 2000 spectrophotometer.

To synthesize cDNA, the SuperScript™ IV First-Strand Synthesis System (Invitrogen, 18091050) was performed according to manufacturer's specifications with each 20 µL reaction containing 4 µL RNA (400 ng/µL). Negative controls with no template (NTC) and no reverse transcriptase (NRT) were also included. Reactions were run at 37°C for 50 min, then 70°C for 15 min in the Mastercycler® pro (Eppendorf UK Ltd., Stevenage, UK). cDNA was diluted 10-fold to give a final volume of 200 µL and stored at -20°C.

RT-qPCR was carried out in 96-well plates (AB0700W, Thermo Fisher Scientific). Each reaction totalled 20 µL and contained 5 µL diluted cDNA, 10 µL SYBR Green JumpStart™ ReadyMix™ (S4438), 1 µL forward primer (10 µM), 1 µL reverse primer (10 µM) and 3 µL dH_20. Primers used are shown in **Table 2.10**. Within each plate, there were technical triplicates for every reaction, including for reference genes polyubiquitin C (*AtUBC*) and TAP42 interacting protein of 41 kDa (*AtTIP41*), NTC and NRT. Each experiment had three independent biological replicates.

Primer name	Sequence	Reference
AtZIP5 FOR	TTGGCGTGGAATCTG GTGAA	Zheng et al.[73]
AtZIP5 REV	TTGAAATTTCCCTGG GCGATG	Zheng et al.[73]
AtZIP3 FOR	TGCACAGGTATTGGA GTTGGG	Zheng et al.[73]
AtZIP3 REV	TGCGAAGAACGTCG ACATGA	Zheng et al.[73]
AtZIP4 FOR	CACGGACATATGCA CGGGAA	Zheng et al.[73]
AtZIP4 REV	ACTGTGCCTGAGAG ATGCAG	Zheng et al.[73]
AtIAR1 FOR	CTTCCCCAAGAGATA GGTGATTTTGG	T. Gate
AtIAR1 REV	CAAGAACTCCAGCA ACAGCTATG	T. Gate
AtZIP9 FOR	ACTCTGCTCGCGGAT TTCAT	Zheng et al.[73]
AtZIP9 REV	TGGAGAGGCTATGA CGGTGA	Zheng et al.[73]
AtMTP2 FOR	GGACAACCATTAAG ATGCTTCG	Sinclair et al.[92]
AtMTP2 REV	TCTCTCGGTGTGCTC TCCATTA	Sinclair et al.[92]
AtBiP3 FOR	CACGGTTCCAGCGTA TTTCAAT	Valencia et al.[347]
AtBiP3 REV	ATAAGCTATGGCAG CACCCGTT	Valencia et al.[347]
AtBiP1/2 FOR	TCAGTCCTGAGGAG ATTAGTGCT	Cho et al.[348]
AtBiP1/2 REV	TGCCTTTGAGCATCA TTGAA	Cho et al.[348]

AtbHLH38 FOR	TTTCACAAACTTCGGTTGGCC	Rodriguez-Celma et al.[157]
AtbHLH38 REV	CTGACGAAACAGATACTCCCAAGCT	Rodriguez-Celma et al.[157]
AtIMA1 FOR	TGATTGTAATTTAGGAGGAAACAAAA	Grillet et al.[161]
AtIMA1 REV	TCAATCCACAAGTAAACATCTATGG	Grillet et al.[161]
AtUBC FOR	CTGCGACTCAGGGAATCTTCTAA	Zheng et al.[73]
AtUBC REV	TTGTGCCATTGAATTGAACCC	Zheng et al.[73]
AtTIP41 FOR	GTGAAAACTGTTGGAGAGAAGCAA	Grillet et al.[161]
AtTIP41 REV	TCAACTGGATACCCTTTCGCA	Grillet et al.[161]

Table 2.10 Primers used in RT-qPCR for gene expression analysis

The PCR programme was then as follows: 95°C for 3 min, followed by 40 cycles of 94°C for 30 s, 63°C for 30 s, 72°C for 30 s and one cycle of 50°C for 30 s. There then followed a melt curve analysis (from 65°C up to 95°C, with increments of 0.5°C). Data were then exported to Excel (Microsoft® Office 2016) using CFX Manager (v. 3.1.1517.0823, Biorad) software. qPCR reactions were run using the C1000TM CFX96 Touch™ Real-Time PCR Detection System (Biorad, Hercules, California, USA). The expression of genes of interest was calculated using the 2-ΔCt method[349] with fold changes represented relative to Col-0 under control conditions.

2.3.6 Microscopy methods

2.3.6.1 *GUS* expression

Sterilised and vernalised seeds were sown onto Hoagland solution-based EDTA-washed agar media with 0, 1 or 150 µM $ZnSO_4$ and with either no auxin, 100 nM IAA or 20 µM IAA-Ala added. After growth in light conditions for 8 days, seedlings were stained overnight in X-Glc (Sigma-Aldrich, 73837) 0.05% (w/v) solution at 37°C, and then transferred to 70% (v/v) ethanol for 8 hours to remove chlorophyll. Cleared seedlings were then imaged with an Axio Imager Z2 microscope (Zeiss) and captured using the AxioCam 506 camera (Zeiss).

2.3.6.2 Root meristem size

Sterilised and vernalised seeds were sown onto Hoagland solution-based EDTA-washed agar media with 0, 1 or 150 µM $ZnSO_4$. 5-day old plants were cleared overnight in chloral hydrate solution, a solution of 67% (w/v) chloral hydrate (Sigma-Aldrich, 23100), 25% (v/v) dH_2O and 8.3% (v/v) glycerol (Fisher G/0650/17). Differential interference microscopy was performed using the Axio Imager Z2 microscope (Zeiss) and captured using the AxioCam 506 camera (Zeiss). Following previous methods[350] cells in the cortical layer can be divided into cells in the meristematic zone (red) transition zone (yellow) and elongation zone (green), whose boundaries were found by the shape of the cell and cytosol appearance (**see Figure 2.7**). Only cells within the meristematic zone were counted.

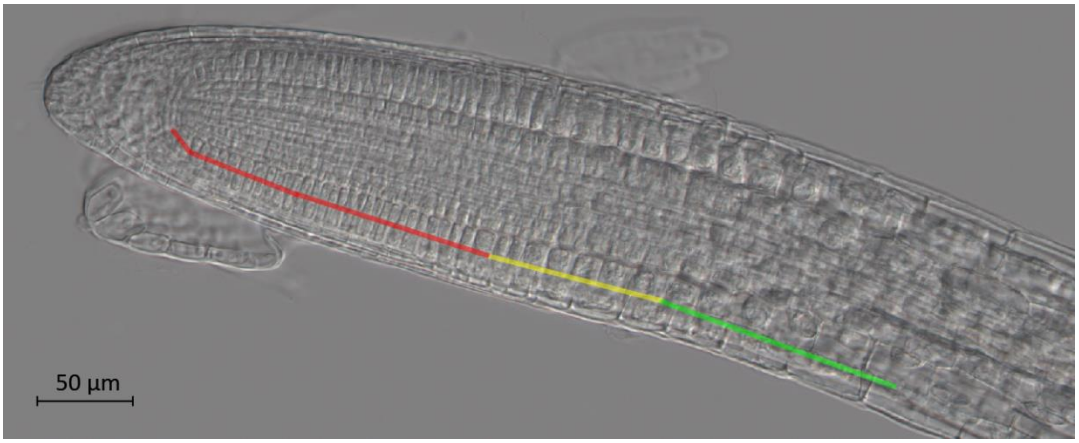

Figure 2.7 Root meristem cortex cell counting. Cortical layer lies above the coloured line. Meristematic zone to be counted shown in red, transition zone in yellow and elongation zone in green. Taken with 40x objective, using tile scan experiment and stitching processing available in ZEN software (Zeiss).

2.3.7 Metabolite analysis

2.3.7.1 Metabolites of interest

To investigate the influence of Zn status and AtIAR1 activity on auxin metabolism, the abundance of several auxin-related metabolites was measured (**Table 2.11** and **Figure 2.8**). These were chosen to represent precursors of IAA (Tryptophan and IAN), IAA itself and IAA conjugation and degradation products (IAA-Ala, IAA-Asp, IAA-Glc and oxIAA).

Metabolite	Source
L-Tryptophan (Trp)	Sigma-Aldrich, T0254
3-Indoleacetonitrile (IAN)	Sigma-Aldrich, 129453
3-Indoleacetic acid (IAA)	Sigma-Aldrich, 45533
Indole-3-acetyl b-D-Glucopyranose (IAA-Glc)	Toronto Research Chemicals, I627020
(2S)-2-[[2-(1H-Indol-3-yl)acetyl]amino]butanedioic acid (IAA-Asp)	Astatech, A11375
N-(3-Indolylacetyl)- L -alanine (IAA-Ala)	Sigma-Aldrich, 345911
2-Oxo-2,3-dihydro-1H-indol-3-yl)acetic acid (oxIAA)	Sigma-Aldrich, CDS009127
Indole-3-acetic-2,2-D_2 acid (D_2-IAA)	Sigma-Aldrich, 492817

Table 2.11 Metabolites measured in this study and sources.

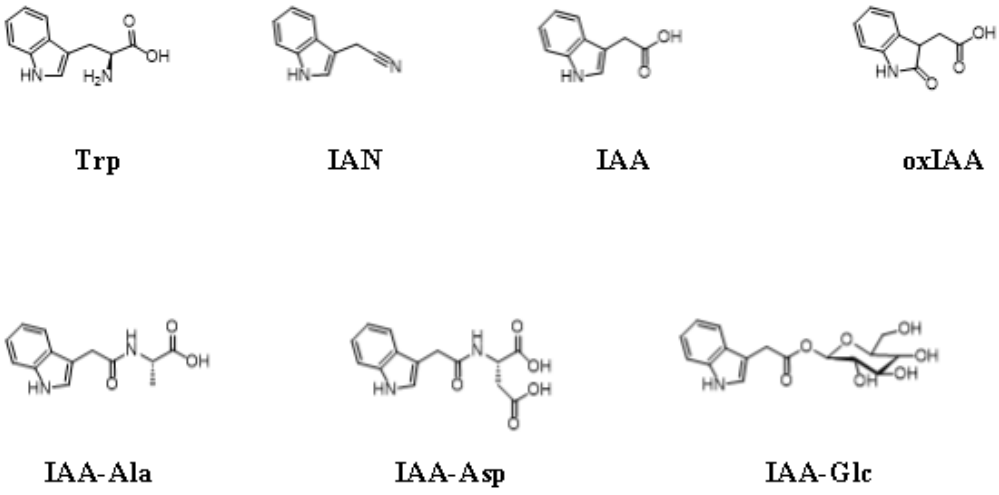

Figure 2.8 Structures of metabolites measured in this study. Created using ChemDraw 2.0 (PerkinElmer)

2.3.7.2 Metabolite extraction

Sterilised and vernalised seeds were sown onto Hoagland solution-based EDTA-washed agar media with 0, 1 or 150 µM $ZnSO_4$ and grown for 16 days. In a protocol adapted from Sugahara et al.[278], 100 mg pools of 16-day old whole seedlings were snap frozen in liquid nitrogen and homogenised with 3 mm tungsten carbide beads with a TissueLyser LT homogeniser. 333 µL 80% (v/v) methanol containing the internal standard deuterated IAA (D_2-IAA) at 500 nM was added to the homogenate, then centrifuged at 10,800 x *g* for one minute and the supernatant extracted and retained in a separate 2 mL Eppendorf vial on ice. Two further rounds of adding 333 µL 80% (v/v) methanol, homogenisation and collecting supernatant were performed resulting in 1 mL of 80% (v/v) methanol solution containing extracted metabolites and 166 nM D_2-IAA.

The 80% (v/v) methanol solution was then subjected to LLE using hexane. After adding 700 µL of hexane and inverting several times, the mixture was separated by centrifugation at 16,000 x *g* for 3 minutes. The upper hexane layer was removed, and the hexane addition, inversion and centrifugation steps repeated twice further.

The resulting fraction was dried in the Genevac EZ-2 Elite Evaporator (SP Scientific), with a temperature limit of 45°C, evaporation time of 90 minutes and a drying time of 30 minutes. Dried samples were then resuspended in 100 µL 80% (v/v) methanol containing no D_2-IAA and passed through a 0.22 µm pore spin filter (8161, Corning Ltd).

2.3.7.3 Liquid chromatography mass spectrometry (LC-MS)

The Xevo TQ-S (Waters) was used for LC-MS separation, detection and quantification of target ions. Separation of the metabolites was performed by passing the sample through a Kinetex® 2.6µm EVO C18 100 Å, LC Column 100 x 2.1 mm (Phenomenex, 00D-4725-AN, see **Table 2.12** for details) which closely resembles the column used by Sugahara et al.[278].

Property of LC column	Value
Internal diameter (mm)	2.1
Length (mm)	100
Stationary phase	C18 with trimethylsilyl endcapping
Solid Support	Organo-silica with ethane cross-linking,
Particle size (µm)	2.6
Pore size (Å)	100

Table 2.12 Properties of LC column used in this study.

The metabolites were separated using reverse phase LC along a methanol gradient as shown in **Table 2.13** using conditions as shown in **Table 2.14** and detected with MS conditions as in **Table 2.15.**

LC condition	Value
Solvent A	0.5% (v/v) formic acid (Supelco, 00940) dissolved in Milli-Q ultrapure water
Solvent B	100% methanol
Column temperature (°C)	40
Flow rate (mL/min)	0.4
Injection volume (µL)	5

Table 2.13 LC conditions used in this study.

Time	Solvent A%	Solvent B%
0	95	5
4	10	90
5	10	90
5.2	95	5
8	STOP	STOP

Table 2.14 Inlet method for LC used in this study.

MS condition	Value
Ionisation mode	Electrospray ionisation
Capillary voltage (kV)	1.5
Cone voltage (V)	20
Source offset (V)	50
Desolvation gas temperature (°C)	500
Desolvation gas flow (L/hr)	1000
Cone gas flow (L/hr)	150
Nebulising gas pressure (bar)	70
Collision gas flow (mL/min)	0.15

Table 2.15 MS conditions used in this study.

2.3.7.4 Calculation of metabolite content

The concentration of the metabolites was established by comparison to the internal standard D_2-IAA. Comparing the known concentration of D_2-IAA in the sample to the detected peak allows calculation of the percent of metabolites that have been lost between sample extraction and detection by MS, labelled (F).

$$\text{Detected response (Standard)} = \text{F x Sample concentration (166 nM)}$$

Due to the co-linearity of the response of metabolites, if the level of detected IAA metabolites of interest (IAA etc) falls within the linear range we can use the F value from the internal standard, D_2-IAA, to calculate the concentration of the IAA metabolites in the samples prior to extraction. Metabolite content was then given as mol/mg of fresh weight.

$$\frac{\text{Detected response (IAA etc)}}{\text{F}} = \text{Sample content (IAA etc (M))}$$

All analysis was carried out in MassLynx software (Waters).

2.4 Bioinformatic methods

2.4.1 Phylogenetic analysis of the ZIP transporter family

To illustrate the relationship of AtIAR1 to other plant ZIPs as well as the wider ZIP transporter family, a phylogenetic tree was constructed. Sequences of ZIP genes were gathered using the tBLASTn function on the BLAST server[351] using AtIAR1 amino acid sequence (Uniprot accession number Q9M647) and AtIRT1 amino acid sequence (Uniprot accession number Q38856) as the query and collecting sequences from organisms within animal (*Drosophila melanogaster* and *Homo sapiens*), plant (*Arabidopsis thaliana*, *Oryza sativa* and *Medicago truncatula*) and fungal (*Saccharomyces cerevisiae*) kingdoms. These sequences were aligned and phylogeny calculated within the MEGA-X software[352]. For alignment, MUSCLE[353] was used, using default settings and phylogeny calculated with the Maximum Likelihood method and Jones-Taylor-Thornton (JTT) matrix-based model[354] with a gamma distribution of 5 categories to model different evolutionary rates at different sites. The phylogenetic tree was then constructed from 100 bootstrap replicates and initial trees using BioNJ and Neighbour-Join algorithms on the JTT-generated matrix.

2.4.2 Bioinformatic analysis of amino acid composition in AtIAR1 homologues

Sequences of *AtIAR1* homologues were gathered using the tBLASTn function on the BLAST server[351] using AtIAR1 amino acid sequence (Uniprot accession number Q9M647) as the query and collecting sequences of from organisms within animal (*Drosophila melanogaster*, *Xenopus laevis*, *Mus musculus*, and *Homo sapiens*), plant (*Arabidopsis thaliana*, *Oryza sativa, Nicotiana tabacum*, *Zea mays*, *Glycine max* and *Marchantia polymorpha*) and fungal (*Saccharomyces cerevisiae*) kingdoms. These sequences were aligned using MUSCLE[353] using default settings.

The aligned sequences were then separated between loop and transmembrane sequences based on the loop positions present in the AtIAR1 AlphaFold model[355]. These loop sequences were analysed for histidine density which could then be plotted.

To further check the conservation of residues involved in the transport of metals, the aligned sequences were also aligned against residues seen in the crystal structure of *Bordetella bronchiseptica* ZIP protein[356] seen to bind metals during their transport through the transmembrane helices 4 and 5.

2.4.3 Subcellular localisation predictions of AtIAR1 homologues

To screen AtIAR1 homologues for putative subcellular location, three different subcellular localisation prediction programmes were used; PProwler v1.2[357], TargetP v2.0[358] and DeepLoc v2[359]. Sequences of AtIAR1 homologues were gathered using the tBLASTn function on the BLAST server[351] with AtIAR1 amino acid sequence (Uniprot accession number Q9M647) as the query and sequences of good quality collected from organisms within a diverse set of plants (*Solanum tuberosum, Nicotiana tabacum, Vitis vinifera, Gossypium hirsutum, Medicago truncatula, Phaseolus vulgaris, Glycine max, Arabidopsis thaliana, Brassica oleracea, Oryza sativa, Sorghum bicolor, Zea mays, Triticum aestivum, Hordeum vulgare, Pinus kesiya, Marchantia polymorpha* and *Physcomitrium patens*).

To examine the potential changed localisation of *AtIAR1* homologues within the Solanaceae family in further detail, sequences from closely related species and Solanaceae family members were gathered. Extra sequences were collected from; *Hibiscus syriacus, Gossypium raimondii, Durio zibethinus, Prunus mume, Prunus armeniaca, Prunus persica, Prunus dulcis, Nyssa sinensis, Actinidia chinensis, Buddleja alternifolia, Olea europaea, Ipomoea triloba, Ipomoea nil, Nicotiana tomentosiformis, Nicotiana attenuata, Nicotiana sylvestris, Capsicum annuum, Capsicum baccatum, Capsicum chinense, Solanum chil*ense, *Solanum pennellii, Solanum lycopersicum* and *Solanum commersonii*.

These sets of sequences were then passed to prediction software with the probability of localising to each sub-cellular compartment outputted for analysis.

2.4.5 Promotor region annotation

Promotor regions were accessed using the TAIR genome browser[360]. Predicted transcription factor binding sites for these regions were found using the PlantCARE database[361] and visualised using the gene feature visualisation server[362].

Chapter 3: Control of *AtMTP2* Expression

3.1 Introduction

3.1.1 Role of *AtMTP2* in ER Zn homeostasis

A wide variety of genes in *Arabidopsis* are upregulated under Zn deficient conditions including metal transporter genes (e.g. *AtZIP9*) and nicotianamine synthase genes (e.g.*AtNAS4*)[1] with further details of this response discussed in **Chapter 1.2**. Some of these genes are regulated by the transcription factors AtbZIP19 and AtbZIP23[71] which are themselves responsive to local Zn levels[120]. Some Zn deficiency responsive genes are upregulated by a shoot-derived Zn deficiency signal, including *AtMTP2* that could override local signals in the root of Zn sufficiency[92]. *AtMTP2* codes for an endoplasmic reticulum (ER) localised Zn transporter in the outer cell layers of the elongation zone, and *Atmtp2* mutants show reduced biomass and lower Zn partitioning to shoot under Zn deficient conditions[92]. It is therefore hypothesised that AtMTP2 facilitates Zn transport symplastically through the ER-luminal continuum in the root cortex[5] to aid root-to-shoot Zn transport. As AtMTP2 is to date the only ER Zn importer shown to be localised to the ER, AtMTP2 appears to be a major regulator of ER Zn homeostasis, and therefore represents a key target for further understanding ER Zn dynamics during systemic Zn deficiency.

In addition to the role of ER Zn in root-to-shoot Zn transport in Zn deficiency conditions, ER Zn levels have been implicated in the response to exogenous auxin conjugates[1,328]. Whether AtMPT2 plays a role in the Zn related response to exogenous auxin conjugates is currently unknown. Further research of the control of ER Zn import through AtMTP2 may prove vital in understanding the control of root-to-shoot Zn translocation in Zn limited conditions and also auxin metabolism in Zn deficient conditions.

3.2 Results

3.2.1 Identifying components in a systemic Zn deficiency response

To begin investigating the components of the systemic regulation of genes by shoot Zn deficiency, a group of genes upregulated by this systemic signal were identified from data within Sinclair et al.[92]. All genes identified as systemically regulated by Sinclair et al.[92] were taken forward for promotor analysis and included *AtMTP2*, *AtMLO9*, *AtRPS15B*, *AtNWMU2-2S*, *AtSAUR28*, *AT5G03620*. *AT1G03890*, *AT1G73510*, *AT3G28770*, *AT2G05400*, *AT2G19420*, *AT4G39753*, *AT2G36780*, *AT2G03160* and *AT2G04720*. Unfortunately, a search for conserved motifs in promotors of these genes using Multiple Em for Motif Elicitation (MEME) analysis[363] did not result in any obvious potential transcription binding sites. Due to time restraints, and the fact that *AtMTP2* is the only gene in the list with a known link to Zn homeostasis, only *AtMTP2* was investigated further, although in future work, expression of other genes could be assessed.

Another method to find components involved in the shoot-to-root Zn deficiency signal was to use a forward genetic screen. A luciferase-based screen was decided upon, based on previous success for measuring cadmium response in plants[364] and the ability to quantify expression by emission at 560 nm during the cleavage of exogenous D-luciferin to oxyluciferin[365]. Therefore, *Arabidopsis* Col-0 ecotype plants were transformed with *Agrobacterium* containing a plasmid with the promotor and terminator sequences of *AtMTP2* (2.6 and 1 kbp) upstream and downstream of a firefly luciferase gene (see **Chapter 2.2.2**). These transformed *AtMTP2*::*LUC* lines were then taken to the fourth generation through several rounds of selection (see **Chapter 2.2.5**) and were used for further analysis below.

3.2.2 *AtMTP2*::*LUC* lines respond to Zn deficiency

To determine which *AtMTP2*::*LUC* lines would be best for use in a forward screen and for general *AtMTP2* expression profiling, seedlings were screened for highest luciferase expression in 0 Zn media relative to control Zn levels as seen in **Figure 3.1**.

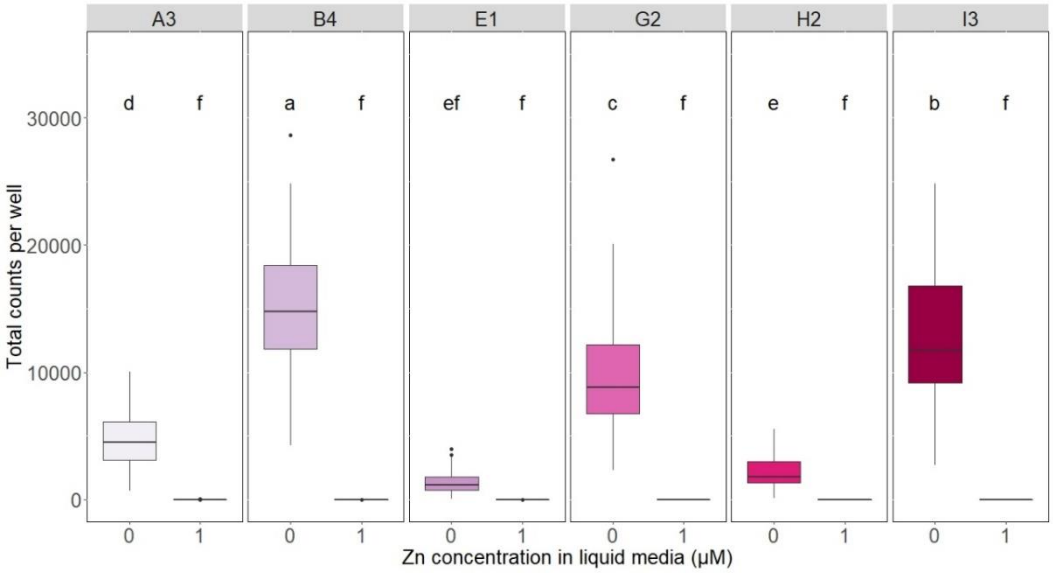

Figure 3.1 *AtMTP2*::*LUC* transformants respond differently to Zn deficiency. Data are split by different parental lines (labelled A3-I3). Three independent sets of 32 plants were analysed for each condition, with data displayed using R version 4.1.1. Lower case lettering indicates statistically significant differences between groups (labelled sequentially from 'a' in order of estimated mean) as calculated using analysis of variance (ANOVA) using Tukey's method for p-value adjustment[366] for 12 groups using a p-value cut-off of 0.05.

As shown in **Figure 3.1** the *AtMTP2*::*LUC* lines showed a variety of responsiveness to Zn deficient conditions and all showed almost no detectable response in replete Zn conditions. *AtMTP2*::*LUC* line B4 was the line with the highest counts per well, indicating highest luciferase activity in Zn deficient

conditions, and had minimal expression in replete conditions. This line was therefore taken forward for further expression analysis and could be used in a future forward genetic screen.

3.2.3 *AtMTP2*::*LUC* B4 line responds to Zn deficiency specifically

Specificity of response is important for reporter lines used in forward genetic screens in order to find mutants only involved in the transcriptional response under investigation. Divalent metal ions such as Zn^{2+}, Mn^{2+} and Fe^{2+} have similar ionic radius and so compete with each other for metalation of proteins according to the Irving-Williams series[125]. To check whether the *AtMTP2*::*LUC* B4 line was responsive to this metal cross-homeostasis, the *AtMTP2*::*LUC* B4 line was screened in excess or deficient Zn, Fe and Mn conditions (**Figure 3.2**).

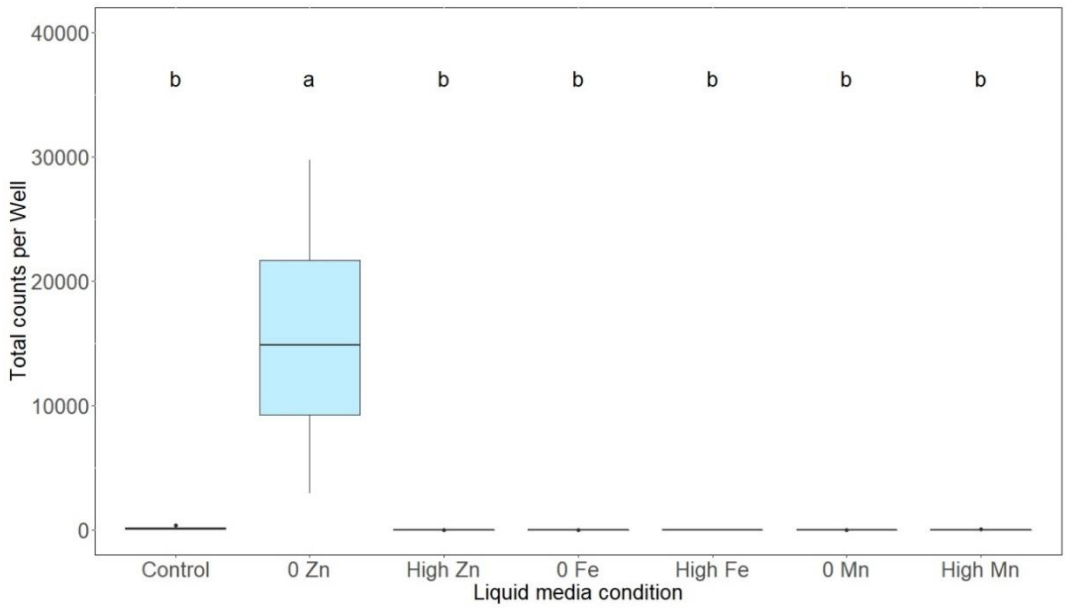

Figure 3.2 Metal specificity of the *AtMTP2*-driven luciferase expression. Three independent sets of 32 plants were analysed for each condition. High Mn, Fe and Zn levels were 500, 250 and 100 µM respectively, with MS media as a control. Data displayed using R version 4.1.1. Statistically significant differences between groups were calculated and displayed as in **Figure 3.1**.

As **Figure 3.2** illustrates, the chosen line shows significantly higher luciferase activity in Zn deficiency conditions compared to all other conditions including control conditions. Firstly, this further emphasises the Zn deficiency responsiveness of this reporter line, and secondly, shows that *AtMTP2* expression and by extension the shoot-derived Zn deficiency signal is not responsive to the altered Mn and Fe conditions tested.

With this experiment, it became obvious that the differences in size of plants grown under different conditions were influencing the luciferase activity reported because plants under high Zn and Fe deficiency conditions were smaller than those grown in other conditions. In future experiments, this heterogeneity could be corrected for by including a constitutively expressed GFP module within the plasmids used for transformation and measuring luciferase activity as a percentage of GFP fluorescence.

Unfortunately, due to time restrictions, the mutagenesis and screening for mutants in *AtMTP2* expression were not carried out. However, the *AtMTP2*::*LUC* B4 line has been shown to respond with high intensity and specificity to Zn deficiency and so could be used in a screen at a later date.

3.2.4 Promotor analysis of *AtMTP2* showed multiple potential regulators of expression

To predict the conditions in which *AtMTP2* expression might be induced, the promotor region of *AtMTP2* was analysed (shown below in **Figure 3.3)**. The promotor was found to contain elements for response to light (G-box, TCT-motif, Box 4, chs-CMA1, AE-box), anaerobic induction (ARE), salicylic acid (TCA-element), abscisic acid (AAGAA motif), gibberellin (P-box), ethylene (ERE), wounding (WRE3) and also elements thought to be involved in leaf development (CCAAT box). In addition, the promotor was found to contain myc and TGACG motifs that are important for binding of MYC and TGA transcription factors respectively which have varied roles but include expression in response to exogenous auxin and heavy metals[367,368]. This promotor analysis has indicated that *AtMTP2* expression and by extension Zn transport into the ER may be controlled by a wide range of stimuli, including a variety of plant hormones including auxin, any of which could prove important in root-to-shoot Zn transport.

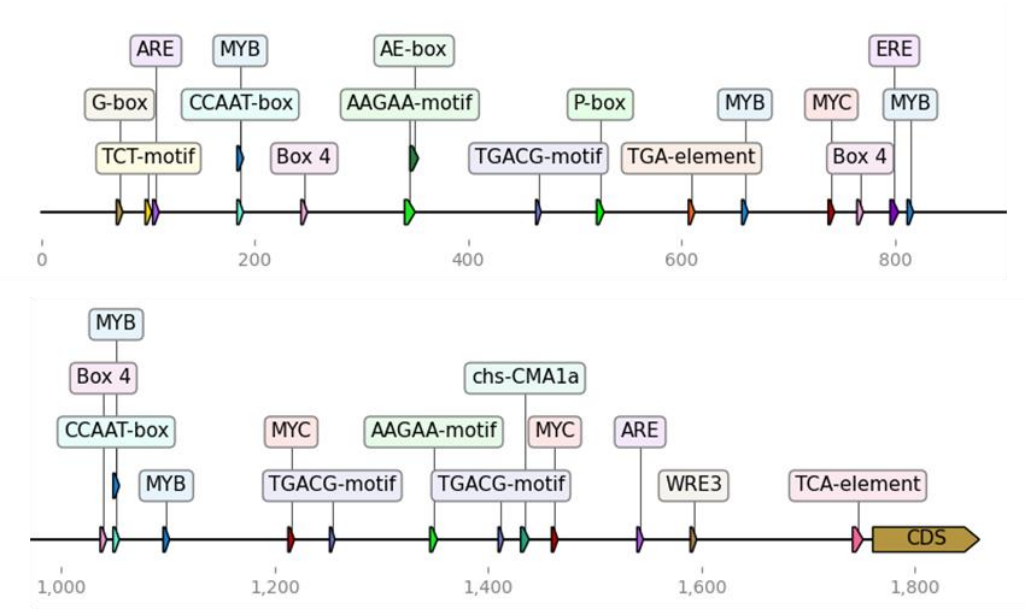

Figure 3.3. Promotor elements present in *AtMTP2* promotor. Promotor elements as identified by PlantCARE[361] from sequences upstream of the coding sequence (CDS). CAAT (common cis-acting element) and TATA-box (common core promotor region) annotations were removed for clarity. Numbers indicate base pairs from 5' end of the promotor sequence used for generation of *AtMTP2*::*GUS* constructs.

3.2.5 *AtMTP2*::*LUC* expression in Zn deficiency is reduced by exogenous auxins

Previous work has suggested that plant hormones including auxin may interact with Zn nutrition to co-ordinate nutritional requirements of developing tissues. *AtSAUR28,* a gene upregulated by auxin and involved in temperature-induced rosette architecture changes[369], was found within the group of genes regulated by this systemic Zn deficiency signal by Sinclair et al.[92]. In addition, *AtMTP2* controls Zn transport into the ER where metal balance is thought to play a role in auxin conjugation[1,328] and promotor analysis found binding sites of transcription factors, some of which are influenced by auxin. It was therefore hypothesised that either unconjugated or conjugated auxin may influence *AtMTP2* expression. Thus,

luciferase expression was assayed in the *AtMTP2*::*LUC* B4 line in media with either no auxin, unconjugated (IAA) or conjugated auxin (IAA-Ala) added.

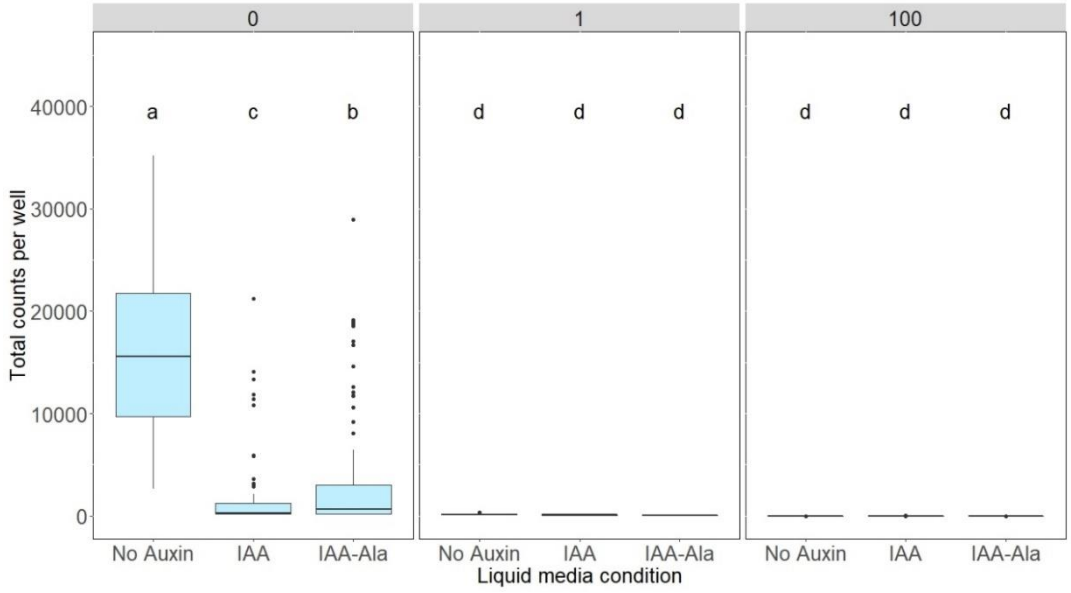

Figure 3.4 Auxin responsiveness of *AtMTP2* driven luciferase expression. Data are split into columns by Zn concentration in the media (0, 1, 100 µM) with either no auxin, 100 nM IAA or 20 µM IAA-Ala in the media. Three independent sets of 32 plants were analysed for each condition, with data displayed using R. Statistically significant differences between groups were calculated and displayed as in **Figure 3.1**

As the results in **Figure 3.4** show, both exogenous IAA and IAA-Ala reduce the luciferase activity observed, indicating a reduction in *AtMTP2* expression. The size of plants was reduced in the auxin treatments which may have contributed to the drop in reported luciferase activity, which was not taken into account here. A future experiment using a lower concentration of auxin could be used to elicit an auxin transcriptional response without the associated reduction in size. In addition, long term treatment with IAA and IAA-Ala such as this and in experiments in following chapters will lead to many indirect effects which could account here for any changes in expression. Furthermore, IAA and IAA-Ala will degrade in light

conditions over time further complicating this result and that of future chapters. In future experiments a more stable auxin analogue could be used such as 1-naphthalene acetic acid (NAA).

3.3 Discussion

In this study a luciferase-based reporter plant which responds specifically to Zn deficient conditions has been generated. Because the expression of luciferase is driven by an *AtMTP2* promotor, this reporter plant can be used to probe the components of the systemic Zn deficiency response along with other responses to control ER Zn import in *Arabidopsis*. The results of further work on the *AtMTP2*::*LUC* B4 line could provide useful information which would be used to help generate crops with higher Zn translocation into the shoot and into grains.

The expression of *AtMTP2* was found to be potentially regulated by many mechanisms with exogenous auxin leading to a reduction in *AtMTP2* expression in Zn deficient conditions. AtMTP2 activity is thought to increase Zn levels in the ER where conjugate hydrolases are localised[279-282], and high Zn levels lead to a reduction in auxin conjugate hydrolysis *in vitro*[281]. Therefore, AtMTP2 activity in Zn deficiency would reduce hydrolysis of auxin conjugates. However, with high levels of exogenous auxin or auxin conjugate, if reduction in *AtMTP2* expression results in a reduction in ER Zn levels, this would promote auxin hydrolysis over conjugation. A larger portion of the auxin pool would therefore exist in the active unconjugated form, creating a positive feedback loop. In contrast, previous work has shown that when supplied with exogenous auxin, *YUCCA* genes, responsible for the rate limiting step in auxin production are transcriptionally downregulated to reduce the active auxin pool[307,308] whilst genes for auxin conjugation and inactivation are upregulated[283]. Therefore, future work is required to establish whether *AtMTP2* expression correlates with ER Zn levels and auxin conjugate hydrolysis, such as through investigating the sensitivity of *Atmtp2* mutants to auxin conjugates. This further work may provide insights into the developmental changes associated with Zn deficiency and the role of auxin metabolism on Zn nutrition.

Chapter 4: IAR1 fundamentals: Transport, Localisation and Expression

4.1 Introduction

4.1.1 *AtIAR1* was found to influence auxin conjugate hydrolysis

Indole-3-acetic acid (IAA, auxin) is a major plant hormone involved in many developmental processes in plants. The concentration of auxin is controlled by many factors including biosynthesis, transport, degradation, and conjugation (see **Chapter 1.3** for more details).

Conjugation of auxin to inactive conjugates is an evolutionarily conserved mechanism of controlling the concentration of IAA[370]. One of these conjugate groups are IAA-amino acid conjugates (IAA-aas). The enzymatic conjugation to IAA-aa in some cases is reversible through hydrolysis which is governed by hydrolases with different substrate specificities[281] and appears to take place in the endoplasmic reticulum (ER)[279-282]. These hydrolase enzymes are metalloenzymes and have their activity enhanced by availability of Mn^{2+} ions[279,281]. Other divalent ions such as Zn^{2+} or Cu^{2+} compete with Mn^{2+} for these binding sites and thus bring about inhibition of these enzymes *in vitro*[281].

In a screen for genes involved in hydrolysis of IAA-aa conjugates, *Arabidopsis* mutants were isolated that showed insensitivity to the growth inhibitory effect of exogenous IAA-alanine (IAA-Ala). The growth inhibitory effect of IAA-Ala is due to the hydrolysis of inactive IAA-Ala to active IAA and so sensitivity to IAA-Ala derives from IAA-Ala hydrolysis and IAA sensitivity. From this screen, mutants in the gene *AtIAR1* (*IAA-Ala resistance1*) were found[328] which were relatively insensitive to IAA-Ala but remained sensitive to IAA. *AtIAR1* was found to be a member of the ZRT, IRT-like Protein (ZIP) family, a ubiquitous family of metal transporters that transport metal ions into the cytosol[64].

4.1.2 AtIAR1 is likely an ER and/or Golgi-based Zn transporter

Several pieces of existing evidence point to AtIAR1 functioning as a Zn transporter localised to the secretory pathway. Firstly, the auxin conjugate hydrolases, which AtIAR1 is thought to influence, are present within the ER[279-282] and are inhibited by Zn[281]. The phenotypes of the *Atiar1-1* and *Atiar1-2* mutants found in the screen were also complemented by excess Mn[328] which is thought to compete with the Zn^{2+} for hydrolase binding sites. The *Atiar1-3* mutant, which has a frameshift mutation at the end of the *AtIAR1* coding region, has its phenotype compensated by additional mutations in *AtMTP5*, a member of the Zn-Cation Diffusion Facilitator (CDF) transporter family responsible for metal transport out of the cytosol[1].

Interestingly, AtMTP5 was later confirmed to have one splice variant localised to the Golgi, and showed Zn transporting activity only when in a complex with *cis*-Golgi-localised AtMTP12[89]. Both human and mouse ZIP7 have been shown to be localised to the ER[371] as well as the Golgi apparatus and both transport Zn into the cytosol[335]. In addition, DmCatsup[372] has been shown also to transport Zn out of the secretory pathway into the cytosol. Interestingly, ScYke4 is thought to transport Zn bidirectionally between the ER and cytosol[336]. However, this bidirectional nature of transport has yet to be identified directly in other homologues. Altogether, this evidence was used to generate a model of AtIAR1 activity shown below in **Figure 4.1**.

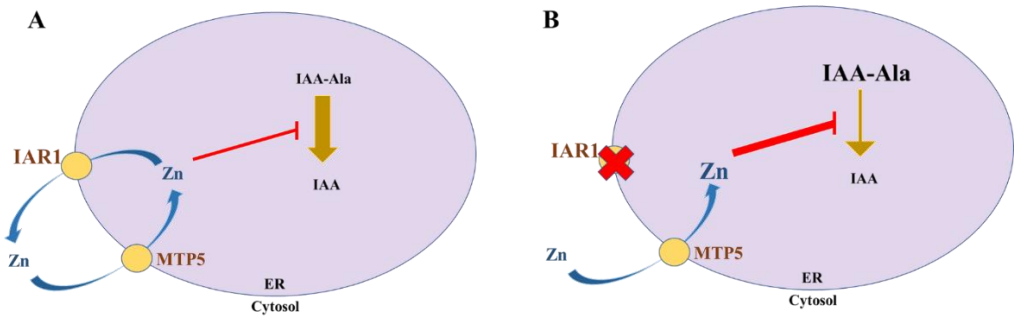

Figure 4.1 Adapted Rampey et al, 2013[1] model on metal transport in the ER and IAA-Ala hydrolysis in wildtype and *Atiar1* mutant plants. (A) *AtMTP5* and *AtIAR1* antagonistically control levels of metals including Zn in the ER which then controls the activity of IAA-Ala hydrolases. (B) *Atiar1* mutants lose Zn transport activity, causing ER Zn levels to increase which inhibits IAA-Ala hydrolases. Model adapted with permission to focus on Zn as the inhibitory cation.

Confirming the fundamentals of this model is vital for clarifying the interaction between metal ions and auxin metabolism. Therefore, this study will focus on AtIAR1 transport activity, localisation and expression, as well as how the mutations within the *Atiar1-3* mutant from Lasswell et al.[328] affect these features. The *Atiar1-3* mutant was chosen as its phenotype was complemented by *AtMTP5* mutations and represents the only *AtIAR1* mutant in a Col-0 background without deletion of neighbouring genes (as in *Atiar1-4*).

4.2 Results

4.2.1 *AtIAR1* is a LIV-1 subfamily member of the ZIP family

The transport activity and localisation of ZIPs varies across the family. For example, ScYKE4 transports Zn^{2+} out of the cytosol from the ER[336], AtZIP1 is responsible for Mn^{2+} mobilisation from the vacuole[68] and the AtIRT1 protein can import extracellular Fe^{2+} along with other divalent metals[67]. Phylogenetic analysis of ZIP transporters was key to understanding the role of AtIAR1 in auxin conjugate hydrolysis. Looking to the closest characterised homologue of *AtIAR1* was therefore a useful starting point to investigate functionality. The phylogeny of the ZIP family including members from the plant, animal and fungal kingdoms is illustrated below in **Figure 4.2**.

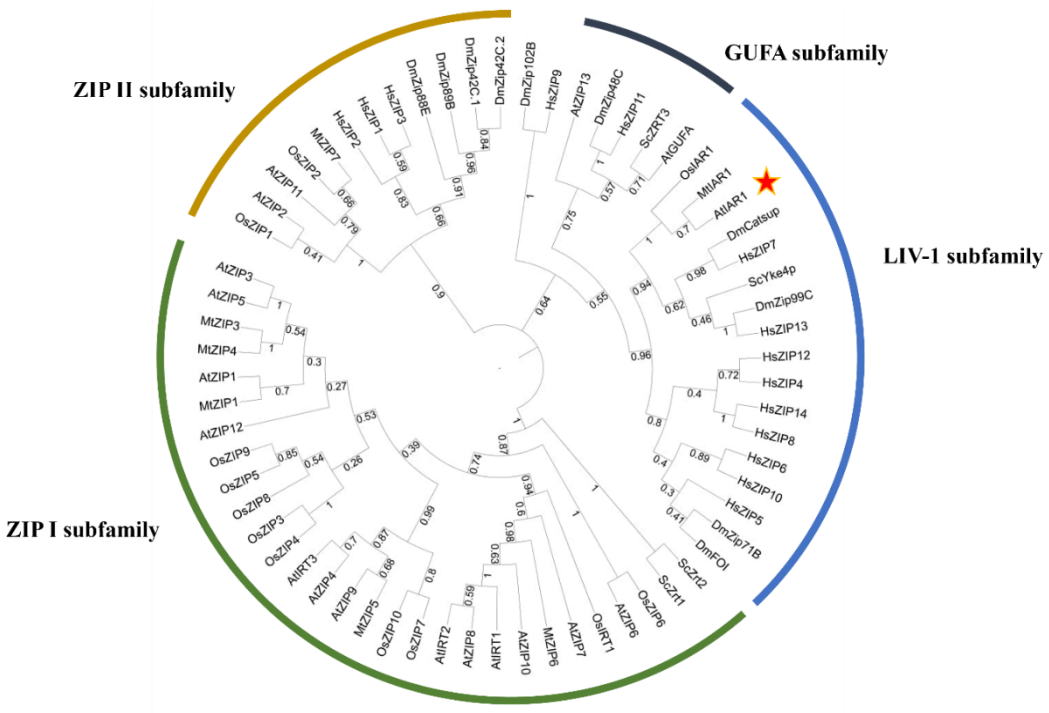

Figure 4.2 Phylogenetic analysis of the ZIP family. *AtIAR1* is indicated by the red star. Sequences taken from within animal (*Drosophila melanogaster* and *Homo sapiens*), plant (*Arabidopsis thaliana*, *Oryza sativa* and *Medicago truncatula*) and fungal (*Saccharomyces cerevisiae*) kingdoms. Sequences were aligned using MUSCLE [353] and phylogeny calculated within the MEGA-X software[352] with the Maximum Likelihood method and Jones-Taylor-Thornton (JTT) matrix-based model[354]. To model different evolutionary rates a gamma distribution of 5 categories was used. The phylogenetic tree was then constructed from 100 bootstrap replicates and initial trees using BioNJ and Neighbour-Join algorithms on the JTT-generated matrix. Numbers by branches show bootstrap support values. As seen in previous analyses, *HsZIP9* does not fit easily into any of the four subfamilies[373], but is classed as being part of the ZIP I subfamily[374].

The ZIP family can be split into four subfamilies[375] with *AtIAR1* found in the LIV-1 subfamily. The closest characterised homologues within this subfamily are human and mouse *ZIP7*, *DmCatsup* and *ScYke4*. Constitutive expression of the mouse homologue *MmZIP7* in *Atiar1* mutants restored IAA-Ala sensitivity[328], and in *ScYKE4* mutants restored calcofluor white resistance[336] suggesting that AtIAR1 and its homologues show a high degree of conservation of function across kingdoms.

4.2.2 Transport

Crucial to the model of AtIAR1 activity is its ability to transport inhibitory metals including Zn out of the ER into the cytosol. Several ZIP transporters are known to transport many divalent metals with varying levels of specificity such as AtIRT1[67], which can transport Fe^{2+} but also Mn^{2+} and Zn^{2+}. Given that auxin conjugate hydrolysis relies on Mn-dependant enzymes and is thought to be inhibited by Zn ions[281], the metal transport specificity of AtIAR1 is vital to understand. In addition, potential bidirectional transport has been demonstrated in the yeast homologue[336] which adds a potential additional layer of complexity to the interaction of Zn and auxin in the model. For both these points, yeast mutant complementation provides an ideal tool for assessing protein functionality.

4.2.2.1 *AtIAR1* and *Atiar1-3* expression complements *yke4*Δ phenotype

It has already been demonstrated that the mouse homologue *MmZIP7* gene, when constitutively expressed, can fully complement the *Atiar1-3* mutant phenotype[328] and the calcofluor sensitivity phenotype of the yeast *yke4*Δ mutant strain[336]. The *yke4*Δ mutants show reduced growth on media containing calcofluor white which binds to cell wall components including chitin, causing cell wall stress, allowing screening for cell wall mutants[376]. This phenotype was complemented by growth on high Zn. As such the cell wall defects were hypothesised to be caused by metal dyshomeostasis in the secretory system, from lack of Zn transport into the ER, thus representing a direction of transport so far not seen in other homologues. Expression of the *MmZIP7* gene was able to complement *yke4*Δ[336], but MmZIP7 has only been shown to transport Zn out of the secretory system in mice[335,377] therefore casting doubt on whether *yke4*Δ complementation is an accurate indicator of Zn transport into the secretory system.

Complementation of the yeast *yke4*Δ strain with the wildtype *AtIAR1* gene and the mutated *Atiar1-3* gene has not been performed. To test whether expression of *AtIAR1* or *Atiar1-3* could functionally restore metal homeostasis in *yke4*Δ mutants, and therefore indicate possible bidirectional transport of AtIAR1, *AtIAR1* and *Atiar1-3* heterologous expression plasmids were constructed and transformed into *yke4*Δ mutants (see **Chapter 2.1**).

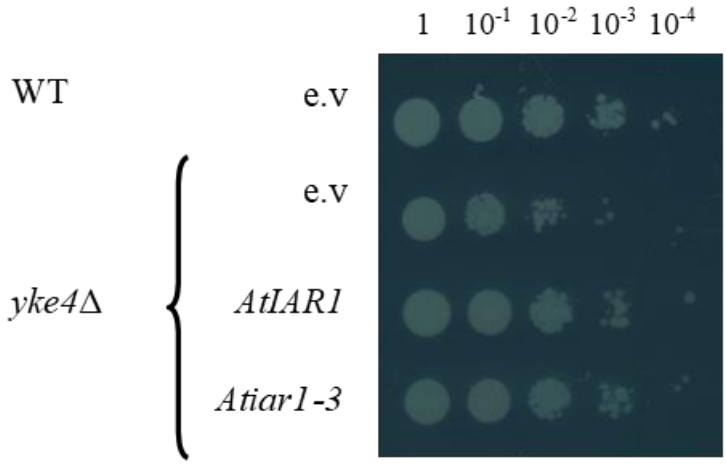

Figure 4.3 *AtIAR1* and *Atiar1-3* expression complements *yke4*Δ strain. Serial 10-fold dilutions (left to right) of transformed yeast cultures were pipetted onto media containing 20 µg/ml calcofluor white and 10 µg/ml evans blue dye. Wildtype (WT) or *yke4Δ* mutant strains sensitive to calcofluor white were transformed with e.v (empty vector), *AtIAR1* or *Atiar1-3* recombinant plasmids. Image shown from an experiment that was representative of 3 biological repeats.

Expression of both the *AtIAR1* and *Atiar1-3* genes complements the *yke4*Δ phenotype on calcofluor white-containing plates. It is surprising that in yeast both versions of the *AtIAR1* gene are functional, which is in contrast to the model, where Atiar1-3 proteins should be incapable of Zn transport. Further work may include changing conditions to increase the severity of the *yke4*Δ phenotype to show this complementation more clearly. As this experiment provided only a single form of assessment of metal transport capabilities, it was therefore important to expand the

complementation assays to include more measurements of transport activity into the cytosol.

4.2.2.2 AtIAR1 can transport Zn but not Fe or Mn

Complementation of yeast strains incapable of importing metals is a commonly used method for assessing the metal transport capabilities of plant ZIP proteins including from *Arabidopsis*[68], *Medicago*[378] and *Poncirus*[379] species. Therefore, a collection of strains incapable of importing Zn^{2+}, Mn^{2+} and Fe^{2+} was transformed with *AtIAR1*-based constructs. The transformed strains were then assessed for their growth on Zn, Mn or Fe restrictive media as described in **Chapter 2.1.** The complementation of the Zn import mutant strain *zrt1Δ zrt2Δ* with *AtIAR1* has previously failed[328] which was reasoned to be because of poor trafficking of the predicted ER-localised AtIAR1 to the plasma membrane to allow Zn uptake. Therefore, in the present study the signal peptide of AtIRT1 was swapped for that of AtIAR1 in some of the constructs to allow increased trafficking to the plasma membrane, as occurred for the ER-localised AtZIP29 protein[80]. The ability of the AtIRT1 signal peptide to traffic AtIAR1 successfully from the secretory pathway was seen by the loss of *yke4*Δ complementation when the swapped constructs were expressed (data not shown). Additionally, the constructs in this study used codon optimised sequences to reduce the likelihood of low expression of the constructs.

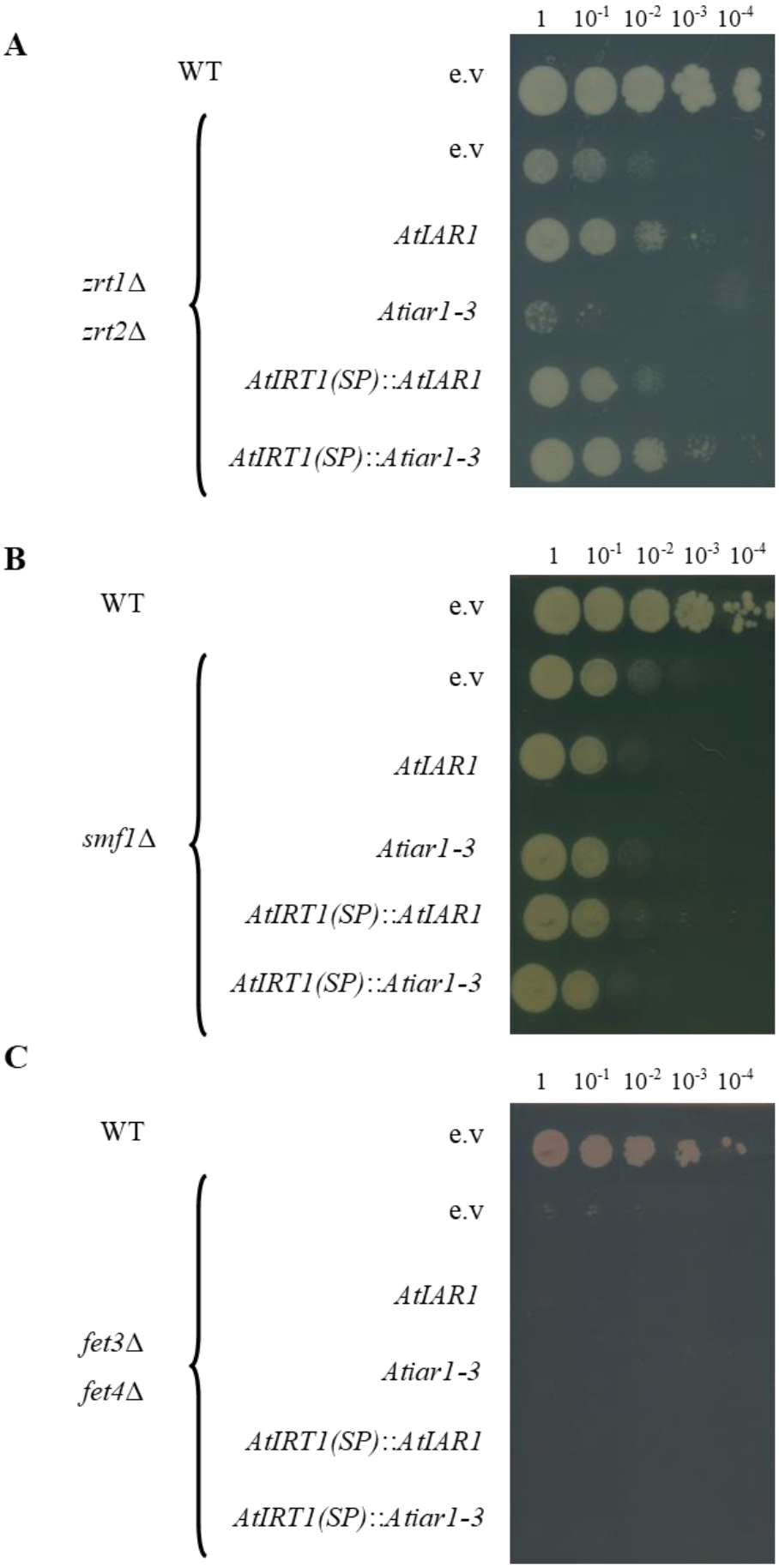
A
1 10-1 10-2 10-3 10-4
WT
e.v
e.v
AtIAR1
zrt1Δ
zrt2Δ
Atiar1-3
AtIRT1(SP)::AtIAR1
AtIRT1(SP)::Atiar1-3
B
1 10-1 10-2 10-3 10-4
WT
e.v
e.v
AtIAR1
smf1Δ
Atiar1-3
AtIRT1(SP)::AtIAR1
AtIRT1(SP)::Atiar1-3
C
1 10-1 10-2 10-3 10-4
WT
e.v
e.v
AtIAR1
fet3Δ
fet4Δ
Atiar1-3
AtIRT1(SP)::AtIAR1
AtIRT1(SP)::Atiar1-3

Figure 4.4 Complementation of metal import mutants by *AtIAR1* constructs. Serial 10-fold dilutions (left to right) of transformed yeast cultures were pipetted onto restrictive media. Wildtype (WT) or mutant strains defective in the import of Zn (*zrt1Δ zrt2Δ*), Mn (*smf1Δ*), Fe (*fet3Δ fet4Δ*) were transformed with e.v (empty vector), *AtIAR1*, *Atiar1-3*, *AtIRT1(SP)*::*AtIAR1* (signal peptide sequence swapped for that of AtIRT1), and *AtIRT1(SP)*::*Atiar1-3*. Transformed strains were then grown on (A) Zn-restrictive media, (B) Mn-restrictive media or (C) Fe-restrictive media. Images shown from experiments that were representative of 3 biological repeats.

As **Figure 4.4** shows, the *AtIAR1* construct lacks the ability to complement the Mn and Fe uptake mutants, while being able to partially complement the Zn uptake mutant, which was not seen in previous studies[328] and implies AtIAR1 shows specific transport activity for Zn as predicted. The increased trafficking of AtIAR1 proteins to the plasma membrane by signal peptide swapping with AtIRT1 led to a decrease in complementation which was unexpected and suggests that potentially the swapped signal peptide may be interfering with Zn transport activity in this instance. Transformation with the *Atiar1-3* construct did not lead to complementation, unlike in transformations with *AtIRT1*(SP)::*Atiar1-3* constructs. Given that plasma membrane expression is required to complement the *zrt1*Δ *zrt2*Δ strain, this suggests that Atiar1-3 may be incapable of being trafficked to the plasma membrane without the AtIRT1 signal peptide. Additionally, AtIRT1(SP)::Atiar1-3 may in fact have higher Zn transport activity than AtIRT1(SP)::AtIAR1, as shown by the more complete complementation. This suggests the interference of Zn transport seen in AtIRT1(SP)::AtIAR1 does not occur in AtIRT1(SP)::Atiar1-3. Further work to confirm these results could involve expression in *Xenopus* oocytes, followed by measurements of cation uptake.

Translation of this work in *Arabidopsis* to other plant species of interest, including agricultural crops, is important to establish how widespread this link between Zn transport and auxin metabolism is. Therefore, the conservation of structural features

thought to be important in metal transport across IAR1 homologues in eukaryotes were examined.

4.2.2.3 AtIAR1 plant homologues show similar transport-related structural features

Conservation of structural features is an indication of shared function. This property was used to give insights to transporter activity on AtIAR1 homologues across eukaryotes. AtIAR1 is predicted to be a transmembrane protein with 8 transmembrane helices (see **Figure 4.5**) with histidine (H) rich segments in loops either side of the membrane including on the 'variable loop' between helices α3 and 4.

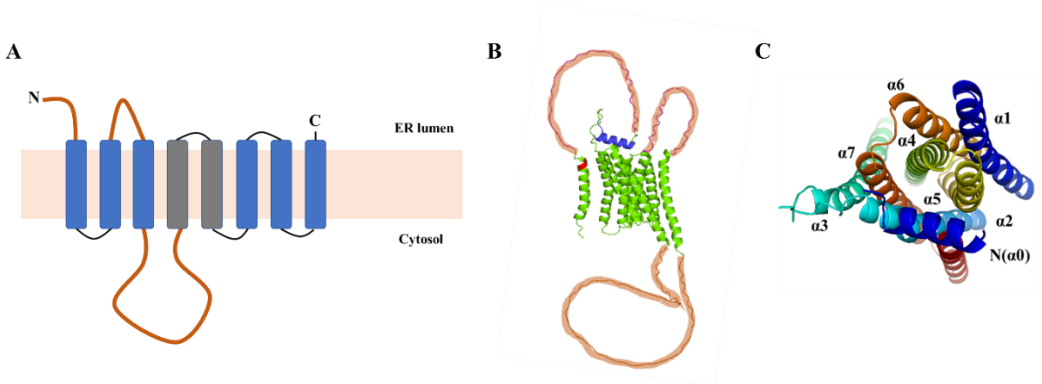

Figure 4.5 AtIAR1 protein topology and predicted structure. (A) ZIP transporter structural model adapted from Guerinot.[64] with histidine rich loops in orange and helices with conserved metal transport residues in grey. (B) AlphaFold[355] structural model of AtIAR1 with signal peptide cleavage site as predicted by SignalP-5.0[339] in red, histidine (H) containing extracellular loops shaded orange, and acidic N(α0) helix shaded blue. (C) Top-down view from 'extracellular' side of AlphaFold model of AtIAR1. Helices labelled α0 to α8, N to C terminal, blue to red, removing signal peptide for clarity.

Key features of this structure with respect to metal binding include the highly conserved sequences within helices α4 and α5 and the H-rich loops. Crystal structures of a bacterial ZIP protein, BbZIP, showed that residues from α4 and α5 contribute together to form two sites for binding metals within the protein during transport[356]. Conservation of these residues in the binuclear site and surrounding residues may indicate the same transport metal selectivity and mechanism and so equivalent sequences in AtIAR1 homologues across a spectrum of eukaryotes were aligned against those found in the crystal structure of BbZIP (**Figure 4.6**).

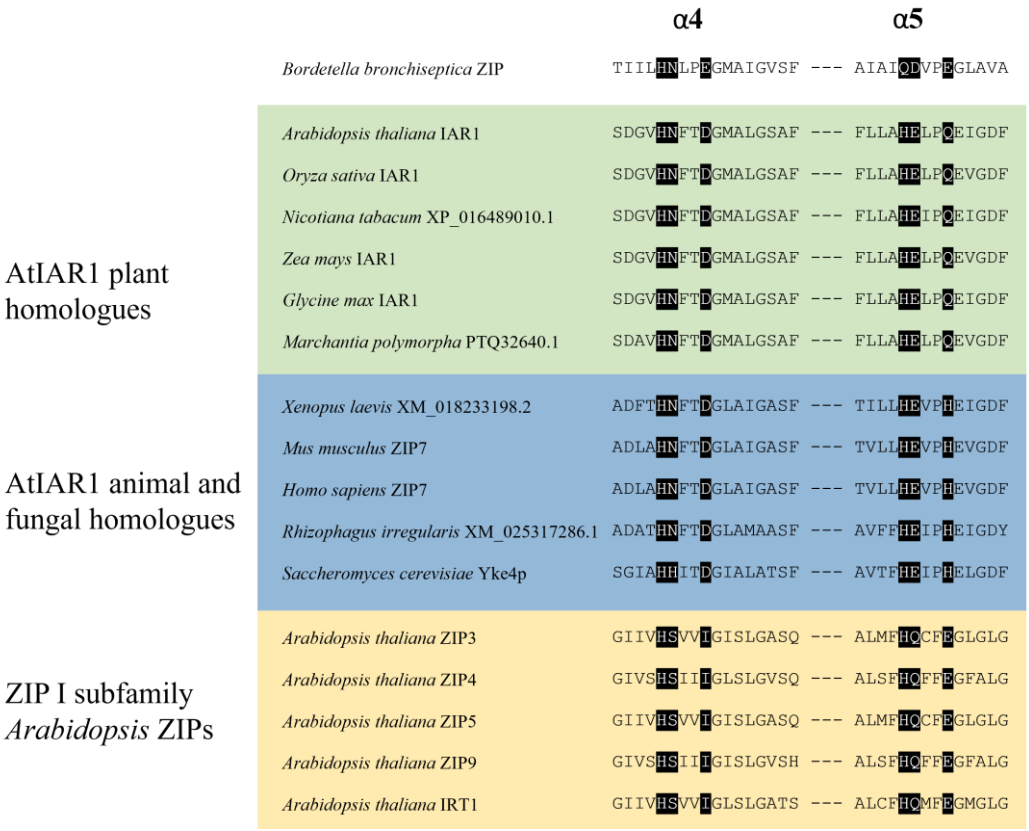

Figure 4.6 Conservation of equivalent metal-contacting residues present in BbZIP crystal structure. Sequences within helices α4 and 5 were taken from AtIAR1 homologues in plants (green), animal and fungi (blue) as well as from the ZIP I subfamily (yellow) and aligned against residues within the binuclear site seen the crystal structure of BbZIP[356]. Residues in direct contact to the transporting metal and the equivalents in the chosen ZIP transporters are highlighted in black.

As shown above, the residues that might contact the metal in AtIAR1 are not identical but similar to those of BbZIP. Within the α4 helix, the contacting residues are highly similar with E substituted with D, and the wider surrounding residues are not identical but again biochemically similar. A possibly significant difference is the change of the LP residues between the contacting residues to FT, which may lack the inflexibility that proline provides and therefore may indicate a slight difference in conformational changes during transport between AtIAR1 and BbZIP.

Residues in the α4 and α5 helices are highly conserved in AtIAR1 plant homologues, with the residues predicted to contact transporting metals being 100% conserved. In addition, surrounding residues on these helices are biochemically similar which implies a similar metal binding site and transport mechanism, suggesting that the metal transport activity observed for AtIAR1 is representative of other plant AtIAR1 homologues.

Interestingly, this conservation of predicted metal contacting residues extends into homologues in the animal and fungal kingdom for the α4 but not the α5 helices. The change from Q to H in the α5 residues may lead to a change in transport activity and so functional characterisation of mammalian or yeast AtIAR1 homologues may not be an accurate estimation for plant homologues. The conservation of putative transported metal-binding residues is higher among plant IAR1 homologues and animal or fungal IAR1 homologues than with *Arabidopsis* ZIP I subfamily transporters. This further emphasises the point that *Arabidopsis* AtIAR1 is more closely related to LIV-1 subfamily members in the animal and fungal kingdom than to other ZIPs within *Arabidopsis*.

In addition to the residues within the transport channel, metal binding loops also may act as transport selectivity determinants by acting as a chaperone, transporting Zn to the transport channel such as in the case of a H rich loop in HvMTP1[337]. In the AtIRT1 protein, another H-rich motif in the 'variable loop' which faces the cytosolic side of the plasma membrane acts as a sensor for Zn^{2+} and Mn^{2+} ions to promote endocytosis of the transporter[124]. The metal binding activity of loops within AtIAR1 and its homologues may therefore play a role both in metal transport but also metal sensing and localisation changes. Sequences for these loop regions

were therefore extracted for AtIAR1 homologues in the plant, animal and fungal kingdom as well as ZIP transporters from the ZIP I subfamily. As histidine is the major metal binding residue used by ZIP transporters, these loops were then analysed for histidine content as shown in **Figure 4.7**.

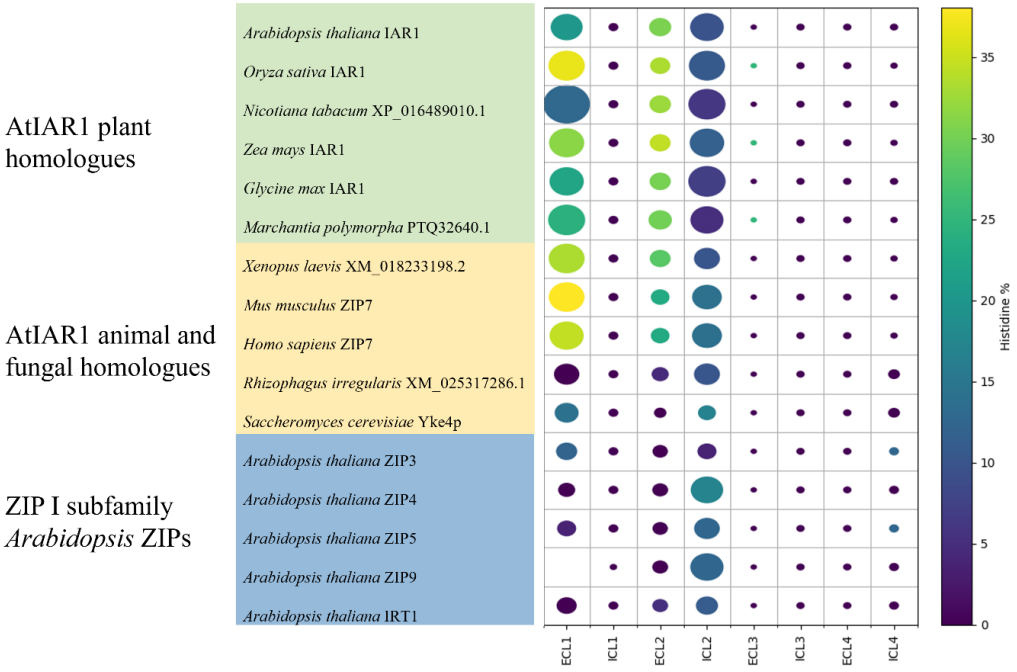

Figure 4.7. Histidine density of loops is similar in AtIAR1 homologues in plants and animals. Loops are classified by their direction of facing if present on the plasma membrane, either extracellular, (ECL) or intracellular (ICL) and numbered from N-terminal to C-terminal. Histidine density is shown by colour and loop size is indicated by diameter of the dot. Data visualised using Python 3.

As shown in **Figure 4.7**, large H-rich loops predicted to face into the ER/Golgi lumen (ECL1 and ECL2) are present in all AtIAR1 homologues in plants and animals. In addition, ICL2 (the 'variable loop') is consistently larger than other loops in AtIAR1 plant and animal homologues. It is interesting to note that the size and histidine density decreases in the two fungal homologues, suggesting a change in metal binding and potentially transport activity regulation. This could be

explored further and confirmed by expanding this analysis to include more samples from the fungal kingdom. Comparing AtIAR1 homologues in plants and animals to ZIP I subfamily members, the large 'variable loop' is a common feature but H-richness in ECL1 and 2 is distinct to the AtIAR1 homologues. This implies a role of metal sensing or binding in the luminal side of IAR1 which is lacking in the sample of ZIP I subfamily chosen.

Taken together, the conservation of metal binding residues within the transport metal-binding site and within surrounding loops on both sides of the membrane suggest plant IAR1 homologues will transport and interact with metals similarly to AtIAR1 and so transport Zn between the secretory pathway and the cytosol. It is possible that the metal binding loops facilitate Zn sensing and so control some aspect of this Zn transport. In comparison to the conservation of histidine density in the loop regions, it appears that there are small differences in the binuclear metal site between animal and plant IAR1 homologues, which could influence transport mechanics.

Future work on metal transport could include testing the complementation of yeast transporter mutants with *AtIAR1* constructs containing mutated sequences for loop regions or binuclear metal binding sites. This would enable the testing of hypotheses that these regions are determining factors in metal transport specificity and directionality. For the current model on AtIAR1 function, the Zn ion transported is from ER to the cytosol, and so localisation of AtIAR1 and its homologues were tested.

4.2.3 Localisation

The subcellular localisation of AtIAR1 is important for confirming the role of AtIAR1 in auxin conjugate hydrolysis, and as yet has not been directly verified. In addition, the localisation of other plant AtIAR1 homologues is potentially different where mutant data on IAA-Ala sensitivity is unknown, which would lead to changes in the predicted role of the gene in Zn-auxin interactions. The localisation

was therefore investigated with a green fluorescent protein (GFP) tagging approach and a bioinformatic approach.

4.2.3.1 *AtIAR1*::*GFP* complementation lines did not yield observable GFP fluorescence

GFP tagging is a method that can be utilised to visualise subcellular localisation of proteins where GFP is expressed fused to the protein of interest[380]. In the cloning of GFP-tagged membrane proteins, GFP presence can result in non-functional proteins due to misfolding or interruption of functional sites. To reduce the likelihood of interruption, in this study GFP was cloned with surrounding G-rich flexible linkers (see **Chapter 2.2.2.3**) and was designed to be inserted separately into three areas. The GFP insertion sites were the N-terminus after a predicted signal peptide cleavage site, within ICL3 and at the C-terminus. Previous GFP tagging of AtIRT1 utilised ECL1 to insert GFP into[123], but as outlined above, ECL1 has conserved metal binding properties and so was thought unsuitable for GFP insertion. GFP constructs were then transformed into *Atiar1-3* plants as detailed in **Chapter 2.2.5** and a total of nine independently transformed lines were subsequently checked for complementation by measuring the insensitivity to IAA-Ala as shown in **Figure 4.8**.

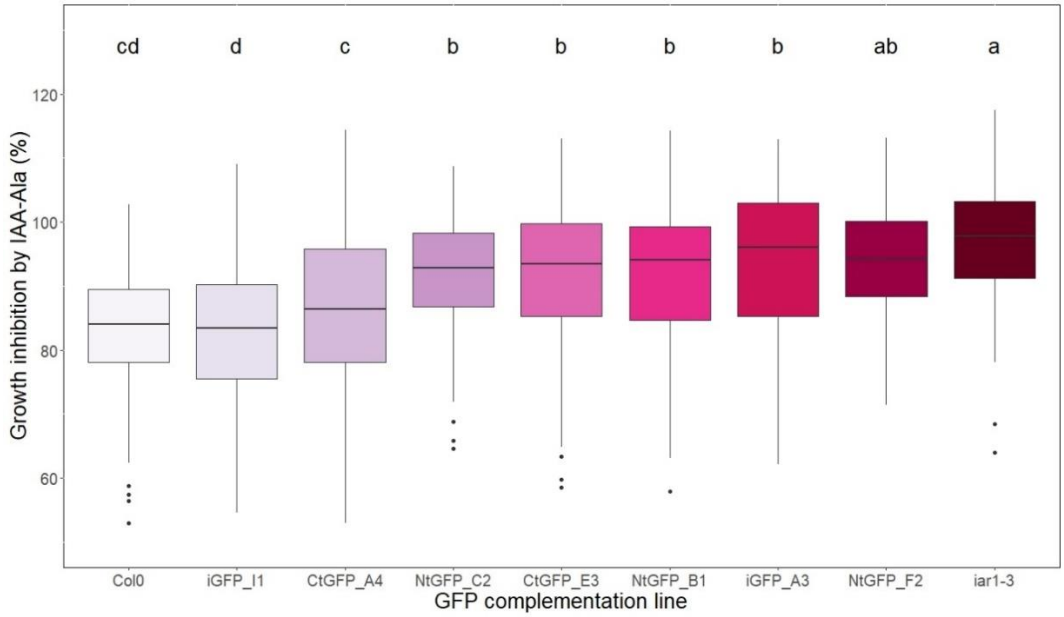

Figure 4.8 GFP complementation lines show a range of complementation. Complementation lines from plants transformed with N-terminal tagged GFP (NtGFP), ICL3-tagged GFP (iGFP) and C-terminal-tagged GFP (CtGFP) constructs arranged from lowest percentage growth in IAA-Ala conditions to highest. Percentage growth determined as root length in media with IAA-Ala relative to mean root length in media without IAA-Ala. Three independent sets of at least 50 homozygous T3 plants were analysed for each condition, with data displayed using R version 4.1.1. Lower case lettering indicates statistically significant differences between groups (labelled sequentially from 'a' in order of estimated mean) as calculated using analysis of variance (ANOVA) using Tukey's method for p-value adjustment[366] for 9 groups using a p-value cut-off of 0.05.

As shown in **Figure 4.8** a range of complementation from no complementation (NtGFP_F2 line) to full complementation (iGFP_I1 line) was seen. The complementation level did not seem to be correlated with the placement of the GFP within AtIAR1 and so was therefore thought to be due to expression levels, which in future could be checked using reverse transcriptase quantitative PCR (RT-qPCR). iGFP_I1 and CtGFP_A4 lines displayed the strongest complementation but showed no GFP fluorescence above background and so could not be used for

subcellular localisation. Future work could involve testing more conditions which induce *AtIAR1* to a higher level or antibody-mediated detection of GFP which may increase signal to noise ratio.

4.2.3.2 AtIAR1 and the majority of the plant AtIAR1 homologues are predicted to have ER or Golgi localisation

In addition to GFP tagging, software has been developed to predict subcellular localisation of proteins. Prediction software is particularly useful here as it allows quick screening of AtIAR1 homologues for putative localisation. Software was chosen based on ability to accurately predict localisation of plant ZIPs with experimentally verified localisation. The software chosen was PProwler v1.2[357], TargetP v2.0[358] and DeepLoc v2[359] which all use neural networks to predict localisation. PProwler v1.2 is built upon the original TargetP software[381] which predicts localisation based on the N-terminal sequence, to the secretory pathway, mitochondria, or chloroplast with everything else classed as 'other'. TargetP v2.0, unlike PProwler v1.2 and DeepLoc v2 can also predict thylakoid luminal transit peptides and DeepLoc v2 enables further distinctions such as between ER and Golgi localisation. Comparing localisation predictions from these three software packages together in **Figure 4.9** allows for a more accurate prediction of localisation of AtIAR1 and its homologues.

Figure 4.9 Most plant AtIAR1 homologues are predicted to localise to the secretory pathway. Red asterisk denotes AtIAR1. Probability of localisation prediction is shown by colour. 'OTHER' contains either non-identifiable signal peptides in the case of TargetP v2 or 'other' localisation predicted in the case of DeepLoc v2 or PProwler v1.2. The 'Mitochondria' group contains predictions for presence of a mitochondrial targeting peptide by TargetP v2 and PProwler v1.2 as well as mitochondrial localisation predicted by DeepLoc v2. The 'Chloroplast' group contains the summed probability of TargetP v2 predicting a chloroplast transit peptide and a thylakoid luminal transit peptide, the probability of a chloroplast transit peptide by PProwler v1.2 and chloroplastic localisation by DeepLoc v2.

All localisation software tested showed AtIAR1 and many AtIAR1 homologues to have ER or secretory pathway localisation as the highest probability. DeepLoc v2 interestingly suggested lysosome, Golgi apparatus and cell membrane as most likely localisations after ER (probability of 0.62, 0.47 and 0.38 respectively), but it should be noted that lysosome localisation was predicted with high probability (greater than 0.5) for many test ZIP proteins which have not shown lysosome localisation measured *in vivo*. Together this supports the localisation of IAR1 to the ER but potentially suggests some additional localisation including the plasma membrane and Golgi. Interestingly, outliers in the foregoing analysis were for

AtIAR1 homologues within *Solanum tuberosum* and *Nicotiana tabacum*. These sequences were identified to have a thylakoid luminal transit peptide by TargetP v2, a mitochondrial targeting peptide by PProwler v1.2, and ER localisation by DeepLoc v2. To further investigate this, a higher resolution sampling of the *Solanaceae* family and closely related families was undertaken as shown in **Figure 4.10** below.

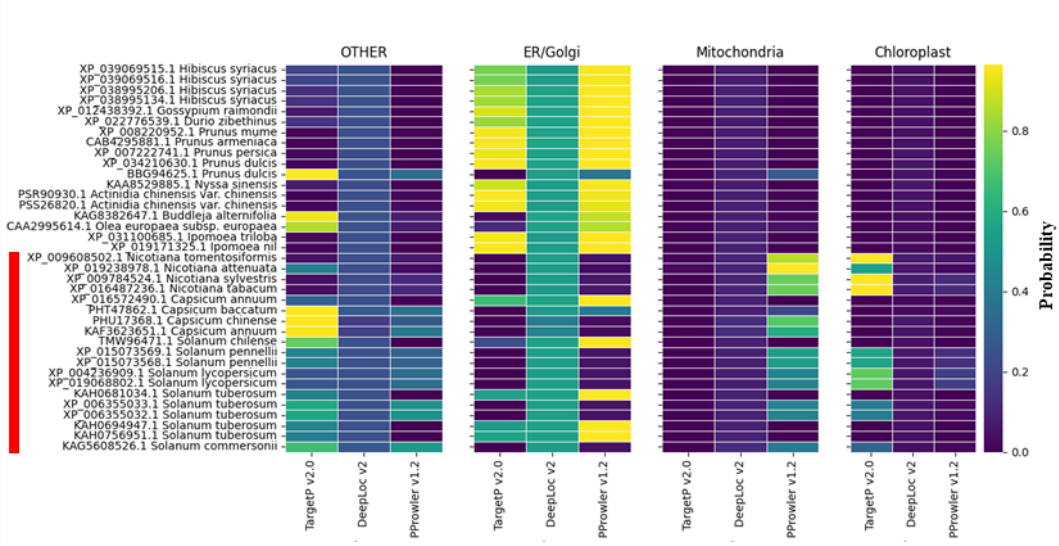

Figure 4.10 AtIAR1 homologues in many *Solanaceae* species are predicted to localise outside the secretory pathway. *Solanaceae* family members are indicated by the red bar. Predictions of localisation are shown by colour. 'OTHER' contains either non-identifiable signal peptide in the case of TargetP v2 or other localisations predicted such as in the case of DeepLoc v2 or PProwler v1.2. The 'Mitochondria' group contains predictions for presence of a mitochondrial targeting peptide by TargetP v2 and PProwler v1.2 and mitochondrial localisation predicted by DeepLoc v2. The 'Chloroplast' group contains the accumulated probability of TargetP v2 predicting a chloroplast transit peptide and a thylakoid luminal transit peptide, the probability of a chloroplast transit peptide by PProwler v1.2 and chloroplast localisation by DeepLoc v2.

As **Figure 4.10** illustrates, both TargetP v2 and PProwler v1.2 software consistently predict different non-secretory pathway localisations for AtIAR1 homologues specifically within the *Solanaceae* family. In many cases, such as in the commercially important *Nicotiana tabacum*, this AtIAR1 homologue is the only AtIAR1 homologue present and so this potential altered localisation has not occurred through duplication and neofunctionalization. TargetP v2 is the only software utilised that can accurately predict thylakoid luminal transit peptides which may be a contributing factor to why these predictions are different. In addition, PProwler v1.2 was developed much earlier than TargetP v2 and DeepLoc v2 and so used a much different training set which could have led to altered prediction. Confirming the localisation of IAR1 proteins in these species and the associated IAA conjugate sensitivity in *iar1* mutants is important for testing whether this changed localisation represents a shift in the Zn-auxin interaction landscape in these species.

Overall, localisation of AtIAR1 is most likely to be present in the ER or Golgi, potentially both, and this is consistent across the plant kingdom apart from *Solanaceae* family members which may exhibit alternate localisations. Therefore, the evidence suggests that the localisation part of the model for AtIAR1 function is partially accurate on a cellular level. However, to expand the model from the cellular level to the level of tissues and organs, understanding how *AtIAR1* is regulated at a whole plant level is required. The first step of this investigation was to assess what regulates the expression of *AtIAR1*.

4.2.4 Expression

Auxin synthesis and action are dynamically regulated and spatially separated by transporters which create auxin gradients in tissues and organs to produce developmental responses (see **Chapter 1.3.1**). The role of auxin conjugates and therefore *AtIAR1* could thus be location- and condition-dependant, which is not currently considered in the model of IAR1 activity. Therefore, to investigate what may be transcriptionally regulating *AtIAR1*, promotor analysis was conducted and

followed up with investigations of how Zn and auxin levels influence *AtIAR1* expression using qPCR and *AtIAR1* promotor controlled β-glucuronidase (GUS) reporter plants.

4.2.4.1 Promotor analysis of *AtIAR1* illustrates multiple potential inducers of expression

In silico analysis of the *AtIAR1* promotor for known transcription factor binding sites found that *AtIAR1* expression is likely responsive to a wide range of conditions. The promotor was found to contain elements for response to abscisic acid (AAGAA-motif), light (AE-box, GATA motif, I box, MRE, TCT motif), anaerobic conditions (ARE), low temperature (LTR), seed development (O2-site), general stress (STRE, TC-rich) and wounding (WRE3, WUN-box) (**Figure 4.11**). In addition, the promotor was found to contain myc and TGACG motifs that are important for binding of MYC and TGA transcription factors respectively which have varied roles. Some TGACG motifs have been known to be associated with expression in response to exogenous auxin[367] and heavy metals, including cadmium[368]. Given the potential interaction between Zn and auxin in the relation to *AtIAR1*, GUS reporter plants were analysed across conditions of varying Zn and auxin levels.

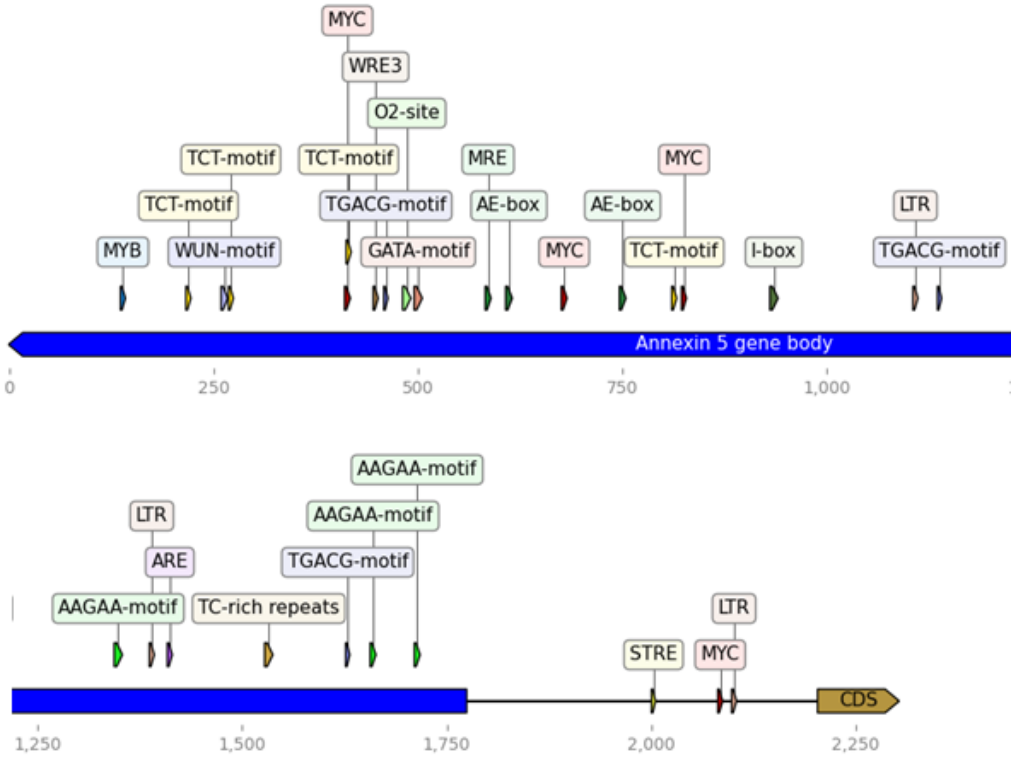

Figure 4.11 Promotor elements present in *AtIAR1* promotor. Promotor elements as identified by PlantCARE[361] from sequences upstream of the coding sequence (CDS). CAAT (common cis-acting element) and TATA-box (common core promotor region) annotations were removed for clarity. The Annexin 5 gene body highlighted represents AT1G68090, a gene involved in Ca-dependant membrane trafficking[382], which may have overlapping regulatory sequences with *AtIAR1*. Numbers indicate base pairs from 5' end of the promotor sequence used for generation of *AtIAR*1::*GUS* constructs.

4.2.4.2 *AtIAR1* expression is dependent on Zn, IAA and IAA-Ala

As AtIAR1 appears to operate as a Zn transporter important in auxin metabolism, and there are potential auxin and heavy metal stress responsive elements in the *AtIAR1* promotor, it was hypothesised that *AtIAR1* expression was regulated through both auxin and Zn levels. Promotor-controlled *GUS* expression has been

developed in plants as a common methodology for visualising the location of expression of a gene of interest[383]. The expressed GUS enzyme will cleave β-glucuronides including 5-Bromo-4-chloro-3-indolyl-β-D-glucuronic Acid (X-Glc) to produce an insoluble product[384] which can then be visualised by microscopy.

Firstly, to visualise where *AtIAR1* is expressed without any exogenous auxin added to the media, *AtIAR1*::*GUS* plasmids were generated and transformed into Col-0 *Arabidopsis* (see **Chapter 2.2.2.3**, and **Chapter 2.2.5** respectively). These reporter plants were then grown on three different Zn conditions determined to induce conditions of Zn deficiency, Zn-replete and Zn excess conditions which led to *GUS* expression as shown below in **Figure 4.12**.

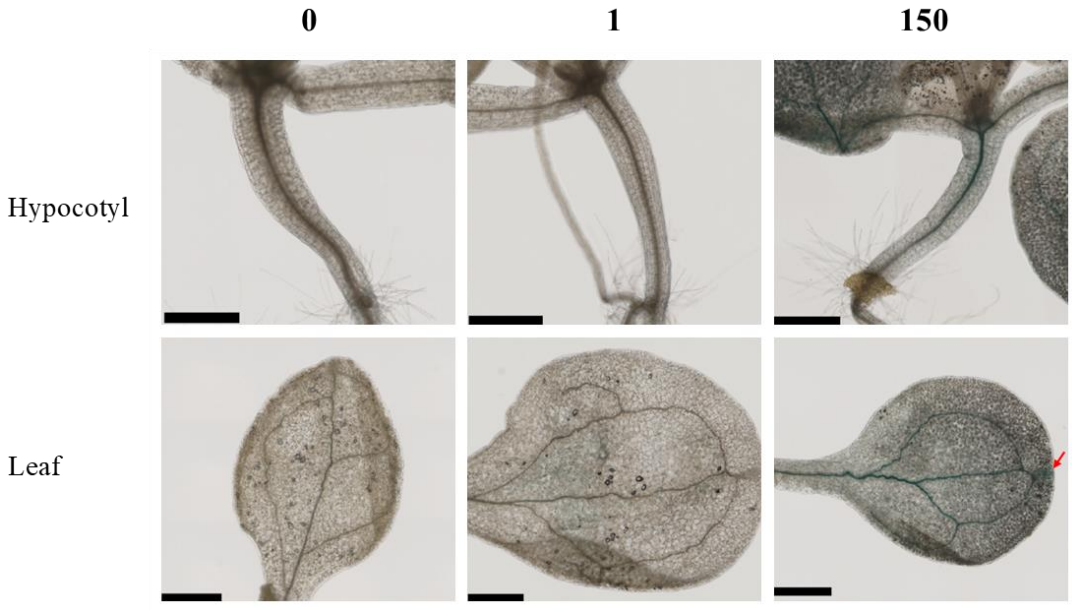

Figure 4.12 *AtIAR1*::*GUS* reporter plants show increased *GUS* expression in the hypocotyl and leaf under excess Zn. GUS reporter plants grown on modified Hoagland's media containing EDTA-washed agar, with either (left to right) 0 Zn added (deficiency), 1 µM Zn (control) or 150 µM Zn (excess). After 8 days of growth, whole seedlings were then stained overnight in X-Glc solution, and then cleared in 70% (v/v) ethanol for 8 h before imaging. Red arrow indicates small staining in leaf tip. Images represent the most common expression pattern achieved by 7 independently transformed homozygous T3 lines. Black scale bars indicate 500 µm.

As **Figure 4.12** illustrates, *GUS* expression visualised through staining is only seen in excess Zn conditions when no exogenous auxin is present. In particular, the leaf and hypocotyl vasculature show strong staining with some additional stain highlighted by the red arrow in the leaf tip. No staining was observed in the root. To investigate whether the Zn-dependant *GUS* expression seen above was responsive to exogenous auxin, the GUS reporter plants were grown on the same Zn conditions but additionally with IAA and IAA-Ala added (see **Figure 4.13**)

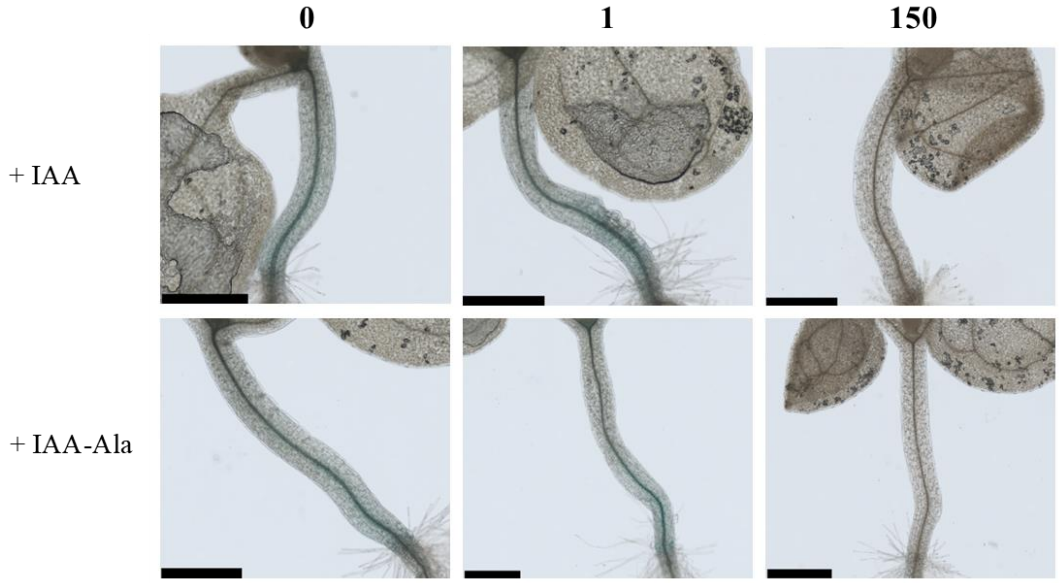

Figure 4.13 *AtIAR1*::*GUS* reporter plants show *GUS* expression in Zn deficient and control conditions with exogenous auxin. GUS reporter plants grown on modified Hoagland's media containing EDTA-washed agar, with either (left to right) 0 Zn added (deficiency), 1 µM Zn (control) or 150 µM Zn (excess) and either 100 nM IAA or 20 µM IAA-Ala. After 8 days of growth, whole seedlings were then stained overnight in X-Glc solution, and then cleared in 70% (v/v) ethanol for 8 h before imaging. Images represent the most common expression pattern achieved by 7 independently transformed homozygous T3 lines. Black scale bars indicate 500 µm.

The response of exogenous IAA and IAA-Ala was very similar which was as expected because IAA amide conjugates are inactive until hydrolysed to IAA. Staining was most prominently seen in the hypocotyl vasculature under control and Zn deficiency conditions, in contrast to "no auxin" treatment in **Figure 4.12**. Furthermore, there was no staining observed in either hypocotyl nor leaf vasculature under Zn excess conditions. As with the no auxin treatments, no staining was observed in the roots.

Confirmation of these *GUS* expression results can be assessed by qPCR. As **Figure 4.14** displays, due to highly variable expression of *AtIAR1* any difference in expression at high Zn is not statistically significant. In future work, this qPCR-mediated expression analysis could be expanded to include conditions with exogenous auxin and further repeated.

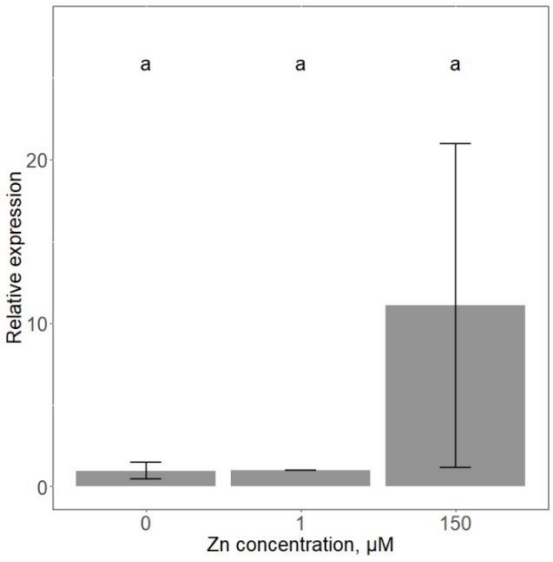

Figure 4.14 *AtIAR1* expression under different Zn conditions. RNA extracted from whole plants grown for 16 days in Zn deficient (0 Zn added), Zn control (1 µM) and Zn excess (150 µM) conditions on modified Hoagland's media containing EDTA-washed agar. Expression is calculated using the 2-ΔCt method[349], using internal reference genes of *AtUBC* and *AtTIP41*, and relative to the mean expression seen within control Zn conditions for each of three biological repetitions. Error bars show standard error of the mean. Data displayed using R version 4.1.1. Statistically significant differences between groups were calculated and displayed as in **Figure 4.8**.

In summary, promotor analysis appears to show that *AtIAR1* expression is regulated by a wide range of developmental and abiotic stimuli. Through the use of *AtIAR1*::*GUS* reporter plants, *AtIAR1* was shown to be induced in excess Zn conditions, but induced in Zn deficient and control conditions only if IAA or IAA-Ala is also present, suggesting Zn-auxin crosstalk in *AtIAR1* regulation. On a tissue level, *AtIAR1* expression was shown to be localised mostly to the vasculature in hypocotyls and leaves. This differential expression is not currently taken into consideration within the IAR1 model.

4.3 Discussion

The working IAR1 hypothesis by Rampey et al, 2013[1] has AtIAR1 localised to the ER, transporting metal ions inhibitory to IAA-aa hydrolases into the cytosol. In *AtIAR1* mutants including *Atiar1-3*, this Zn transport is lost and so leads to a build-up of ER Zn. Confirming the fundamentals of this model, and its applicability across different tissues and species is crucial to further understanding the AtIAR1-dependent Zn-auxin interaction.

4.3.1 AtIAR1 and plant homologues transport Zn

Heterologous expression of constructs containing *AtIAR1* and *AtIRT1*(SP):*AtIAR1* have been demonstrated in this study to complement the yeast Zn import mutant, *zrt1Δ zrt2Δ*, which indicates that AtIAR1 does transport Zn ions into the cytosol. However, additionally, expression of constructs containing *AtIAR1* complemented the yeast *AtIAR1* homologue mutant, *yke4Δ*, which may suggest that AtIAR1 can also transport Zn in the reverse direction into the secretory pathway which is not taken into account in the published model. Further testing of this potential Zn import into the ER could involve complementation of mutant yeast strains sensitive to Zn excess such as *zrc1Δ cot1Δ* or expression of *AtIAR1* and *Atiar1-3* constructs in *Xenopus* oocytes.

Bioinformatic analysis supports the notion that the Zn transport capability is conserved across the plant kingdom and has identified large, conserved H-rich loops which may act as Zn sensors in the lumen to control the activity of AtIAR1.

4.3.2 AtIAR1 and plant homologues predominantly localise to the secretory pathway

AtIAR1 appears to localise across several membranes when expressed in yeast. The complementation of *yke4Δ* strains suggest ER localisation, whereas the complementation of *zrt1Δ zrt2Δ* strains suggest that in yeast, AtIAR1 is localised at least partially to the plasma membrane. Bioinformatic analysis from three separate software packages agreed that the most likely localisation of AtIAR1 in plants was within the secretory system (with ER being the most likely as predicted by DeepLoc v2). DeepLoc v2 did additionally predict a probability of greater than 0.3 for lysosome, Golgi and plasma membrane localisation. Unfortunately, these localisations were unable to be tested in plants using GFP complementation lines due to low expression.

Most plant IAR1 homologues were also predicted to be localised within the secretory pathway, although members of the *Solanaceae* family showed potential deviation as predicted by Target P v2 and PProwler v1.2. This deviation may represent a change in Zn-auxin interaction in these species as the IAR1 model requires IAR1 to localise to the compartment containing auxin hydrolases, and so warrants further investigation.

Therefore, although the model may be partially correct in predicting that IAR1 is localised to the ER membrane, the model may not represent all the sub-cellular localisations of AtIAR1 nor that of IAR1 homologues in *Solanaceae*.

4.3.3 *AtIAR1* is expressed in the vasculature of above ground tissues in a Zn and auxin dependant manner

AtIAR1 promotor analysis has suggested that there are multiple potential regulators of *AtIAR1* expression, including abiotic and developmental stimuli. Using *AtIAR1*::*GUS* reporter plants, this study has shown that three of these induction conditions are Zn excess, exogenous auxin and exogenous auxin conjugate.

Interestingly, Zn and auxin/auxin conjugate seem to interact with each other: expression was observed in conditions of Zn excess with no exogenous auxin or auxin conjugate as well as conditions of deficient or replete Zn with exogenous auxin or auxin conjugate. In both cases the expression was seen in the hypocotyl vasculature, and for the Zn-excess condition additionally in the leaf vasculature and leaf tip.

Therefore, this work suggests that the model IAR1 function of regulating auxin conjugate balance occurs only under specific conditions and in certain tissues. The significance of *AtIAR1* expression in these areas is investigated further with respect to Zn and auxin in later chapters (**Chapter 5** and **Chapter 6** respectively).

4.3.4 Atiar1-3 may have improper dimerization and localisation

Evidence for the IAR1 model came from several different *AtIAR1* mutants, which all showed relative insensitivity to a variety of auxin conjugates including IAA-Ala, predicted to be caused by reduced cation transport out of the ER. One of these mutations identified in these plants, *Atiar1-3*, has been characterised in this study as still able to complement the yeast *AtIAR1* homologue mutant *yke4Δ*, and Zn import mutants, but only when expressed with an *AtIRT1* signal peptide sequence. This suggests that Atiar1-3 is still capable of transporting Zn in yeast, but may have restricted localisation to the ER. Therefore, the model of how *Atiar1* mutants lead to auxin conjugate insensitivity may not apply to *Atiar1-3*.

The *Atiar1-3* mutant contains a frameshift mutation, close to the 3' end of the coding region, which leads only to changing of the final 11 amino acids. However, the C-terminus is highly conserved in plants as shown in **Figure 4.15** and although seemingly not directly involved in transport may play a role in IAR1 functionality by forming dimerization contacts as predicted through analysis of evolutionary coupling of residues in the ZIP family[385]. C-terminal residues are also known to be important for localisation particularly within the secretory pathway: for example the di-lysine motif was shown to promote ER retention of membrane proteins in plants[386]. However, neither the C-terminus of AtIAR1 nor Atiar1-3 show known

retention signals. These features may indeed be linked, as in the case of the membrane protein prenylin in which failed dimerization due to C-terminal substitutions results in improper ER retention[387].

Protein	C-terminal sequence
AtIAR1	SLILGMSVALCISLIE*
OsIAR1	SLTMGMLVALGISLVE*
NtIAR1	SLLSGMAVALCISLVE*
ZmIAR1	SLAMGMLVALGISLVE*
GmIAR1	SLTIGMAVALGISLVE*
MpIAR1	ALTVGMGIAVAISLAE*
Atiar1-3	SLILGPECCSLHLSYRMIS*

Figure 4.15 *Atiar1-3* mutations cause substitutions within the highly conserved C-terminus. Asterisks indicate STOP codons while the sequence in red is that altered through a frame shift mutation in the *Atiar1-3* gene. Residues highlighted in grey are those showing 100% conservation in the sample of plant AtIAR1 homologues shown (*Oryza sativa*, *Nicotiana tabacum*, *Zea mays*, *Glycine max* and *Marchantia polymorpha*).

It is therefore hypothesised that Atiar1-3, loses its ability to dimerise, which causes it to be localised only in the ER, instead of other compartments such as the Golgi, whilst retaining its Zn transport activity. Assuming that functional transport in yeast is an indicator of functional Zn transport in plants and that localisation of IAR1 in yeast represents localisation in plants, this study suggests that this mislocalisation, rather than loss of transport activity, led to the auxin conjugate insensitivity in *Atiar1-3* plants. If Atiar1-3 is indeed functional in the ER, then loss of Zn transport out of the ER is not directly responsible for the IAA-Ala insensitivity of *Atiar1-3*

plants and as such this phenotype may be due to loss of IAR1-related function outside the ER such as in the Golgi.

The compensatory loss of function mutations found within *AtMTP5* gene[1], which when expressed with *AtMTP12* forms a functional Zn transporter in the *cis*-Golgi[89] suggests that the *Atiar1-3* phenotype may be due to disruption of metal homeostasis in the Golgi. Hydrolases specific for auxin-amide conjugates such as IAA-Ala have been shown to localise to the ER, through bioinformatic, proteomic and GFP-tagging experiments[279-282]. Therefore, disruption of Golgi Zn homeostasis in *Atiar1-3* is predicted to lead to disrupted of ER Zn homeostasis.

Testing this hypothesis of restricted localisation, requires high-resolution subcellular localisation data on AtIAR1 and Atiar1-3 which unfortunately was not possible in this study, but could be continued with complementation of full *Atiar1* knock out mutants with *AtIAR1*::*GFP* and *Atiar1-3*::*GFP* constructs.

Overall, through testing of the model for *AtIAR1*, this study has found evidence supporting that AtIAR1 transports Zn out of the ER, localises to other locations in the secretory pathway and is expressed in vasculature of hypocotyls and leaves in a Zn and auxin-dependent manner.

Chapter 5: *AtIAR1* and Zn homeostasis

5.1 Introduction

5.1.1 Zn deficiency in *Arabidopsis thaliana*

5.1.1.1 Zn homeostasis in *Arabidopsis thaliana* in Zn deficient conditions

Zinc (Zn) is a redox-stable transition metal that binds to around 9% of the eukaryotic proteome[2]. Its roles include acting as catalytic centres in enzymes like carbonic anhydrase[3], structural components in some transcription factors[4], stabilisation of membranes[5], as an intracellular second messenger in mammals[6,7], and in reactive oxygen species (ROS) protection[8]. Therefore plants without sufficient Zn show severe phenotypes including stunted growth, leaf chlorosis, increased shoot branching, early senescence of leaves, reduced floral fertility[14,15] and increased ROS levels[16].

Therefore, in conditions of Zn deficiency, plants co-ordinate a range of responses to increase Zn uptake and utilisation. This includes maximizing Zn uptake from the soil into the cytosol of root cells[71,105]. This Zn is then transported into the xylem for root-to-shoot translocation[62,92,112]. During Zn deficiency mobilisation of above-ground Zn stores also occurs from trichromes and cell vacuoles[113,114,388]. For further details of the Zn deficiency response in *Arabidopsis* see **Chapter 1.2.3**.

The regulation of this Zn deficiency response in *Arabidopsis* occurs through a local and systemic Zn deficiency response. The local response involves the Zn-responsive AtbZIP19/23 transcription factor pair[71,118-120]. Whereas the systemic Zn deficiency response operates through an as yet unidentified shoot-derived signal that regulates genes including *AtMTP2*[92]. This regulation of Zn deficiency is summarised below in **Figure 5.1**.

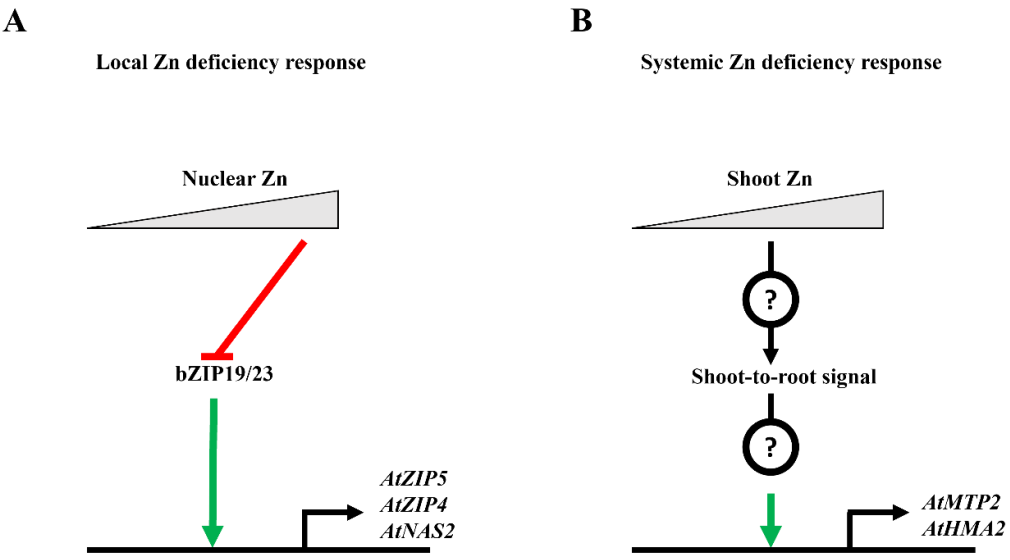

Figure 5.1 Zn deficiency response in *Arabidopsis thaliana*. (A) Local Zn deficiency response. bZIP19/23 transcription factor activity is inhibited by direct binding of Zn. In low Zn conditions, the active transcription factor pair activates the transcription of many genes including those for Zn and Mn import (*AtZIP4*, *AtZIP5*) and nicotianamine synthesis (*AtNAS2*). (B) Systemic Zn deficiency response. Low Zn status in the shoot is transmitted through unknown components to the root leading to induction of genes involved in endoplasmic reticulum (ER) Zn import (*AtMTP2*) and xylem Zn loading (*AtHMA2*). For further details see **Chapter 1.2.4**.

5.1.1.2 Zn deficiency sensitive mutants give insights into the Zn deficiency response

Mutants in components of the Zn deficiency homeostasis system show sensitivity to Zn deficiency. It should be noted that each of the components involved in Zn homeostasis is part of a plastic network[117]. This means that the mutant phenotypes of singular *ZIP* genes such as in *Atzip9* and *Atzip12* plants[119] are often marginal, in this case the phenotypes were slightly reduced root length with reduced Zn content in roots in Zn deficient conditions. Higher order mutants of *ZIP* genes including

quadruple *Atzip* mutants are often required to combat this redundancy to produce a strong Zn phenotype[72]. *Atmtp2* mutants also show sensitivity to Zn deficiency, in particular reduced biomass and reduced shoot Zn levels in Zn deficient conditions[92]. Mutants in the components of the deficiency response produce more significant phenotypes in Zn deficiency compared to individual transporter mutants. The *Atbzip19 Atbzip23* double mutants show reduced fresh weight of shoots and roots relative to controls under Zn deficient conditions[71]. Together, this suggests root length, shoot fresh weight and elemental analysis can be used to characterise mutants potentially sensitive to Zn deficiency.

The current model for AtIAR1 involves the transport of divalent cations (most likely Zn) from the endoplasmic reticulum (ER)[1,328]. Zn ER levels have been implicated in the systemic Zn deficiency response which involves Zn import into the ER through AtMTP2 activity[92]. However, Zn release from the ER has not been investigated as a potentially important factor in Zn deficiency. This study therefore aims to address whether Zn transport by AtIAR1 is an important component of the Zn deficiency response.

5.1.2 Zn excess in *Arabidopsis thaliana*

5.1.2.1 Zn and Fe homeostasis within *Arabidopsis thaliana* in Zn excess conditions

Under Zn excess, plants suffer from inhibition of photosynthetic enzymes[126,127] and increased oxidative stress[128,129] and so show reduced fresh weight and chlorosis[135]. Some of these symptoms come from the competition of Zn with other divalent cations for binding sites in particular Fe^{2+} according to the Irving-Williams series[125,135]. Therefore, *Arabidopsis thaliana* responds to Zn excess by sequestering Zn in the cell wall[130,131], vacuole[91,93,389] and the Golgi[76]. In addition, Fe availability is also increased to combat Fe deficiency that accompanies Zn excess including

from vacuolar Fe release[98,99] and Fe uptake[35,135-138]. For further details on the Zn excess response in *Arabidopsis* see **Chapter 1.2.5**.

Although in *Arabidopsis*, no Zn excess specific signalling pathways are known, the Fe deficiency response which is activated under Zn excess is well characterised. Fe-deficiency genes are upregulated through a cascade of basic helix-loop-helix (bHLH) transcription factors[148,150-153]. At the end of the cascade in Fe deficient conditions, active AtFIT, in dimerization with other bHLHs including AtbHLH38, then induces the transcription of Fe deficiency machinery including for reduction of Fe^{3+} to Fe^{2+} and import of Fe^{2+} in the roots[136-138]. BRUTUS (BTS) and BRUTUS-LIKE (BTSL) E3 ligases regulate this cascade by degrading members of the bHLHs involved in the cascade in Fe sufficient conditions[156-158] and these E3 ligases are themselves inhibited by Fe deficiency-induced IRON MAN (IMA) peptides[159-161]. This regulatory cascade is shown below in **Figure 5.2.**

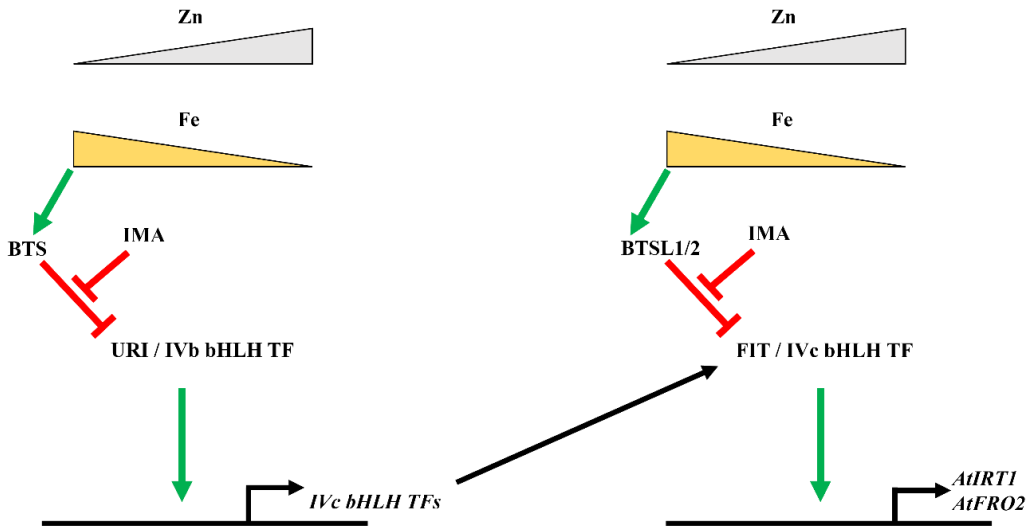

Figure 5.2 Fe deficiency response induced by Zn excess. In Fe replete conditions, BTS and BTSL proteins are active and degrade members of the bHLH transcription factor (TF) cascade reducing expression of Fe deficiency genes. In low Fe conditions, BTS and BTSL proteins are inactive thus stabilising URI and IVb bHLH TFs. URI IVb bHLH TFs then induce expression of *AtFIT* and IVc *bHLH* TF genes which then induce genes including those involved in Fe uptake (*AtIRT1* and *AtFRO2*). For further details see **Chapter 1.2.6**.

5.1.2.2 Zn excess sensitive mutants show common phenotypes associated with Fe deficiency

Phenotypes in Zn excess often are associated with Fe deficiency. The most easily seen phenotype in Zn excess and Fe deficiency is chlorosis, partially due to the Fe-dependence of chlorophyll biosynthetic enzymes[390,391]. This chlorosis is worsened in many Fe deficiency sensitive mutants such as the *Atirt1* mutants[77]. Similar phenotypes are seen in mutants sensitive to Zn toxicity such as *Atmtp1* mutant plants which show reduced root growth and chlorosis in elevated Zn levels[93,389,392] similar to that seen in *Atpcr2* mutants in similar conditions[81]. Mutants within regulatory portions of the Fe deficiency signalling cascade also show reduced root growth and enhanced chlorosis in Fe deficiency conditions such as in the *Atbhlh34*

and *Atbhlh104* mutants[150]. This suggests these features are common to Fe deficiency in Zn excess and can be used to characterise mutants for sensitivity to Zn excess and Fe deficiency conditions.

Previous work has shown that Zn transport into the Golgi through AtZIP13 is important in the Zn detoxification strategy in *Arabidopsis thaliana*[76]. Given that previous work in this study on AtIAR1 suggested Zn transport activity and potential localisation to the Golgi (see **Chapter 4.3**), the potential role of AtIAR1 in Zn excess tolerance is important to clarify.

5.1.3 ER stress is regulated by ER Zn levels

Maintaining optimal Zn levels within the ER is essential for correct metalation of metalloproteins across kingdoms. The ER stress response in plants can be split into two pathways. In the first, INOSITOL REQUIRING ENZYME 1 (IRE1) functions as a protein kinase and ribonuclease[393-395] with homologues of IRE1 and downstream factors also found in yeast, plants and mammals[396]. In *Arabidopsis*, sensing of ER stress is thought to lead to dimerization and auto-transphosphorylation which activates the ribonuclease activity of AtIRE1 to splice *AtbZIP60* mRNA[397-400]. This splicing changes the localisation of the resulting AtZIP60 protein to facilitate nuclear localisation enabling transcriptional activity[399]. In the second pathway of ER stress activation, type II transmembrane proteins, including ATF6, bZIP17 and bZIP28 are firstly migrated to the Golgi where they are cleaved once again to allow nuclear localisation and transcriptional activity[401-406]. Transcriptional activation from these two pathways is distinct but one of the common features is expression of genes encoding Binding Proteins (BiPs)[407-409]. BiPs are Heat Shock Protein 70 family members that contain an ATPase domain and a protein binding domain, together allowing BiP proteins to act as ATP-dependant protein chaperones[410]. *Arabidopsis* contains three *BiP* genes[411], with *AtBiP1* and *AtBiP2* showing high sequence identity, all three of which are upregulated in ER stress[348,400].

Lack of Zn transport into the ER in yeast produces an exacerbated ER stress response in low Zn conditions[412]. Yeast strains with a knock-out mutation in the gene homologous to *AtIAR1, yke4*Δ, thought to lead to increased ER Zn levels, show reduced ER stress in Zn deficient conditions[336]. In mammals, Zn deficiency was seen to transcriptionally upregulate the mammalian ER stress response[412]. In addition, mice with mutations in genes homologous to *AtIAR1* show increased ER stress in secretory epithelial cells[413]. In plants, ER stress has also been shown to be Zn sensitive. Addition of Zn to growth media containing NaCl reduced the salt-induced ER stress in *Arabidopsis thaliana.* In addition, mutants in the gene encoding the ER Zn exporter AtZTP29, a member of the ZIP family[80], show inability to induce the ER stress response in high salt conditions. Overall, this indicates that Zn levels in the ER and *AtIAR1* may regulate the ER stress levels in plants.

5.1.4 Measurements of Zn content in plants

Measuring the Zn content of plants is a key method for assessing Zn homeostatic changes in different conditions and genetic backgrounds. The visualisation or quantification of Zn in plants can be performed through a variety of methods including inductively coupled plasma-optical emission spectroscopy (ICP-OES) and mass spectrometry (ICP-MS), fluorescent dyes such as zinquin and zinypr[104,414], and more recently, genetically encoded Förster resonance energy transfer (FRET) sensors[46]. Genetically encoded FRET sensors have several advantages over ICP including greater spatial resolution, subcellular targeting, and measurement of biologically available Zn not just the total Zn. Genetically encoded sensors also can quantify the *in vivo* Zn concentration, unlike the fluorescent dyes, which is vital for comparative studies.

Currently, three different Zn FRET sensors are being used in subcellular Zn studies. The ZapCY sensors[415] and the eCALWY sensors[416] both have a CFP-YFP FRET pair and the recently developed eZinCH-2 utilises a Cerulean and Citrine FRET pair[417]. The amino acids that bind Zn in these sensors are histidine and cysteine

residues and both are pH and redox sensitive[418,419] and therefore require *in vivo* calibration. This is especially important for Zn quantification in the ER which is a much more oxidising environment than the cytosol and so could obscure calculations[420]. To date using this careful approach with a range of different sensors of differing affinities, cytosolic Zn concentration in *Arabidopsis* roots has been calculated to be in the 400 pM range, differing between biological replicates and different areas of the root[46]. ER Zn concentration has not been calculated in plants. Experimental values in mammalian cell lines using genetically encoded FRET sensors and targetable fluorescent sensors show Zn levels 10-100 times lower than the cytosol[415,421] whereas other studies using eCALWY sensors show free Zn concentration of around 5 nM, higher than the cytosol[422]. These conflicting data highlights the difficulty in assaying Zn levels in the ER.

Unfortunately, work with genetically encoded Zn FRET reporter plants in this study was not taken to completion but could be carried on in the future. Instead, gene expression analysis has been used as a proxy to investigate subcellular levels of Zn and Fe. The advantage of using gene expression analysis is the speed at which results can be gathered in contrast to the use of genetically encoded FRET sensors. However, expression of genes may not be a direct read out of transport activity due to post-transcriptional regulation, for example the activity of the ZIP transporter AtIRT1 is controlled by endocytosis and degradation when its cytosolic loop binds non-target metals such as Zn and Mn[124]. The occurrence of such regulation in other ZIPs including those tested in this study is currently unknown.

5.2 Results

5.2.1 *Atiar1-3* and *Atiar1-t* mutants are predicted to have differing severity of phenotype

To investigate the role of *AtIAR1* in Zn homeostasis, two different *Arabidopsis* mutants were used in this study; *Atiar1-3* and *Atiar1-t* mutants shown below in **Figure 5.3**. *Atiar1-3* is a partially characterised mutant found during a screen for IAA-Ala insensitivity by Lasswell et al[328] and contains a frame shift mutation leading to amino acid substitutions in the C-terminus of the protein. By contrast *Atiar1-t* is a T-DNA insertion line (SALK_ 047876C) not yet characterised, with the T-DNA insertion site within an exon coding for part of the helix α5. Therefore, *Atiar1-t* is predicted to be a full knockout whereas *Atiar1-3* is predicted to show expression of the *Atiar1-3* gene which lacks some *AtIAR1* functionality.

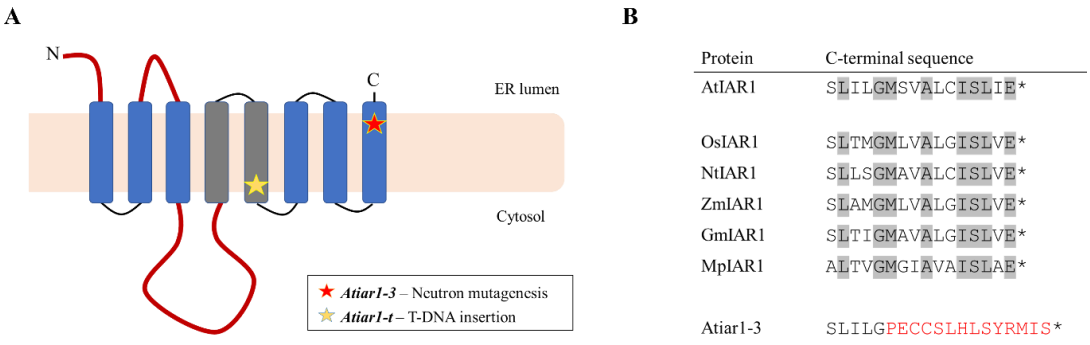

Figure 5.3 *Atiar1* mutants used in this study. (A) Schematic of AtIAR1 topology with the yellow and red asterisks representing the amino acid positions corresponding to the site of T-DNA insertion or neutron mutagenesis in *Atiar1-t* and *Atiar1-3* plants respectively. Transmembrane helices containing conserved transport-associated residues are in grey and histidine rich loops shown in red. (B) Amino acid sequences at the C-terminus in AtIAR1, AtIAR1 plant homologues and Atiar1-3. Asterisks indicate STOP codons while the residues in red are those altered through a frame shift mutation in the *Atiar1-3* gene. Residues highlighted in grey are those showing 100% conservation in the sample of plant AtIAR1 homologues shown (*Oryza sativa*, *Nicotiana tabacum*, *Zea mays*, *Glycine max* and *Marchantia polymorpha*).

To firstly check whether *Atiar1-3* and *Atiar1-t* showed disruption of expression of *AtIAR1*, transcription level was measured using reverse transcriptase quantitative PCR (RT-qPCR) as shown in **Figure 5.4**.

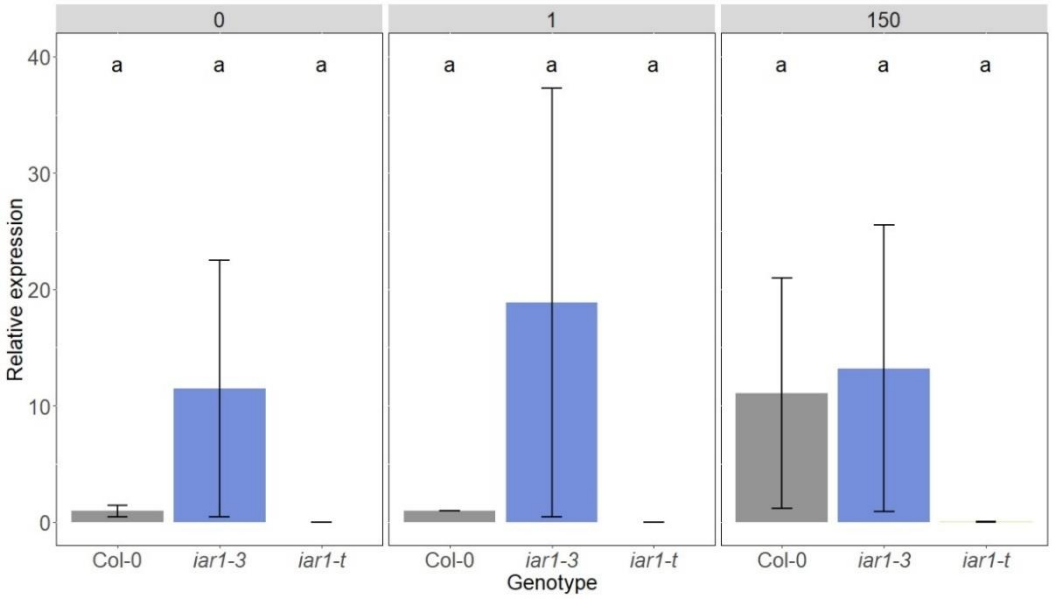

Figure 5.4 *AtIAR1* expression in *Atiar1-3* and *Atiar1-t* plants. RNA extracted from whole plants grown for 16 days in Zn deficient (0 Zn added), Zn control (1 µM) and Zn excess (150 µM) conditions on modified Hoagland's media containing EDTA-washed agar. Expression was calculated using the 2-ΔCt method[349], using internal reference genes *AtUBC* and *AtTIP41*, and relative to the mean expression seen in the Col-0 genotype within control Zn conditions for each of three biological replicates. Data displayed using R version 4.1.1. Error bars display the standard error of the mean (SEM). Lower case lettering indicates statistically significant differences between groups (labelled sequentially from 'a' in order of estimated mean) as calculated using analysis of variance (ANOVA) using Tukey's method for p-value adjustment[366] for 9 groups using a p-value cut-off of 0.05.

As shown above, the predicted differences in expression between Col-0 and the *Atiar1* mutants were not seen in the expression level of *AtIAR1*, possibly due to low signal to noise ratio. Additionally, a complete absence of *AtIAR1* transcript was detected for *Atiar1-t* across all Zn conditions. To assess the effect of these mutations on Zn homeostasis a selection of phenotypes associated with sensitivity to Zn deficiency and excess was assayed for Col-0, *Atiar1-3* and *Atiar1-t* genotypes.

5.2.2 Root and shoot phenotypes vary across Zn conditions and genotypes

5.2.2.1 *Atiar1-3* and *Atiar1-t* show different primary root growth responses to altered Zn

Primary root length has been reported as reduced in mutants sensitive to Zn deficiency (*Atbzip19 Atbzip23* double mutants[71]) and Zn excess (*Atmtp1* mutants[389]). Therefore, the primary root length of *Atiar1-3* and *Atiar1-t* was measured in Zn deficiency and excess conditions as shown below in **Figure 5.5**.

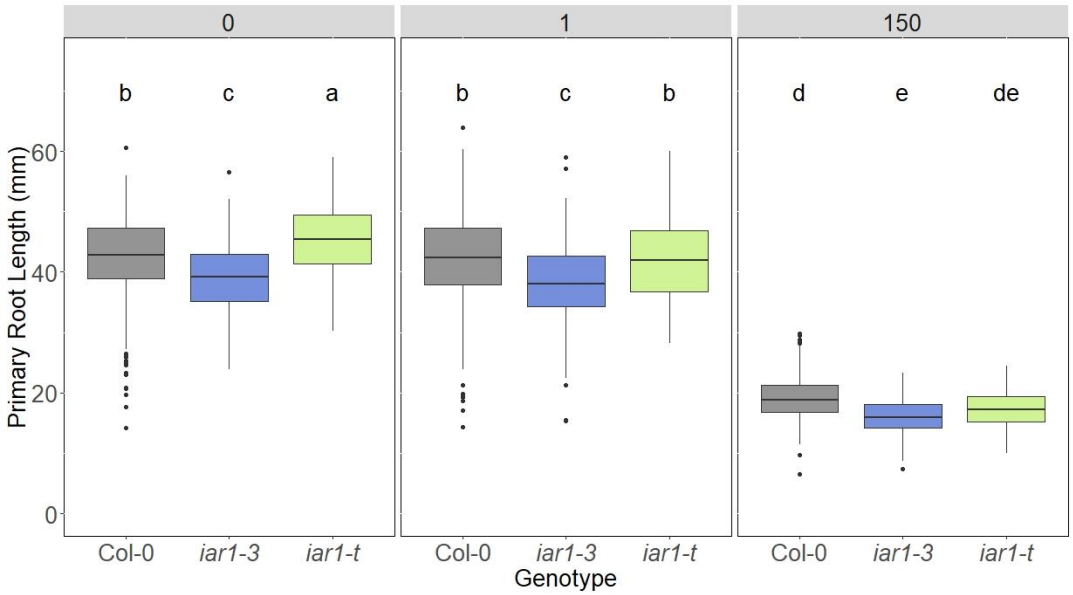

Figure 5.5 Primary root length of *Atiar1* mutants grown on different Zn levels. Primary root length was measured from Col-0 (grey), *Atiar1-3* (blue) and *Atiar1-t* (green) plants grown for 10 days in Zn deficient (0 Zn added), Zn control (1 µM) and Zn excess (150 µM) conditions on modified Hoagland's media containing EDTA-washed agar. At least 50 plants were measured in each of three biological replicates. Data displayed using R version 4.1.1. Statistically significant differences between groups were calculated and displayed as in **Figure 5.4**.

As shown above, in Zn deficient conditions, there is a significant reduction in primary root length in *Atiar1-3* mutants relative to the control, and this difference persists across all Zn conditions. On the other hand, the *Atiar1-t* mutant shows increased primary root length only in Zn deficient conditions. This suggests the two mutants are responding to Zn differently with the *Atiar1-3* mutant showing a Zn-independent root growth reduction relative to Col-0. All genotypes responded similarly to Zn excess conditions with a reduction in primary root length.

5.2.2.2 *Atiar1-3* and *Atiar-t* show altered shoot development

Shoot fresh weight and chlorophyll content have been shown to be influenced by Zn deficiency[110] and excess[81,423] in *Arabidopsis*. Therefore, to assess the impact of *AtIAR1* activity on these features, the shoot fresh weight was recorded along with chlorophyll content for Col-0, *Atiar1-3,* and *Atiar1-t* plants.

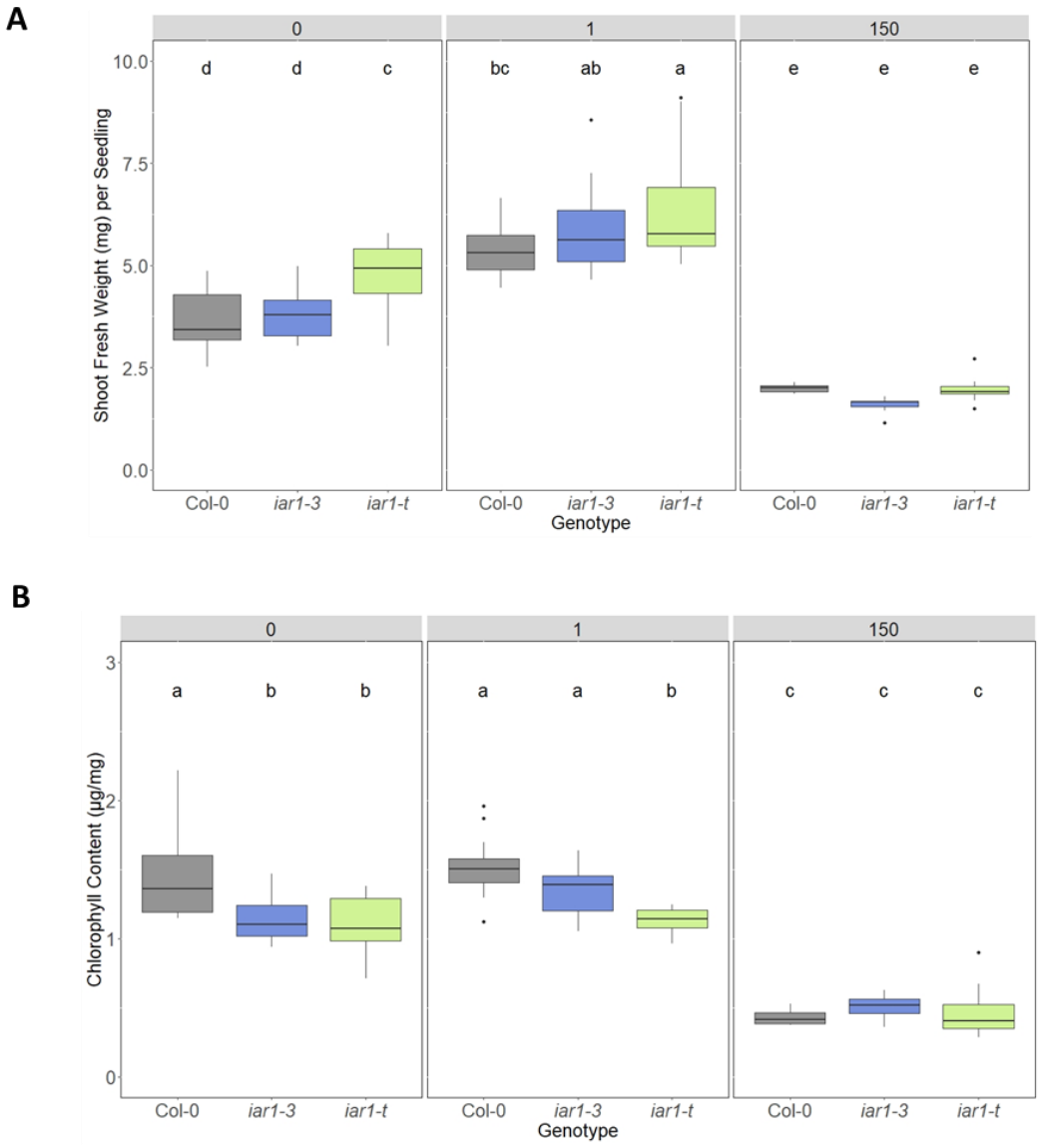

Figure 5.6 Shoot phenotypes of *Atiar1* mutants grown on different Zn levels. (A) Shoot fresh weight and (B) chlorophyll content was measured from Col-0 (grey), *Atiar1-3* (blue) and *Atiar1-t* (green) plants grown for 16 days in Zn deficient (0 Zn added), Zn control (1 µM) and Zn excess (150 µM) conditions on modified Hoagland's media containing EDTA-washed agar. Data displayed using R version 4.1.1. For each of 3 biological replicates, plant shoot tissue from at least 30 plants was separated into 50 mg pools before measuring. Statistically significant differences between groups were calculated and displayed as in **Figure 5.4**.

Firstly, the Col-0 response to deficient and excess Zn conditions is to reduce shoot fresh weight. Under Zn deficient conditions and control optimal Zn conditions, the *Atiar1-3* mutant is similar to the Col-0 genotype for shoot fresh weight but shows reduced chlorophyll content in Zn deficient conditions. The *Atiar1-t* mutant under Zn deficient and control conditions shows increased shoot fresh weight with reduced chlorophyll content. The magnitude of the differences increases between the *Atiar1-3* mutant and the *Atiar1-t*, suggesting that the *Atiar1-t* mutant has a more severe shoot growth phenotype. In Zn excess conditions, no differences were seen between Col-0 and either *Atiar1* mutant.

This reduction of chlorophyll content along with increased shoot fresh weight for *Atiar1-t* under deficient and control conditions suggest that in these conditions, the *Atiar1-t* plants and to a lesser extent the *Atiar1-3* plants show a greater proportion of low-chlorophyll density tissues such as hypocotyl and petioles. This may imply that the shoot response seen in Zn is a developmental one. Interestingly, in Zn excess conditions this trend is reversed or lost in *Atiar1-3* and *Atiar1-t* plants respectively suggesting that Zn excess may interact with this phenotype.

The Zn deficiency sensitive *Atbzip19 Atbzip23* double mutants are unable to increase the expression of Zn transporters and show reduced root length and shoot weight in Zn deficient conditions[71]. Neither *Atiar1-3* nor *Atiar1-t* plants showed both these features, suggesting *AtIAR1* is not involved in Zn deficiency. However, a small reduction in root length under all Zn conditions similar to that seen in *Atzip9* and *Atzip12* mutants was observed for *Atiar1-3* mutants[119]. This could suggest a similar mechanism for root shortening driven by reduced Zn availability in *Atiar1-3* mutants, which is further investigated below.

The Zn excess sensitive *Athma1* mutants are unable to detoxify Zn effectively and show a reduction in root length, shoot fresh weight and chlorophyll content in excess Zn conditions[423]. Neither *Atiar1-3* nor *Atiar1-t* mutants show a similarly consistent phenotype in excess Zn conditions, suggesting *AtIAR1* is not involved in plant-wide Zn detoxification.

Overall, this highlights that these mutants may show divergent phenotypes across Zn conditions, which may relate to the differing severity of the mutations. Further investigation of the role of *AtIAR1* in Zn homeostasis can be achieved by assessing

the transcriptional response of *Atiar1-3* and *Atiar1-t* mutants to Zn deficiency and excess conditions.

5.2.3 Expression analysis reveals altered Zn deficiency and excess response in *Atiar1-3* and *Atiar1-t* plants

5.2.3.1 Parts of the local Zn deficiency response may be reduced in *Atiar1-t* mutants

Yeast[336] and animal homologues[377] of *AtIAR1* have been shown to be contributors to control of cytosolic Zn levels in Zn deficient conditions. A proxy for direct measurement of intracellular Zn in *Arabidopsis* using gene expression relies on the local Zn deficiency response that is bZIP19/23 dependant. Nuclear Zn deficiency increases activity of the bZIP19/23 transcription factor pair[120] and resultant expression of bZIP19/23 regulated genes can be monitored. Proxy genes (*AtZIP3,4,5,9*) were selected based on presence of a Zn deficiency response element (ZDRE) and reduced expression in *Atbzip19/23* double mutants[71].

AtZIP3 has been shown to transport Zn in yeast mutant complementation assays[68] and has its expression induced in both roots and shoots during Zn deficiency induced by *AtMTP1* overexpression[424]. AtZIP4 is localised on the plasma membrane[72] was shown to transport Zn[68,72] in addition to Cu[56] and although is expressed in roots and shoots[70,425] has its expression upregulated predominantly in roots under Zn deficiency[72]. AtZIP5 in yeast complementation assays has been shown to transport Mn[68] but also Fe and Zn[75]. *AtZIP5* has previously been shown to be induced in roots and shoots under Zn deficiency[71,426] and in the leaf vasculature under Fe excess conditions[75,427]. The transport specificity of plasma membrane localised AtZIP9[72] is questionable as it has been shown in independent yeast complementation assays to transport Mn but not Zn[68] but also Zn and not Mn[72]. Expression of *AtZIP9* was seen in roots and shoots[425], but like *AtZIP4*, is induced mainly in the roots in Zn deficiency[72]. In addition to expression during Zn deficiency *AtZIP9* was also seen to be induced in shoot and roots in low Fe in a

AtbHLH100/*AtbHLH101*-dependant manner[428]. How these different genes are regulated in Col-0, *Atiar1-3* and *Atiar1-t* plants is shown below in **Figure 5.7**.

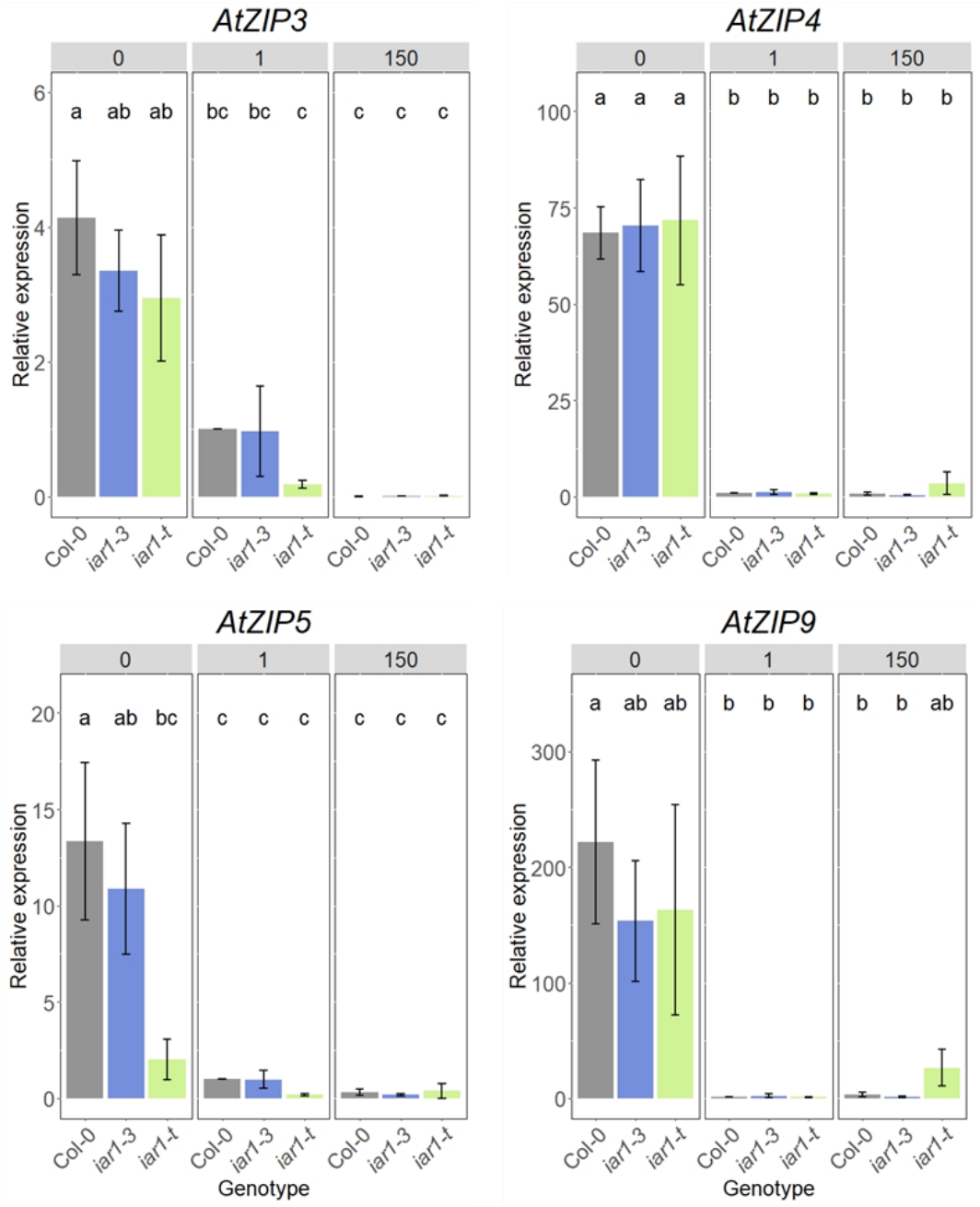

Figure 5.7 Expression of genes involved in *AtbZIP19/23* dependant regulation. . For each of 3 biological replicates, RNA was extracted from whole Col-0 (grey), *Atiar1-3* (blue) and *Atiar1-t* (green) plants grown for 16 days in Zn deficient (0 Zn added), Zn control (1 µM) and Zn excess (150 µM) conditions on modified Hoagland's media containing EDTA-washed agar. Expression and statistically significant differences between groups was calculated and displayed as in **Figure 5.4**.

As shown, all genes selected show an increase in expression in Zn deficient conditions in Col-0 as expected. *AtZIP4* shows statistically significant increases in expression under Zn deficient conditions in all genotypes. *AtZIP3* and *9* expression show no statistically significant differences between genotypes within the same Zn condition. However, expression of *AtZIP3* and *9* is not statistically significantly induced in Zn deficiency in either *Atiar1* mutant. Additionally, *AtZIP5* is not induced in *Atiar1-t* unlike Col-0 and *Atiar1-3* in Zn deficiency conditions.

In comparison to the local Zn deficiency response seen in bZIP19/23 dependant expression, *AtMTP2* is thought to be regulated by a shoot-derived Zn deficiency signal[92] representing systemic Zn deficiency. AtMTP2 is thought to transport Zn into the ER in the roots which may help root-to-shoot translocation of Zn. This led to the hypothesis that AtMTP2 activity and therefore the systemic Zn deficiency response may be regulated by AtIAR1 activity which could transport Zn in the opposite direction according to the AtIAR1 model of Rampey et al, 2013[1]. It was therefore important to check whether *AtMTP2* expression changed in *Atiar1* mutants (**Figure 5.8**).

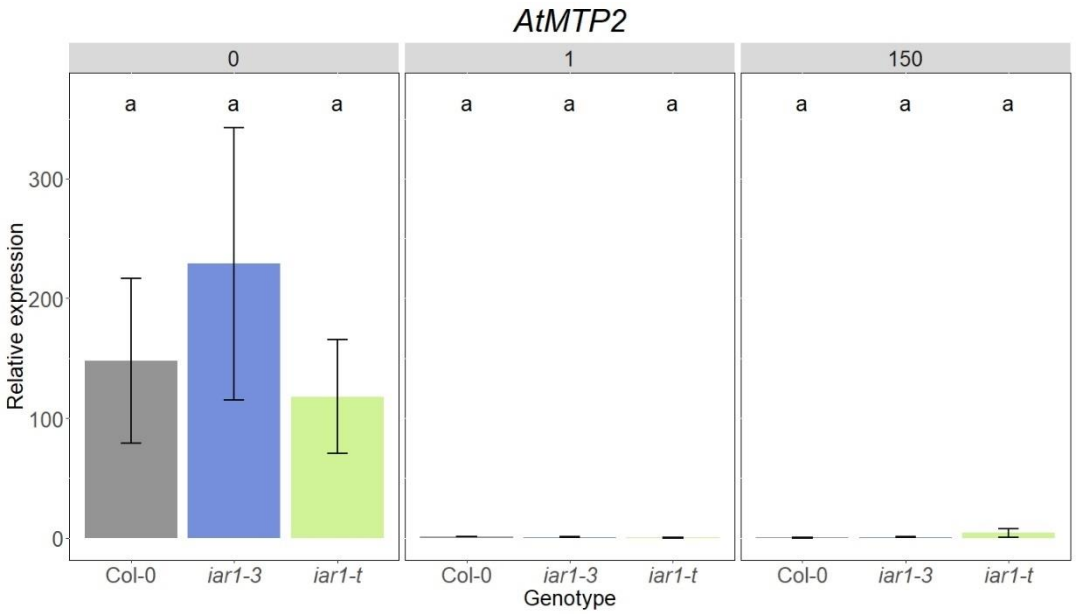

Figure 5.8 Expression of *AtMTP2* in *Atiar1* mutants. For each of 3 biological replicates, RNA was extracted from whole Col-0 (grey), *Atiar1-3* (blue) and *Atiar1-t* (green) plants grown for 16 days in Zn deficient (0 Zn added), Zn control (1 µM) and Zn excess (150 µM) conditions on modified Hoagland's media containing EDTA-washed agar. Expression and statistically significant differences between groups was calculated and displayed as in **Figure 5.4**.

As shown in **Figure 5.8**, there is no statistically significant difference between genotypes or Zn treatment groups. However, there is a possible trend of increased expression of *AtMTP2* in Zn deficient conditions in all genotypes, which may warrant further repeats of this experiment. Transcription of the chosen *AtZIP* genes and *AtMTP2* is repressed under excess Zn and so a different set of genes was analysed for assessing the influence of *AtIAR1* in the Zn excess response.

5.2.3.2 *Atiar1-3* mutants show an enhanced Fe deficiency response

In Zn excess, Zn outcompetes Fe for Fe-binding sites and so leads to functional Fe deficiency. Therefore, a transcriptional output for Zn excess is expression of genes

responsible for Fe deficiency. Genes chosen to be measured for the Fe deficiency response were *AtIMA1* and *AtHLH38* because of their known upregulation in response to Fe deficiency[151,161].

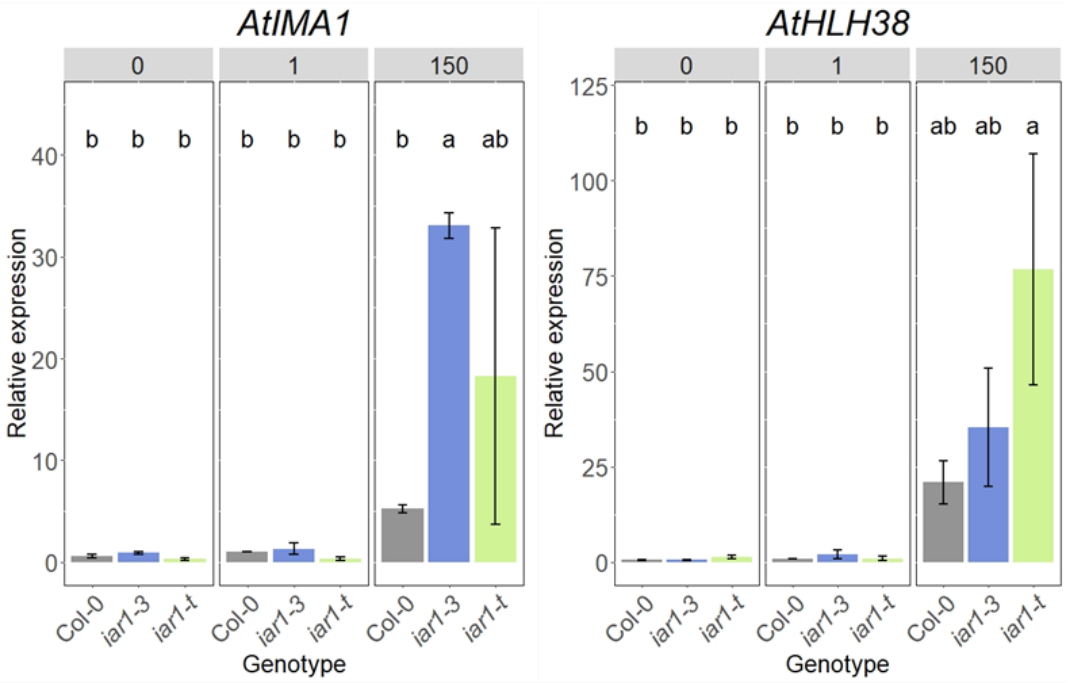

Figure 5.9 Expression of Fe-deficiency genes in *Atiar1* mutants. For each of 3 biological replicates, RNA was extracted from whole Col-0 (grey), *Atiar1-3* (blue) and *Atiar1-t* (green) plants grown for 16 days in Zn deficient (0 Zn added), Zn control (1 µM) and Zn excess (150 µM) conditions on modified Hoagland's media containing EDTA-washed agar. Expression and statistically significant differences between groups was calculated and displayed as in **Figure 5.4**.

As shown in **Figure 5.9**, *AtIMA1* is more upregulated in *Atiar1-3* mutant plants under excess Zn conditions relative to Col-0. In addition, there appears to be no statistically significant differences in mean expression of *AtHLH38* in *Atiar1-3* and *Atiar1-t* plants relative to Col-0, although only in *Atiar1-t* in Zn excess is *AtHLH38* expression level significantly different from that in control Zn conditions. This suggests that Zn excess may be more severe in *Atiar1-3* and *Atiar1-t* mutants

leading to an increased Fe deficiency response. Further work on other genes induced in Fe deficiency such as *AtIRT1* and *AtFRO2* may help test this hypothesis.

The gene expression data shown so far are responsive mostly to cytosolic or nuclear Zn levels. As AtIAR1 is likely located on the ER membrane and probably transports Zn, genes responsive to ER Zn levels were also investigated. It is hypothesised that low Zn in the ER causes ER stress in yeast[412] and in *Arabidopsis*[80]. Therefore, expression of *AtBiP* genes, which are responsive to ER stress, was therefore investigated to determine if *Atiar1* mutants showed altered Zn-dependant ER stress.

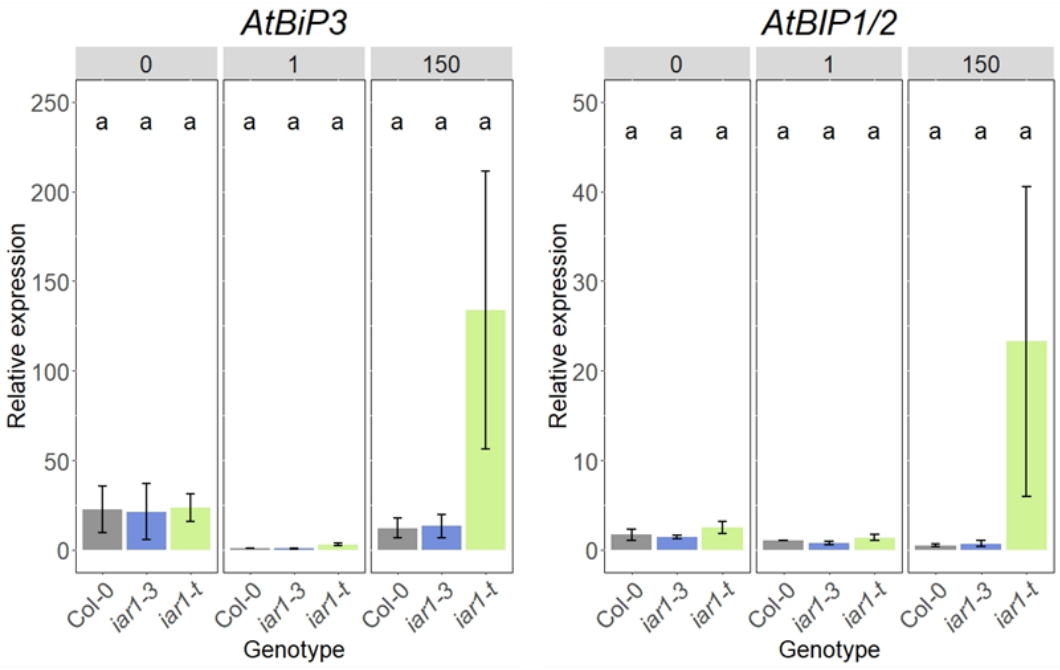

Figure 5.10 Expression of *AtBiP* genes in *Atiar1* mutants. For each of 3 biological replicates, RNA was extracted from whole Col-0 (grey), *Atiar1-3* (blue) and *Atiar1-t* (green) plants grown for 16 days in Zn deficient (0 Zn added), Zn control (1 µM) and Zn excess (150 µM) conditions on modified Hoagland's media containing EDTA-washed agar. Expression and statistically significant differences between groups was calculated and displayed as in **Figure 5.4**.

It was seen for *AtBiP* genes that there was no significant change in expression under any Zn condition or between genotypes. However, under high Zn there is a possible trend of increased *AtBiP* expression for *Atiar1-t*. Further repeats along with protein quantification could be carried out to investigate this possible trend. Increasing ER stress with growth in high salt conditions may also help investigate the role of AtIAR1 in ER stress.

Overall, under Zn excess, there is an increase in Fe deficiency in the *Atiar1-3* mutant. This implies AtIAR1 may function to reduce Zn toxicity such as through transport of Zn into the secretory pathway from the cytosol. To further test this hypothesis, and investigate any potential root and shoot metal distribution changes, measurements of Zn levels were performed in roots and shoots using ICP-OES.

5.2.4 ICP-OES analysis show no change in Mn, Zn and Fe levels in *Atiar1-3* plants

Mutants in metal uptake or root-to-shoot translocation show differences in metal abundance in root and shoot. Since *Atiar1* mutants showed altered gene expression in Zn deficiency and excess conditions, it was hypothesised that this response may correlate with altered metal distribution in the plant. Therefore ICP-OES was used to measure metal abundance in the roots and shoots separately. The metals chosen to be measured were Zn, Mn and Fe which reflect the most common metals altered in changing Zn conditions. Unfortunately, only the *Atiar1-3* mutant was analysed alongside the Col-0 background.

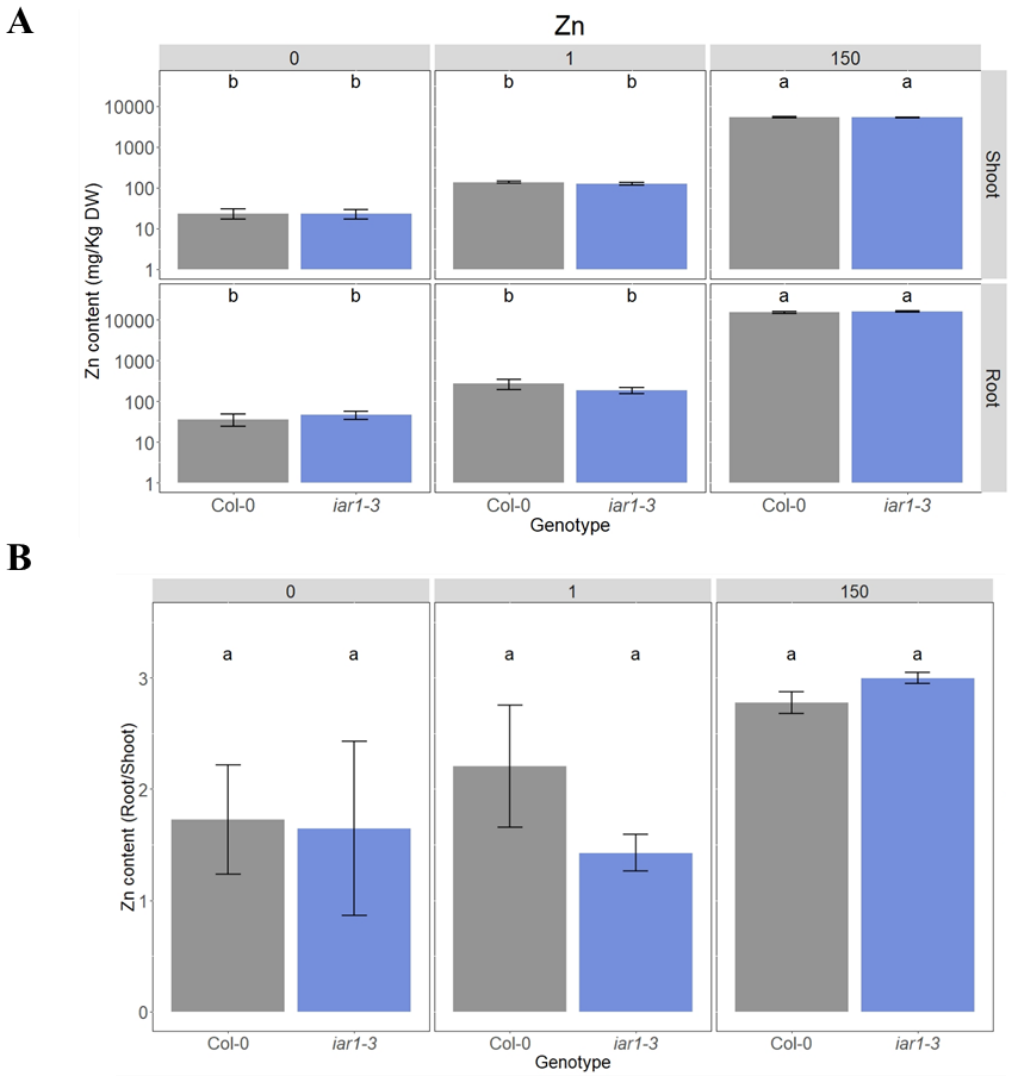

Figure 5.11 Zn content in root and shoot of Col-0 and *Atiar1-3* plants. (A) Zn content in roots and shoots separately or (B) root/shoot ratio for Col-0 (grey) and *Atiar1-3* (blue) plants grown for 16 days in Zn deficient (0 Zn added), Zn control (1 µM) and Zn excess (150 µM) conditions on modified Hoagland's media containing EDTA-washed agar. Data displayed for 3 biological replicates using R version 4.1.1. Error bars and statistically significant differences between 6 groups were calculated and displayed as in **Figure 5.4**.

As shown in **Figure 5.11A**, Zn content significantly increases in Zn excess in both root and shoot samples. Further analysis of the root/shoot Zn ratio in **Figure 5.11B** shows that in all conditions, Zn is preferentially stored in roots, which is counter to

what is seen in the Zn hyperaccumulator species *Arabidopsis halleri*[112]. There were no differences observed between Zn content in Col-0 or *Atiar1-3* plants under any Zn condition.

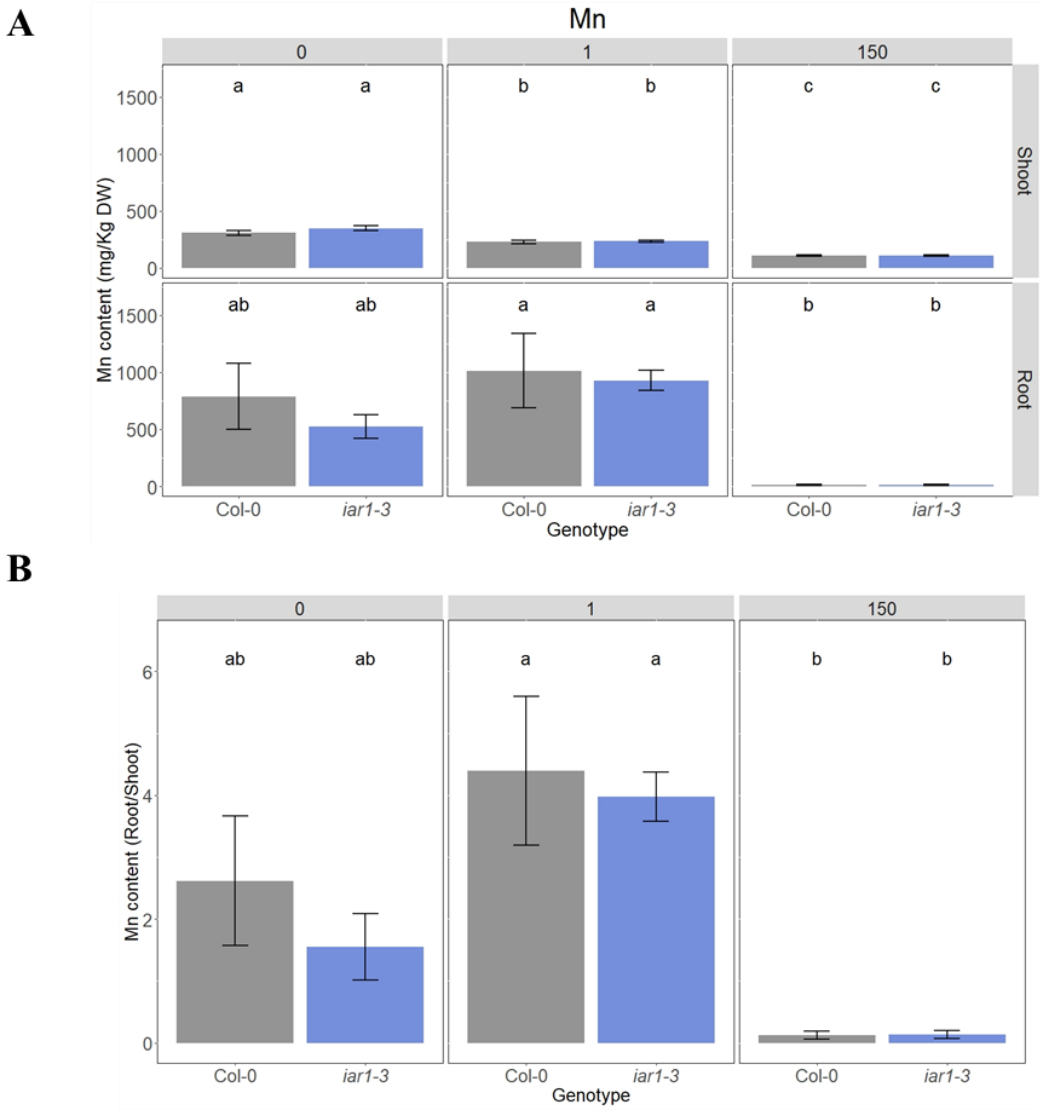

Figure 5.12 Mn content in root and shoot of Col-0 and *Atiar1-3* plants. (A) Mn content in roots and shoots separately or (B) root/shoot ratio for Col-0 (grey) and *Atiar1-3* (blue) plants grown for 16 days in Zn deficient (0 Zn added), Zn control (1 µM) and Zn excess (150 µM) conditions on modified Hoagland's media containing EDTA-washed agar. Data displayed for three biological replicated using R version 4.1.1. Error bars and statistically significant differences between 6 groups were calculated and displayed as in **Figure 5.4**.

With increasing Zn concentration in the media, Mn content was seen to progressively decrease in the shoot (**Figure 5.12**) indicating potential competition with Mn transport by Zn. No statistically significant changes in Mn content in roots or shoots were observed between Col-0 and *Atiar1-3* mutants within any of the Zn supply conditions. Root-to-shoot ratio of Mn decreased severely in Zn excess conditions, where root Mn levels are decreased to a higher extent in the root than the shoot. This suggests Mn demand is higher in the shoot than the root under these Mn-limiting conditions.

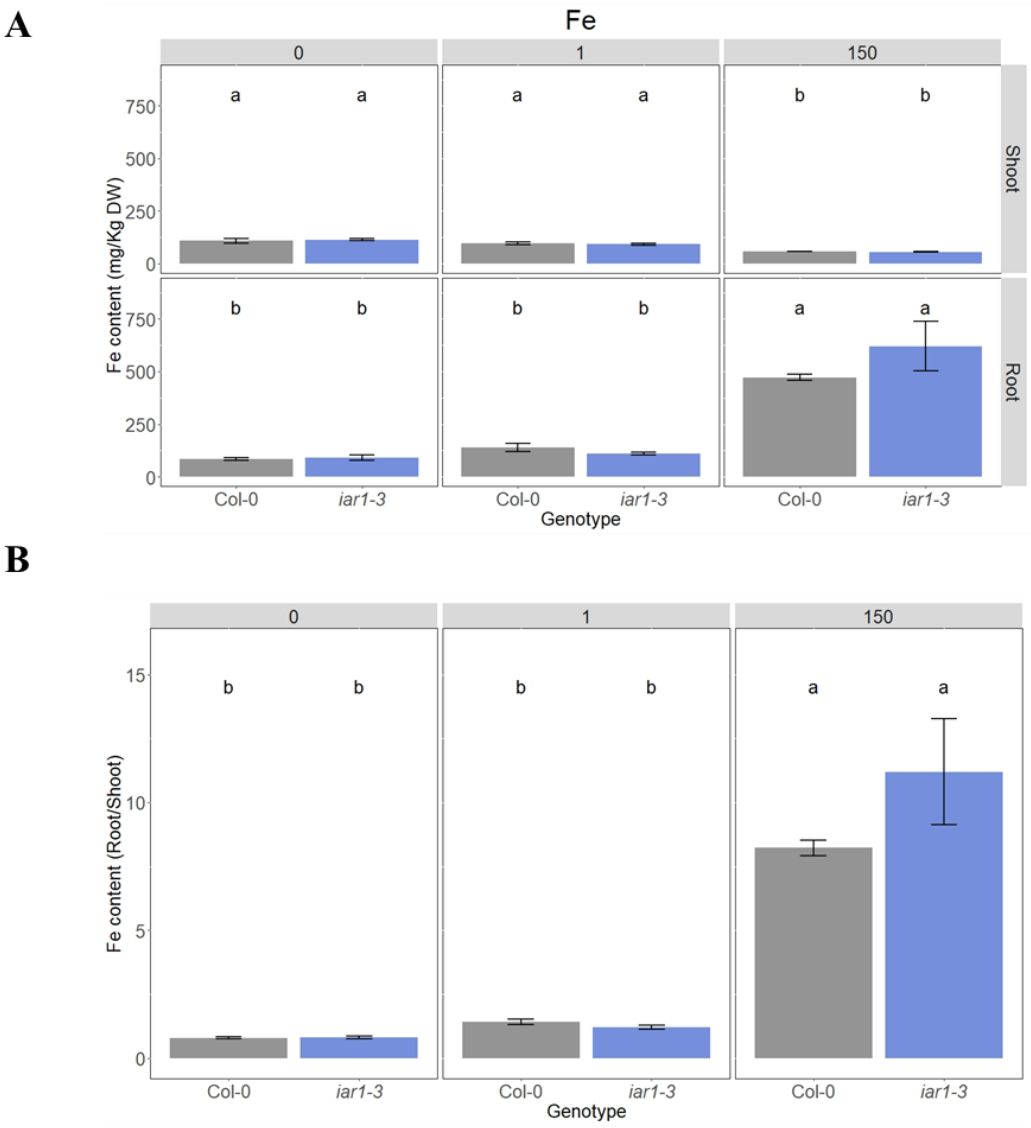

Figure 5.13 Fe content in root and shoot of Col-0 and *Atiar1-3* plants. (A) Fe content in roots and shoots separately or (B) root/shoot ratio for Col-0 (grey) and *Atiar1-3* (blue) plants grown for 16 days in Zn deficient (0 Zn added), Zn control (1 µM) and Zn excess (150 µM) conditions on modified Hoagland's media containing EDTA-washed agar. Data displayed for three biological replicates using R version 4.1.1. Error bars and statistically significant differences between 6 groups were calculated and displayed as in **Figure 5.4**.

With excess Zn conditions, Fe content was seen to decrease in the shoot and increase in the root (**Figure 5.13A**). This can be seen in the root to shoot ratio of Fe

which increased in excess Zn conditions. This suggests Fe may be increased in the root to maintain available Fe levels in a background of increasing competition for binding sites with Zn. There was however, no differences in Fe content between Col-0 and *Atiar1-3* plants in this experiment.

Overall, no changes in Zn, Mn or Fe levels were seen between Col-0 and *Atiar1-3*, suggesting any changed subcellular ion homeostasis has not impacted wider metal homeostasis in Zn deficiency or excess conditions.

5.2.5 Hydroponic long-term growth showed little difference between Col-0 and *Atiar1-3* plants

To determine whether the effects seen when grown on Zn deficient or excess agar were representative of longer-term growth under these conditions, Col-0 and *Atiar1-3* mutants were grown in hydroponic conditions, designed to elicit Zn deficiency, control and Zn excess conditions. However, there were no statistically significant changes in the fresh weight of shoot or root tissue between Col-0 and *Atiar1-3* plants after six weeks of hydroponic culture (data not shown). Further work optimising growth conditions to elicit appropriate Zn deficiency and excess conditions may prove helpful in investigating long term growth trends in Col-0 and *Atiar1* mutant plants.

5.3 Discussion

5.3.1 *Atiar1* mutants show mostly developmental phenotypes in Zn deficiency and control Zn conditions

Growth on EDTA-washed agar achieved Zn deficient conditions as demonstrated with all genotypes showing reduced shoot fresh weight and induction of Zn deficiency genes when compared to control replete conditions. It is interesting to note that these conditions did not lead to a measured reduction in Zn content in the plant, potentially due to the compensatory mechanisms employed to maintain sufficient Zn.

The *Atiar1-3* mutant does not show sensitivity to Zn deficiency relative to Col-0. *Atiar1-3* showed decreased primary root length and reduced chlorophyll content when compared to Col-0 in deficient and control Zn conditions, perhaps suggesting developmental control of root and shoot growth may be a contributing factor rather than Zn deficiency sensitivity. The *Atiar1-3* mutant showed no statistically significant changes in expression of genes during Zn deficiency compared to Col-0 which correlated with ICP-OES analysis showing no change in metal content or distribution in Zn deficient conditions.

In Zn deficient media *Atiar1-t* showed increased primary root length and reduced chlorophyll content alongside increased shoot fresh weight when compared to Col-0, but this phenotype was also seen in control Zn conditions suggesting developmental control of hypocotyl and petiole length may be a contributing factor for both *Atiar1* mutants rather than Zn deficiency sensitivity. The *Atiar1-t* mutant showed no induction of *AtZIP5* in Zn deficient conditions, unlike Col-0 and *Atiar1-3* suggesting some portion of Zn homeostasis is disrupted in *Atiar1-t*. Further work characterising the expression profile of these differently regulated genes may provide insight into the potential mechanism behind this reduced expression in *Atiar1-t*.

Taken together, it appears that AtIAR1 is unlikely to play a role in Zn homeostasis in Zn deficiency.

5.3.2 Slight Zn excess sensitivity is seen in *Atiar1-3*

Despite showing no strong growth phenotype, the *Atiar1-3* mutant showed a statistically significant increase in expression of *AtIMA1* suggesting an increase in the Fe deficiency response through reduced Zn detoxification. Expression of *AtIMA1* is associated with increased expression of Fe uptake genes however the effect of this is not seen in the ICP-OES data where the *Atiar1-3* mutant shows similar Fe content to Col-0. This may suggest the disturbance of the Zn excess response is limited to subcellular compartments and doesn't interfere with whole plant Zn and Fe homeostasis, or that regulation of *AtIMA1* may be separated from that of Fe import genes.

Atiar1-t mutants showed similar root phenotypes, shoot phenotypes and expression profiles to Col-0 in Zn excess conditions. In addition to completing ICP-OES analysis on *Atiar1-t* plants, further work on AtIAR1 and Fe deficiency response could include the inclusion of more Fe deficiency regulated genes in the analysis and testing growth and metal content of both *Atiar1-3* and *Atiar1-t* mutants in Fe deficient conditions containing 1 µM Zn. Together this may reveal details on the mechanism behind the AtIMA1 upregulation in *Atiar1-3* plants.

Overall, it appears that *Atiar1-3* may be slightly sensitive to Zn excess although further work is needed to explore this possibility, and the mechanisms behind it.

5.3.3 *Atiar1-3* and *Atiar1-t* mutants differ in their Zn related phenotypes

Atiar1-t is predicted to be a knockout mutant, whilst *Atiar1-3* is predicted to express *Atiar1-3* which lacks some *AtIAR1* functionality. In shoot growth

phenotypes, *Atiar1-3* plants showed a phenotype intermediate between Col-0 and *Atiar1-t* of higher shoot fresh weight and reduced chlorophyll in Zn deficient and control conditions. However, in the root growth phenotype of *Atiar1-3* did not match that of *Atiar1-t*. For example, in Zn deficiency *Atiar1-3* had smaller primary roots whilst *Atiar1-t* had longer primary roots than Col-0. This difference in phenotype may reflect the partial functionality of Atiar1-3 proteins, which may interfere with root-specific processes in a way not seen in the *Atiar1-t* knockout mutants.

As AtIAR1 activity has been shown in this study to influence shoot and root development and is thought to control auxin conjugate hydrolysis[1,328], the Zn dependence of developmental changes related to auxin are examined further in **Chapter 6**.

Chapter 6: *AtIAR1* and auxin homeostasis

6.1 Introduction

6.1.1 Auxin signalling, metabolism, and transport

Auxin is a major plant hormone involved in many developmental processes in plants. Auxin has been shown to signal through indole-3-acetic acid (IAA, auxin) binding to intracellular receptors including TRANSPORT INHIBITOR RESPONSE1 / AUXIN SIGNALLING F-BOX PROTEIN (TIR1/AFB) and AUXIN / IAA (Aux/IAA) coreceptors which then leads to release of AUXIN RESPONSE FACTORS (ARFs) from repression to bring about a transcriptional response[216,217,219,225]. IAA binding has also been demonstrated for AUXIN BINDING PROTEIN1 (ABP1)[235] which localises to the endoplasmic reticulum (ER) and plasma membrane[236] and is thought to be responsible for signalling from extracellular IAA potentially through TRANSMEMBRANE KINASE 1 (TMK1)[238-240]. For further information on auxin signalling see **Chapter 1.3.2**.

One of the ways to control auxin signalling is through altering the concentration of cellular IAA through regulation of the synthesis, conjugation and degradation of IAA, as shown below in **Figure 6.1**.

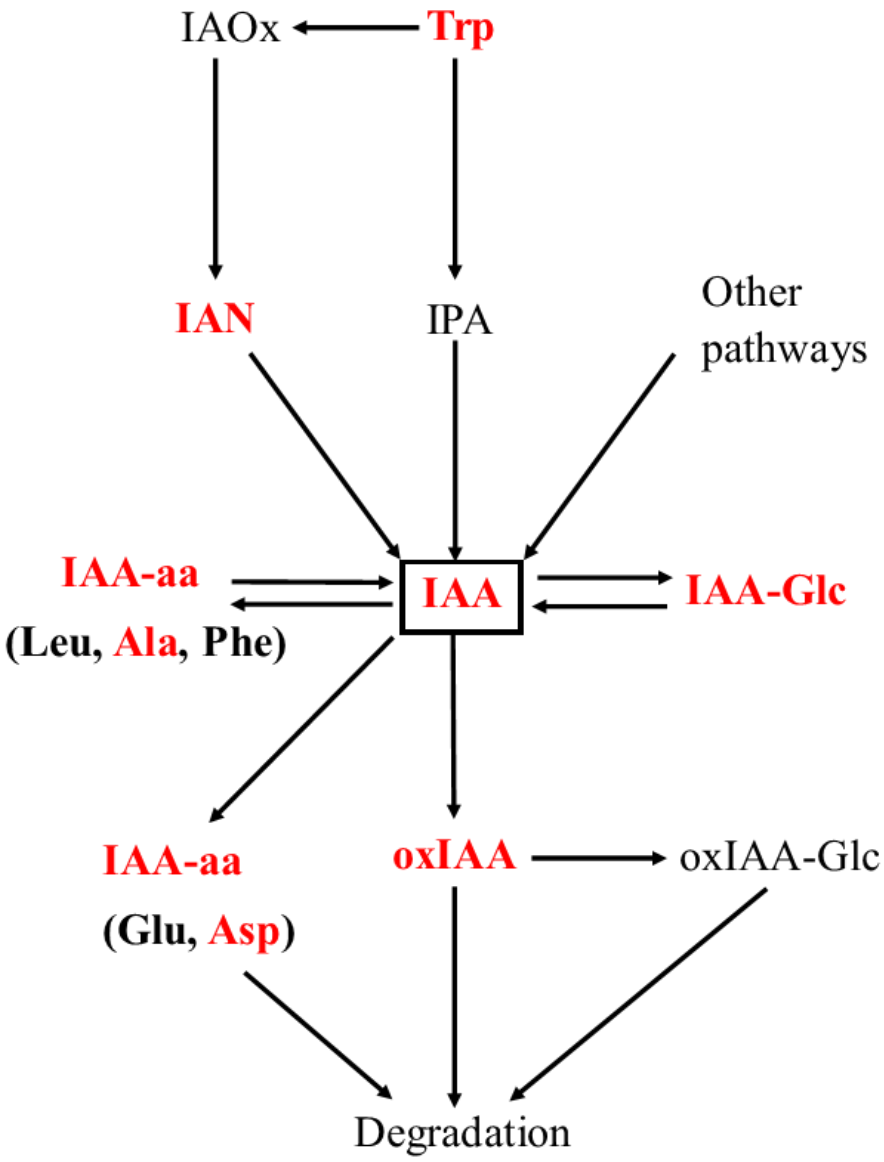

Figure 6.1 Auxin synthesis, conjugation, and degradation pathways.
Metabolites in red represent metabolites investigated in this study. For details of metabolic conversions see text and **Chapter 1.3.3** and **Chapter 1.3.4**.

In young seedlings, the majority of IAA synthesis occurs in above-ground tissue particularly cotyledons, but all tissues do show localised *de novo* synthesis[241,242]. IAA can be synthesised mostly from tryptophan (Trp) but also Trp-independent sources[243]. The pathway of IAA synthesis from Trp can take two routes; via indole-3-acetaldoxime (IAOx) or via indole-3-pyruvic acid (IPA). The route via IAOx involves reactions catalysed by AtCYP79B2/B3[257,258] and AtCYP71A13[262] to

produce indole-3-acetonitrile (IAN) which can then be converted to IAA through the activity of AtNITRILASE1[263,264]. The route via IPA involves TAA/TAR and YUCCA enzymes[247-249] and is thought to be the major pathway to synthesis IAA[252,253].

The concentration of active IAA is then also controlled through its conjugation into inactive storage forms and degradation via oxidation. These inactive conjugates include methylated IAA, amide-linked IAA and ester-linked IAA. Methylated IAA is formed through IAA CARBOXYMETHYLTRANSFERASE 1 (AtIAMT1)[301] and this process is reversed via esterases including AtMES17[302]. Amide-linked IAAs include amino acid linked IAAs (IAA-aas), peptide linked IAA and protein linked IAA. IAA-aas are formed from IAA through the action of enzymes in the Gretchen Hagen 3 (GH3) family[270,271]. In some cases (IAA-Asp and IAA-Glu), this conjugation is irreversible[276] whereas in other cases (IAA-Ala, IAA-Leu, IAA-Phe among others) the conjugation is reversible through the activity of ER-localised IAA-aa hydrolases[279-282]. The major ester-linked IAA conjugate observed in *Arabidopsis* is IAA-glucose (IAA-Glc). This conjugation to glucose occurs through the activity of UDP-glucosyltransferases (UGTs), predominantly AtUGT84B1[288-293]. The glycosylation of IAA is reversible in rice[294] and maize[295], and although a hydrolysis step has not yet been demonstrated in *Arabidopsis*, it is suspected[296]. Oxidation is the main pathway by which IAA is catabolised. DIOXYGENASE FOR AUXIN OXIDATION enzymes (AtDAO1/2)[304-306] catalyse the oxidation of IAA to oxIAA, which can then become glucosylated to oxIAA-Glc through the action of AtUGT74D1[297].

The concentration of active IAA is also controlled by polar transport between and within cells and tissues to create gradients. In order to create auxin concentration gradients across tissues to generate a developmental response, various auxin transporters are required. These transporters include the polarly localised long PINFORMED (PIN) auxin exporters[183-187], AUXIN-RESISTANT1/ LIKE AUX1 (AUX1/LAX) auxin importers[200,202,429], ATP-BINDING CASSETTE (ABC) transporters[207,430] and AtNRT1.1[209]. In addition, subcellular compartmentalisation of IAA is also controlled by transporters. Transporters such as short PINs and PIN-LIKES (PILS) family members localise to the ER and co-ordinate IAA transport between the ER and cytosol[191-195]. In addition, WALLS ARE THIN1 (AtWAT1)

was shown to be important for release of vacuolar stores of IAA[196]. For further details on auxin transporters see **Chapter 1.3.1**.

Transport of IAA also occurs at the whole plant level from IAA sources to sinks and appears to progress through narrow routes including the vasculature system. These auxin transport pathways are reinforced in a positive feedback loop in a process referred to as canalization that requires IAA-dependant changes in PIN localisation[283,311-315].

6.1.2 Auxin in development

6.1.2.1 Auxin homeostasis and primary root growth

Primary root length is an essential feature of root architecture to aid nutrient and water acquisition. Root growth is maintained by the root apical meristem (RAM). There are three domains within the RAM; the stem cell niche (SCN), the proliferation zone and the transition zone, with the elongation zone lying above the transition zone, outside of the RAM. In the SCN a population of stem cells is maintained; these then divide asymmetrically into transit amplifying cells which move into the proliferation zone where they divide further. These cells then begin differentiating in the transition zone which includes elongation that continues into the elongation zone above the RAM[431-433]. This balance of division and differentiation in the RAM is a tightly controlled process which leads to root growth[170]. Root growth is therefore determined by division rate in the meristem and the extent of elongation in the elongation zone[434]. A major part of this control comes from the cross talk and antagonism between auxin and cytokinin with auxin promoting division and cytokinin promoting differentiation and elongation[171,275].

Auxin, sourced redundantly from the shoots and synthesised locally, is important for maintaining the SCN in the meristem and therefore root elongation[241,251,435]. To generate an auxin gradient, auxin is transported via the stele (made of pericycle and vasculature tissue) towards the quiescent centre (QC) through the activity of

AtPIN1[184] and AtPIN7[172]. Auxin is then further concentrated to the root tip by activity of AtPIN2 localised to the basal membrane of cells in the cortical layer[172,185,436] and AtPIN4 localised to the basal layer of cells surrounding the QC and provascular cells[172]. AtPIN3 and AtPIN7 are localised on the membrane symmetrically in the columella cells, but react to changing gravitational stimuli such as during root skewing by polarising their localisation to induce gravitropism[186,437]. Auxin is then transported to the epidermal layers and up in a shootward direction through the action of AtPIN2 localised to the apical layer of epidermal cells[172,436]. AtAUX1, which facilitates auxin uptake into cells, has been shown in modelling to be vital for maintaining auxin gradients within the root tip and elongation zone by preventing flow of auxin from the root-to-shoot stream in the epidermis into the shoot-to-root stream in the stele[438]. This IAA transport in the root tip is summarised in **Figure 6.2.**

Cytokinin acts antagonistically to auxin in the root to promote cellular differentiation instead of division thereby reducing the root meristem size[179]. Cytokinin activity through SHORT HYPOCOTYL2 (SHY2) represses auxin signalling and downregulates *AtPIN1, 3, 7* expression reducing auxin concentration at the QC whilst auxin activity causes degradation of AtSHY2[171]. Cytokinin also acts through upregulation of the short PIN gene *AtPIN5*, and *AtGH3.17* which promote the uptake of auxin into the ER and conjugation, including to IAA-Glu respectively[191].

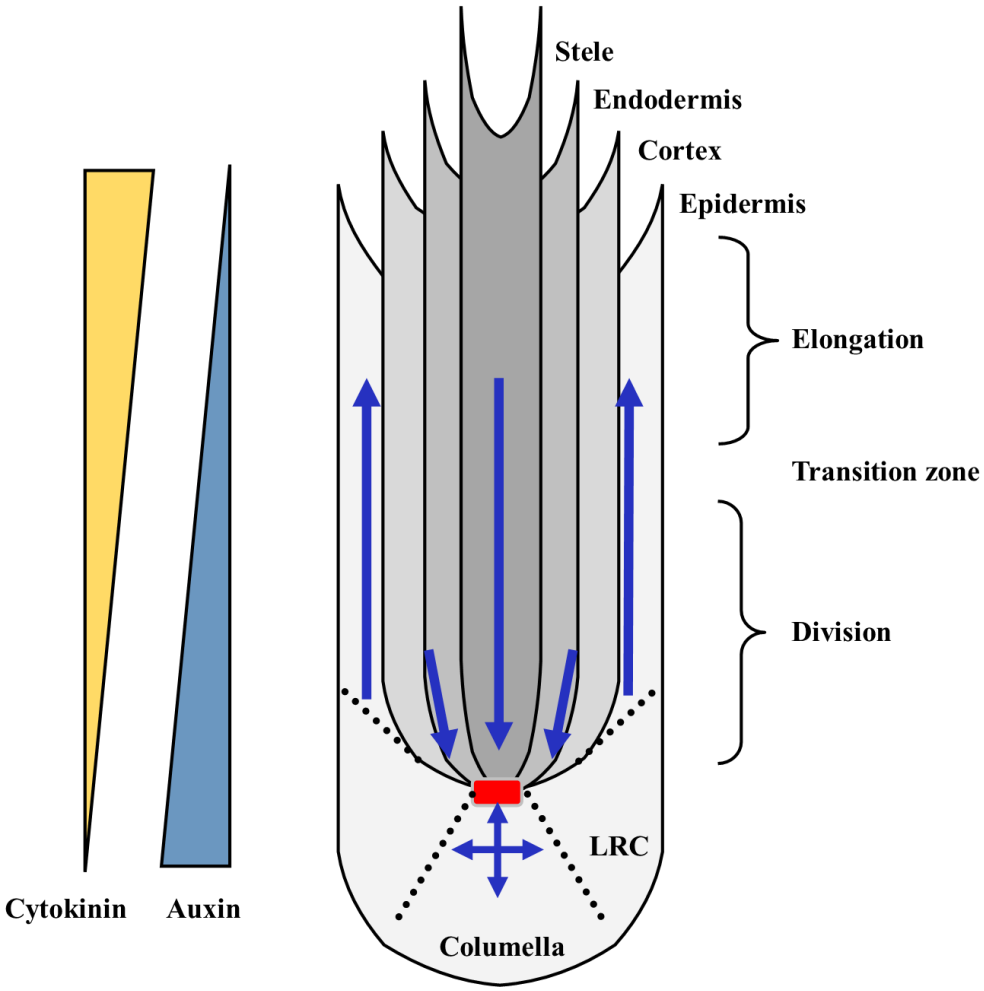

Figure 6.2 Auxin transport in the root tip. Quiescent centre in red where a stem cell niche (SCN) is maintained. Auxin transport shown by blue arrows maintains the SCN and determines the ratio of division to differentiation in the root tip. Auxin (blue) and cytokinin (yellow) concentration gradients can be seen to decrease and increase respectively as cells transition from division to elongation as they move away from the SCN. LRC denotes the lateral root cap.

The elongation of root cells is also influenced by auxin levels through apoplastic pH changes[439]. According to the acid growth hypothesis, a drop in apoplastic pH loosens cell walls and so enables elongation[440-442] and indeed the apoplastic pH decreases in the transition zone relative to the elongation and division zone, coincident with the beginning of elongation[443]. However, when IAA is applied exogenously at high concentration, root length decreases[444] through apoplastic

alkalinisation requiring TIR1 auxin signalling, which at high auxin concentration dominates over the TMK1-mediated phosphorylation and activation of proton pumps on the plasma membrane[240,443]. At lower concentrations, the TMK1 pathway domain dominates and so promotes root cell elongation. These results display the concentration-dependence of the activity of auxin that has been illustrated in a variety of contexts[283,445,446].

Other factors that change during cell expansion include cytoskeletal reorganisation and vacuolar expansion which control the ratio of cell elongation to radial expansion[447-452] and turgidity of the cells respectively[453,454].

6.1.2.2 Auxin homeostasis and lateral root formation

Lateral root (LR) formation is an important part of root architecture that dynamically exploits new areas of soil. LR formation involves four stages; pre-branch site formation, initiation, primordium formation and emergence[455]. LR pre branch site formation starts from the priming of xylem pole pericycle (XPP) cells. This priming is responsive to changes in cell shape and gravitropism that are accompanied with root skewing, in a process dependant on AtAUX1 and AtPIN1 activity[456,457]. The auxin that is required in this context is derived from programmed cell death releasing IAA from indole butyric acid in the LRC[458-460].

An auxin threshold is required to be reached within these XPP cells for initiation, wherein the XPP cells re-enter the cell cycle and undergo asymmetric division[461] in a process that utilises shoot-derived auxin[462-464], locally synthesised auxin[461,465] and auxin transporters[466]. AtPIN3 acts in endodermal layers to transport auxin back into XPP cells[467] while AtAUX1 is important in mobilisation of auxin from source tissue in the shoot and auxin uptake in XPP cells[468]. This high level of auxin activates auxin signalling components that mediate the cell specification required for undergoing the asymmetric division[469].

After initiation, cells undergo primordium formation and emergence in which the primordium undergoes rapid division to push through the outer layers of root cells[204]. Following outgrowth, the LR emerges from the primary root and becomes

organised similarly to the primary root tip with epidermal, cortex and endodermal layers[455]. This process of emergence requires a very localised expression of an auxin uptake transporter (*AtLAX3*) to the endodermal and cortical cell layers enabling auxin concentration in these cells[204]. This concentration of auxin can then stimulate the expression of genes for cell wall modification enzymes enabling LR emergence[470]. This process is illustrated below in **Figure 6.3.**

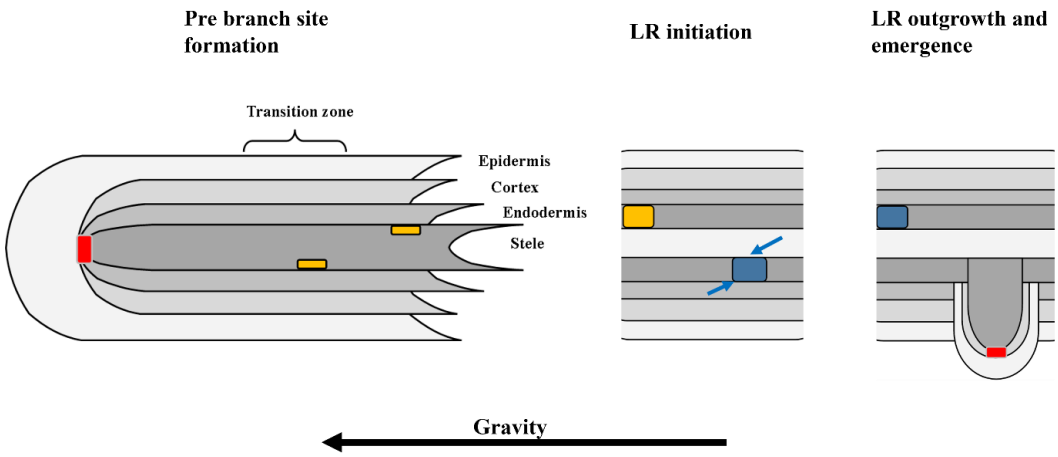

Figure 6.3 Lateral root formation. Within the primary root, pre branch site formation starts from priming xylem pole pericycle (XPP) cells (orange cells). To initiate LR formation, auxin transporters (blue arrows) create an auxin local maximum in primed XPP cells (blue cells). Once initiated, LR outgrowth and emergence breaches the outer root layers to form a stem cell niche (red cells) with similar structure to that of the primary root.

6.1.2.3 Auxin homeostasis and hypocotyl length

The *Arabidopsis* hypocotyl epidermis is formed of around 20 cells from top to bottom which co-ordinate hypocotyl length exclusively through cell expansion[471]. Many hormones are involved in regulating this expansion including auxin[472,473],

ethylene[474,475] and gibberellins[476,477] which all interact[478]. In addition, the cell elongation depends on cell wall integrity[479,480], cytoskeletal components[481] and vacuole-mediated cell turgidity[482-484]. All these factors are influenced differently by light, which inhibits hypocotyl elongation[475,476,478,485-487].

In both light and dark conditions, auxin promotes cell expansion in shoot hypocotyls through acid-induced growth, where auxin induces apoplastic acidification and so promotes wall-loosening and cell extension[488,489]. Auxin-dependant cell elongation requires TMK1[490], the TIR1/AFB signalling pathway[491,492] and expression of *SMALL AUXIN UP RNA* (*SAUR*) genes, together leading to activation of a plasma membrane H^+-ATPase[489,491,493,494].

Emergence of seedlings from soil involves rapid hypocotyl elongation through cell elongation alone, along with the development of an apical hook which acts to protect the shoot apical meristem as the plant pushes upwards[163,471]. This developmental programme in the dark is referred to as skotomorphogenesis. Interestingly, there is heterogeneity in the rate of elongation within skotomorphogenesis, with the initial 24 hours of hypocotyl elongation occurring slowly where high levels of auxin are seen to inhibit *AtSAUR* expression[495]. This is then followed by a phase of faster elongation which spreads upwards in the hypocotyl when auxin concentration is reduced to levels where *AtSAUR* expression is induced[471,495,496]. This further exemplifies the concentration dependence of the auxin response.

Formation of the apical hook requires co-ordination of ethylene and auxin signalling[497,498], which interact[499] and are responsive to light[230]. Within the apical hook, the hook structure is created through the inhibition of cell expansion on the concave side of the hook[500]. This inhibition of cell expansion is correlated with an auxin maximum created through auxin transporters including AtPIN1, AtPIN2, AtPIN4, AtAUX1 and AtLAX1[501,502]. Auxin accumulation on the concave side of the hook leads to signalling through the TMK1 pathway[239], leading to TIR1/ARB activity which causes inhibition of apoplastic acidification through *AtSAUR* repression[495].

The detection of light of various wavelengths through photoreceptors[503-507] leads to large transcriptional responses[508] including expression which evokes inhibition of

hypocotyl elongation[509,510]. The main components in this response are PHYTOCHROME INTERACTING FACTORS (PIFs)[511-517], ETHYLENE-INSENSITIVE 3/EIN3-LIKE 1 (EIN3/EIL1)[518-520] and ELONGATED HYPOCOTYL 5 (HY5)[521,522]. These light dependant factors then go on to cause changes to hormone activity such as increasing auxin activity in dark conditions and decreasing auxin activity in light conditions[293,516,523,524]. Light is also associated with changes of *PIN* transporter expression and localisation such that auxin transport in the root and shoot favours root growth over shoot growth unlike in skotomorphogenesis[525-528]. Further increases of auxin activity are responsible for the hypocotyl elongation that occurs in conditions of elevated temperature[529,530] and shade avoidance[274,531]. This auxin comes from both local sources[274] and from synthesis in the cotyledons[487,532,533].

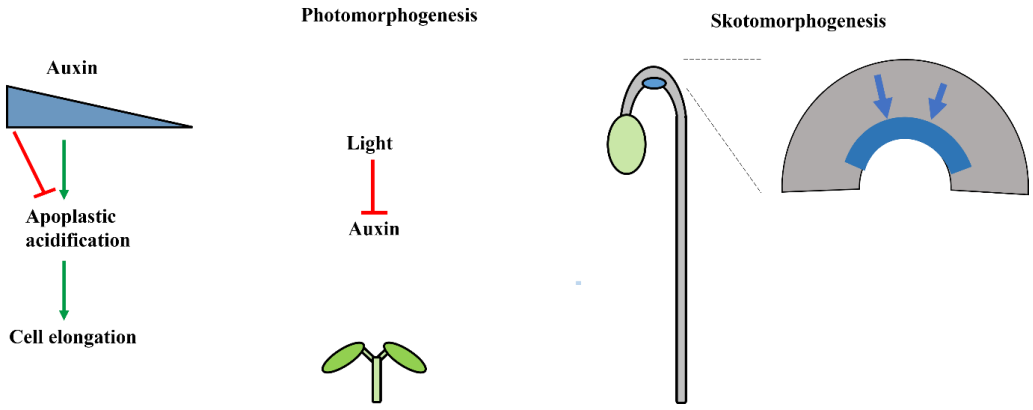

Figure 6.4 Role of auxin in hypocotyl elongation. Auxin stimulates apoplastic acidification in a concentration-dependant manner. Light among many other activities, inhibits auxin activity leading to short hypocotyls during photomorphogenesis. During skotomorphogenesis, auxin acts in a concentration dependant manner to induce hypocotyl cell elongation. However high levels of auxin within the concave side of the apical hook (blue region) created through auxin transport (blue arrows) restrict cell elongation and lead to apical hook formation. See text for further details.

6.1.2.4 Mutants in auxin related genes show characteristic phenotypes

Mutations within genes responsible for auxin sensing, synthesis, and metabolism, provide a framework for establishing key auxin-related phenotypes to test within this study. *Attmk* loss of function mutants show reduced response to exogenous IAA along with reduced cell elongation in shoot and root tissue[534], reduced apical hook angle[239], reduced LR number[535] and reduced gravitropism[536].

Overexpression of *AtYUCCA1* increases IAA levels and results in increased hypocotyl length in light conditions and decreased hypocotyl length in dark conditions with no apical hook[537]. These plants also show elongated petioles, shorter roots with increased frequency and density of root hairs[537]. The phenotypes are similar to those observed in *Atsuperroot* mutants[334,538]. These *Atsuperroot* mutants were characterised to be loss of function mutations in genes responsible for IAOx utilisation in the glucosinolate pathway, leading to increased IAOx conversion to IAA[539].

Mutations in genes responsible for IAA conjugate synthesis and degradation illustrate the importance of IAA conjugates on wider development. Loss of function mutations in the gene encoding AtGH3.17, an enzyme thought to be responsible for IAA conjugation to specifically IAA-Glu, showed longer hypocotyls in light conditions[274], whereas overexpression of *AtGH3.6* caused reduced lateral root growth and short hypocotyls in most light conditions but not in darkness[540]. Similarly, *Atilr1 Atiar3 Atill2* IAA-aa hydrolase triple mutants show reduced root length, LR number and hypocotyl length compared with wildtype. Quadruple knockout mutants for *AtUGT76E* genes thought to be involved in IAA conjugation with glucose have elongated hypocotyls in skotomorphogenesis only, and show higher IAA and decreased IAA-Glc levels[290]. Knockout mutations within the *AtDAO1* gene that is responsible for IAA oxidation causes a dramatic increase in IAA-Asp and IAA-Glu levels which correspond to increased lateral root density, reduced apical hook angle and an increase in hypocotyl length in etiolated plants[306]. Therefore, for this study, root length, lateral root density, hypocotyl length and skotomorphogenesis features were used as indicators of auxin activity.

6.1.3 Auxin and Zn interactions can be probed using *Atiar1* mutants

The details of the interactions between Zn and auxin remain mostly unexplored besides the known reduction in root length and meristem size in plants grown in Zn excess[325,327]. For further details on known auxin and Zn interactions see **Chapter 1.4**. Therefore, in this study the Zn and auxin dependency on established auxin phenotypes are measured. The testing of *Atiar1* mutants is used to probe the poorly understood link between subcellular Zn homeostasis, auxin conjugate balance and wider auxin homeostasis. The study includes the already-characterised *Atiar1-3* mutant and the *Atiar1-t* mutant, hypothesised to be a knockout mutant (see **Chapter 5**), whose auxin phenotypes have not yet been examined.

6.2 Results

6.2.1 Auxin related root phenotypes

6.2.1.1 Primary root length and meristem size after 5 days depends on Zn and *AtIAR1*

The balance of division and differentiation rates in the RAM in combination with extent of cell elongation in the elongation zone determine primary root growth[170,434]. This balance between division and differentiation within the RAM can be analysed with microscopy by measuring the number of meristematic cells in the cortex layer of root tips[350]. To determine what role *AtIAR1* and Zn have in early primary root growth and whether any differences are caused by meristem size, both features were measured in Col-0, the *Atiar1-3* mutant and the suspected complete knockout *Atiar1-t* mutant at 5 days as shown in **Figure 6.5.**

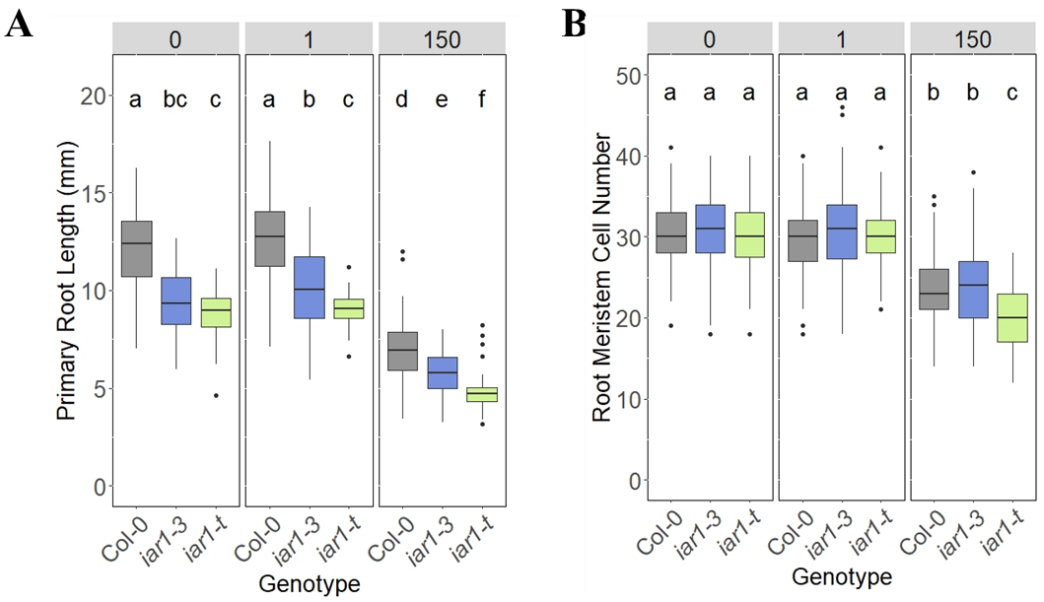

Figure 6.5 Primary root length and meristem size. Primary root length (A) and meristem cell numbers (B) were measured from Col-0 (grey), *Atiar1-3* (blue) and *Atiar1-t* (green) plants grown for 5 days in Zn deficient (0 Zn added), Zn control (1 µM) and Zn excess (150 µM) conditions on modified Hoagland's media containing EDTA-washed agar. At least 30 plants were measured in each of three biological replicates. Data displayed using R version 4.1.1. Lower case lettering indicates statistically significant differences between groups (labelled sequentially from 'a' in order of estimated mean) as calculated using analysis of variance (ANOVA) using Tukey's method for p-value adjustment[366] for 9 groups using a p-value cut-off of 0.05.

As shown in **Figure 6.5**, excess Zn conditions, as expected lead to reduction in primary root length. This reduction in root length is mirrored by reduction in meristem size, suggesting similar to previous studies that reduction of meristem size is at least partially responsible for the primary root growth reduction in Zn excess conditions[325,327]. After 5 days of growth, both *Atiar1-3* and *Atiar1-t* mutants show reduced primary root length compared with Col-0 in all Zn conditions with this reduced primary root growth more severe in *Atiar1-t* than *Atiar1-3* mutants, aligning with the suspected decrease in AtIAR1 functionality between these two mutants. However, the differences between genotypes observed in primary root

length is not seen in root meristem cell numbers, except in excess Zn conditions. The lack of coherence between primary root length and root meristem size could be due to reduction in the extent of elongation of cells in both the *Atiar1* mutants. Under excess Zn conditions, *Atiar1-t* additionally shows reduced meristem size indicating that *AtIAR1* activity might influence several different aspects of primary root growth in a Zn dependant manner.

AtDR5 promotor-driven *GFP* expression has proved a useful tool for investigating sites of auxin transcriptional activity[541]. In the *DR5*::*NLS-2GFP* expressing reporter plants, nuclear localised tandem GFP is the auxin-signalling driven output. These reporter plants were crossed with the *Atiar1-3* mutant, and in line with the meristem size data (**Figure 6.5B**) did not display any inter-genotype differences between itself and the wildtype reporter plants in the RAM (data not shown). Future work could involve crossing the *DR5*::*NLS-2GFP* expression reporter plants with *Atiar1-t* mutants to investigate whether the changed meristem size under excess Zn correlates with changed auxin signalling.

6.2.1.2 *Atiar1* mutants show different levels of IAA-Ala insensitivity depending on Zn status

The *AtIAR1* gene was discovered and characterised through a screen for mutants showing insensitivity to the root growth inhibition effect in media with exogenous IAA-Ala[328]. The mutant phenotype was complemented by excess Mn conditions, however the IAA-Ala sensitivity was not tested across in different Zn conditions. Therefore, this study aimed to address how IAA-Ala sensitivity is influenced by Zn level. To test the sensitivity to the response, primary root lengths after 10 days were first measured in media without any additional IAA or IAA-Ala, as shown below, which has been presented previously (**Figure 5.5**, repeated below in **Figure 6.6**).

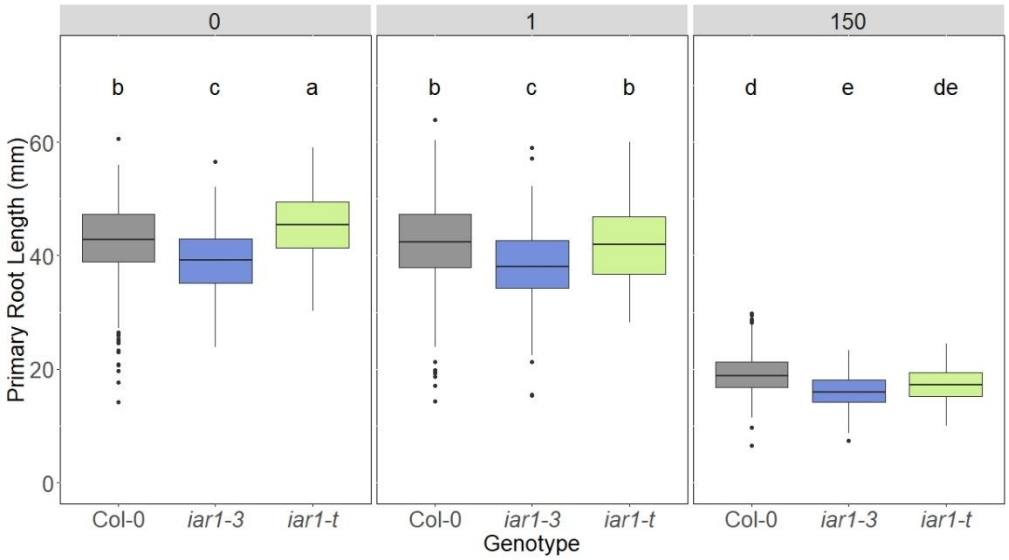

Figure 6.6 Primary root length of *Atiar1* mutants grown at different Zn concentrations. Primary root length was measured from Col-0 (grey), *Atiar1-3* (blue) and *Atiar1-t* (green) plants grown for 10 days in Zn deficient (0 Zn added), Zn control (1 µM) and Zn excess (150 µM) conditions on modified Hoagland's media containing EDTA-washed agar. At least 50 plants were measured in each of three biological replicates with statistically significant differences between groups calculated and displayed as in **Figure 6.5**.

Interestingly, the relationship between genotypes in primary root length differs between day 5 and day 10. At day 10, *Atiar1-t* has a longer primary root length than Col-0 and *Atiar1-3* in Zn deficient conditions, and similar to Col-0 in control Zn conditions. This suggests that the phenotype of *Atiar1-t* is developmental stage-dependant, unlike that of *Atiar1-3*. Meristem size is predicted to be constant after 5 days[350], although this assumption was not tested in this study so the origin of this root length change has not been further examined.

To determine plant sensitivity to IAA-Ala and its Zn dependence, the percentage change in primary root growth after 10 days growth in media containing IAA-Ala was compared to 10 days of growth in media without added auxin or auxin conjugate (presented in **Figure 6.6**). This sensitivity of primary root growth to IAA-Ala is shown below in **Figure 6.7**.

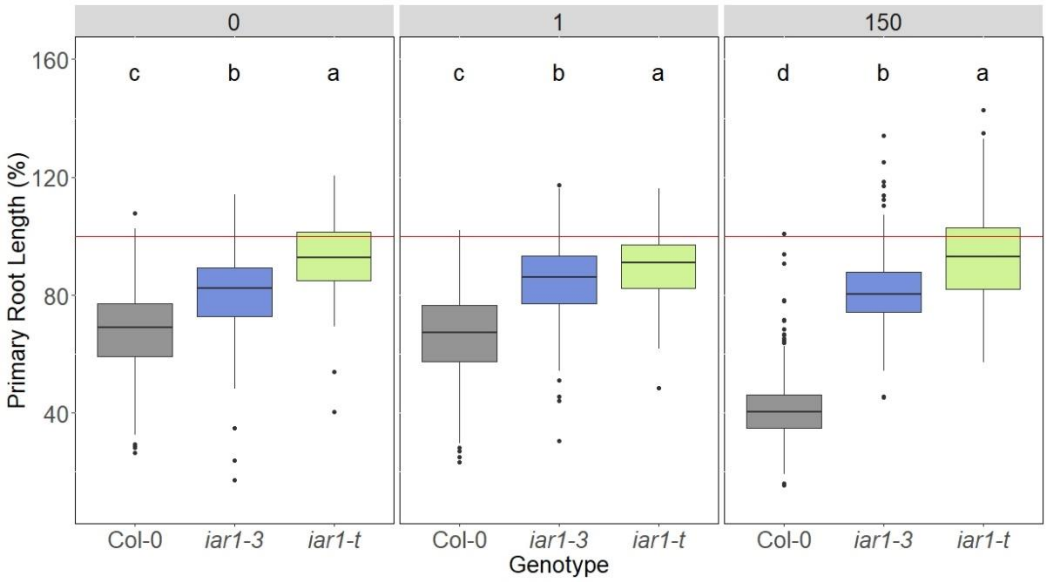

Figure 6.7 Primary root length percentage change in IAA-Ala media.
Percentage primary root length in media containing 20 µM IAA-Ala compared to media with no auxin conjugate added with all other media conditions as **Figure 6.6**. 100% (no response) is indicated by the red line. At least 50 plants were measured in each of three biological replicates with statistically significant differences between groups calculated and displayed as in **Figure 6.5**.

As shown above, the insensitivity to IAA-Ala is seen in both *Atiar1* mutants across all Zn conditions. The phenotype of IAA-Ala insensitivity is greater in *Atiar1-t* relative to *Atiar1-3* mutants, which again aligns with the suspected increased severity of the *Atiar1-t* mutant. Interestingly, the sensitivity of IAA-Ala increases in Zn excess conditions only for Col-0 and not in either of the *Atiar1* mutants suggesting an *AtIAR1*-dependant sensitisation that occurs in high Zn. Additionally, the high insensitivity to IAA-Ala response in the *Atiar1-t* mutants shows that most of the IAA-Ala hydrolysis is occurring in an *AtIAR1*-regulated environment rather than extracellularly before uptake by the plant. However, this high degree of insensitivity may have masked any Zn excess dependant auxin hypersensitisation in the mutant under these conditions.

The effect of IAA-Ala is a function of IAA-Ala uptake, hydrolysis and then transport, metabolism and signalling of IAA. To determine where within this sequence the Zn and genotype-related phenotypes are acting, the percentage change in primary root length under exogenous IAA was assayed (**Figure 6.8**).

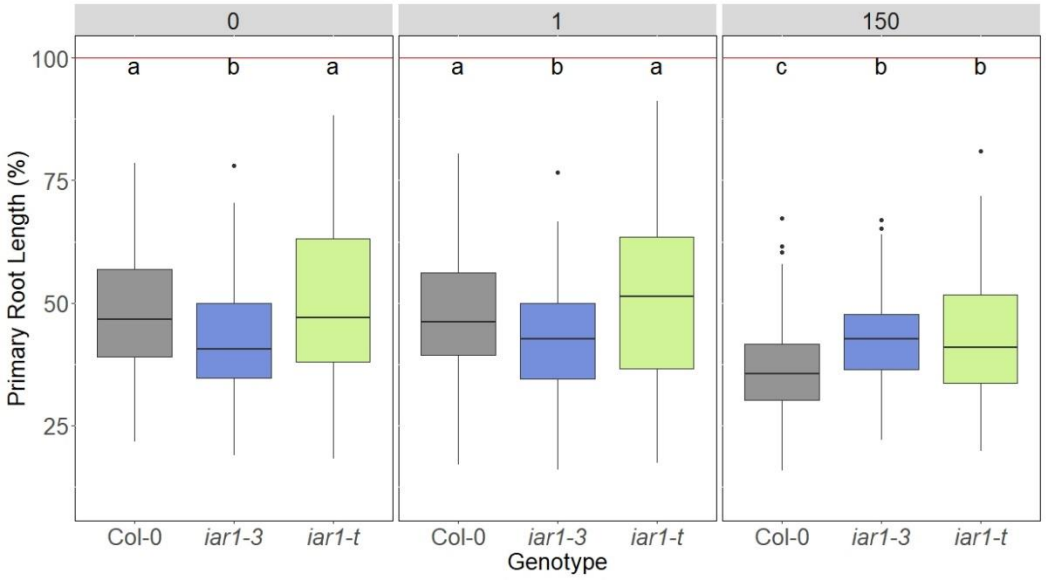

Figure 6.8 Primary root length percentage change in IAA media. Percentage primary root length in media containing 100 nM IAA compared to media with no auxin added with all other media conditions as **Figure 6.6**. 100% (no response) is indicated by the red line. At least 50 plants were measured in each of three biological replicates with statistically significant differences between groups calculated and displayed as in **Figure 6.5**.

Firstly, IAA at 100 nM has greater potency in primary root length reduction than 20 µM IAA-Ala in Col-0 under Zn deficiency and control Zn conditions. Given that IAA-Ala is inactive, and activated by hydrolysis to IAA, this suggests that IAA levels in the plant after IAA-Ala hydrolysis are different from those induced by direct application of IAA and thus lead to a different level of response. Also, as seen above in **Figure 6.8**, insensitivity is no longer seen in *Atiar1* mutants across Zn deficiency and control conditions implying this insensitivity effect is restricted

to the influence of AtIAR1 on auxin conjugate hydrolysis, as suspected. Additionally, Col-0 shows a reduction in primary root length change under Zn excess conditions. This implies that the Zn excess influence on auxin sensitivity occurs post IAA-Ala hydrolysis. However, in contrast to exogenous IAA-Ala conditions, *Atiar1-t* mutants also show a slight reduction in primary root length change under Zn excess conditions. Interestingly, the *Atiar1-3* mutant, as seen in exogenous IAA-Ala conditions, shows no change in percentage root length across Zn conditions. *Atiar1-3* also shows increased sensitivity in Zn deficient and control conditions compared to Col-0 and *Atiar1-t*, which together indicates a difference between the two *Atiar1* mutants in Zn dependence of IAA sensitivity.

Overall, it seems that two factors are involved in the *AtIAR1*-mediated intersection of Zn and auxin; conjugate hydrolysis, and also a novel Zn excess-mediated effect which warrants further investigation. To determine whether further auxin-related phenotypes in the root show similar Zn, auxin and AtIAR1 dependence, lateral root (LR) density and its sensitivity to IAA-Ala and IAA were measured.

6.2.1.3 *Atiar1-t* mutant shows increased lateral root density

As a classic symptom of auxin homeostasis disruption, LR density was examined in *Atiar1* mutants across Zn conditions. LR density was measured alongside primary root length after 10 days seen above and so firstly, LR density in media with no exogenous auxin added was measured (**Figure 6.9**).

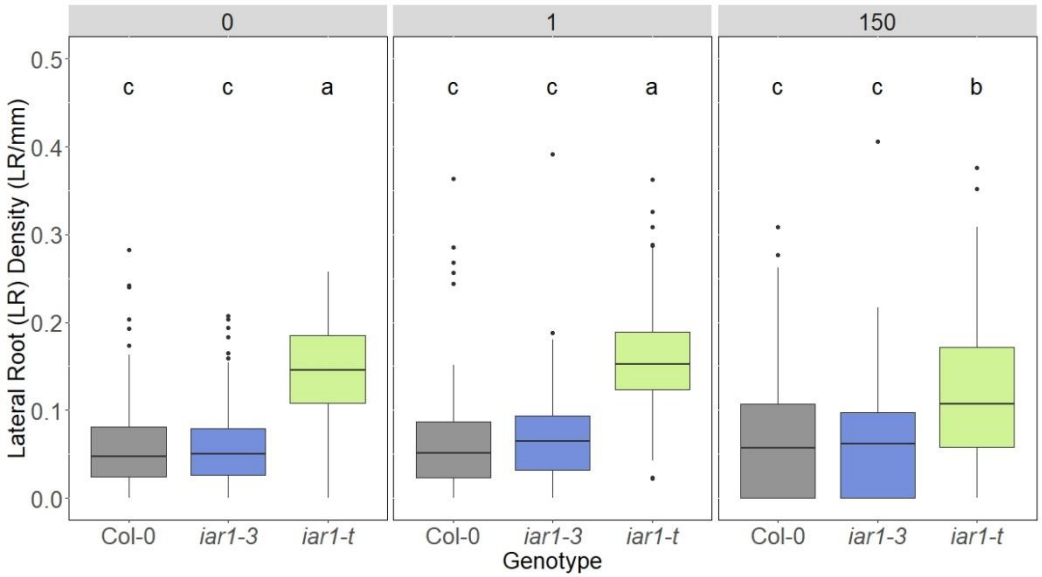

Figure 6.9 Lateral root density across Zn conditions. LR density measured for each individual seedling grown in media conditions as **Figure 6.6**. At least 50 plants were measured in each of three biological replicates with statistically significant differences between groups calculated and displayed as in **Figure 6.5**.

As seen above in **Figure 6.9**, LR density is increased in *Atiar1-t* mutants in all Zn conditions but not in *Atiar1-3* mutants. Additionally, LR density is not Zn-responsive in wildtype and *Atiar1-3* genotypes but in high Zn conditions the LR density of *Atiar1-t* decreases. To test whether this LR density is responsive to IAA-Ala and Zn in the same way as primary root length, LR density was measured in exogenous IAA-Ala conditions (**Figure 6.10**).

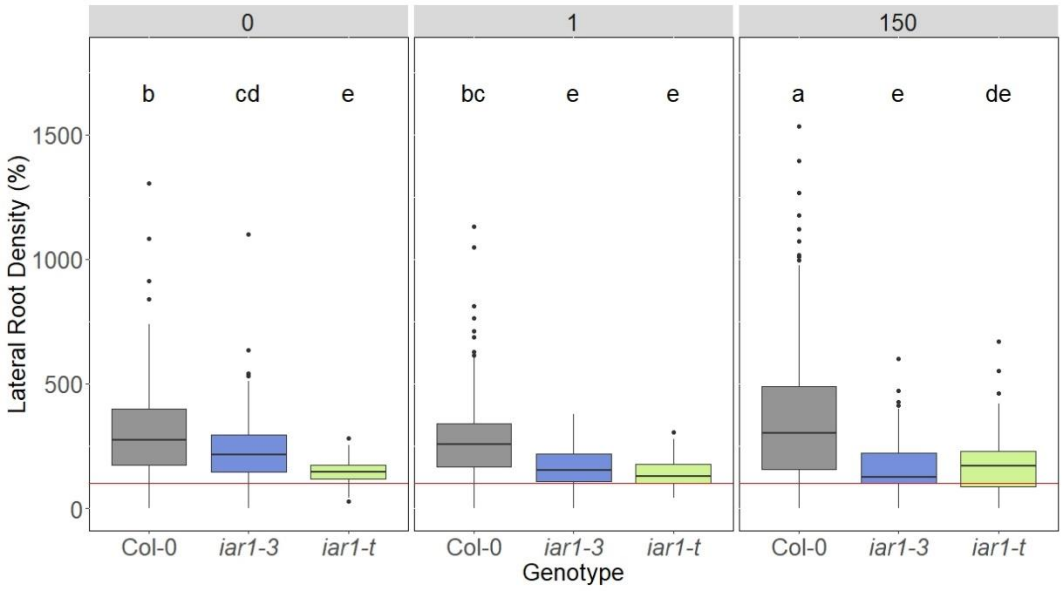

Figure 6.10 Lateral root density percentage change in IAA-Ala media.
Percentage change of LR density in media containing 20 µM IAA-Ala compared to media with no auxin conjugate added with all other media conditions as **Figure 6.6**. 100% (no response) is indicated by the red line. At least 50 plants were measured in each of three biological replicates with statistically significant differences between groups calculated and displayed as in **Figure 6.5**.

LR density changes in Col-0 in IAA-Ala containing media is enhanced in Zn excess conditions. *Atiar1-3* and *Atiar1-t* plants show increased insensitivity to IAA-Ala and a lack of a Zn excess response, although due to low responsiveness to IAA-Ala any Zn excess interaction could be masked in *Atiar1-t* plants. As these data mirrored the Zn excess effect seen in primary root length, this response of LR density to IAA was investigated further (**Figure 6.11**).

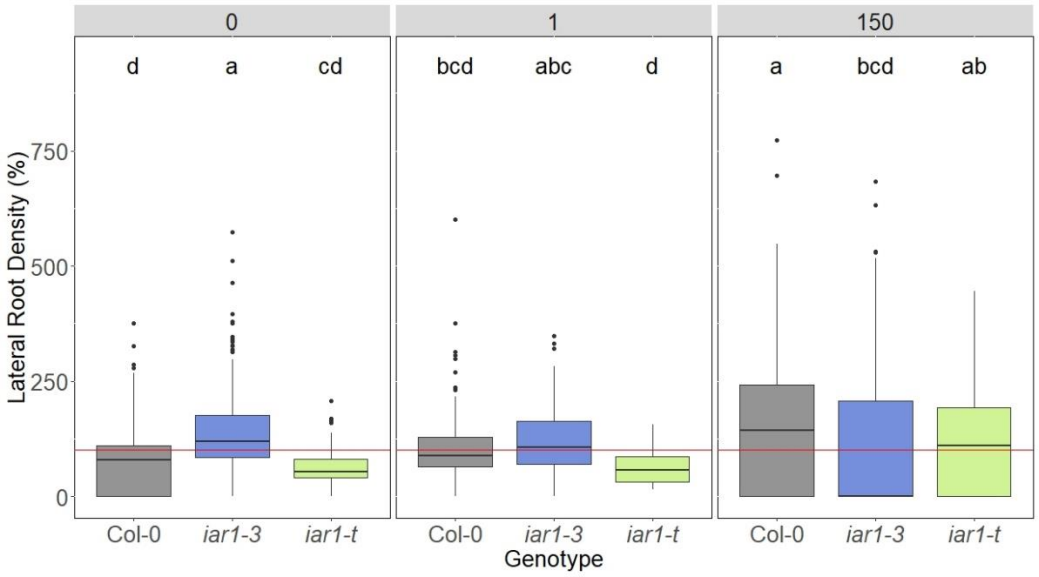

Figure 6.11 Lateral root density percentage change in IAA media. Percentage LR density in media containing 100 nM IAA compared to media with no auxin added, with all other media conditions as **Figure 6.6**. 100% (no response) is indicated by the red line. At least 50 plants were measured in each of three biological replicates with statistically significant differences between groups calculated and displayed as in **Figure 6.6**.

In contrast to the LR density changes in IAA-Ala containing media, in exogenous IAA conditions no large increase in LR density was seen across any Zn conditions, indicating as for primary root length, the auxin response of the IAA-Ala and IAA treatments are different. Although IAA application is classically associated with increasing LR density, this effect is reduced and reversed at higher concentrations[542], in line with the results shown in this study. The exogenous IAA led to a reduction in LR density percentage change in the *Atiar1-t* mutant in Zn deficient and control conditions relative to *Atiar1-3* plants. Additionally, as in the IAA-Ala treatment, the largest lateral root density increases were seen in excess Zn conditions in Col-0 and for *Atiar1-t*, whereas no Zn excess dependant hypersensitisation was seen in *Atiar1-3*.

In summary, *Atiar1-t* plants show an elevated LR density in media with no exogenous IAA-Ala or IAA. Exogenous auxin treatment responses broadly mirror

those seen for primary root growth. IAA-Ala treatment had less effect in both *Atiar1* mutants than Col-0, which additionally showed a Zn excess mediated hypersensitivity to the IAA-Ala treatment not seen in the *Atiar1* mutants. Additionally, Col-0 and *Atiar1-t* genotypes showed evidence of Zn excess-dependant hypersensitisation to the IAA treatment.

6.2.2 Auxin related shoot phenotypes

6.2.2.1 Hypocotyl length after 10 days is reduced in *Atiar1-t* plants in Zn deficient and control conditions

Many of the disruptions in auxin homeostasis cause changes in the hypocotyl length. Building from previous results in the root, the novel excess Zn – exogenous auxin interaction was investigated in the shoot hypocotyl. Shoot hypocotyls were therefore firstly measured after 10 days of growth in conditions with no exogenous auxin or auxin conjugate (**Figure 6.12**).

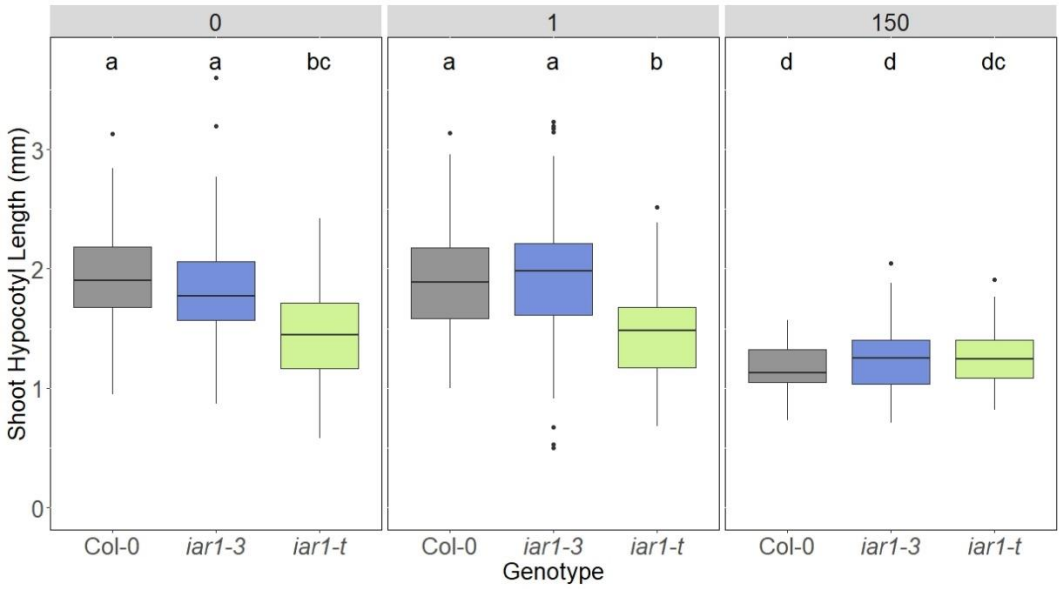

Figure 6.12 Shoot hypocotyl length across Zn conditions. Hypocotyl length was measured for each seedling grown in media conditions as **Figure 6.6**. At least 50 plants were measured in each of three biological replicates with statistically significant differences between groups calculated and displayed as in **Figure 6.5**.

For Col-0 and *Atiar1-3* plants at 10 days, Zn excess conditions caused a reduction in shoot hypocotyl length. In Zn deficiency and control Zn conditions, *Atiar1-t* plants showed a reduction in hypocotyl length compared to both Col-0 and *Atiar1-3* plants. The lack of difference across genotypes in excess Zn conditions could indicate complementation of the *Atiar1-t* phenotype or that hypocotyl length had reached a lower threshold in this condition.

Previous work has shown that hypocotyl length is responsive to IAA-Ala and that the *Atiar1-3* mutant is partially insensitive to its effects[328]. To determine whether shoot hypocotyl length responds similarly to IAA-Ala across a Zn gradient, these features were measured in both genotypes as well as in the *Atiar1-t* knockout mutant (**Figure 6.13**).

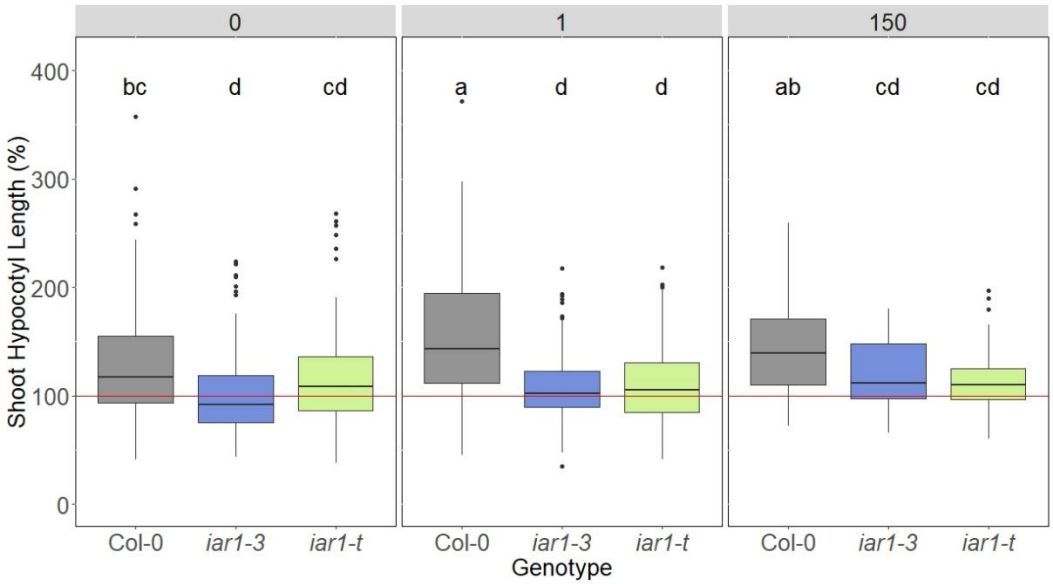

Figure 6.13 Shoot hypocotyl length percentage change in IAA-Ala media. Percentage shoot hypocotyl length in media containing 20 µM IAA-Ala compared to media with no auxin conjugate added with all other media conditions as **Figure 6.6**. 100% (no response) is indicated by the red line. At least 50 plants were measured in each of three biological replicates with statistically significant differences between groups calculated and displayed as in **Figure 6.5**.

Shoot hypocotyl length increases in Col-0 were more sensitive to IAA-Ala than in both *Atiar1* mutants across control Zn and excess Zn conditions. Additionally, there were no statistically significant differences between *Atiar1* mutants and no shift in IAA-Ala activity in excess Zn conditions, unlike previous root phenotypes. To determine whether this response is conserved in exogenous IAA conditions, shoot hypocotyl length in exogenous IAA conditions was measured (**Figure 6.14**)

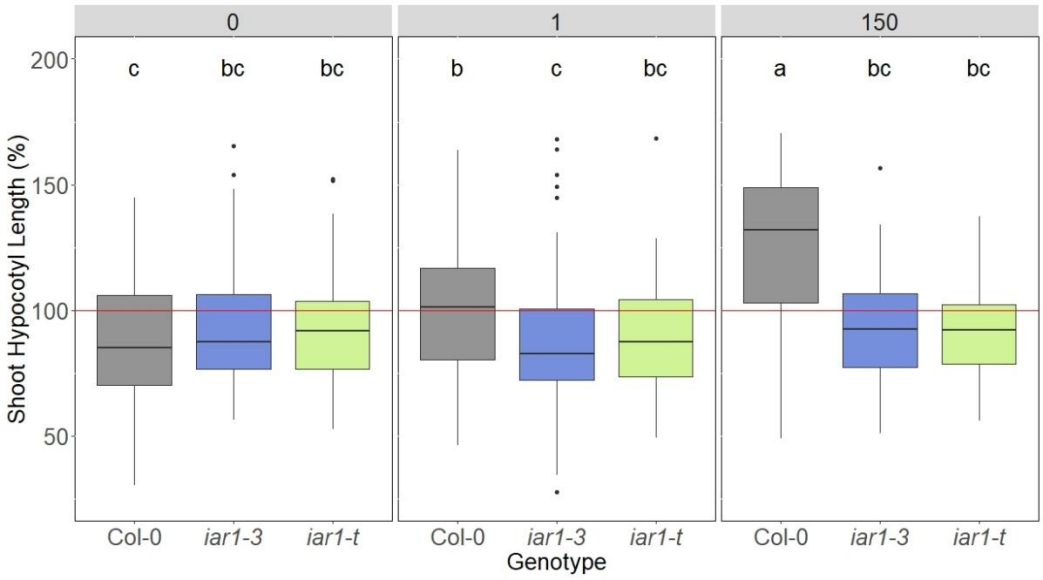

Figure 6.14 Shoot hypocotyl length percentage change in IAA media. Percentage hypocotyl length in media containing 100 nM IAA compared to media with no auxin added with all other media conditions as **Figure 6.6**. 100% (no response) is indicated by the red line. At least 50 plants were measured in each of three biological replicates with statistically significant differences between groups calculated and displayed as in **Figure 6.5**.

As shown above, shoot hypocotyl length in exogenous IAA in Col-0 plants increases in excess Zn conditions. This Zn-dependant change does not occur in either *Atiar1* mutant lines.

In summary, the *Atiar1-t* mutant after 10 days has a shorter hypocotyl than Col-0 and *Atiar1-3* plants in Zn deficiency and control conditions. In accord with previous results *Atiar1* mutants remain partially insensitive to the hypocotyl elongation effect of IAA-Ala. Shoot hypocotyl length is influenced differently by IAA-Ala and IAA treatments. In excess Zn conditions, IAA treatment led to an increase in hypocotyl length only in Col-0 plants, but this effect was not seen in IAA-Ala.

6.2.2.2 Hypocotyl length is increased in *Atiar1-t* plants after 5 days in light and dark conditions.

During skotomorphogenesis, auxin plays a key role in hypocotyl elongation and apical hook formation. To determine the potential role of Zn and *AtIAR1* on this process, Col-0 and *Atiar1* mutants were grown in light for 8 hours then either kept in the light or transferred to darkness for four days and then had their hypocotyl length (**Figure 6.15**) and apical hook angle measured (**Figure 6.16**)

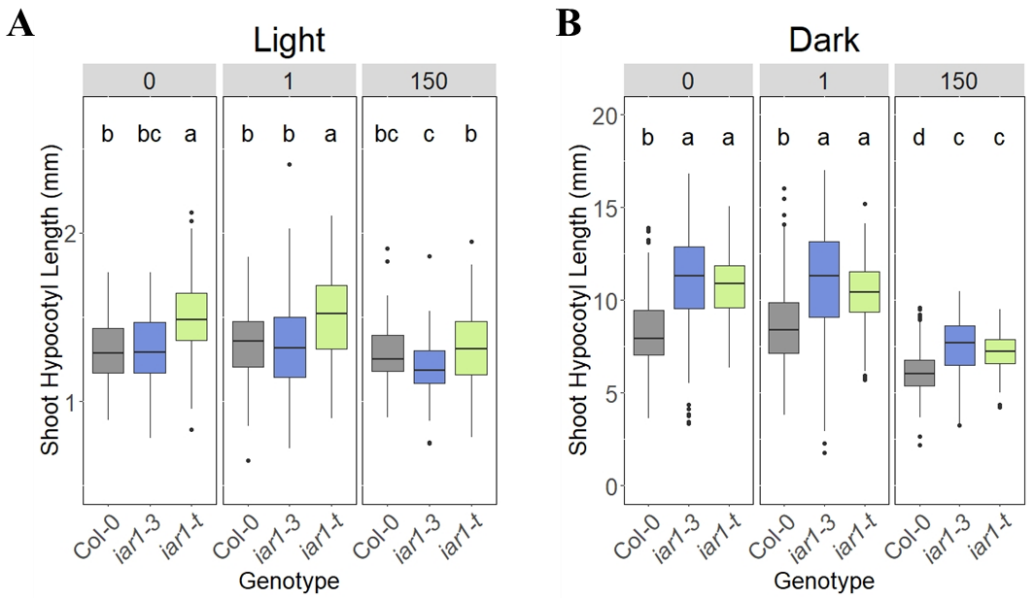

Figure 6.15 Shoot hypocotyl length in light and dark conditions. Hypocotyl length after growth in light (A) or darkness (B) was measured for each seedling grown in media conditions as **Figure 6.6**. At least 30 plants were measured in each of three biological replicates with statistically significant differences between groups calculated and displayed as in **Figure 6.5.**

Firstly, after growth for 5 days in light (**Figure 6.15A**) under Zn deficiency and control Zn conditions, *Atiar1-t* plants showed a larger shoot hypocotyl length. This contrasts with data after 10 days where *Atiar1-t* plants showed smaller hypocotyls

(**Figure 6.12**). This suggests a time dependence of *Atiar1-t* phenotypes as shown with primary root length. Growth in darkness, produced a large increase in hypocotyl length as expected in all genotypes (**Figure 6.15B**). However, the hypocotyl length in skotomorphogenesis was significantly greater in both *Atiar1* mutants in all Zn conditions. There was also no difference detected between the *Atiar1* mutants in any Zn condition. After 5 days in darkness, cell length is asymmetrically distributed in the hypocotyl[543] and so further work examining cell length distributions within these hypocotyls might be used to investigate this increased skotomorphogenesis response.

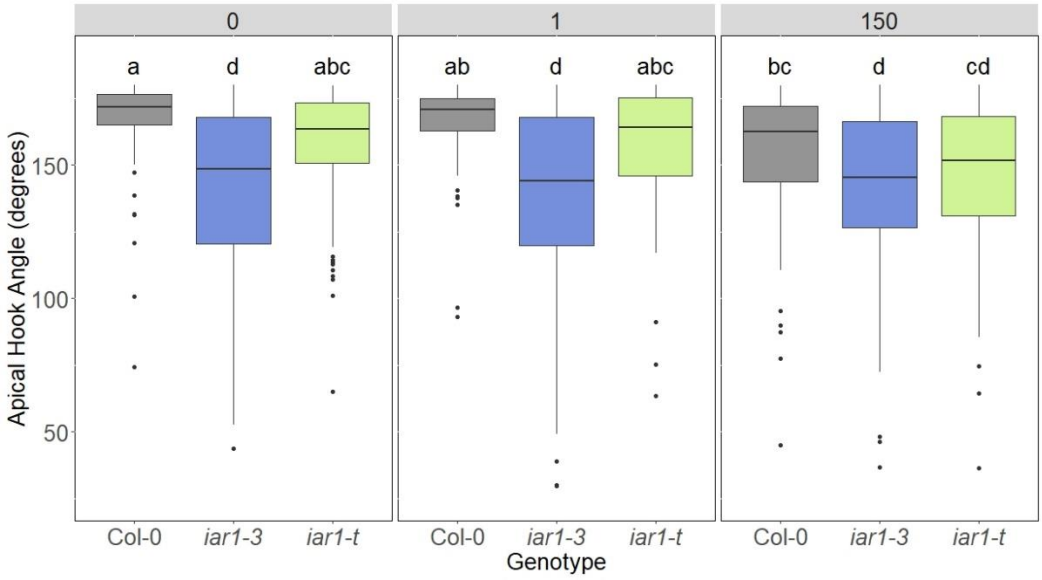

Figure 6.16 Apical hook angle across Zn conditions. Apical hook length was measured after growth in darkness for each seedling grown in media conditions as **Figure 6.6**. At least 20 plants were measured in each of three biological replicates with statistically significant differences between groups calculated and displayed as in **Figure 6.5.**

Interestingly, the apical hook angle was reduced only for the *Atiar1-3* mutant. This suggests *Atiar1-3* but not *Atiar1-t* may lack the ability to form a strong IAA gradient for bending of tissue. Further work could be extended to investigate other

responses that require auxin gradients mediating tissue bending such as in root gravitropism.

Overall, skotomorphogenesis is disturbed in both *Atiar1* mutants, with the two *Atiar1* mutants being differently able to form an apical hook. However, both mutants share the phenotype of an extended hypocotyl in skotomorphogenesis relative to Col-0.

To help explain some of these phenotypes and the wider impact on IAA metabolism, it was important to investigate the levels of IAA precursors, conjugates, and degradation pathway intermediates. Therefore, metabolite analysis was conducted on whole seedlings.

6.2.3 Auxin-related metabolite analysis

6.2.3.1 Generation of a method to simultaneously measure IAA and IAA-related metabolites

Precise quantification of metabolite levels is essential to understanding changes in IAA metabolism. A combination of IAA precursors (Trp, IAN), IAA, IAA conjugates (IAA-Ala, IAA-Asp, IAA-Glc) and degradation pathway intermediates (oxIAA) was measured with the aim to measure changes in all aspects of IAA metabolism. Liquid chromatography mass spectrometry (LC-MS) was used for this simultaneous quantification of IAA and IAA-related metabolites using D_2-IAA as an internal standard based on previous literature[278]. As shown below in **Table 6.1** this adapted methodology produced an appropriate linear response range for metabolite analysis in *Arabidopsis* seedlings. Therefore, the methodology developed could be used for simultaneous quantification of IAA metabolites in whole seedlings.

Metabolite	Retention time (min)	Product detection (m/z)	Linear range (nM)	R^2
Trp	1.0400	204.968 > 117.914	5 - 1000	0.9973
IAN	2.2800	157.032 > 129.981	5 - 10000	0.9974
IAA	1.8900	175.968 > 129.948	5 - 1000	0.9929
oxIAA	1.4900	192.096 > 145.954	1 - 1000	0.9962
IAA-Ala	1.7800	247.032 > 89.998	0.5 - 500	0.9998
IAA-Asp	1.5700	291.16 > 129.94	0.5 - 500	0.9999
IAA-Glc	1.5300	338.096 > 130.004	5 - 1000	0.9991

Table 6.1 LC-MS detection parameters for IAA-related metabolites. Serial dilutions of metabolite standards were separated and identified by LC-MS as described in **Chapter 2.3.7**. Retention time window used for detection was the stated retention time ± 0.2 min.

6.2.3.2 IAA-Glc levels are decreased in *Atiar1* mutants under Zn deficiency and excess conditions

Previous work has shown Trp synthesis is increased *in vitro* when low concentrations of Zn are added but is inhibited in Zn excess[323]. The utilisation of Trp in the TAA/TAR-YUCCA pathway has also been suggested to be regulated by Zn although reports on how Zn affects this pathway are conflicting[324,325]. Using the LC-MS methodology described above, IAA precursors Trp and IAN were measured

to determine whether Zn levels or IAR1 activity may alter IAA synthesis (**Figure 6.17**).

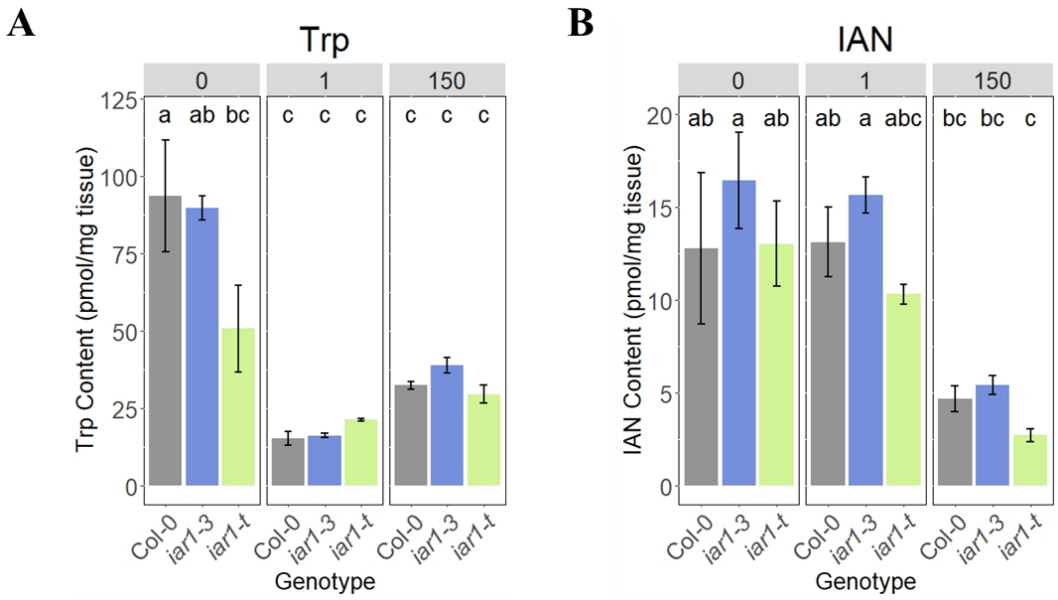

Figure 6.17 IAA precursor content. Metabolite content was measured as in **Chapter 2.3.7.4** from whole seedlings grown for 16 days in media conditions as in **Figure 6.6**. 100 mg of fresh tissue was used in each of three biological replicates with statistically significant differences between groups calculated and displayed as in **Figure 6.5**.

Here analysis shows that Trp levels are elevated in Zn deficient conditions in Col-0 and *Atiar1-3*, but not in *Atiar1-t*. This aligns with findings that Zn deficiency reduces protein synthesis and is associated with increases in the concentration of amino acids including Trp[544-546]. There was also a trend seen of decreasing IAN levels under high Zn which would accord with increased glucosinolate biosynthesis seen in cabbage species under high Zn, which removes IAOx from the IAA synthesis pathway[547,548].

IAA-Ala and IAA-Glc are thought to be reversibly synthesised from IAA, perhaps representing a pool of mobilizable inactive storage compounds, so along with IAA quantification of these compounds was attempted (**Figure 6.18**). Unfortunately,

during this analysis, IAA-Ala levels were too low to detect, a result that aligns with previous work suggesting the content of IAA-Ala is below that of other conjugates including IAA-Glc and IAA-Asp[278].

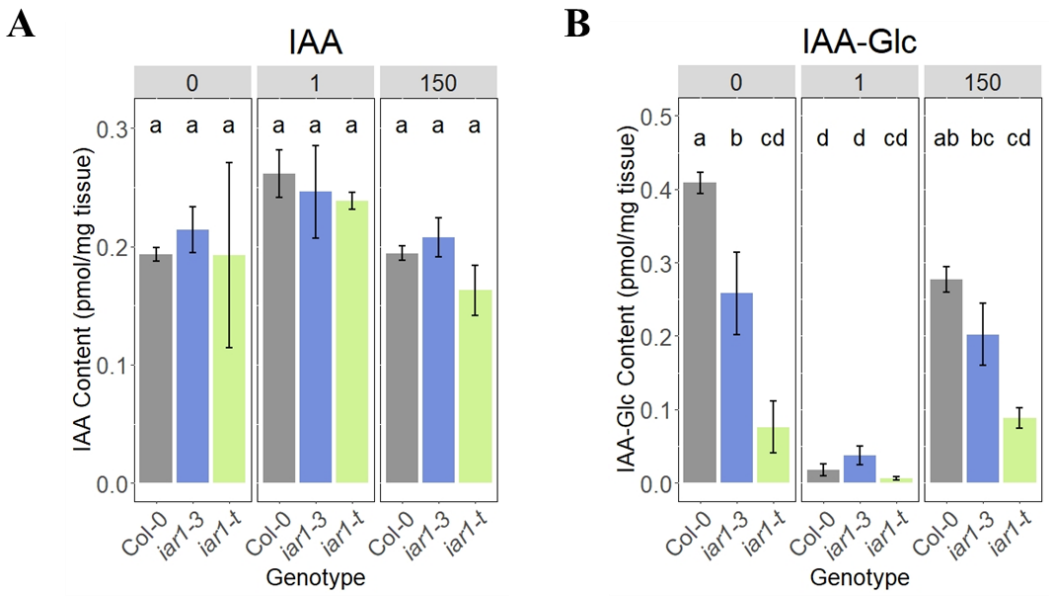

Figure 6.18 IAA and IAA-Glc content. Metabolite content was measured as in **Chapter 2.3.7.4** from whole seedlings grown for 16 days in media conditions as in **Figure 6.6**. 100 mg of fresh tissue was used in each of three biological replicates with statistically significant differences between groups calculated and displayed as in **Figure 6.6**.

IAA levels did not significantly change in any Zn condition or genotype suggesting that a change in IAA precursors is a poor indicator of IAA content, probably due to the many layers of regulation involved in IAA metabolism. The IAA levels measured in this study were greater than previous estimates of IAA content in shoots using a similar method (0.02 pmol/mg tissue)[278], but are closer to that recorded from combined root and shoot samples from 7 day old plants (approximately 0.35 pmol/mg tissue)[290]. Interestingly, IAA-Glc shows an increase in Zn deficient and Zn excess conditions in Col-0 and *Atiar1-3* plants. However, no

rise in IAA-Glc was seen in *Atiar1-t* mutants and the levels in Zn deficient conditions was less in *Atiar1-3* and *Atiar1-t* than in Col-0 plants.

IAA-Asp is thought to be incapable of being hydrolysed and so along with oxIAA are thought of as intermediates in the IAA degradation pathway. This degradation may be influenced by Zn or *AtIAR1* and so were also measured (**Figure 6.19**).

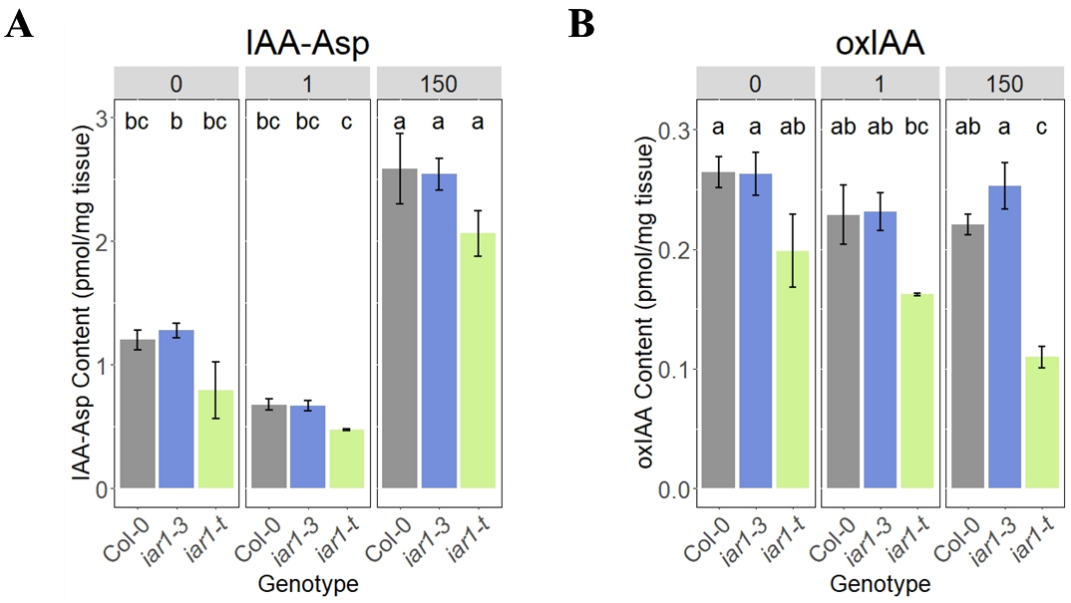

Figure 6.19 IAA-Asp and oxIAA content. Metabolite content was measured as in **Chapter 2.3.7.4** from whole seedlings grown for 16 days in media conditions as in **Figure 6.6**. 100 mg of fresh tissue was used in each of three biological replicates with statistically significant differences between groups calculated and displayed as in **Figure 6.5**.

IAA-Asp levels increase in all genotypes under Zn excess conditions. The lack of changes between Col-0 and *Atiar1* mutants provides further evidence that IAA-Asp is not hydrolysed *in vivo* by Zn-regulated hydrolases, which if so would have been hypothesised to have increased levels in *Atiar1* mutants. oxIAA was shown not to change significantly for Col-0 but was reduced between Zn deficiency and Zn excess conditions in *Atiar1-t*. This decrease suggests oxidation rates of IAA are dependent on Zn levels and *AtIAR1* activity.

In summary, this metabolite analysis has shown that IAA metabolites change in a Zn and *AtIAR1*-dependant manner. As IAA metabolism is controlled through several feedback loops[241,304,307,309,310], disruption of one part of IAA metabolism might lead to concomitant changes in other areas of the metabolic network and as such, changes seen in different Zn conditions and *AtIAR1* genotypes may reflect indirect effects rather than direct effects. The largest differences seen in Zn deficient conditions in Col-0 were the increases in Trp and IAA-Glc levels. By contrast, under Zn excess the largest changes were a reduction in IAN levels and an increase in IAA-Glc and IAA-Asp levels. These changes hint to differing Zn-dependant accumulation of the separate IAA conjugates. The fact that the largest Zn-dependant changes were seen in inactive IAA conjugates instead of the active form of IAA displays the importance of IAA conjugates in maintaining IAA levels at the context-specific appropriate levels. Finally, greater metabolite changes, such as in oxIAA under Zn excess which is decreased in *Atiar1-t*, were seen in *Atiar1-t* than in *Atiar1-3* suggesting that most of the metabolite changes observed in this study are related to the differing ability to hydrolyse IAA-Ala, and similarly hydrolysed IAA-aa conjugates. Overall, these changes are summarised below in **Figure 6.20**.

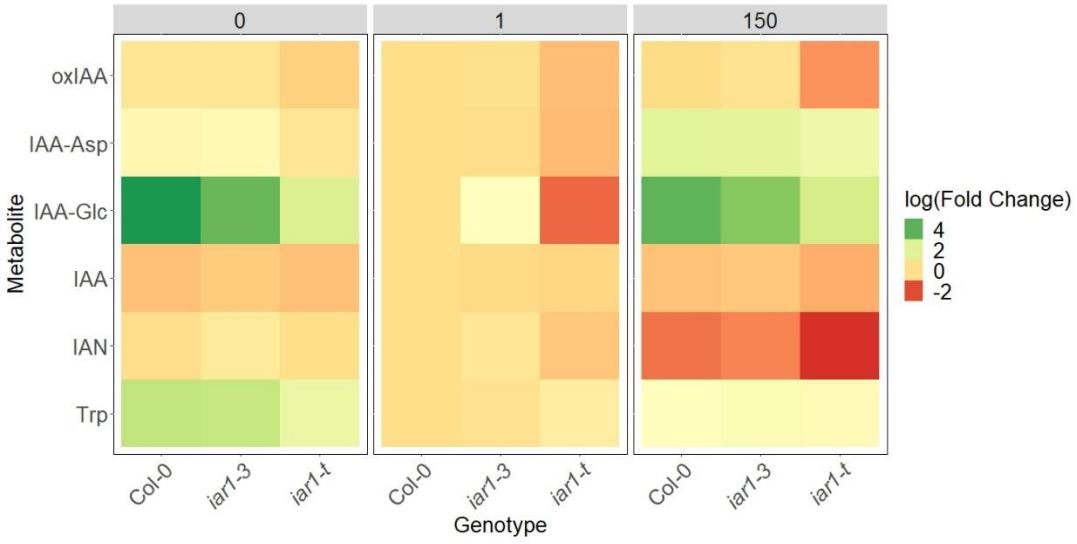

Figure 6.20 Summary of IAA-related metabolite changes. All metabolite content was compared relative to the content observed in Col-0 under control Zn conditions, with the comparative fold change shown on a log2 scale.

It should be noted that although insightful, metabolite levels do not reflect flux between different pools of metabolites, and lack of sub-cellular and tissue resolution may be obscuring potential insights into the different shoot and root metabolite profile of these mutants. Future work may increase the tissue resolution of this data and further enzymatic and expression analysis may prove helpful to understand potential mechanisms of how Zn and *AtIAR1* levels and activity regulate IAA metabolism as a whole.

6.3 Discussion

6.3.1 IAA glucose and amino acid conjugates appear to show crosstalk

Within the metabolite analysis the largest differences between Col-0 and the *Atiar1* mutants were the reduction in IAA-Glc levels. However, this large difference in metabolite profiles was apparent in Zn deficiency and Zn excess conditions, which does not match the pattern of phenotype severity shown elsewhere. Localised IAA metabolism is important for auxin responses, and therefore causative IAA conjugate level changes in a localised area such as the RAM may not be reflected in plant wide metabolite levels, demonstrating the potential limitations of this whole seedling metabolite approach.

IAA-Glc synthesis through various UGTs is predicted through DeepLoc v2.0[359] to be synthesised in the cytosol (data not shown), and hydrolysis has not been characterised in *Arabidopsis*. Given that AtIAR1 is thought to influence hydrolysis of IAA-aas and not influence IAA-Glc metabolism directly, it is interesting that the largest mutational differences occur in IAA-Glc and not IAA-Asp levels, suggesting a high degree of crosstalk in the reversible IAA conjugation pathways. A similar example of crosstalk was shown through overexpression of the *UGT84B1* gene which led to increased IAA-Glc and IAA along with decreased IAA-Asp and IAA-Glu levels[291]. This suggests that to maintain optimal IAA levels, both IAA-aa and IAA-Glc pools can be independently regulated. This crosstalk should be taken into account when analysing mutants with genes responsible for controlling these different conjugation steps. As high levels of auxin promote conjugation to IAA-aa and IAA-Glc[283,290], *Atiar1* mutants therefore represent the opposite, a 'low auxin' metabolic state due to a hypothesised inappropriate build-up of hydrolysable IAA-aas. 'Low auxin' metabolic state mutants with inability to metabolise indole butyric acid, methylated IAA and IAA-aas leads to compensatory increases in IAA synthesis through TAA/YUCCA induction[310] and so could also account for the lower Trp levels in Zn deficiency in the *Atiar1-t* mutant. However, IAA-Asp

synthesis would be predicted to be decreased in a ‘low auxin’ metabolic state but IAA-Asp levels do not decrease in either *Atiar1* mutant.

Hydrolysable IAA-aa conjugates such as IAA-Leu or IAA-Ala were not measured or detectable and would be worth further study to test whether these IAA-aas show increases in concentration. In addition, testing the expression of IAA-involved *AtUGT* genes in different Zn conditions in Col-0 and both *Atiar1* mutants used in this study may help test whether this IAA-aa IAA-Glc crosstalk is mediated transcriptionally. This crosstalk is discussed further in **Chapter 7.2.2**.

6.3.2 *Atiar1-t* mutants show time dependence in their phenotypes

At 5 days of growth in the light, *Atiar1-t* relative to Col-0 had shorter roots and longer hypocotyls, a phenotype similar to that seen in *AtYUCCA1* overexpression high auxin mutants[537]. Unlike *AtYUCCA1* overexpressing plants, however, *Atiar1-t* also showed increased hypocotyl length in skotomorphogenesis suggesting this is not a classical ‘high auxin’ phenotype, or that the auxin concentration differences between these different mutants could influence skotomorphogenesis differently.

However, after 10 days of growth, *Atiar1-t* plants had similar root lengths and shorter hypocotyls than Col-0 in Zn deficient and control conditions. These findings align with the ‘low auxin’ metabolic state predicted for *Atiar1* plants through metabolite analysis. Increased LR density is considered a ‘high auxin’ phenotype and is present after 10 days of growth in *Atiar1-t* and so is hypothesised to be caused by the ‘high auxin’ state in early growth rather than the ‘low auxin’ state present at 10 days. Measurement of LR density after longer term growth may help further elucidate the time dependence of the LR phenotype in *Atiar1-t*. This time dependence of the *Atiar1-t* phenotype is further discussed in **Chapter 7.2**.

6.3.3 Both *Atiar1* mutants are less sensitive to exogenous IAA-Ala than IAA

The phenotype under which *Atiar1-3* was discovered was relative insensitivity to IAA-Ala over IAA in primary root length and hypocotyl length in replete Zn conditions[328]. The present study has confirmed this finding and extended the insensitivity phenotypes to include LR density. In addition, *Atiar1-t* was found to be even less sensitive to IAA-Ala than *Atiar1-3* in the case of primary root length, which further adds to the hypothesis that *Atiar1-t* represents a knockout mutant whereas *Atiar1-3* represents a mutant with some residual *AtIAR1*-like activity.

The near total insensitivity of *Atiar1-t* to IAA-Ala across phenotypes suggests that IAA-Ala is not hydrolysed in the media and its effect is the result of AtIAR1-mediated hydrolysis. Interestingly, IAA-Ala and IAA treatments did not yield the same extent of phenotypic changes in primary root length, LR density and hypocotyl length. This difference in activity probably originates from non-equivalent concentrations of active IAA in the plants in the two treatments.

6.3.4 Zn excess and exogenous IAA-Ala and IAA interact in Col-0

Through measuring the percentage change in different growth parameters in different exogenous IAA and IAA-Ala treatments, this study was able to compare the relative sensitivity of plants to IAA and IAA-Ala in different Zn conditions. For Col-0, primary root length percentage reduction in IAA and IAA-Ala was increased in Zn excess conditions relative to both Zn deficiency and control Zn conditions. This increased sensitivity was also seen in LR density increases for both IAA and IAA-Ala treatments and in an increase in shoot hypocotyl length in IAA treatments. Together these observations imply that in Col-0, the interaction between Zn excess and exogenous auxins is acting downstream of hydrolysis.

This synergy was not observed in *Atiar1-3* mutants but was present albeit reduced in the IAA response in *Atiar1-t* plants for phenotypes including primary root length

and LR density but not hypocotyl length. Although the synergy was not observed in *Atiar1-t* plants in exogenous IAA-Ala conditions, this feature may have been obscured by the near total insensitivity of *Atiar1-t* to IAA-Ala. Together, the present work suggests that AtIAR1 activity may interact with the IAA-Zn synergy as depicted in **Figure 6.21**.

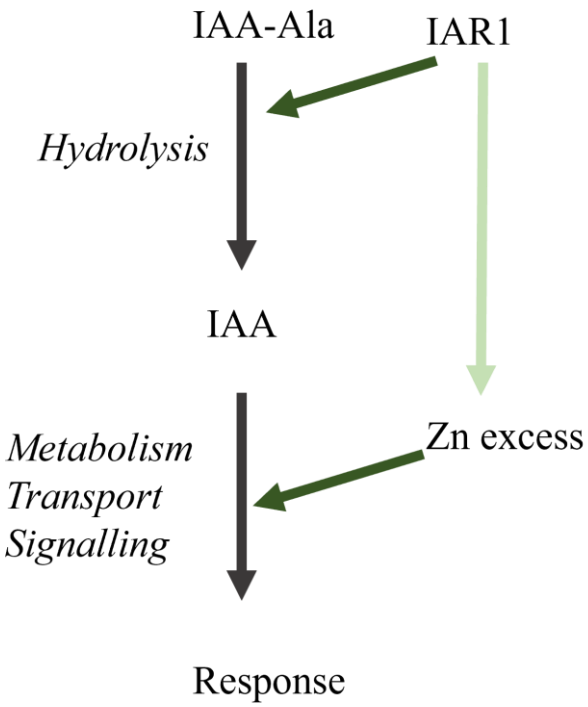

Figure 6.21 Interaction of AtIAR1, Zn and exogenous auxins. AtIAR1 activity increases IAA-Ala hydrolysis but also changes IAA activity post hydrolysis in Zn excess. Processes involved in growth responses from exogenous IAA-Ala treatment are shown in italics. Green arrow indicates a positive effect in Col-0 in primary root length reduction.

Potential mechanisms for the Zn excess – exogenous auxin interaction including its total absence in *Atiar1-3* plants is further discussed in **Chapter 7.3**.

6.3.5 Potential confounding factors include cell wall integrity

Many factors influence the phenotypes tested in this study, not just auxin. Zn and auxin themselves interact with several other nutrients and hormones that could potentially be involved in these phenotypes. Of particular importance to discuss here is cell wall integrity. Cell wall expansion is vital for acid growth[440-442] which is a vital part linking auxin to some of the cell expansion-based phenotypes discussed in this study, such as hypocotyl elongation.

O and N-linked glycosylation occurs in the ER, and is important for synthesis of cell wall components[549-552] using highly conserved machinery[553] including Mn-utilising enzymes[554-556]. Yeast strains with the *AtIAR1* homologue knocked out show cell wall defects[336]. Analysis using ATTED-II v11[557] has shown in addition to *AtMTP5*, *AtIAR1* is co-expressed with *AtALG9* and *AtTBL32* genes, characterised to be involved in glycosylation mediated quality control in the ER and secondary cell wall biosynthesis respectively[558,559]. Therefore, there is a potential role in maintaining optimal glycosylation and cell wall integrity for *AtIAR1*. An illustration of how cell wall integrity may change auxin related phenotypes is seen in *Arabidopsis* mutants in Golgi-localised K^+/Na^+ - proton antiporter *AtKEA3,4,5* genes. *Atkea* mutants show disrupted cell wall synthesis, and reduced skotomorphogenesis[560]. In addition, acetylated pectin components from the cell wall, which are reduced in Zn excess conditions[132,561] have been shown to be required for inducing skotomorphogenesis. *de-etiolated by Zn* (*dez*) mutants show reduced skotomorphogenesis that is enhanced in Zn excess conditions, and complemented by addition of exogenous cell wall components[132]. Cell wall pectin synthesis components are localised in the Golgi[562-565] and mutants in a pectin synthesis related methylesterase encoding gene *AtPME3* show hypersensitivity to Zn excess suggesting a link in *Arabidopsis* between cell wall related phenotypes and Zn homeostasis in the secretory system[133].

Further work on characterising any cell wall specific phenotypes could be helpful in resolving any cell wall and auxin effects within the *Atiar1* mutants. This may

involve measuring cell wall component levels and the influence of media pH on *Atiar1* mutant plants.

Chapter 7: Conclusion

7.1 This study has advanced understanding in how ER Zn control plays a role in Zn and auxin homeostasis

During this study, *proAtMTP2*::*LUC* reporter lines were generated with the purpose of screening for novel regulators of Zn endoplasmic reticulum (ER) import. Initial characterisation suggested that exogenous indole-3-acetic acid (IAA, auxin) and IAA-Ala caused a reduction in Zn deficiency-induced *AtMTP2* expression, implying a reduction in Zn import into the ER. This work was followed by testing of the adapted model of *AtIAR1* function shown below in **Figure 7.1**. Work in this study has found that Zn is transported by AtIAR1 which is likely localised to the secretory pathway, which is also predicted for all plant AtIAR1 homologues other than those from the *Solanaceae* family.

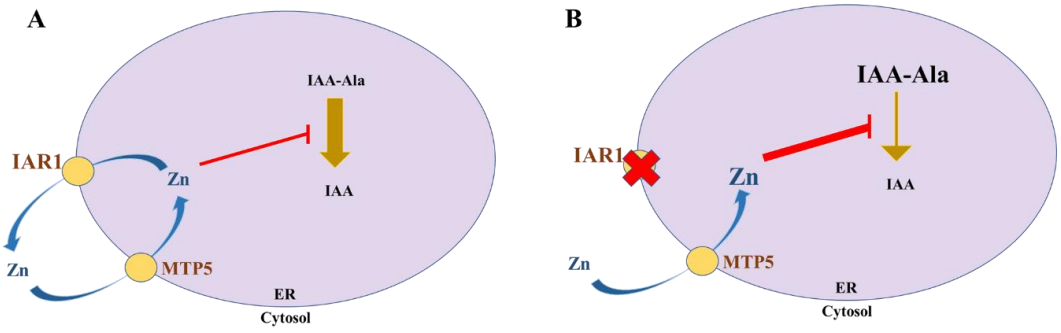

Figure 7.1 Adapted Rampey et al, 2013[1] model of metal transport in the ER and IAA-Ala hydrolysis in wildtype and *Atiar1* mutant plants. (A) AtMTP5 and AtIAR1 antagonistically control levels of metals including Zn in the ER which then control the activity of IAA-Ala hydrolases. (B) *Atiar1* mutants lose Zn transport activity, causing ER Zn levels to increase which inhibits IAA-Ala hydrolases. Figure adapted with permission focussing on the role of Zn as the inhibitory ion.

However, in yeast complementation experiments, Atiar1-3 was shown to transport Zn, unlike the hypothesised lack of transport activity shown in **Figure 7.1B** for

Atiar1 mutants, and may in fact have its localisation restricted to the ER. Furthermore, this study and work on the localisation of Zn^{89} and auxin transporters[191,192] within the secretory system necessitates an expansion of the model to include new features as shown in **Figure 7.2**. In summary these new features are antagonistic Zn transport by AtMTP5-AtMTP12 and AtIAR1 in the Golgi, Zn movement between the Golgi and ER through retrograde trafficking and ER auxin transport.

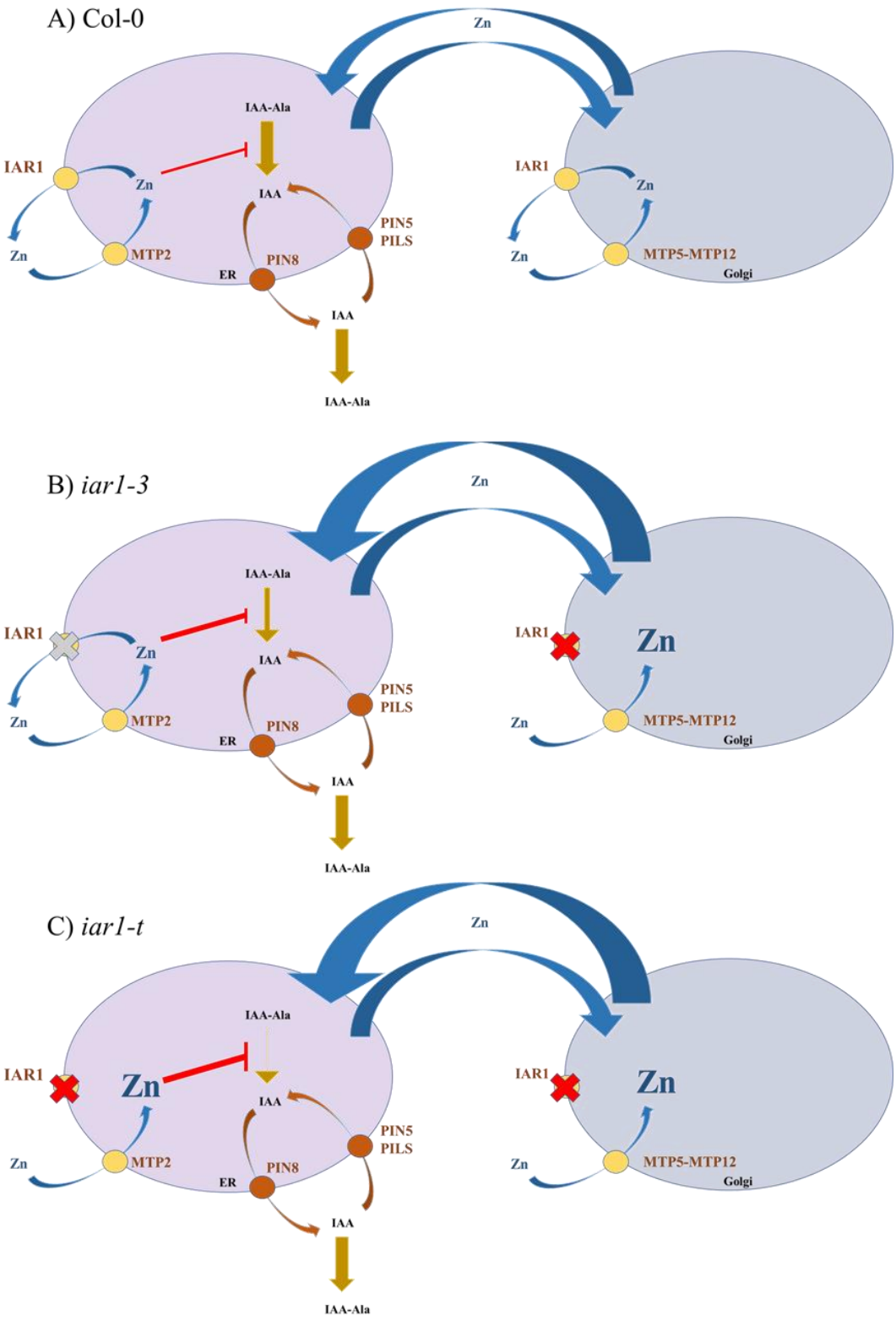

Figure 7.2 Updated model of auxin conjugation and Zn homeostasis within the secretory pathway. A) Col-0. In the wildtype Zn homeostasis in the ER is regulated antagonistically by AtMTP2 and AtIAR1 in addition to AtZTP29 in high

salt conditions[80] (not shown for clarity). Within the ER, IAA-amino acid (IAA-aa) conjugates are hydrolysed to IAA which can be transported between the ER and cytosol through short PINs including PIN5, 8 and PILS[191,192,195]. Auxin conjugation so far has been shown to occur in the cytosol[271,272] and transporters of IAA-aa from the cytosol into the ER have not yet been demonstrated. Zn homeostasis in the Golgi requires the antagonistic activity of the AtMTP5-AtMTP12 complex and AtIAR1, with this Golgi Zn homeostasis influencing ER Zn levels through retrograde trafficking of vesicles. B) In the *Atiar1-3* mutant, although Zn transport may be present (grey cross) in the ER, localisation is likely to be restricted to the ER causing loss of Golgi Zn export. Thus, Golgi and therefore ER Zn levels would rise to inhibit the IAA-aa hydrolases. C) In the *Atiar1-t* mutant, Golgi and ER Zn export is lost (red crosses) leading to a much greater rise in ER Zn levels causing dramatic reduction of IAA-aa hydrolase activity.

Additionally, *AtIAR1* expression was found to be restricted to the above ground vasculature and upregulated in a Zn- and exogenous auxin-dependant manner, which adds an extra layer of complexity to this new model.

To investigate the interactions of Zn and auxin, particularly in the ER, characterisation of the Zn- and auxin-dependant phenotypes of *Atiar1* mutants including *Atiar1-3* and the knockout mutant *Atiar1-t*, revealed that AtIAR1 activity is not necessary for the Zn deficiency response but may be involved in reducing the severity of the Zn excess response. The majority of the phenotypes observed were seen as auxin-related and were present in the shoot and root, which correlated with changes in whole plant IAA-related metabolite levels. Additionally, a partial AtIAR1-dependant excess Zn - exogenous IAA interaction was observed - a novel interaction warranting further characterisation as explored below. Throughout this study, *Atiar1-3* and *Atiar1-t* mutants have behaved differently, indicating that *Atia1-3* is partially functional in plants, and in addition showing a potential further Zn excess sensitivity indicative of a small role for AtIAR1 in Zn detoxification.

Overall, the major advances in this work have been in the gathering of evidence to update the model in **Figure 7.1** and in expanding it to include how ER Zn transport influences wider auxin and Zn homeostasis, and how these interact in

developmental phenotypes. Application of this work for future breeding programmes or genetic engineering of crops could help improve Zn uptake and root-to-shoot translocation in Zn poor soils through understanding *AtMTP2* regulation. Additionally, the role of *AtIAR1* homologues in determining early seedling development could be particularly useful to understand in an agricultural setting. For example, the altered lateral root density of *Atiar1-t* mutants could be used in breeding programmes in the future to optimise a crops nutrient acquisition in a particular fertiliser regime.

Understanding this work holistically requires the formation of a plant wide model in different Zn conditions. However due to the complexities of the Zn-auxin interaction several different models are required for the temporally distinct roles of AtIAR1 in plant Zn-auxin interactions as explored below. These will mostly focus on *Atiar1-t* mutant because the *Atiar1-3* mutant shows additional phenotypes which will be examined separately.

7.2 *Atiar1-t* phenotypes show time-dependence

7.2.1 AtIAR1 may influence light-related auxin signalling in early development up to 5 days

One of the interesting aspects of the growth phenotypes of the *Atiar1-t* mutant was its time-dependence, with early development (5 days of growth after germination) showing a phenotype of longer hypocotyls in light and reduced root length. However, this differential hypocotyl and growth phenotype in the *Atiar1-t* mutant is reversed or complemented after 10 days of growth. One of the key signalling pathways involved in early development involves light, and in the context of light signalling, the *Atiar1-t* mutant shows an enhanced dark response, further evidenced by enhanced hypocotyl growth in darkness and reduced chlorophyll content, synthesis of which is increased in light[566-569]. This potential link between light and *AtIAR1* may also exist on a transcriptional level as *AtIAR1* promotor analysis found several light response elements including the AE-box[570], GATA motif[571], I box[572], MRE[573] and TCT motifs[574], although further work is required to gather *AtIAR1* expression data in different light regimes to confirm this.

How AtIAR1 activity might be linked to this light response is still unclear. Linkage may potentially involve the alteration of a cell wall signalling molecule that positively regulates skotomorphogenesis[132] or AtIAR1 may be involved in light mediated changes in auxin levels or auxin transport[293,472,516,523,524,527]. In one scenario lack of IAA formation from pools of IAA-aa conjugates may be of particular importance in early photomorphogenesis and cause an overcorrection of IAA synthesis to generate the high auxin phenotype. Disruption of activation of multiple different IAA stores has been shown to increase IAA synthesis[310] and specific disruption of IAA-Glc metabolism through *AtUGT84B1* overexpression did lead to increased IAA levels[288], suggesting such an overcompensation may occur. However, mutants unable to mobilise IAA from IAA-aa, methylated IAA and indole butyric acid (IBA) pools combined showed phenotypes typical of low auxin responsiveness after 7 days of growth[310], although the time dependence of this

phenotype was not measured. A possible alternative is that AtIAR1 promotes the changes in auxin transport during photomorphogenesis. Studies on photomorphogenesis has found that *Atkai2* mutants show reduced light-dependant changes in PIN localisation and show enhanced lateral root (LR) density hypothesised to be due to IAA build up in the upper root[525]. This could suggest a potential similarity in early development to the *Atiar1-t* mutant which shares this LR phenotype[525]. It should be noted however that *Atkai2* mutants do not show any hypocotyl changes when grown in darkness, nor primary root length changes[525], unlike the *Atiar1-t* mutant. In addition, unlike hypocotyl elongation in the light, elongation in the dark does not require auxin transport[487], suggesting that although auxin transport may be part of the mechanism in early photomorphogenesis, it does not account for the skotomorphogenesis phenotypes. A different hypothesis could be that activity of AtIAR1 increases the abundance of a cell wall derived skotomorphogenesis signal[132], however, this study has not examined the cell wall of Col-0 nor *Atiar1* mutants across Zn conditions, and so the early enhanced dark phenotype of *Atiar1-t* remains unresolved (**Figure 7. 3**). Further work on cell wall composition, auxin transporter localisation and auxin content in different tissues of Col-0 and *Atiar1* mutants at 5 days of growth in both light and darkness could help resolve this.

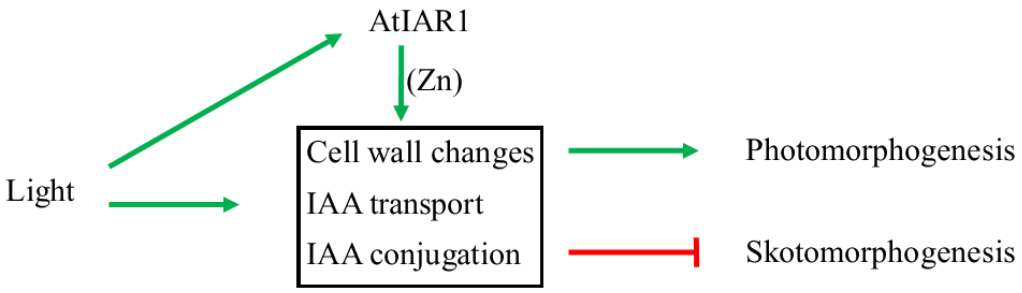

Figure 7.3 Potential involvement of AtIAR1 in light-induced changes during early development.

7.2.2 After 5 days a developmental switch leads to a change in *Atiar1-t* phenotypes

The differential hypocotyl and growth phenotype of *Atiar1-t* mutants after 5 days is reversed or complemented after 10 days of growth, indicating a loss of this early enhanced dark phenotype as *Atiar1-t* shows reduced hypocotyl length and primary root length similar to Col-0. The reason for this switch may be related to the eventual degradation of a cell wall-derived dark signal or differing auxin requirements during the 5 day to 10 day transition, although this is currently unclear. IAA-related metabolites were measured after 16 days and so cannot be directly attributed to phenotypes measured at 10 days. This emphasises the need for future studies to focus on the same time point for collecting data from, particularly when considering developmental phenotypes.

However, assuming no further changes in auxin phenotype between day 10 and day 16, these auxin-related phenotypes after 10 days are associated with no change in total IAA content measured in the plants which were similar across all genotypes. This could suggest compensatory changes in other aspects of IAA metabolism to create a negative feedback loop to stabilise IAA levels for a specific cellular context within these conditions. It has been previously demonstrated that high IAA levels reduce IAA synthesis[307] and promote IAA conjugation to both amino acids and glucose transcriptionally[283,290]. In the 'low auxin' model of the *Atiar1-t* mutant, IAA levels are reduced by the lower level of IAA-aa hydrolysis, which promotes the reverse of the characterised feedback loop where a 'low auxin' signal leads to decrease in IAA-Glc levels as part of a negative feedback loop to maintain IAA levels.

Combining metabolite analysis, *AtMTP2* expression data and IAA-Ala sensitivity from this study, a model for the AtIAR1 and Zn dependency on this IAA-IAA conjugate feedback loop can be constructed as shown below in **Figure 7.4**.

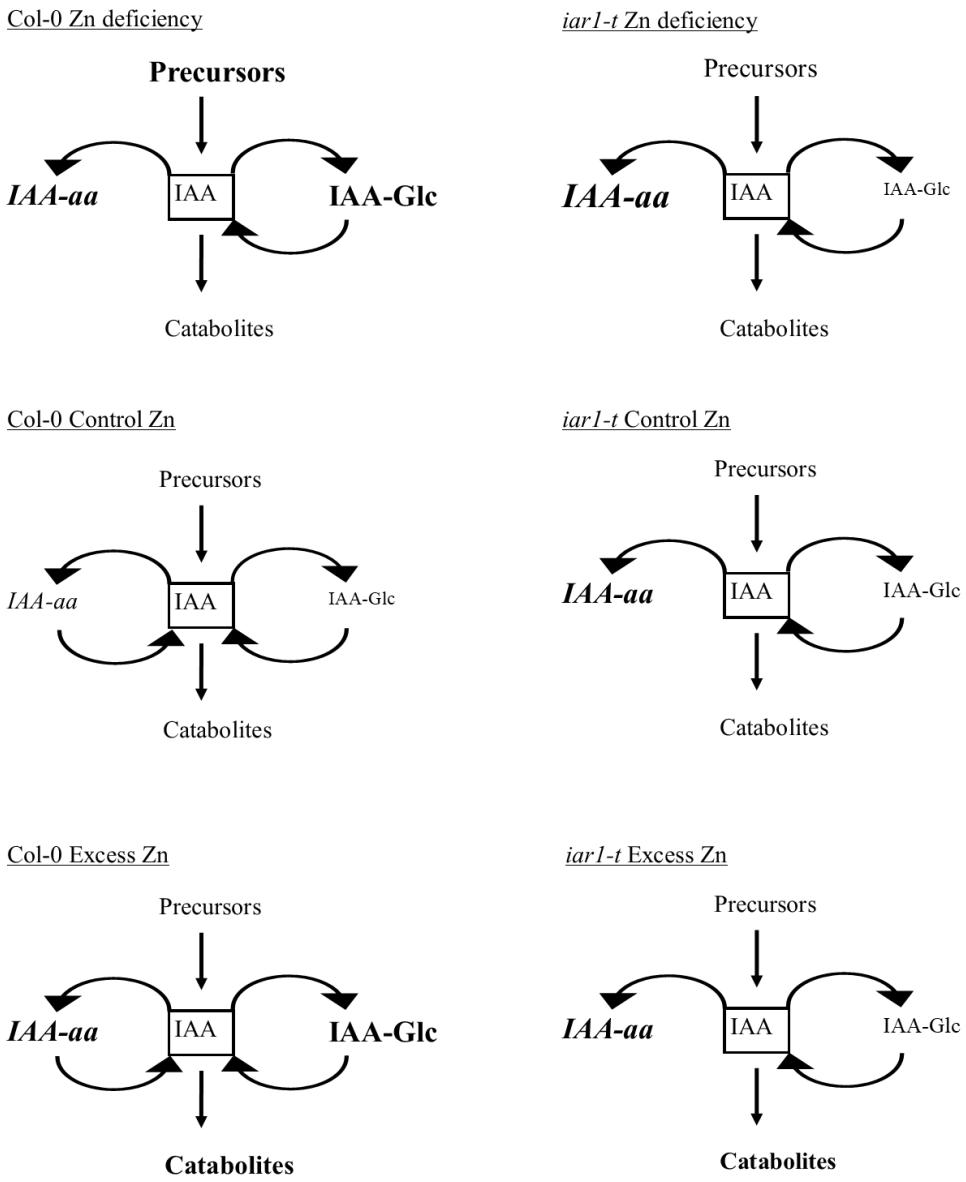

Figure 7.4 Auxin metabolism pools predicted and measured across Zn and *AtIAR1* genotypes. All metabolite levels were either measured or predicted (italics). Arrows represent conversion rates between metabolite pools and are predicted.

In Zn deficiency, Zn import into the ER in the root through enhanced AtMTP2 activity is hypothesised to restrict IAA-aa hydrolysis, although further work on the IAA-aa sensitivity of *Atmtp2* mutants is needed to confirm this takes place. In

addition to high tryptophan (Trp) and IAA-Glc levels, the current findings indicate that Zn deficiency comprises a 'high auxin' metabolic state, and so leads to increasing auxin conjugation. This does not appear to lead to a 'high auxin' growth phenotype relative to control Zn conditions, implying the metabolite phenotype is not associated with a growth phenotype in this instance. Currently, the auxin-related developmental changes in Zn deficiency are poorly characterised with only minor phenotypes shown in this study which were found independent of AtIAR1 and so warrant further investigation. Experiments with plants under Zn deficiency conditions for longer periods of time, using mutants of ER/Golgi Zn importer genes such as *AtMTP5* or *AtMTP2* may prove informative in future work.

In Zn excess, high IAA-Glc and catabolite concentrations indicate another but different 'high auxin' metabolic state. This 'high auxin' metabolic state is not reflected in the hypocotyl, which undergoes growth restriction, but is reflected in the roots which show growth suppression. The shoot and root auxin link in Zn excess will be expanded further below.

Across all these conditions, the *Atiar1-t* mutant showed reduced IAA storage in IAA-Glc and reduced catabolism to oxIAA but only in high Zn conditions. Therefore, the *Atiar1-t* mutant is hypothesised to be in a 'low auxin' metabolic state due to reduced IAA-aa hydrolysis. This 'low auxin' metabolic state might then be responsible for the growth phenotype seen in *Atiar1-t* plants after 10 days of reduced hypocotyl length and regaining wildtype-like root lengths.

In this study, there were no changes in total IAA content of the plant, but dramatic changes in auxin precursors, conjugates and catabolites. This indicates a potential role of IAA conjugates as buffers to smoothen any IAA concentration changes in an Zn-sensitive manner to establish a required developmental response.

This model has assumed that different IAA conjugates are functionally redundant IAA buffers and are regulated similarly, which may not be the case. Indeed, it appears in this study and others that disruption of mobilisation of one IAA conjugate cannot be fully complemented by extra mobilisation of another[274,290,310]. However, due to limited research in the preferential synthesis and hydrolysis of these separate IAA conjugates, it is currently hard to define what these differences are. This model has also assumed that the whole plant metabolite data gathered are

representative of key auxin pools dictating the phenotypes measured, which is unlikely to be the case, particularly if *Atiar1* mutants show disrupted auxin distribution as predicted. Further spatial and temporal resolution on this metabolite analysis would therefore be beneficial to understanding further the Zn and AtIAR1 dependant changes to auxin metabolism and testing the model above.

7.3 The Zn excess response involves auxin transport from shoots

7.3.1 Zn excess response in conditions with no exogenous auxin involves AtIAR1-mediated auxin transport from shoots

In Zn excess conditions, regardless of developmental stage or genotype, shoot hypocotyl and root length are reduced. Although the precise mechanisms of Zn excess-induced growth changes are mostly unknown, there is some evidence of altered PIN distribution causing reduced auxin accumulation in the root meristem[324,325,575]. The absence of change in plant IAA levels measured in this study in Zn excess conditions suggest auxin distribution rather than whole plant auxin level is important here.

Removal of auxin from the shoot could be hypothesised to be partially responsible for the reduced hypocotyl growth in Zn excess. Given *AtIAR1* is induced in the leaf and hypocotyl vasculature in Zn excess conditions, it is hypothesised that AtIAR1 may aid this increased shoot mobilisation of auxin in Zn excess. It is therefore possible that AtIAR1 plays a role in auxin canalisation, where auxin signalling induces development of vasculature tissue carrying auxin in narrow channels from source to sink[313]. This process occurs through auxin-induced PIN localisation changes and the endocytic trafficking of PIN transporters[312,576-578] some of which are expressed in similar tissues to *AtIAR1*[501,527]. Indeed, mutants in genes responsible for activation of storage forms of auxin, including IAA-aas, show leaf venation phenotypes[310]. However, these experiments have not been carried out with *Atiar1* mutants and so warrant further investigation to test this potential role of AtIAR1.

In roots under Zn excess, root apical meristem (RAM) size is reduced, an effect that is accentuated in *Atiar1-t* mutants, whilst reducing the LR density. Auxin is involved at several different points during LR development, and auxin transport at the shoot-root junction is required for LR formation[462]. Zn excess applied after 5

days of growth on control Zn media resulted in increased LR density[324], however in this study continual exposure to Zn excess did not lead to a similar increase. This implies that Zn excess may be acting to increase auxin in the upper roots to promote the later stages of LR development rather than the early stages which occur closer to the root tip. Given that excess Zn reduces expression of genes in the YUCCA-TAA pathway[325], this upper root auxin may be derived from the shoot via AtIAR1-mediated transport rather than synthesis. In *Atiar1-t*, early dark-associated changes in auxin distribution may contribute to increased LR density, in a similar way to *Atkai2* mutants and Zn excess conditions, with increased auxin in the upper root. However, unlike in Zn excess, control and Zn-deficient conditions allow sufficient local auxin synthesis to potentially maintain pre-branch LR sites in *Atiar1-t* mutants. In Zn excess conditions, local root auxin synthesis is reduced and so would lead to a reduced LR density in *Atiar1-t* plants. Experiments involving the Zn dependency of the LR density phenotype of *Atkai2* plants would help test this hypothesis.

Previous work has shown long term Zn excess leads to a reduction in auxin accumulation and size of the RAM, correlated with reduced *PIN* expression and increased reactive oxygen species[325,575]. Potential reasons for *Atiar1-t* plants being more sensitive to this RAM restriction may be due to the already altered auxin distribution predicted during early growth of *Atiar1-t*. *Atiar1-t* therefore becomes over-reliant on local root auxin synthesis for meristem maintenance and so *Atiar1-t* is sensitive to when local synthesis of auxin in roots is reduced in Zn excess conditions[325].

This together leads to the generation of a model shown below in **Figure 7.5**, involving the intersection of local auxin synthesis and transport in Zn-dependant manner**.** Further work on PIN localisations, auxin activity and synthesis would be required to test this hypothesis including crossing *PIN::GFP* and *DR5* reporter lines with *Atiar1-t* lines and investigating expression of auxin synthesis genes in *Atiar1* mutants.

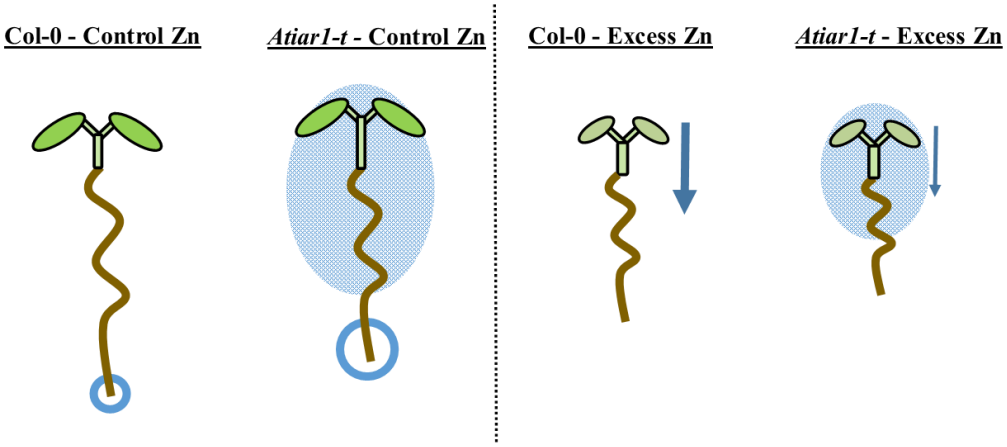

Figure 7.5 Model for Zn dependant auxin mobilisation in 5-day-old Col-0 and *Atiar1-t* plants. Under control Zn conditions, the *Atiar1-t* mutant shows reduced light signalling, which includes enhanced auxin activity in the shoot and upper roots (filled blue circle) enhancing shoot growth and LR growth, with increased local auxin biosynthesis in root tips maintaining meristem size similar to Col-0 (empty blue circle). Under Zn excess, local auxin biosynthesis in roots is reduced, and auxin is mobilised from the shoots (blue arrow), but restricted to the upper root, restricting RAM size. Due to the reduced auxin transport from the shoots in *Atiar1-t* plants this root meristem reduction is enhanced in the *Atiar1-t* mutant and LR formation reduced.

Within this model, it is interesting to note that excess Zn conditions are represented as 'high auxin' metabolic states, with IAA-Glc being a major storage form of IAA, which has been found mostly in the roots in control Zn conditions[290]. Potentially, this shoot-to-root transport of auxin in Col-0 in Zn excess conditions is aided by high levels of auxin conjugation and oxidation in the roots.

7.3.2 The excess Zn–exogenous auxin interaction requires AtIAR1-mediated auxin transport

This model of auxin transport in Zn excess is important to understanding the excess Zn-exogenous auxin interaction. Given that *GUS* expression was not observed in plants grown in excess Zn with exogenous IAA but that these conditions showed the greatest difference in phenotype between *Atiar1-t* and Col-0 plants, this implies that the role of AtIAR1 may have occurred prior to staining and that *AtIAR1* expression was then repressed. As previously established, during early development, the *Atiar1-t* mutant shows an enhanced dark phenotype, due to reduced light signalling through an undetermined mechanism. This can be checked in future work investigating growth and *AtIAR1* expression at earlier time points in control and exogenous IAA conditions.

In high exogenous IAA and IAA-Ala conditions there is a large increase in IAA which generates a high auxin response in roots and shoots, including a reduced RAM size[579]. It is interesting that the excess Zn-exogenous IAA interaction shows differently in roots and shoots. In roots, this interaction further restricts root length and increases LR density, whilst in shoots this interaction extends hypocotyls, indicative of a reduction to the high and inhibitory levels of IAA for shoot hypocotyl extension. Therefore, it is hypothesised that the excess Zn-exogenous IAA interaction is due to increased auxin removal from shoots as a result of the altered auxin distribution in Zn excess seen in **Figure 7.5**. The increase in LR density in Zn excess with exogenous IAA can be explained through added IAA compensating for the low root auxin synthesis that is proposed in Zn excess conditions. Additionally, the reduced root length could be explained by the exogenous IAA-induced changes in PIN distributions[312,318], operating alongside those induced in Zn excess to mediate additional shortening of root length, presumably through reducing meristem size.

In both *Atiar1* mutants, the excess Zn-exogenous IAA interaction in the shoots is lost, but is partially maintained in the lateral root and primary root growth phenotypes only in *Atiar1-t* plants. This fits with a role of AtIAR1 in Zn excess-mediated shoot IAA removal as shown in the model in **Figure 7.4** and is suggestive

of an additional smaller role of AtIAR1 in co-ordinating the auxin transport within the root. Further work to confirm this hypothesis will also involve testing where the AtIAR1-dependant root growth restriction is taking place, either through meristem size reduction or in extent of elongation in the exogenous auxin treatments. In addition, testing of auxin response and PIN localisation in these conditions will be vital in establishing auxin activity distribution in Zn excess conditions.

Finally, the mechanism behind this dependency on AtIAR1 for auxin transport is unclear, as is whether this auxin transport link is also responsible for the enhanced dark phenotype observed for *Atiar1-t* plants during early development. Potential clues of this mechanism may be in further understanding of the roles of auxin conjugation in auxin canalisation. With increased AtIAR1 expression, ER Zn levels are thought to decrease, aiding auxin conjugate hydrolysis, which would further enhance auxin levels in the vasculature, and which may be important in establishing or maintaining narrow auxin transport routes, potentially through auxin-mediated secondary cell wall formation, similarly to AtWAT1 activity[196,197]. Additionally, further characterisation of the *Atiar1-3* mutant which shows no Zn dependency on any aspect of IAA sensitivity in the roots may elucidate this mechanism as outlined below.

7.4 The *Atiar1-t* and *Atiar1-3* mutants show different phenotypes

Across this study, it has become evident that *Atiar1-3* and *Atiar1-t* mutations result in different phenotypic severity. The ability of the AtIAR1-3 protein to transport Zn across the yeast plasma membrane suggests that AtIAR1-3 does not act as a completely non-functional protein as predicted in the Rampey et al, 2013[1] model in **Figure 7.1B**. As *Atiar1-3* shows intermediate sensitivity between *Atiar1-t* and Col-0 to exogenous IAA-Ala, it is hypothesised that ER Zn levels in *Atiar1-3* are intermediate between Col-0 and *Atiar1-t*, as shown in **Figure 7.2** and that this leads to many phenotypes of *Atiar1-3* plants being a milder version of those of *Atiar1-t* plants, including metabolite levels and developmental changes across different Zn and auxin conditions. Further work to establish these ER Zn levels should be pursued using ER-targeted Zn-responsive Förster resonance energy transfer (FRET) sensors or dyes, which has not yet been performed in plants.

Some phenotypes of *Atiar1-3* mutants have however been distinct from both *Atiar1-t* and Col-0 plants. This includes an increase in Fe deficiency response in Zn excess, as well as a lack of the excess Zn -exogenous IAA interactions in root phenotypes. Whether these phenotypes are related is unknown, but it could be hypothesised that the increased Zn toxicity seen in *Atiar1-3* plants may alter the PIN distribution which is relevant to the Zn excess-exogenous IAA interactions in the root.

In addition to Zn excess-specific changes, the *Atiar1-3* mutant also shows phenotypes distinct from Col-0 and *Atiar1-t* across Zn deficiency and control Zn conditions. This includes persistent decreases in primary root length, not showing the time dependence of the *Atiar1-t* phenotype, decreased apical hook angle, and increased IAA sensitivity compared to Col-0 and *Atiar1-t* in Zn deficiency and control Zn conditions. Further understanding of localisation and activity of AtIAR1 and Atiar1-3 is necessary to unpick the mechanisms here, but particular attention should paid to functionality of the C-terminal region which is disrupted in Atiar1-3, and could be related to dimerization[385], either homodimerization or

heterodimerisation with other secretory pathway ZIPs. The restricted localisation of Atiar1-3 predicted in the updated model in **Figure 7.2** would mean any Atiar1-3 interacting protein which could be trafficked to the Golgi in *Atiar1-t* plants is retained in *Atiar1-3* plants. Retention of this protein may then lead to increased sensitivity to Zn toxicity, changed auxin gradients and show a time-dependant function. Therefore, future work should involve investigating the interactome of AtIAR1 to further unpick this.

7.5 The ER and Golgi are differently regulated Zn stores

One of the questions surrounding ER and Golgi Zn homeostasis involves whether Zn levels are higher or lower in the secretory pathway than the cytosol. The concentration of free Zn in the cytosol of plant cells has been calculated using FRET sensors to be around 400 pM[46] similar to estimates in mammalian cells[415,416]. Plant ER Zn concentration has not been measured, but calculations of ER Zn in mammalian cells has shown diverging estimates of close to 1 pM[415,421] or 1-5 nM[417,422]. Given a compartment with a volume of 1 pL with a Zn concentration of 1 pM would be calculated to contain 0.6 Zn ions and that HeLa cells have a total volume of 1-2 pl[580,581], it is therefore unlikely that the ER has a Zn concentration of 1 pM in mammalian cells[582]. Additionally, to date in plants, AtMTP2 proteins are the only proteins known to be responsible for Zn import into the ER, requiring proton antiport[86,87] which is favourable given the more acidic pH of the ER relative to the cytosol[583]. AtZTP29[80] and AtIAR1 which release Zn from the ER are ZIP transporters which are suspected to symport HCO_3^- in a similar way to HsZIP2, 8 and 14, and so would also be transporting against the pH gradient[584-586]. It therefore seems most likely that Zn levels in the ER are higher that of the cytosol.

The situation is more complicated in the Golgi which retains a lower pH than the ER[583] but in addition to AtMTP5-AtMTP12 transporting Zn into the *cis*-Golgi[1,89], AtZIP13 also can transport Zn into the Golgi[76]. However, AtZIP13 is an atypical ZIP, transporting a metal out of the cytosol with predicted 14 transmembrane helices and so its transport mechanism may be atypical of previously characterised eukaryotic ZIP transporters. Therefore, it is possible that Golgi Zn levels are also higher than that in the cytosol, but further work is needed using ER and Golgi targeted FRET sensors to test these hypotheses.

The regulation of these two Zn compartments are different. Only Golgi Zn is thought used as a storage compartment during excess Zn conditions[76], unlike ER Zn which is increased in Zn deficient conditions[92] and reduced by salt stress[80]. The strongest *Atiar1* mutant phenotypes seen in this study are related to auxin rather than Zn deficiency and excess responses suggesting AtIAR1 may not be involved in

the dynamic regulation of ER/Golgi Zn stores in these changing Zn conditions, but instead to developmental cues. Further work on the regulation of *AtIAR1* expression and activity will help further characterise how AtIAR1-mediated ER/Golgi Zn mobilisation is controlled and interacts with other mobilisation cues such as salt stress.

7.6 Studies on hormone-nutrient interaction require high spatial and temporal resolution

As shown in this study, the complexity of the hormonal and developmental responses in changing Zn conditions are vast and contain a multitude of overlapping factors. It is therefore difficult to determine one specific change between the different conditions as key. Future work on the nutrient-hormone interaction landscape would do well to focus in on a single aspect of a developmental change in the altered nutrient/hormone conditions and acquire data with high spatial and temporal resolution on this point to advance the field further. This is particularly the case when considering further work on *AtIAR1*, whose mutants show varied phenotypes indicative of pleiotropic effects of mutations at this locus.

Bibliography

1 Rampey, R. A., Baldridge, M. T., Farrow, D. C., Bay, S. N. & Bartel, B. Compensatory mutations in predicted metal transporters modulate auxin conjugate responsiveness in Arabidopsis. *G3: Genes, Genomes, Genetics* **3**, 131-141 (2013).

2 Andreini, C., Bertini, I. & Rosato, A. Metalloproteomes: a bioinformatic approach. *Acc. Chem. Res.* **42**, 1471-1479 (2009).

3 Whitney, P. L., Fölsch, G., Nyman, P. O. & Malmström, B. G. Inhibition of human erythrocyte carbonic anhydrase B by chloroacetyl sulfonamides with labeling of the active site. *J. Biol. Chem.* **242**, 4206-4211 (1967).

4 Devaiah, B. N., Nagarajan, V. K. & Raghothama, K. G. Phosphate homeostasis and root development in Arabidopsis are synchronized by the zinc finger transcription factor ZAT6. *Plant Physiol.* **145**, 147-159 (2007).

5 O'Dell, B. L. Role of Zinc in Plasma Membrane Function. *The Journal of Nutrition* **130**, 1432S-1436S (2000).

6 Lin, C.-W., Chang, H.-B. & Huang, H.-J. Zinc induces mitogen-activated protein kinase activation mediated by reactive oxygen species in rice roots. *Plant Physiol. Biochem.* **43**, 963-968 (2005).

7 Sensi, S. L., Yin, H. Z. & Weiss, J. H. AMPA/kainate receptor-triggered Zn2+ entry into cortical neurons induces mitochondrial Zn2+ uptake and persistent mitochondrial dysfunction. *Eur. J. Neurosci.* **12**, 3813-3818 (2000).

8 Cakmak, I. Possible Roles of Zinc in Protecting Plant Cells from Damage by Reactive Oxygen Species **146**, 185-205 (2000).

9 Sillanpaa, M. Micronutrient assessment at the country level: an international study. *FAO Soils Bulletin* **63** (1990).

10 Alloway, B. J. *Micronutrient deficiencies in global crop production*. (Springer Science & Business Media, 2008).

11 Barber, S. A. *Soil nutrient bioavailability: a mechanistic approach*. (John Wiley & Sons, 1995).

12 Sims, J. T. Soil pH Effects on the Distribution and Plant Availability of Manganese, Copper, and Zinc 1. *Soil Sci. Soc. Am. J.* **50**, 367-373 (1986).

13 Lu, X. *et al.* Effects of zinc fertilization on zinc dynamics in potentially zinc-deficient calcareous soil. *Agron. J.* **104**, 963-969 (2012).

14 Marschner, H. Mineral nutrition of higher plants. 2nd. *Edn. Academic Pres* (1995).

15 Wissuwa, M., Ismail, A. M. & Yanagihara, S. Effects of zinc deficiency on rice growth and genetic factors contributing to tolerance. *Plant Physiol.* **142**, 731-741 (2006).

16 Cakmak, I. & Marschner, H. Enhanced superoxide radical production in roots of zinc-deficient plants. *J. Exp. Bot.* **39**, 1449-1460 (1988).

17 Höller, S., Meyer, A. & Frei, M. Zinc deficiency differentially affects redox homeostasis of rice genotypes contrasting in ascorbate level. *J. Plant Physiol.* **171**, 1748-1756 (2014).

18 Cakmak, I. *et al.* Dry matter production and distribution of zinc in bread and durum wheat genotypes differing in zinc efficiency. *Plant Soil* **180**, 173-181 (1996).

19 Winterbourn, C. C. Toxicity of iron and hydrogen peroxide: the Fenton reaction. *Toxicol. Lett.* **82**, 969-974 (1995).

20 Cakmak, I., Ozkan, H., Braun, H., Welch, R. & Romheld, V. Zinc and iron concentrations in seeds of wild, primitive, and modern wheats. *Food and Nutrition Bulletin* **21**, 401-403 (2000).
21 Hambidge, K. M., Miller, L. V., Westcott, J. E., Sheng, X. & Krebs, N. F. Zinc bioavailability and homeostasis. *The American journal of clinical nutrition* **91**, 1478S-1483S (2010).
22 Group, I. Z. N. C. International Zinc Nutrition Consultative Group (IZiNCG) technical document# 1. Assessment of the risk of zinc deficiency in populations and options for its control. *Food Nutr Bull* **25**, S99-S203 (2004).
23 Black, R. E. *et al.* Maternal and child undernutrition: global and regional exposures and health consequences. *The lancet* **371**, 243-260 (2008).
24 Caggiano, V. *et al.* Zinc deficiency in a patient with retarded growth, hypogonadism, hypogammaglobulinemia and chronic infection. *American Journal of Medical Sciences* **257**, 305-319 (1969).
25 Hambidge, K. M., Hambidge, C., Jacobs, M. & Baum, J. D. Low levels of zinc in hair, anorexia, poor growth, and hypogeusia in children. *Pediatric Research* **6**, 868-874 (1972).
26 Beck, F. W., Kaplan, J., Fine, N., Handschu, W. & Prasad, A. S. Decreased expression of CD73 (ecto-5'-nucleotidase) in the CD8+ subset is associated with zinc deficiency in human patients. *Journal of Laboratory and Clinical Medicine* **130**, 147-156 (1997).
27 Beck, F., Prasad, A., Kaplan, J., Fitzgerald, J. & Brewer, G. Changes in cytokine production and T cell subpopulations in experimentally induced zinc-deficient humans. *American Journal of Physiology-Endocrinology and Metabolism* **272**, E1002-E1007 (1997).
28 Prasad, A. S. *et al.* Serum thymulin in human zinc deficiency. *The Journal of clinical investigation* **82**, 1202-1210 (1988).
29 Cakmak, I. Enrichment of fertilizers with zinc: An excellent investment for humanity and crop production in India. *J. Trace Elem. Med Biol.* **23**, 281-289 (2009).
30 Borrill, P. *et al.* Biofortification of wheat grain with iron and zinc: integrating novel genomic resources and knowledge from model crops. *Frontiers in plant science* **5**, 53 (2014).
31 Menguer, P. K. *et al.* Improving zinc accumulation in cereal endosperm using Hv MTP 1, a transition metal transporter. *Plant Biotechnol. J.* **16**, 63-71 (2018).
32 Harrington, S. A. *et al.* A two-gene strategy increases the iron and zinc concentration of wheat flour and improves mineral bioaccesibility for human nutrition. *Plant Physiol.* (2022).
33 Sutherland, R. A. & Tolosa, C. A. Variation in total and extractable elements with distance from roads in an urban watershed, Honolulu, Hawaii. *Water, Air, Soil Pollut.* **127**, 315-338 (2001).
34 Fontes, R. & Cox, F. Zinc toxicity in soybean grown at high iron concentration in nutrient solution. *J. Plant Nutr.* **21**, 1723-1730 (1998).
35 Shanmugam, V. *et al.* Differential expression and regulation of iron-regulated metal transporters in Arabidopsis halleri and Arabidopsis thaliana–the role in zinc tolerance. *New Phytol.* **190**, 125-137 (2011).
36 Krämer, U. Metal hyperaccumulation in plants. *Annu. Rev. Plant Biol.* **61**, 517-534 (2010).
37 Cappa, J. J. & Pilon-Smits, E. A. Evolutionary aspects of elemental hyperaccumulation. *Planta* **239**, 267-275 (2014).

38 Hanikenne, M. & Nouet, C. Metal hyperaccumulation and hypertolerance: a model for plant evolutionary genomics. *Curr. Opin. Plant Biol.* **14**, 252-259 (2011).
39 Corso, M. *et al.* Adaptation of Arabidopsis halleri to extreme metal pollution through limited metal accumulation involves changes in cell wall composition and metal homeostasis. *New Phytol.* **230**, 669-682 (2021).
40 Schvartzman, M. S. *et al.* Adaptation to high zinc depends on distinct mechanisms in metallicolous populations of Arabidopsis halleri. *New Phytol.* **218**, 269-282 (2018).
41 Seregin, I., Kozhevnikova, A. & Schat, H. Correlated Variation of the Zn Accumulation and Tolerance Capacities among Populations and Ecotypes of the Zn Hyperaccumulator, Noccaea caerulescens. *Russian Journal of Plant Physiology* **68**, S26-S36 (2021).
42 Shah, K. & Nongkynrih, J. Metal hyperaccumulation and bioremediation. *Biol. Plant.* **51**, 618-634 (2007).
43 Castro, P. H. *et al.* Phylogenetic analysis of F-bZIP transcription factors indicates conservation of the zinc deficiency response across land plants. *Scientific reports* **7**, 1-14 (2017).
44 Clemens, S. How metal hyperaccumulating plants can advance Zn biofortification. *Plant Soil* **411**, 111-120 (2017).
45 Broadley, M. R., White, P. J., Hammond, J. P., Zelko, I. & Lux, A. Zinc in plants. *New Phytol.* **173**, 677-702 (2007).
46 Lanquar, V. *et al.* Dynamic imaging of cytosolic zinc in Arabidopsis roots combining FRET sensors and RootChip technology. *New Phytol.* **202**, 198-208 (2014).
47 Yang, Z., Wu, Y., Li, Y., Ling, H.-Q. & Chu, C. OsMT1a, a type 1 metallothionein, plays the pivotal role in zinc homeostasis and drought tolerance in rice. *Plant Mol. Biol.* **70**, 219-229 (2009).
48 Tennstedt, P., Peisker, D., Böttcher, C., Trampczynska, A. & Clemens, S. Phytochelatin synthesis is essential for the detoxification of excess zinc and contributes significantly to the accumulation of zinc. *Plant Physiol.* **149**, 938-948 (2009).
49 Guo, W. J., Bundithya, W. & Goldsbrough, P. B. Characterization of the Arabidopsis metallothionein gene family: tissue-specific expression and induction during senescence and in response to copper. *New Phytol.* **159**, 369-381 (2003).
50 Grennan, A. K. Metallothioneins, a diverse protein family. *Plant Physiol.* **155**, 1750-1751 (2011).
51 Lee, J., Donghwan, S., Won-yong, S., Inhwan, H. & Youngsook, L. Arabidopsis metallothioneins 2a and 3 enhance resistance to cadmium when expressed in Vicia faba guard cells. *Plant Mol. Biol.* **54**, 805-815 (2004).
52 Guo, W.-J., Meetam, M. & Goldsbrough, P. B. Examining the specific contributions of individual Arabidopsis metallothioneins to copper distribution and metal tolerance. *Plant Physiol.* **146**, 1697-1706 (2008).
53 Cobbett, C. & Goldsbrough, P. Phytochelatins and metallothioneins: roles in heavy metal detoxification and homeostasis. *Annu. Rev. Plant Biol.* **53**, 159-182 (2002).
54 Hirata, K. *et al.* Strong induction of phytochelatin synthesis by zinc in marine green alga, Dunaliella tertiolecta. *J. Biosci. Bioeng.* **92**, 24-29 (2001).
55 Mendoza-Cózatl, D. G. *et al.* Identification of high levels of phytochelatins, glutathione and cadmium in the phloem sap of Brassica napus. A role for thiol-peptides in the long-distance transport of cadmium and the effect of cadmium on iron translocation. *The Plant Journal* **54**, 249-259 (2008).

56 Wintz, H. *et al.* Expression profiles of Arabidopsis thaliana in mineral deficiencies reveal novel transporters involved in metal homeostasis. *J. Biol. Chem.* **278**, 47644-47653 (2003).
57 Salt, D. E., Prince, R. C., Baker, A. J., Raskin, I. & Pickering, I. J. Zinc ligands in the metal hyperaccumulator Thlaspi caerulescens as determined using X-ray absorption spectroscopy. *Environ. Sci. Technol.* **33**, 713-717 (1999).
58 Takahashi, M. *et al.* Role of nicotianamine in the intracellular delivery of metals and plant reproductive development. *The Plant Cell* **15**, 1263-1280 (2003).
59 Cornu, J. Y. *et al.* Contrasting effects of nicotianamine synthase knockdown on zinc and nickel tolerance and accumulation in the zinc/cadmium hyperaccumulator Arabidopsis halleri. *New Phytol.* **206**, 738-750 (2015).
60 Douchkov, D., Gryczka, C., Stephan, U., Hell, R. & Bäumlein, H. Ectopic expression of nicotianamine synthase genes results in improved iron accumulation and increased nickel tolerance in transgenic tobacco. *Plant, Cell Environ.* **28**, 365-374 (2005).
61 Curie, C. *et al.* Metal movement within the plant: contribution of nicotianamine and yellow stripe 1-like transporters. *Ann. Bot.* **103**, 1-11 (2009).
62 Waters, B. M. *et al.* Mutations in Arabidopsis yellow stripe-like1 and yellow stripe-like3 reveal their roles in metal ion homeostasis and loading of metal ions in seeds. *Plant Physiol.* **141**, 1446-1458 (2006).
63 Uraguchi, S., Weber, M. & Clemens, S. Elevated root nicotianamine concentrations are critical for Zn hyperaccumulation across diverse edaphic environments. *Plant, Cell Environ.* **42**, 2003-2014 (2019).
64 Guerinot, M. L. The ZIP family of metal transporters. *Biochimica et Biophysica Acta (BBA)-Biomembranes* **1465**, 190-198 (2000).
65 Lehtovirta-Morley, L. E., Alsarraf, M. & Wilson, D. Pan-domain analysis of ZIP zinc transporters. *International journal of molecular sciences* **18**, 2631 (2017).
66 Rogers, E. E., Eide, D. J. & Guerinot, M. L. Altered selectivity in an Arabidopsis metal transporter. *Proceedings of the National Academy of Sciences* **97**, 12356-12360 (2000).
67 Korshunova, Y. O., Eide, D., Clark, W. G., Guerinot, M. L. & Pakrasi, H. B. The IRT1 protein from Arabidopsis thaliana is a metal transporter with a broad substrate range. *Plant Mol. Biol.* **40**, 37-44 (1999).
68 Milner, M. J., Seamon, J., Craft, E. & Kochian, L. V. Transport properties of members of the ZIP family in plants and their role in Zn and Mn homeostasis. *J. Exp. Bot.* **64**, 369-381 (2013).
69 Winter, D. *et al.* An "Electronic Fluorescent Pictograph" browser for exploring and analyzing large-scale biological data sets. *PloS one* **2** (2007).
70 Lin, Y.-F., Hassan, Z., Talukdar, S., Schat, H. & Aarts, M. G. Expression of the ZNT1 zinc transporter from the metal hyperaccumulator Noccaea caerulescens confers enhanced zinc and cadmium tolerance and accumulation to Arabidopsis thaliana. *PloS one* **11**, e0149750 (2016).
71 Assunção, A. G. *et al.* Arabidopsis thaliana transcription factors bZIP19 and bZIP23 regulate the adaptation to zinc deficiency. *Proceedings of the National Academy of Sciences* **107**, 10296-10301 (2010).
72 Lee, S. *et al.* Redundant roles of four ZIP family members in zinc homeostasis and seed development in Arabidopsis thaliana. *The Plant Journal* **108**, 1162-1173 (2021).
73 Zheng, X., Chen, L. & Li, X. Arabidopsis and rice showed a distinct pattern in ZIPs genes expression profile in response to Cd stress. *Botanical Studies* **59**, 22 (2018). https://doi.org:10.1186/s40529-018-0238-6

74 Klepikova, A. V., Kasianov, A. S., Gerasimov, E. S., Logacheva, M. D. & Penin, A. A. A high resolution map of the Arabidopsis thaliana developmental transcriptome based on RNA-seq profiling. *The Plant Journal* **88**, 1058-1070 (2016).
75 Nguyen, N. T. *et al.* Iron Availability within the Leaf Vasculature Determines the Magnitude of Iron Deficiency Responses in Source and Sink Tissues in Arabidopsis. *Plant and Cell Physiology* (2022).
76 Wang, Y., Yang, J., Miao, R., Kang, Y. & Qi, Z. A Novel Zinc Transporter Essential for Arabidopsis Zinc and Iron-Dependent Growth. *J. Plant Physiol.* **256**, 153296 (2020).
77 Vert, G. *et al.* IRT1, an Arabidopsis transporter essential for iron uptake from the soil and for plant growth. *The Plant Cell* **14**, 1223-1233 (2002).
78 Vert, G., Briat, J. F. & Curie, C. Arabidopsis IRT2 gene encodes a root-periphery iron transporter. *The Plant Journal* **26**, 181-189 (2001).
79 Lin, Y. F. *et al.* Arabidopsis IRT3 is a zinc-regulated and plasma membrane localized zinc/iron transporter. *New Phytol.* **182**, 392-404 (2009).
80 Wang, M., Xu, Q., Yu, J. & Yuan, M. The putative Arabidopsis zinc transporter ZTP29 is involved in the response to salt stress. *Plant Mol. Biol.* **73**, 467-479 (2010).
81 Song, W.-Y. *et al.* Arabidopsis PCR2 is a zinc exporter involved in both zinc extrusion and long-distance zinc transport. *The Plant Cell* **22**, 2237-2252 (2010).
82 Axelsen, K. B. & Palmgren, M. G. Inventory of the superfamily of P-type ion pumps in Arabidopsis. *Plant Physiol.* **126**, 696-706 (2001).
83 Axelsen, K. B. & Palmgren, M. G. Evolution of substrate specificities in the P-type ATPase superfamily. *J. Mol. Evol.* **46**, 84-101 (1998).
84 Hussain, D. *et al.* P-type ATPase heavy metal transporters with roles in essential zinc homeostasis in Arabidopsis. *The Plant Cell* **16**, 1327-1339 (2004).
85 Morel, M. l. *et al.* AtHMA3, a P1B-ATPase Allowing Cd/Zn/Co/Pb Vacuolar Storage in Arabidopsis *Plant Physiol.* **149**, 894-904 (2008).
86 Guffanti, A. A., Wei, Y., Rood, S. V. & Krulwich, T. A. An antiport mechanism for a member of the cation diffusion facilitator family: divalent cations efflux in exchange for K+ and H+. *Mol. Microbiol.* **45**, 145-153 (2002).
87 Chao, Y. & Fu, D. Kinetic study of the antiport mechanism of an Escherichia coli zinc transporter, ZitB. *J. Biol. Chem.* **279**, 12043-12050 (2004).
88 Montanini, B., Blaudez, D., Jeandroz, S., Sanders, D. & Chalot, M. Phylogenetic and functional analysis of the Cation Diffusion Facilitator (CDF) family: improved signature and prediction of substrate specificity. *BMC Genomics* **8**, 107 (2007).
89 Fujiwara, T. *et al.* A high molecular mass zinc transporter MTP 12 forms a functional heteromeric complex with MTP 5 in the Golgi in Arabidopsis thaliana. *The FEBS journal* **282**, 1965-1979 (2015).
90 Bloß, T., Clemens, S. & Nies, D. H. Characterization of the ZAT1p zinc transporter from Arabidopsis thaliana in microbial model organisms and reconstituted proteoliposomes. *Planta* **214**, 783-791 (2002).
91 Arrivault, S., Senger, T. & Krämer, U. The Arabidopsis metal tolerance protein AtMTP3 maintains metal homeostasis by mediating Zn exclusion from the shoot under Fe deficiency and Zn oversupply. *The Plant Journal* **46**, 861-879 (2006).
92 Sinclair, S. A. *et al.* Systemic upregulation of MTP2-and HMA2-mediated Zn partitioning to the shoot supplements local Zn deficiency responses. *The Plant Cell* **30**, 2463-2479 (2018).
93 Desbrosses-Fonrouge, A.-G. *et al.* Arabidopsis thaliana MTP1 is a Zn transporter in the vacuolar membrane which mediates Zn detoxification and drives leaf Zn accumulation. *FEBS Lett.* **579**, 4165-4174 (2005).

94 Gunshin, H. *et al.* Cloning and characterization of a mammalian proton-coupled metal-ion transporter. *Nature* **388**, 482-488 (1997).
95 Chen, X.-Z. *et al.* Yeast SMF1 mediates H+-coupled iron uptake with concomitant uncoupled cation currents. *J. Biol. Chem.* **274**, 35089-35094 (1999).
96 Tandy, S. *et al.* Nramp2 expression is associated with pH-dependent iron uptake across the apical membrane of human intestinal Caco-2 cells. *J. Biol. Chem.* **275**, 1023-1029 (2000).
97 Thomine, S., Wang, R., Ward, J. M., Crawford, N. M. & Schroeder, J. I. Cadmium and iron transport by members of a plant metal transporter family in Arabidopsis with homology to Nramp genes. *Proceedings of the National Academy of Sciences* **97**, 4991-4996 (2000).
98 Lanquar, V. *et al.* Export of vacuolar manganese by AtNRAMP3 and AtNRAMP4 is required for optimal photosynthesis and growth under manganese deficiency. *Plant Physiol.* **152**, 1986-1999 (2010).
99 Lanquar, V. *et al.* Mobilization of vacuolar iron by AtNRAMP3 and AtNRAMP4 is essential for seed germination on low iron. *The EMBO journal* **24**, 4041-4051 (2005).
100 Haydon, M. J. & Cobbett, C. S. A novel major facilitator superfamily protein at the tonoplast influences zinc tolerance and accumulation in Arabidopsis. *Plant Physiol.* **143**, 1705-1719 (2007).
101 Haydon, M. J. *et al.* Vacuolar nicotianamine has critical and distinct roles under iron deficiency and for zinc sequestration in Arabidopsis. *The Plant Cell* **24**, 724-737 (2012).
102 Remy, E. *et al.* Intron retention in the 5′ UTR of the novel ZIF2 transporter enhances translation to promote zinc tolerance in Arabidopsis. *PLoS Genet.* **10**, e1004375 (2014).
103 Barton, D. A. *et al.* Cell-to-cell transport via the lumen of the endoplasmic reticulum. *The Plant Journal* **66**, 806-817 (2011).
104 Sinclair, S. A., Sherson, S. M., Jarvis, R., Camakaris, J. & Cobbett, C. S. The use of the zinc-fluorophore, Zinpyr-1, in the study of zinc homeostasis in Arabidopsis roots. *New Phytol.* **174**, 39-45 (2007).
105 Cakmak, I. & Marschner, H. Increase in membrane permeability and exudation in roots of zinc deficient plants. *J. Plant Physiol.* **132**, 356-361 (1988).
106 Broadley, M. R. *et al.* Response to zinc deficiency of two rice lines with contrasting tolerance is determined by root growth maintenance and organic acid exudation rates, and not by zinc-transporter activity. *New Phytol.* **186**, 400-414 (2010).
107 Cakmak, I., Öztürk, L., Karanlik, S., Marschner, H. & Ekiz, H. Zinc-efficient wild grasses enhance release of phytosiderophores under zinc deficiency. *J. Plant Nutr.* **19**, 551-563 (1996).
108 Obata, H., Kawamura, S., Senoo, K. & Tanaka, A. Changes in the level of protein and activity of Cu/Zn-superoxide dismutase in zinc deficient rice plant, Oryza sativa L. *Soil Sci. Plant Nutr.* **45**, 891-896 (1999).
109 Cakmak, I. *et al.* Concentration of zinc and activity of copper/zinc-superoxide dismutase in leaves of rye and wheat cultivars differing in sensitivity to zinc deficiency. *J. Plant Physiol.* **151**, 91-95 (1997).
110 Nakayama, S. *et al.* Manganese Treatment Alleviates Zinc Deficiency Symptoms in Arabidopsis Seedlings. *Plant and Cell Physiology* (2020).
111 Jain, A., Sinilal, B., Dhandapani, G., Meagher, R. B. & Sahi, S. V. Effects of deficiency and excess of zinc on morphophysiological traits and spatiotemporal regulation of zinc-responsive genes reveal incidence of cross talk between micro- and macronutrients. *Environ. Sci. Technol.* **47**, 5327-5335 (2013).

112 Becher, M., Talke, I. N., Krall, L. & Krämer, U. Cross-species microarray transcript profiling reveals high constitutive expression of metal homeostasis genes in shoots of the zinc hyperaccumulator Arabidopsis halleri. *The Plant Journal* **37**, 251-268 (2004).
113 Küpper, H., Lombi, E., Zhao, F.-J. & McGrath, S. P. Cellular compartmentation of cadmium and zinc in relation to other elements in the hyperaccumulator Arabidopsis halleri. *Planta* **212**, 75-84 (2000).
114 Erenoglu, E. B., Kutman, U. B., Ceylan, Y., Yildiz, B. & Cakmak, I. Improved nitrogen nutrition enhances root uptake, root-to-shoot translocation and remobilization of zinc (65Zn) in wheat. *New Phytol.* **189**, 438-448 (2011).
115 Eguchi, M., Kimura, K., Makino, A. & Ishida, H. Autophagy is induced under Zn limitation and contributes to Zn-limited stress tolerance in Arabidopsis (Arabidopsis thaliana). *Soil Sci. Plant Nutr.* **63**, 342-350 (2017).
116 Shinozaki, D. *et al.* Autophagy Increases Zinc Bioavailability to Avoid Light-Mediated ROS Production under Zn Deficiency. *Plant Physiol.*, pp.01522.02019 (2020). https://doi.org:10.1104/pp.19.01522
117 Pita-Barbosa, A., Ricachenevsky, F. K., Wilson, M., Dottorini, T. & Salt, D. E. Transcriptional plasticity buffers genetic variation in zinc homeostasis. *Scientific Reports* **9**, 1-11 (2019).
118 Lilay, G. H., Castro, P. H., Campilho, A. & Assunção, A. G. The Arabidopsis bZIP19 and bZIP23 activity requires zinc deficiency–insight on regulation from complementation lines. *Frontiers in plant science* **9**, 1955 (2019).
119 Inaba, S. *et al.* Identification of putative target genes of bZIP19, a transcription factor essential for Arabidopsis adaptation to Zn deficiency in roots. *The Plant Journal* **84**, 323-334 (2015).
120 Lilay, G. H. *et al.* Arabidopsis bZIP19 and bZIP23 act as zinc sensors to control plant zinc status. *Nature plants* **7**, 137-143 (2021).
121 Lilay, G. H. *et al.* Rice F-bZIP transcription factors regulate the zinc deficiency response. *J. Exp. Bot.* **71**, 3664-3677 (2020).
122 Henriques, A., Farias, D. d. R. & de Oliveira, A. C. Identification and characterization of the bZIP transcription factor involved in zinc homeostasis in cereals. *Gen. Mol. Res.* **16**, 1-10 (2017).
123 Barberon, M. *et al.* Monoubiquitin-dependent endocytosis of the iron-regulated transporter 1 (IRT1) transporter controls iron uptake in plants. *Proceedings of the National Academy of Sciences* **108**, E450-E458 (2011).
124 Dubeaux, G., Neveu, J., Zelazny, E. & Vert, G. Metal sensing by the IRT1 transporter-receptor orchestrates its own degradation and plant metal nutrition. *Mol. Cell* **69**, 953-964 (2018).
125 Irving, H. & Williams, R. Order of stability of metal complexes. *Nature* **162**, 746-747 (1948).
126 Van Assche, F. & Clijsters, H. Inhibition of photosynthesis in Phaseolus vulgaris by treatment with toxic concentration of zinc: effect on ribulose-1, 5-bisphosphate carboxylase/oxygenase. *J. Plant Physiol.* **125**, 355-360 (1986).
127 Van Assche, F. & Clijsters, H. Inhibition of photosynthesis in Phaseolus vulgaris by treatment with toxic concentrations of zinc: effects on electron transport and photophosphorylation. *Physiol. Plant.* **66**, 717-721 (1986).
128 Remans, T. *et al.* Exposure of Arabidopsis thaliana to excess Zn reveals a Zn-specific oxidative stress signature. *Environ. Exp. Bot.* **84**, 61-71 (2012).
129 Chaoui, A., Mazhoudi, S., Ghorbal, M. H. & El Ferjani, E. Cadmium and zinc induction of lipid peroxidation and effects on antioxidant enzyme activities in bean (Phaseolus vulgaris L.). *Plant Sci.* **127**, 139-147 (1997).

130 Dronnet, V., Renard, C., Axelos, M. & Thibault, J.-F. Heavy metals binding by pectins: selectivity, quantification and characterisation. *Prog. Biotechnol.* **14**, 535-540 (1996).
131 Kartel, M. T., Kupchik, L. A. & Veisov, B. K. Evaluation of pectin binding of heavy metal ions in aqueous solutions. *Chemosphere* **38**, 2591-2596 (1999).
132 Sinclair, S. A. *et al.* Etiolated seedling development requires repression of photomorphogenesis by a small cell-wall-derived dark signal. *Curr. Biol.* **27**, 3403-3418 (2017).
133 Weber, M. *et al.* A mutation in the Arabidopsis thaliana cell wall biosynthesis gene pectin methylesterase 3 as well as its aberrant expression cause hypersensitivity specifically to Zn. *The Plant Journal* **76**, 151-164 (2013).
134 van de Mortel, J. E. *et al.* Large expression differences in genes for iron and zinc homeostasis, stress response, and lignin biosynthesis distinguish roots of Arabidopsis thaliana and the related metal hyperaccumulator Thlaspi caerulescens. *Plant Physiol.* **142**, 1127-1147 (2006).
135 Fukao, Y. *et al.* iTRAQ analysis reveals mechanisms of growth defects due to excess zinc in Arabidopsis. *Plant Physiol.* **155**, 1893-1907 (2011).
136 Robinson, N. J., Procter, C. M., Connolly, E. L. & Guerinot, M. L. A ferric-chelate reductase for iron uptake from soils. *Nature* **397**, 694-697 (1999).
137 Eide, D., Broderius, M., Fett, J. & Guerinot, M. L. A novel iron-regulated metal transporter from plants identified by functional expression in yeast. *Proceedings of the National Academy of Sciences* **93**, 5624-5628 (1996).
138 Colangelo, E. P. & Guerinot, M. L. The essential basic helix-loop-helix protein FIT1 is required for the iron deficiency response. *The Plant Cell* **16**, 3400-3412 (2004).
139 Vert, G. *et al.* Arabidopsis IRT2 cooperates with the high-affinity iron uptake system to maintain iron homeostasis in root epidermal cells. *Planta* **229**, 1171-1179 (2009).
140 Rogers, E. E. & Guerinot, M. L. FRD3, a Member of the Multidrug and Toxin Efflux Family, Controls Iron Deficiency Responses in Arabidopsis. *The Plant Cell* **14**, 1787-1799 (2002).
141 Durrett, T. P., Gassmann, W. & Rogers, E. E. The FRD3-Mediated Efflux of Citrate into the Root Vasculature Is Necessary for Efficient Iron Translocation. *Plant Physiol.* **144**, 197-205 (2007).
142 Pineau, C. *et al.* Natural variation at the FRD3 MATE transporter locus reveals cross-talk between Fe homeostasis and Zn tolerance in Arabidopsis thaliana. *PLoS Genet.* **8**, e1003120 (2012).
143 Pottier, M. *et al.* Identification of mutations allowing Natural Resistance Associated Macrophage Proteins (NRAMP) to discriminate against cadmium. *The Plant Journal* **83**, 625-637 (2015).
144 Shinozaki, D., Tanoi, K. & Yoshimoto, K. Optimal Distribution of Iron to Sink Organs via Autophagy Is Important for Tolerance to Excess Zinc in Arabidopsis. *Plant and Cell Physiology* **62**, 515-527 (2021).
145 Smeets, K. *et al.* Cadmium-induced transcriptional and enzymatic alterations related to oxidative stress. *Environ. Exp. Bot.* **63**, 1-8 (2008).
146 Remans, T. *et al.* Metal-specific and NADPH oxidase dependent changes in lipoxygenase and NADPH oxidase gene expression in Arabidopsis thaliana exposed to cadmium or excess copper. *Funct. Plant Biol.* **37**, 532-544 (2010).
147 Zhang, H. *et al.* PuHSFA4a enhances tolerance to excess zinc by regulating reactive oxygen species production and root development in Populus. *Plant Physiol.* **180**, 2254-2271 (2019).

148 Gao, F. *et al.* The transcription factor bHLH121 interacts with bHLH105 (ILR3) and its closest homologs to regulate iron homeostasis in Arabidopsis. *The Plant Cell* **32**, 508-524 (2020).
149 Zhang, J. *et al.* The bHLH transcription factor bHLH104 interacts with IAA-LEUCINE RESISTANT3 and modulates iron homeostasis in Arabidopsis. *The Plant Cell* **27**, 787-805 (2015).
150 Li, X., Zhang, H., Ai, Q., Liang, G. & Yu, D. Two bHLH transcription factors, bHLH34 and bHLH104, regulate iron homeostasis in Arabidopsis thaliana. *Plant Physiol.* **170**, 2478-2493 (2016).
151 Liang, G., Zhang, H., Li, X., Ai, Q. & Yu, D. bHLH transcription factor bHLH115 regulates iron homeostasis in Arabidopsis thaliana. *J. Exp. Bot.* **68**, 1743-1755 (2017).
152 Yuan, Y. *et al.* FIT interacts with AtbHLH38 and AtbHLH39 in regulating iron uptake gene expression for iron homeostasis in Arabidopsis. *Cell Res.* **18**, 385-397 (2008).
153 Wang, N. *et al.* Requirement and functional redundancy of Ib subgroup bHLH proteins for iron deficiency responses and uptake in Arabidopsis thaliana. *Molecular plant* **6**, 503-513 (2013).
154 Long, T. A. *et al.* The bHLH transcription factor POPEYE regulates response to iron deficiency in Arabidopsis roots. *The Plant Cell* **22**, 2219-2236 (2010).
155 Tissot, N. *et al.* Transcriptional integration of the responses to iron availability in Arabidopsis by the bHLH factor ILR3. *New Phytol.* **223**, 1433-1446 (2019).
156 Hindt, M. N. *et al.* BRUTUS and its paralogs, BTS LIKE1 and BTS LIKE2, encode important negative regulators of the iron deficiency response in Arabidopsis thaliana. *Metallomics* **9**, 876-890 (2017).
157 Rodríguez-Celma, J. *et al.* Arabidopsis BRUTUS-LIKE E3 ligases negatively regulate iron uptake by targeting transcription factor FIT for recycling. *Proceedings of the National Academy of Sciences* **116**, 17584-17591 (2019).
158 Selote, D., Samira, R., Matthiadis, A., Gillikin, J. W. & Long, T. A. Iron-binding E3 ligase mediates iron response in plants by targeting basic helix-loop-helix transcription factors. *Plant Physiol.* **167**, 273-286 (2015).
159 Li, Y. *et al.* IRON MAN interacts with BRUTUS to maintain iron homeostasis in Arabidopsis. *Proceedings of the National Academy of Sciences* **118**, e2109063118 (2021).
160 Lichtblau, D. M. *et al.* The iron deficiency-regulated small protein effector FEP3/IRON MAN1 modulates interaction of BRUTUS-LIKE1 with bHLH subgroup IVc and POPEYE transcription factors. *Frontiers in Plant Science* **13** (2022).
161 Grillet, L., Lan, P., Li, W., Mokkapati, G. & Schmidt, W. IRON MAN is a ubiquitous family of peptides that control iron transport in plants. *Nature plants* **4**, 953-963 (2018).
162 Ciesielski, T. *Untersuchungen über die Abwärtskrümmung der Wurzel*. Vol. 2 (1871).
163 Darwin, C. & Darwin, F. *The Power of Movement in Plants* (John Murray, London, 1881).
164 Kögl, F., Haagen-Smit, A. & Erxleben, H. Über ein neues Auxin "Hetero-auxin" aus Harn. *Mitteilung über pflanzliche Wachstumsstoffe* **11** (1934).
165 Berger, J. & Avery Jr, G. S. Isolation of an auxin precursor and an auxin (indoleacetic acid) from maize. *Am. J. Bot.*, 199-203 (1944).
166 Schiavone, F. M. & Cooke, T. J. Unusual patterns of somatic embryogenesis in the domesticated carrot: developmental effects of exogenous auxins and auxin transport inhibitors. *Cell differentiation* **21**, 53-62 (1987).

167 Liu, C., Xu, Z. & Chua, N.-h. Auxin polar transport is essential for the establishment of bilateral symmetry during early plant embryogenesis. *The Plant Cell* **5**, 621-630 (1993).
168 Fischer, C. & Neuhaus, G. Influence of auxin on the establishment of bilateral symmetry in monocots. *The Plant Journal* **9**, 659-669 (1996).
169 Fischer, C., Speth, V., Fleig-Eberenz, S. & Neuhaus, G. Induction of zygotic polyembryos in wheat: influence of auxin polar transport. *The Plant Cell* **9**, 1767-1780 (1997).
170 Moubayidin, L. *et al.* The rate of cell differentiation controls the Arabidopsis root meristem growth phase. *Curr. Biol.* **20**, 1138-1143 (2010).
171 Ioio, R. D. *et al.* A genetic framework for the control of cell division and differentiation in the root meristem. *Science* **322**, 1380-1384 (2008).
172 Blilou, I. *et al.* The PIN auxin efflux facilitator network controls growth and patterning in Arabidopsis roots. *Nature* **433**, 39-44 (2005).
173 Shi, B. *et al.* Feedback from lateral organs controls shoot apical meristem growth by modulating auxin transport. *Dev. Cell* **44**, 204-216. e206 (2018).
174 Vernoux, T. *et al.* The auxin signalling network translates dynamic input into robust patterning at the shoot apex. *Mol. Syst. Biol.* **7**, 508 (2011).
175 Reinhardt, D., Mandel, T. & Kuhlemeier, C. Auxin regulates the initiation and radial position of plant lateral organs. *The Plant Cell* **12**, 507-518 (2000).
176 Reinhardt, D. *et al.* Regulation of phyllotaxis by polar auxin transport. *Nature* **426**, 255-260 (2003).
177 Růžička, K. *et al.* Cytokinin regulates root meristem activity via modulation of the polar auxin transport. *Proceedings of the National Academy of Sciences* **106**, 4284-4289 (2009).
178 Pierdonati, E. *et al.* Cytokinin-Dependent Control of GH3 Group II Family Genes in the Arabidopsis Root. *Plants* **8**, 94 (2019).
179 Ioio, R. D. *et al.* Cytokinins determine Arabidopsis root-meristem size by controlling cell differentiation. *Curr. Biol.* **17**, 678-682 (2007).
180 Yang, W. *et al.* Molecular mechanism of cytokinin-activated cell division in Arabidopsis. *Science* **371**, 1350-1355 (2021).
181 Rubery, P. H. & Sheldrake, A. R. Carrier-mediated auxin transport. *Planta* **118**, 101-121 (1974).
182 Raven, J. Transport of indoleacetic acid in plant cells in relation to pH and electrical potential gradients, and its significance for polar IAA transport. *New Phytol.* **74**, 163-172 (1975).
183 Okada, K., Ueda, J., Komaki, M. K., Bell, C. J. & Shimura, Y. Requirement of the auxin polar transport system in early stages of Arabidopsis floral bud formation. *The plant cell* **3**, 677-684 (1991).
184 Galweiler, L. *et al.* Regulation of polar auxin transport by AtPIN1 in Arabidopsis vascular tissue. *Science* **282**, 2226-2230 (1998).
185 Müller, A. *et al.* AtPIN2 defines a locus of Arabidopsis for root gravitropism control. *The EMBO journal* **17**, 6903-6911 (1998).
186 Friml, J., Wiśniewska, J., Benková, E., Mendgen, K. & Palme, K. Lateral relocation of auxin efflux regulator PIN3 mediates tropism in Arabidopsis. *Nature* **415**, 806-809 (2002).
187 Friml, J. *et al.* AtPIN4 mediates sink-driven auxin gradients and root patterning in Arabidopsis. *Cell* **108**, 661-673 (2002).
188 Kashkan, I. *et al.* Mutually opposing activity of PIN7 splicing isoforms is required for auxin-mediated tropic responses in Arabidopsis thaliana. *New Phytol.* **233**, 329-343 (2022).

189 Křeček, P. *et al.* The PIN-FORMED (PIN) protein family of auxin transporters. *Genome biology* **10**, 1-11 (2009).
190 Ganguly, A., Park, M., Kesawat, M. S. & Cho, H.-T. Functional analysis of the hydrophilic loop in intracellular trafficking of Arabidopsis PIN-FORMED proteins. *The Plant Cell* **26**, 1570-1585 (2014).
191 Mravec, J. *et al.* Subcellular homeostasis of phytohormone auxin is mediated by the ER-localized PIN5 transporter. *Nature* **459**, 1136-1140 (2009).
192 Ding, Z. *et al.* ER-localized auxin transporter PIN8 regulates auxin homeostasis and male gametophyte development in Arabidopsis. *Nature communications* **3**, 1-11 (2012).
193 Bosco, C. D. *et al.* The endoplasmic reticulum localized PIN8 is a pollen-specific auxin carrier involved in intracellular auxin homeostasis. *The Plant Journal* **71**, 860-870 (2012).
194 Simon, S. *et al.* PIN6 auxin transporter at endoplasmic reticulum and plasma membrane mediates auxin homeostasis and organogenesis in Arabidopsis. *New Phytol.* **211**, 65-74 (2016).
195 Barbez, E. *et al.* A novel putative auxin carrier family regulates intracellular auxin homeostasis in plants. *Nature* **485**, 119-122 (2012).
196 Ranocha, P. *et al.* Arabidopsis WAT1 is a vacuolar auxin transport facilitator required for auxin homoeostasis. *Nature communications* **4**, 1-9 (2013).
197 Ranocha, P. *et al.* Walls are thin 1 (WAT1), an Arabidopsis homolog of Medicago truncatula NODULIN21, is a tonoplast-localized protein required for secondary wall formation in fibers. *The Plant Journal* **63**, 469-483 (2010).
198 Pickett, F. B., Wilson, A. K. & Estelle, M. The aux1 mutation of Arabidopsis confers both auxin and ethylene resistance. *Plant Physiol.* **94**, 1462-1466 (1990).
199 Maher, E. & Martindale, S. Mutants of Arabidopsis thaliana with altered responses to auxins and gravity. *Biochem. Genet.* **18**, 1041-1053 (1980).
200 Bennett, M. J. *et al.* Arabidopsis AUX1 gene: a permease-like regulator of root gravitropism. *Science* **273**, 948-950 (1996).
201 Marchant, A. *et al.* AUX1 regulates root gravitropism in Arabidopsis by facilitating auxin uptake within root apical tissues. *The EMBO journal* **18**, 2066-2073 (1999).
202 Yang, Y., Hammes, U. Z., Taylor, C. G., Schachtman, D. P. & Nielsen, E. High-affinity auxin transport by the AUX1 influx carrier protein. *Curr. Biol.* **16**, 1123-1127 (2006).
203 Young, G., Jack, D., Smith, D. & Saier Jr, M. The amino acid/auxin: proton symport permease family. *Biochimica et Biophysica Acta (BBA)-Biomembranes* **1415**, 306-322 (1999).
204 Swarup, K. *et al.* The auxin influx carrier LAX3 promotes lateral root emergence. *Nat. Cell Biol.* **10**, 946-954 (2008).
205 Péret, B. *et al.* AUX/LAX genes encode a family of auxin influx transporters that perform distinct functions during Arabidopsis development. *The Plant Cell* **24**, 2874-2885 (2012).
206 Blakeslee, J. J. *et al.* Interactions among PIN-FORMED and P-glycoprotein auxin transporters in Arabidopsis. *The Plant Cell* **19**, 131-147 (2007).
207 Kamimoto, Y. *et al.* Arabidopsis ABCB21 is a facultative auxin importer/exporter regulated by cytoplasmic auxin concentration. *Plant and Cell Physiology* **53**, 2090-2100 (2012).
208 Terasaka, K. *et al.* PGP4, an ATP binding cassette P-glycoprotein, catalyzes auxin transport in Arabidopsis thaliana roots. *The Plant Cell* **17**, 2922-2939 (2005).
209 Krouk, G. *et al.* Nitrate-regulated auxin transport by NRT1. 1 defines a mechanism for nutrient sensing in plants. *Dev. Cell* **18**, 927-937 (2010).

210 Hershko, A., Heller, H., Elias, S. & Ciechanover, A. Components of ubiquitin-protein ligase system. Resolution, affinity purification, and role in protein breakdown. *J. Biol. Chem.* **258**, 8206-8214 (1983).
211 Van Nocker, S., Deveraux, Q., Rechsteiner, M. & Vierstra, R. D. Arabidopsis MBP1 gene encodes a conserved ubiquitin recognition component of the 26S proteasome. *Proceedings of the National Academy of Sciences* **93**, 856-860 (1996).
212 Skowyra, D., Craig, K. L., Tyers, M., Elledge, S. J. & Harper, J. W. F-box proteins are receptors that recruit phosphorylated substrates to the SCF ubiquitin-ligase complex. *Cell* **91**, 209-219 (1997).
213 Gray, W. M., Kepinski, S., Rouse, D., Leyser, O. & Estelle, M. Auxin regulates SCFTIR1-dependent degradation of AUX/IAA proteins. *Nature* **414**, 271-276 (2001).
214 Gray, W. M. *et al.* Identification of an SCF ubiquitin–ligase complex required for auxin response in Arabidopsis thaliana. *Genes Dev.* **13**, 1678-1691 (1999).
215 Ruegger, M. *et al.* The TIR1 protein of Arabidopsis functions in auxin response and is related to human SKP2 and yeast grr1p. *Genes Dev.* **12**, 198-207 (1998).
216 Dharmasiri, N., Dharmasiri, S. & Estelle, M. The F-box protein TIR1 is an auxin receptor. *Nature* **435**, 441-445 (2005).
217 Kepinski, S. & Leyser, O. The Arabidopsis F-box protein TIR1 is an auxin receptor. *Nature* **435**, 446-451 (2005).
218 Tan, X. *et al.* Mechanism of auxin perception by the TIR1 ubiquitin ligase. *Nature* **446**, 640-645 (2007).
219 Calderón Villalobos, L. I. A. *et al.* A combinatorial TIR1/AFB–Aux/IAA co-receptor system for differential sensing of auxin. *Nat. Chem. Biol.* **8**, 477-485 (2012).
220 Prigge, M. J. *et al.* Genetic analysis of the Arabidopsis TIR1/AFB auxin receptors reveals both overlapping and specialized functions. *elife* **9**, e54740 (2020).
221 Parry, G. *et al.* Complex regulation of the TIR1/AFB family of auxin receptors. *Proceedings of the National Academy of Sciences* **106**, 22540-22545 (2009).
222 Dharmasiri, N. *et al.* Plant development is regulated by a family of auxin receptor F box proteins. *Dev. Cell* **9**, 109-119 (2005).
223 Jurado, S. *et al.* The Arabidopsis Cell Cycle F-Box Protein SKP2A Binds to Auxin *The Plant Cell* **22**, 3891-3904 (2010).
224 del Pozo, J. C., Diaz-Trivino, S., Cisneros, N. & Gutierrez, C. The balance between cell division and endoreplication depends on E2FC-DPB, transcription factors regulated by the ubiquitin-SCFSKP2A pathway in Arabidopsis. *The Plant Cell* **18**, 2224-2235 (2006).
225 Abel, S., Oeller, P. W. & Theologis, A. Early auxin-induced genes encode short-lived nuclear proteins. *Proceedings of the National Academy of Sciences* **91**, 326-330 (1994).
226 Tiwari, S. B., Wang, X.-J., Hagen, G. & Guilfoyle, T. J. AUX/IAA proteins are active repressors, and their stability and activity are modulated by auxin. *The Plant Cell* **13**, 2809-2822 (2001).
227 Ulmasov, T., Murfett, J., Hagen, G. & Guilfoyle, T. J. Aux/IAA proteins repress expression of reporter genes containing natural and highly active synthetic auxin response elements. *The Plant Cell* **9**, 1963-1971 (1997).
228 Szemenyei, H., Hannon, M. & Long, J. A. TOPLESS mediates auxin-dependent transcriptional repression during Arabidopsis embryogenesis. *Science* **319**, 1384-1386 (2008).
229 Mironova, V. V., Omelyanchuk, N. A., Wiebe, D. S. & Levitsky, V. G. Computational analysis of auxin responsive elements in the Arabidopsis thaliana L. genome. *BMC Genomics* **15**, 1-14 (2014).

230 Liscum, E. & Hangarter, R. P. Light-stimulated apical hook opening in wild-type Arabidopsis thaliana seedlings. *Plant Physiol.* **101**, 567-572 (1993).
231 Remington, D. L., Vision, T. J., Guilfoyle, T. J. & Reed, J. W. Contrasting modes of diversification in the Aux/IAA and ARF gene families. *Plant Physiol.* **135**, 1738-1752 (2004).
232 Rademacher, E. H. *et al.* Different auxin response machineries control distinct cell fates in the early plant embryo. *Dev. Cell* **22**, 211-222 (2012).
233 Kuhn, A. *et al.* Direct ETTIN-auxin interaction controls chromatin states in gynoecium development. *Elife* **9**, e51787 (2020).
234 Simonini, S., Bencivenga, S., Trick, M. & Østergaard, L. Auxin-induced modulation of ETTIN activity orchestrates gene expression in Arabidopsis. *The Plant Cell* **29**, 1864-1882 (2017).
235 Löbler, M. & Klämbt, D. Auxin-binding protein from coleoptile membranes of corn (Zea mays L.). II. Localization of a putative auxin receptor. *J. Biol. Chem.* **260**, 9854-9859 (1985).
236 Jones, A. M. & Herman, E. M. KDEL-Containing Auxin-Binding Protein Is Secreted to the Plasma Membrane and Cell Wall. *Plant Physiol.* **101**, 595-606 (1993).
237 Gao, Y. *et al.* Auxin binding protein 1 (ABP1) is not required for either auxin signaling or Arabidopsis development. *Proceedings of the National Academy of Sciences* **112**, 2275-2280 (2015).
238 Friml, J. *et al.* ABP1–TMK auxin perception for global phosphorylation and auxin canalization. *Nature* **609**, 575-581 (2022).
239 Cao, M. *et al.* TMK1-mediated auxin signalling regulates differential growth of the apical hook. *Nature* **568**, 240-243 (2019).
240 Fendrych, M. *et al.* Rapid and reversible root growth inhibition by TIR1 auxin signalling. *Nature plants* **4**, 453-459 (2018).
241 Ljung, K., Bhalerao, R. P. & Sandberg, G. Sites and homeostatic control of auxin biosynthesis in Arabidopsis during vegetative growth. *The Plant Journal* **28**, 465-474 (2001).
242 Ljung, K. *et al.* Sites and regulation of auxin biosynthesis in Arabidopsis roots. *The Plant Cell* **17**, 1090-1104 (2005).
243 Normanly, J., Cohen, J. D. & Fink, G. R. Arabidopsis thaliana auxotrophs reveal a tryptophan-independent biosynthetic pathway for indole-3-acetic acid. *Proceedings of the National Academy of Sciences* **90**, 10355-10359 (1993).
244 Zhang, R., Wang, B., Ouyang, J., Li, J. & Wang, Y. Arabidopsis indole synthase, a homolog of tryptophan synthase alpha, is an enzyme involved in the trp-independent indole-containing metabolite biosynthesis. *Journal of integrative plant biology* **50**, 1070-1077 (2008).
245 Wang, B. *et al.* Tryptophan-independent auxin biosynthesis contributes to early embryogenesis in Arabidopsis. *Proceedings of the National Academy of Sciences* **112**, 4821-4826 (2015).
246 Nonhebel, H. M. Tryptophan-independent indole-3-acetic acid synthesis: critical evaluation of the evidence. *Plant Physiol.* **169**, 1001-1005 (2015).
247 Won, C. *et al.* Conversion of tryptophan to indole-3-acetic acid by TRYPTOPHAN AMINOTRANSFERASES OF ARABIDOPSIS and YUCCAs in Arabidopsis. *Proceedings of the National Academy of Sciences* **108**, 18518-18523 (2011).
248 Stepanova, A. N. *et al.* The Arabidopsis YUCCA1 Flavin Monooxygenase Functions in the Indole-3-Pyruvic Acid Branch of Auxin Biosynthesis. *The Plant Cell* **23**, 3961-3973 (2011).
249 Mashiguchi, K. *et al.* The main auxin biosynthesis pathway in Arabidopsis. *Proceedings of the National Academy of Sciences* **108**, 18512-18517 (2011).

250 Poulet, A. & Kriechbaumer, V. Bioinformatics analysis of phylogeny and transcription of TAA/YUC auxin biosynthetic genes. *International journal of molecular sciences* **18**, 1791 (2017).
251 Chen, Q. *et al.* Auxin overproduction in shoots cannot rescue auxin deficiencies in Arabidopsis roots. *Plant and Cell Physiology* **55**, 1072-1079 (2014).
252 Stepanova, A. N. *et al.* TAA1-mediated auxin biosynthesis is essential for hormone crosstalk and plant development. *Cell* **133**, 177-191 (2008).
253 Cheng, Y., Dai, X. & Zhao, Y. Auxin synthesized by the YUCCA flavin monooxygenases is essential for embryogenesis and leaf formation in Arabidopsis. *The Plant Cell* **19**, 2430-2439 (2007).
254 Cheng, Y., Dai, X. & Zhao, Y. Auxin biosynthesis by the YUCCA flavin monooxygenases controls the formation of floral organs and vascular tissues in Arabidopsis. *Genes Dev.* **20**, 1790-1799 (2006).
255 Hornitschek, P. *et al.* Phytochrome interacting factors 4 and 5 control seedling growth in changing light conditions by directly controlling auxin signaling. *The Plant Journal* **71**, 699-711 (2012).
256 Li, L. *et al.* Linking photoreceptor excitation to changes in plant architecture. *Genes Dev.* **26**, 785-790 (2012).
257 Hull, A. K., Vij, R. & Celenza, J. L. Arabidopsis cytochrome P450s that catalyze the first step of tryptophan-dependent indole-3-acetic acid biosynthesis. *Proceedings of the National Academy of Sciences* **97**, 2379-2384 (2000).
258 Mikkelsen, M. D., Hansen, C. H., Wittstock, U. & Halkier, B. A. Cytochrome P450 CYP79B2 from Arabidopsis catalyzes the conversion of tryptophan to indole-3-acetaldoxime, a precursor of indole glucosinolates and indole-3-acetic acid. *J. Biol. Chem.* **275**, 33712-33717 (2000).
259 Glawischnig, E., Hansen, B. G., Olsen, C. E. & Halkier, B. A. Camalexin is synthesized from indole-3-acetaldoxime, a key branching point between primary and secondary metabolism in Arabidopsis. *Proceedings of the National Academy of Sciences* **101**, 8245-8250 (2004).
260 Sugawara, S. *et al.* Biochemical analyses of indole-3-acetaldoxime-dependent auxin biosynthesis in Arabidopsis. *Proceedings of the National Academy of Sciences* **106**, 5430-5435 (2009).
261 Zhao, Y. *et al.* Trp-dependent auxin biosynthesis in Arabidopsis: involvement of cytochrome P450s CYP79B2 and CYP79B3. *Genes Dev.* **16**, 3100-3112 (2002).
262 Nafisi, M. *et al.* Arabidopsis Cytochrome P450 Monooxygenase 71A13 Catalyzes the Conversion of Indole-3-Acetaldoxime in Camalexin Synthesis. *The Plant Cell* **19**, 2039-2052 (2007).
263 Normanly, J., Grisafi, P., Fink, G. R. & Bartel, B. Arabidopsis mutants resistant to the auxin effects of indole-3-acetonitrile are defective in the nitrilase encoded by the NIT1 gene. *The Plant Cell* **9**, 1781-1790 (1997).
264 Lehmann, T. *et al.* Arabidopsis NITRILASE 1 contributes to the regulation of root growth and development through modulation of auxin biosynthesis in seedlings. *Frontiers in Plant Science* **8**, 36 (2017).
265 Doskočilová, A. *et al.* NITRILASE 1 regulates the exit from proliferation, genome stability and plant development. *New Phytol.* **198**, 685-698 (2013).
266 Novák, O. *et al.* Tissue-specific profiling of the Arabidopsis thaliana auxin metabolome. *The Plant Journal* **72**, 523-536 (2012).
267 Gao, Y. *et al.* Two homologous INDOLE-3-ACETAMIDE (IAM) HYDROLASE genes are required for the auxin effects of IAM in Arabidopsis. *Journal of genetics and genomics* **47**, 157-165 (2020).

268 Zolman, B. K., Martinez, N., Millius, A., Adham, A. R. & Bartel, B. Identification and characterization of Arabidopsis indole-3-butyric acid response mutants defective in novel peroxisomal enzymes. *Genetics* **180**, 237-251 (2008).
269 Zolman, B. K., Yoder, A. & Bartel, B. Genetic analysis of indole-3-butyric acid responses in Arabidopsis thaliana reveals four mutant classes. *Genetics* **156**, 1323-1337 (2000).
270 Staswick, P. E. *et al.* Characterization of an Arabidopsis Enzyme Family That Conjugates Amino Acids to Indole-3-Acetic Acid. *The Plant Cell* **17**, 616-627 (2005).
271 Di Mambro, R. *et al.* The lateral root cap acts as an auxin sink that controls meristem size. *Curr. Biol.* **29**, 1199-1205 (2019).
272 Ludwig-Müller, J., Jülke, S., Bierfreund, N. M., Decker, E. L. & Reski, R. Moss (Physcomitrella patens) GH3 proteins act in auxin homeostasis. *New Phytol.* **181**, 323-338 (2009).
273 Brunoni, F. *et al.* Conifers exhibit a characteristic inactivation of auxin to maintain tissue homeostasis. *New Phytol.* **226**, 1753-1765 (2020).
274 Zheng, Z. *et al.* Local auxin metabolism regulates environment-induced hypocotyl elongation. *Nature plants* **2**, 1-9 (2016).
275 Di Mambro, R. *et al.* Auxin minimum triggers the developmental switch from cell division to cell differentiation in the Arabidopsis root. *Proceedings of the National Academy of Sciences* **114**, E7641-E7649 (2017).
276 Östin, A., Kowalyczk, M., Bhalerao, R. P. & Sandberg, G. r. Metabolism of Indole-3-Acetic Acid in Arabidopsis. *Plant Physiol.* **118**, 285-296 (1998).
277 Kowalczyk, M. & Sandberg, G. Quantitative analysis of indole-3-acetic acid metabolites in Arabidopsis. *Plant Physiol.* **127**, 1845-1853 (2001).
278 Sugahara, K., Kitao, K., Yamagaki, T. & Koyama, T. Practical optimization of liquid chromatography/mass spectrometry conditions and pretreatment methods toward the sensitive quantification of auxin in plants. *Rapid Commun. Mass Spectrom.* **34**, e8625 (2020).
279 Bartel, B. & Fink, G. R. ILR1, an amidohydrolase that releases active indole-3-acetic acid from conjugates. *Science* **268**, 1745-1748 (1995).
280 Davies, R. T., Goetz, D. H., Lasswell, J., Anderson, M. N. & Bartel, B. IAR3 encodes an auxin conjugate hydrolase from Arabidopsis. *The Plant Cell* **11**, 365-376 (1999).
281 LeClere, S., Tellez, R., Rampey, R. A., Matsuda, S. P. & Bartel, B. Characterization of a family of IAA-amino acid conjugate hydrolases from Arabidopsis. *J. Biol. Chem.* **277**, 20446-20452 (2002).
282 Sanchez Carranza, A. P. *et al.* Hydrolases of the ILR1-like family of Arabidopsis thaliana modulate auxin response by regulating auxin homeostasis in the endoplasmic reticulum. *Scientific Reports* **6**, 1-11 (2016).
283 Paponov, I. A. *et al.* Comprehensive transcriptome analysis of auxin responses in Arabidopsis. *Molecular Plant* **1**, 321-337 (2008).
284 Bialek, K. & Cohen, J. D. Amide-Linked Indoleacetic Acid Conjugates May Control Levels of Indoleacetic Acid in Germinating Seedlings of Phaseolus vulgaris. *Plant Physiol.* **100**, 2002-2007 (1992).
285 Bialek, K. & Cohen, J. D. Free and conjugated indole-3-acetic acid in developing bean seeds. *Plant Physiol.* **91**, 775-779 (1989).
286 Walz, A. *et al.* A gene encoding a protein modified by the phytohormone indoleacetic acid. *Proceedings of the National Academy of Sciences* **99**, 1718-1723 (2002).
287 Rampey, R. A. *et al.* A Family of Auxin-Conjugate Hydrolases That Contributes to Free Indole-3-Acetic Acid Levels during Arabidopsis Germination. *Plant Physiol.* **135**, 978-988 (2004).

288 Jackson, R. G. *et al.* Over-expression of an Arabidopsis gene encoding a glucosyltransferase of indole-3-acetic acid: phenotypic characterisation of transgenic lines. *The Plant Journal* **32**, 573-583 (2002).
289 Jin, S.-H. *et al.* UGT74D1 is a novel auxin glycosyltransferase from Arabidopsis thaliana. *PLoS One* **8**, e61705 (2013).
290 Mateo-Bonmatí, E., Casanova-Sáez, R., Šimura, J. & Ljung, K. Broadening the roles of UDP-glycosyltransferases in auxin homeostasis and plant development. *New Phytol.* **232**, 642-654 (2021).
291 Aoi, Y. *et al.* UDP-glucosyltransferase UGT84B1 regulates the levels of indole-3-acetic acid and phenylacetic acid in Arabidopsis. *Biochem. Biophys. Res. Commun.* **532**, 244-250 (2020).
292 Jackson, R. G. *et al.* Identification and biochemical characterization of an Arabidopsis indole-3-acetic acid glucosyltransferase. *J. Biol. Chem.* **276**, 4350-4356 (2001).
293 Chen, L. *et al.* IPyA glucosylation mediates light and temperature signaling to regulate auxin-dependent hypocotyl elongation in Arabidopsis. *Proceedings of the National Academy of Sciences* **117**, 6910-6917 (2020).
294 Ishimaru, K. *et al.* Loss of function of the IAA-glucose hydrolase gene TGW6 enhances rice grain weight and increases yield. *Nat. Genet.* **45**, 707-711 (2013).
295 Jakubowska, A. & Kowalczyk, S. A specific enzyme hydrolyzing 6-O (4-O)-indole-3-ylacetyl-β-d-glucose in immature kernels of Zea mays. *J. Plant Physiol.* **162**, 207-213 (2005).
296 Casanova-Sáez, R., Mateo-Bonmatí, E. & Ljung, K. Auxin metabolism in plants. *Cold Spring Harbor Perspectives in Biology* **13**, a039867 (2021).
297 Tanaka, K. *et al.* UGT74D1 catalyzes the glucosylation of 2-oxindole-3-acetic acid in the auxin metabolic pathway in Arabidopsis. *Plant and Cell Physiology* **55**, 218-228 (2014).
298 Nicholls, P. The isolation of indole-3-acetyl-2-O-myo-inositol from Zea mays. *Planta* **72**, 258-264 (1966).
299 Chisnell, J. R. Myo-inositol esters of indole-3-acetic acid are endogenous components of Zea mays L. shoot tissue. *Plant Physiol.* **74**, 278-283 (1984).
300 Luo, Y. *et al.* D-myo-inositol-3-phosphate affects phosphatidylinositol-mediated endomembrane function in Arabidopsis and is essential for auxin-regulated embryogenesis. *The Plant Cell* **23**, 1352-1372 (2011).
301 Qin, G. *et al.* An Indole-3-Acetic Acid Carboxyl Methyltransferase Regulates Arabidopsis Leaf Development. *The Plant Cell* **17**, 2693-2704 (2005).
302 Yang, Y. *et al.* Inactive Methyl Indole-3-Acetic Acid Ester Can Be Hydrolyzed and Activated by Several Esterases Belonging to the AtMES Esterase Family of Arabidopsis *Plant Physiol.* **147**, 1034-1045 (2008).
303 Abbas, M. *et al.* Auxin methylation is required for differential growth in Arabidopsis. *Proceedings of the National Academy of Sciences* **115**, 6864-6869 (2018).
304 Mellor, N. *et al.* Dynamic regulation of auxin oxidase and conjugating enzymes AtDAO1 and GH3 modulates auxin homeostasis. *Proceedings of the National Academy of Sciences* **113**, 11022-11027 (2016).
305 Zhao, Z. *et al.* A role for a dioxygenase in auxin metabolism and reproductive development in rice. *Dev. Cell* **27**, 113-122 (2013).
306 Zhang, J. *et al.* DAO1 catalyzes temporal and tissue-specific oxidative inactivation of auxin in Arabidopsis thaliana. *Proceedings of the National Academy of Sciences* **113**, 11010-11015 (2016).

307 Suzuki, M. *et al.* Transcriptional feedback regulation of YUCCA genes in response to auxin levels in Arabidopsis. *Plant Cell Rep.* **34**, 1343-1352 (2015).
308 Takato, S. *et al.* Auxin signaling through SCFTIR1/AFBs mediates feedback regulation of IAA biosynthesis. *Biosci., Biotechnol., Biochem.* **81**, 1320-1326 (2017).
309 Porco, S. *et al.* Dioxygenase-encoding AtDAO1 gene controls IAA oxidation and homeostasis in Arabidopsis. *Proceedings of the National Academy of Sciences* **113**, 11016-11021 (2016).
310 Spiess, G. M. *et al.* Auxin input pathway disruptions are mitigated by changes in auxin biosynthetic gene expression in Arabidopsis. *Plant Physiol.* **165**, 1092-1104 (2014).
311 Vieten, A. *et al.* Functional redundancy of PIN proteins is accompanied by auxin-dependent cross-regulation of PIN expression. *Development* **132**, 4521-4531 (2005).
312 Sauer, M. *et al.* Canalization of auxin flow by Aux/IAA-ARF-dependent feedback regulation of PIN polarity. *Genes Dev.* **20**, 2902-2911 (2006).
313 Sachs, T. The induction of transport channels by auxin. *Planta* **127**, 201-206 (1975).
314 Sachs, T. Cell polarity and tissue patterning in plants. *Development* **113**, 83-93 (1991).
315 Sachs, T. The control of the patterned differentiation of vascular tissues. *Adv. Bot. Res.* **9**, 151-262 (1981).
316 Mazur, E., Kulik, I., Hajný, J. & Friml, J. Auxin canalization and vascular tissue formation by TIR1/AFB-mediated auxin signaling in Arabidopsis. *New Phytol.* **226**, 1375-1383 (2020).
317 Prát, T. *et al.* WRKY23 is a component of the transcriptional network mediating auxin feedback on PIN polarity. *PLoS Genet.* **14**, e1007177 (2018).
318 Hajný, J. *et al.* Receptor kinase module targets PIN-dependent auxin transport during canalization. *Science* **370**, 550-557 (2020).
319 Mazur, E. *et al.* Clathrin-mediated trafficking and PIN trafficking are required for auxin canalization and vascular tissue formation in Arabidopsis. *Plant Sci.* **293**, 110414 (2020).
320 Skoog, F. Relationships between zinc and auxin in the growth of higher plants. *Am. J. Bot.*, 939-951 (1940).
321 Zeng, H., Zhang, X., Ding, M., Zhang, X. & Zhu, Y. Transcriptome profiles of soybean leaves and roots in response to zinc deficiency. *Physiol. Plant.* **167**, 330-351 (2019).
322 Mallikarjuna, M. G. *et al.* Comparative transcriptome analysis of iron and zinc deficiency in maize (Zea mays L.). *Plants* **9**, 1812 (2020).
323 Horak, V. & Trčka, I. The influence of Zn 2+ ions on the tryptophan biosynthesis in plants. *Biol. Plant.* **18**, 393-396 (1976).
324 Zhang, P. *et al.* cGMP is involved in Zn tolerance through the modulation of auxin redistribution in root tips. *Environ. Exp. Bot.* **147**, 22-30 (2018).
325 Wang, J. & Yang, S. Dose-dependent responses of Arabidopsis thaliana to zinc are mediated by auxin homeostasis and transport. *Environ. Exp. Bot.* **189**, 104554 (2021).
326 Powell, M., Davies, M. & Francis, D. Effects of Zinc on Meristem Size and Proximity of Root Hairs and Xylem Elements to the Root Tip in a Zinc-tolerant and a Non-tolerant Cultivar of Festuca rubra L. *Ann. Bot.* **61**, 723-726 (1988).

327 Sofo, A. *et al.* Plant architecture, auxin homeostasis and phenol content in Arabidopsis thaliana grown in cadmium-and zinc-enriched media. *J. Plant Physiol.* **216**, 174-180 (2017).
328 Lasswell, J., Rogg, L. E., Nelson, D. C., Rongey, C. & Bartel, B. Cloning and characterization of IAR1, a gene required for auxin conjugate sensitivity in Arabidopsis. *The Plant Cell* **12**, 2395-2408 (2000).
329 Magidin, M., Pittman, J. K., Hirschi, K. D. & Bartel, B. ILR2, a novel gene regulating IAA conjugate sensitivity and metal transport in Arabidopsis thaliana. *The Plant Journal* **35**, 523-534 (2003).
330 Kamitani, M., Okuno, T. & Kudoh, H. Complete genome sequence of a novel partitivirus from a wild brassicaceous plant, Arabidopsis halleri. *Archives of Virology* **165**, 2091-2094 (2020).
331 Nibert, M. L. *et al.* Taxonomic reorganization of family Partitiviridae and other recent progress in partitivirus research. *Virus Res.* **188**, 128-141 (2014).
332 Rampey, R. A. *et al.* An Arabidopsis basic helix-loop-helix leucine zipper protein modulates metal homeostasis and auxin conjugate responsiveness. *Genetics* **174**, 1841-1857 (2006).
333 Celenza, j. J., Grisafi, P. L. & Fink, G. R. A pathway for lateral root formation in Arabidopsis thaliana. *Genes Dev.* **9**, 2131-2142 (1995).
334 Boerjan, W. *et al.* Superroot, a recessive mutation in Arabidopsis, confers auxin overproduction. *The Plant Cell* **7**, 1405-1419 (1995).
335 Huang, L., Kirschke, C. P., Zhang, Y. & Yu, Y. Y. The ZIP7 gene (Slc39a7) encodes a zinc transporter involved in zinc homeostasis of the Golgi apparatus. *J. Biol. Chem.* **280**, 15456-15463 (2005).
336 Kumánovics, A., Poruk, K. E., Osborn, K. A., Ward, D. M. & Kaplan, J. YKE4 (YIL023C) encodes a bidirectional zinc transporter in the endoplasmic reticulum of Saccharomyces cerevisiae. *J. Biol. Chem.* **281**, 22566-22574 (2006).
337 Podar, D. *et al.* Metal selectivity determinants in a family of transition metal transporters. *J. Biol. Chem.* **287**, 3185-3196 (2012).
338 Evens, N. P., Buchner, P., Williams, L. E. & Hawkesford, M. J. The role of ZIP transporters and group F bZIP transcription factors in the Zn-deficiency response of wheat (Triticum aestivum). *The Plant Journal* **92**, 291-304 (2017).
339 Almagro Armenteros, J. J. *et al.* SignalP 5.0 improves signal peptide predictions using deep neural networks. *Nat. Biotechnol.* **37**, 420-423 (2019).
340 Gietz, R. D. & Woods, R. A. in *Methods Enzymol.* Vol. 350 87-96 (Elsevier, 2002).
341 Alonso, J. M. *et al.* Genome-wide insertional mutagenesis of Arabidopsis thaliana. *Science* **301**, 653-657 (2003).
342 Doyle, J. J. & Doyle, J. L. A rapid DNA isolation procedure for small quantities of fresh leaf tissue. *Phytochemical bulletin* **19**, 11-15 (1987).
343 Engler, C. *et al.* A golden gate modular cloning toolbox for plants. *ACS synthetic biology* **3**, 839-843 (2014).
344 Zhang, X., Henriques, R., Lin, S.-S., Niu, Q.-W. & Chua, N.-H. Agrobacterium-mediated transformation of Arabidopsis thaliana using the floral dip method. *Nature protocols* **1**, 641 (2006).
345 Hoagland, D. R. & Arnon, D. I. The water-culture method for growing plants without soil. *California agricultural experiment station* **347** (1950).
346 Porra, R., Thompson, W. & Kriedemann, P. Determination of accurate extinction coefficients and simultaneous equations for assaying chlorophylls a and b extracted with four different solvents: verification of the concentration of chlorophyll standards by atomic absorption spectroscopy. *Biochimica et Biophysica Acta (BBA)-Bioenergetics* **975**, 384-394 (1989).

347 Henriquez-Valencia, C. *et al.* bZIP17 and bZIP60 regulate the expression of BiP3 and other salt stress responsive genes in an UPR-independent manner in Arabidopsis thaliana. *J. Cell. Biochem.* **116**, 1638-1645 (2015).
348 Cho, Y. & Kanehara, K. Endoplasmic reticulum stress response in Arabidopsis roots. *Frontiers in plant science* **8**, 144 (2017).
349 Livak, K. J. & Schmittgen, T. D. Analysis of relative gene expression data using real-time quantitative PCR and the 2− ΔΔCT method. *Methods* **25**, 402-408 (2001).
350 Perilli, S. & Sabatini, S. Analysis of Root Meristem Size Development. *Methods in Molecular Biology* **655**, 177-187 (2010).
351 Boratyn, G. M. *et al.* BLAST: a more efficient report with usability improvements. *Nucleic Acids Res.* **41**, W29-W33 (2013).
352 Kumar, S., Stecher, G., Li, M., Knyaz, C. & Tamura, K. MEGA X: molecular evolutionary genetics analysis across computing platforms. *Mol. Biol. Evol.* **35**, 1547-1549 (2018).
353 Edgar, R. C. MUSCLE: multiple sequence alignment with high accuracy and high throughput. *Nucleic Acids Res.* **32**, 1792-1797 (2004).
354 Jones, D. T., Taylor, W. R. & Thornton, J. M. The rapid generation of mutation data matrices from protein sequences. *Bioinformatics* **8**, 275-282 (1992).
355 Jumper, J. *et al.* Highly accurate protein structure prediction with AlphaFold. *Nature* **596**, 583-589 (2021).
356 Zhang, T. *et al.* Crystal structures of a ZIP zinc transporter reveal a binuclear metal center in the transport pathway. *Science advances* **3**, e1700344 (2017).
357 Hawkins, J. & Bodén, M. Detecting and sorting targeting peptides with neural networks and support vector machines. *J. Bioinf. Comput. Biol.* **4**, 1-18 (2006).
358 Armenteros, J. J. A. *et al.* Detecting sequence signals in targeting peptides using deep learning. *Life science alliance* **2** (2019).
359 Thumuluri, V., Almagro Armenteros, J. J., Johansen, A. R., Nielsen, H. & Winther, O. DeepLoc 2.0: multi-label subcellular localization prediction using protein language models. *Nucleic Acids Res.* (2022).
360 Lamesch, P. *et al.* The Arabidopsis Information Resource (TAIR): improved gene annotation and new tools. *Nucleic Acids Res.* **40**, 1202-1210 (2012).
361 Lescot, M. *et al.* PlantCARE, a database of plant cis-acting regulatory elements and a portal to tools for in silico analysis of promoter sequences. *Nucleic Acids Res.* **30**, 325-327 (2002).
362 Hu, B. *et al.* GSDS 2.0: an upgraded gene feature visualization server. *Bioinformatics* **31**, 1296-1297 (2015).
363 Bailey, T. L., Johnson, J., Grant, C. E. & Noble, W. S. The MEME suite. *Nucleic Acids Res.* **43**, W39-W49 (2015).
364 Jobe, T. O. *et al.* Feedback inhibition by thiols outranks glutathione depletion: a luciferase-based screen reveals glutathione-deficient γ-ECS and glutathione synthetase mutants impaired in cadmium-induced sulfate assimilation. *The Plant Journal* **70**, 783-795 (2012).
365 Aflalo, C. Biologically localized firefly luciferase: a tool to study cellular processes. *Int. Rev. Cytol.* **130**, 269-323 (1991).
366 Tukey, J. W. Comparing individual means in the analysis of variance. *Biometrics*, 99-114 (1949).
367 Csiszár, J., Szabó, M., Tari, I. & Erdei, L. Control of the glutathione S-transferase and mas1' promoter-driven GUS activity in auxin heterotrophic and autotrophic tobacco calli by exogenous 2, 4-d-induced ethylene. *Physiol. Plant.* **113**, 100-107 (2001).

368 Farinati, S., DalCorso, G., Varotto, S. & Furini, A. The Brassica juncea BjCdR15, an ortholog of Arabidopsis TGA3, is a regulator of cadmium uptake, transport and accumulation in shoots and confers cadmium tolerance in transgenic plants. *New Phytol.* **185**, 964-978 (2010).
369 Wang, Z. *et al.* Natural variations of growth thermo-responsiveness determined by SAUR 26/27/28 proteins in Arabidopsis thaliana. *New Phytol.* **224**, 291-305 (2019).
370 Medina, E. A. *et al.* Examination of the M20D Auxin Conjugate Peptidase Family from Hornwort and Implications on the Evolution of the Tracheophytes. *J. Plant Growth Regul.*, 1-12 (2021).
371 Taylor, K. M., Morgan, H. E., Johnson, A. & Nicholson, R. I. Structure-function analysis of HKE4, a member of the new LIV-1 subfamily of zinc transporters. *Biochemical Journal* **377**, 131-139 (2004).
372 Xiao, G., Zhao, M., Liu, Z., Du, F. & Zhou, B. Zinc antagonizes iron-regulation of tyrosine hydroxylase activity and dopamine production in Drosophila melanogaster. *BMC Biol.* **19**, 1-16 (2021).
373 Hu, J. Towards unzipping the ZIP metal transporters: structure, evolution, and implications on drug discovery against cancer. *The FEBS Journal* (2020).
374 Matsuura, W. *et al.* SLC39A9 (ZIP9) regulates zinc homeostasis in the secretory pathway: characterization of the ZIP subfamily I protein in vertebrate cells. *Biosci., Biotechnol., Biochem.* **73**, 1142-1148 (2009).
375 Jeong, J. & Eide, D. J. The SLC39 family of zinc transporters. *Molecular aspects of medicine* **34**, 612-619 (2013).
376 Ram, A. F., Wolters, A., Hoopen, R. T. & Klis, F. M. A new approach for isolating cell wall mutants in Saccharomyces cerevisiae by screening for hypersensitivity to calcofluor white. *Yeast* **10**, 1019-1030 (1994).
377 Woodruff, G. *et al.* The zinc transporter SLC39A7 (ZIP7) is essential for regulation of cytosolic zinc levels. *Mol. Pharmacol.* **94**, 1092-1100 (2018).
378 Lopez-Millan, A.-F., Ellis, D. R. & Grusak, M. A. Identification and characterization of several new members of the ZIP family of metal ion transporters in Medicago truncatula. *Plant Mol. Biol.* **54**, 583-596 (2004).
379 Fu, X.-Z. *et al.* Genome-wide identification, cloning and functional analysis of the zinc/iron-regulated transporter-like protein (ZIP) gene family in trifoliate orange (Poncirus trifoliata L. Raf.). *Frontiers in Plant Science* **8**, 588 (2017).
380 Misteli, T. & Spector, D. L. Applications of the green fluorescent protein in cell biology and biotechnology. *Nat. Biotechnol.* **15**, 961-964 (1997).
381 Emanuelsson, O., Nielsen, H., Brunak, S. & Von Heijne, G. Predicting subcellular localization of proteins based on their N-terminal amino acid sequence. *J. Mol. Biol.* **300**, 1005-1016 (2000).
382 Zhu, J. *et al.* Annexin5 plays a vital role in Arabidopsis pollen development via Ca2+-dependent membrane trafficking. *PloS one* **9**, e102407 (2014).
383 Jefferson, R. A., Kavanagh, T. A. & Bevan, M. W. GUS fusions: beta-glucuronidase as a sensitive and versatile gene fusion marker in higher plants. *The EMBO journal* **6**, 3901-3907 (1987).
384 Stoeber, F. Étude des propriétés et de la biosynthèse de la glucuronidase et de la glucuronide-perméase chez" Escherichia coli.". *Theses de Docteur es Sciences, University of Paris, Paris, France* (1961).
385 Wiuf, A. *et al.* The two-domain elevator-type mechanism of zinc-transporting ZIP proteins. *Science Advances* **8**, eabn4331 (2022).

386 Benghezal, M., Wasteneys, G. O. & Jones, D. A. The C-terminal dilysine motif confers endoplasmic reticulum localization to type I membrane proteins in plants. *The Plant Cell* **12**, 1179-1201 (2000).
387 Liang, Z., Veeraprame, H., Bayan, N. & Li, G. The C-terminus of prenylin is important in forming a dimer conformation necessary for endoplasmic-reticulum-to-Golgi transport. *Biochemical Journal* **380**, 43-49 (2004).
388 Nishiyama, R., Kato, M., Nagata, S., Yanagisawa, S. & Yoneyama, T. Identification of Zn–Nicotianamine and Fe–2′-Deoxymugineic Acid in the Phloem Sap from Rice Plants (Oryza sativa L.). *Plant and Cell Physiology* **53**, 381-390 (2012).
389 Kobae, Y. *et al.* Zinc transporter of Arabidopsis thaliana AtMTP1 is localized to vacuolar membranes and implicated in zinc homeostasis. *Plant and Cell Physiology* **45**, 1749-1758 (2004).
390 Spiller, S. C., Castelfranco, A. M. & Castelfranco, P. A. Effects of iron and oxygen on chlorophyll biosynthesis: I. In vivo observations on iron and oxygen-deficient plants. *Plant Physiol.* **69**, 107-111 (1982).
391 Tottey, S. *et al.* Arabidopsis CHL27, located in both envelope and thylakoid membranes, is required for the synthesis of protochlorophyllide. *Proceedings of the National Academy of Sciences* **100**, 16119-16124 (2003).
392 Kawachi, M. *et al.* A mutant strain Arabidopsis thaliana that lacks vacuolar membrane zinc transporter MTP1 revealed the latent tolerance to excessive zinc. *Plant and Cell Physiology* **50**, 1156-1170 (2009).
393 Morl, K., Ma, W., Gething, M.-J. & Sambrook, J. A transmembrane protein with a cdc2+ CDC28-related kinase activity is required for signaling from the ER to the nucleus. *Cell* **74**, 743-756 (1993).
394 Tirasophon, W., Welihinda, A. A. & Kaufman, R. J. A stress response pathway from the endoplasmic reticulum to the nucleus requires a novel bifunctional protein kinase/endoribonuclease (Ire1p) in mammalian cells. *Genes Dev.* **12**, 1812-1824 (1998).
395 Wang, X.-Z. *et al.* Cloning of mammalian Ire1 reveals diversity in the ER stress responses. *The EMBO journal* **17**, 5708-5717 (1998).
396 Zhang, L., Zhang, C. & Wang, A. Divergence and conservation of the major UPR branch IRE1-bZIP signaling pathway across eukaryotes. *Scientific reports* **6**, 1-14 (2016).
397 Koizumi, N. *et al.* Molecular Characterization of Two Arabidopsis Ire1 Homologs, Endoplasmic Reticulum-Located Transmembrane Protein Kinases. *Plant Physiol.* **127**, 949-962 (2001).
398 Zhang, L., Chen, H., Brandizzi, F., Verchot, J. & Wang, A. The UPR branch IRE1-bZIP60 in plants plays an essential role in viral infection and is complementary to the only UPR pathway in yeast. *PLoS Genet.* **11**, e1005164 (2015).
399 Deng, Y. *et al.* Heat induces the splicing by IRE1 of a mRNA encoding a transcription factor involved in the unfolded protein response in Arabidopsis. *Proceedings of the National Academy of Sciences* **108**, 7247-7252 (2011).
400 Nagashima, Y. *et al.* Arabidopsis IRE1 catalyses unconventional splicing of bZIP60 mRNA to produce the active transcription factor. *Scientific reports* **1**, 1-10 (2011).
401 Liu, J.-X., Srivastava, R., Che, P. & Howell, S. H. An endoplasmic reticulum stress response in Arabidopsis is mediated by proteolytic processing and nuclear relocation of a membrane-associated transcription factor, bZIP28. *The Plant Cell* **19**, 4111-4119 (2007).
402 Gao, H., Brandizzi, F., Benning, C. & Larkin, R. M. A membrane-tethered transcription factor defines a branch of the heat stress response in Arabidopsis

thaliana. *Proceedings of the National Academy of Sciences* **105**, 16398-16403 (2008).

403 Srivastava, R., Chen, Y., Deng, Y., Brandizzi, F. & Howell, S. H. Elements proximal to and within the transmembrane domain mediate the organelle-to-organelle movement of bZIP28 under ER stress conditions. *The Plant Journal* **70**, 1033-1042 (2012).

404 Liu, J. X., Srivastava, R., Che, P. & Howell, S. H. Salt stress responses in Arabidopsis utilize a signal transduction pathway related to endoplasmic reticulum stress signaling. *The Plant Journal* **51**, 897-909 (2007).

405 Shen, J., Chen, X., Hendershot, L. & Prywes, R. ER stress regulation of ATF6 localization by dissociation of BiP/GRP78 binding and unmasking of Golgi localization signals. *Dev. Cell* **3**, 99-111 (2002).

406 Schindler, A. J. & Schekman, R. In vitro reconstitution of ER-stress induced ATF6 transport in COPII vesicles. *Proceedings of the National Academy of Sciences* **106**, 17775-17780 (2009).

407 Tajima, H. & Koizumi, N. Induction of BiP by sugar independent of a cis-element for the unfolded protein response in Arabidopsis thaliana. *Biochem. Biophys. Res. Commun.* **346**, 926-930 (2006).

408 Martínez, I. M. & Chrispeels, M. J. Genomic analysis of the unfolded protein response in Arabidopsis shows its connection to important cellular processes. *The Plant Cell* **15**, 561-576 (2003).

409 Kamauchi, S., Nakatani, H., Nakano, C. & Urade, R. Gene expression in response to endoplasmic reticulum stress in Arabidopsis thaliana. *The FEBS journal* **272**, 3461-3476 (2005).

410 Blond-Elguindi, S. *et al.* Affinity panning of a library of peptides displayed on bacteriophages reveals the binding specificity of BiP. *Cell* **75**, 717-728 (1993).

411 Noh, S.-J., Kwon, C. S., Oh, D.-H., Moon, J. S. & Chung, W.-I. Expression of an evolutionarily distinct novel BiP gene during the unfolded protein response in Arabidopsis thaliana. *Gene* **311**, 81-91 (2003).

412 Ellis , C. D. *et al.* Zinc and the Msc2 zinc transporter protein are required for endoplasmic reticulum function. *J. Cell Biol.* **166**, 325-335 (2004).

413 Ohashi, W. *et al.* Zinc transporter SLC39A7/ZIP7 promotes intestinal epithelial self-renewal by resolving ER stress. *PLoS Genet.* **12** (2016).

414 Sarret, G. *et al.* Trichomes of tobacco excrete zinc as zinc-substituted calcium carbonate and other zinc-containing compounds. *Plant Physiol.* **141**, 1021-1034 (2006).

415 Qin, Y., Dittmer, P. J., Park, J. G., Jansen, K. B. & Palmer, A. E. Measuring steady-state and dynamic endoplasmic reticulum and Golgi Zn2+ with genetically encoded sensors. *Proceedings of the National Academy of Sciences* **108**, 7351-7356 (2011).

416 Vinkenborg, J. L. *et al.* Genetically encoded FRET sensors to monitor intracellular Zn 2+ homeostasis. *Nat. Methods* **6**, 737 (2009).

417 Hessels, A. M. *et al.* eZinCh-2: a versatile, genetically encoded FRET sensor for cytosolic and intraorganelle Zn2+ imaging. *ACS chemical biology* **10**, 2126-2134 (2015).

418 Carter, K. P., Carpenter, M. C., Fiedler, B., Jimenez, R. & Palmer, A. E. Critical comparison of FRET-sensor functionality in the cytosol and endoplasmic reticulum and implications for quantification of ions. *Anal. Chem.* **89**, 9601-9608 (2017).

419 Park, J. G., Qin, Y., Galati, D. F. & Palmer, A. E. New sensors for quantitative measurement of mitochondrial Zn2+. *ACS chemical biology* **7**, 1636-1640 (2012).

420 Hwang, C., Sinskey, A. J. & Lodish, H. F. Oxidized redox state of glutathione in the endoplasmic reticulum. *Science* **257**, 1496-1502 (1992).
421 Liu, R. *et al.* Organelle-Level Labile Zn2+ Mapping Based on Targetable Fluorescent Sensors. *ACS Sensors* (2022).
422 Chabosseau, P. *et al.* Mitochondrial and ER-targeted eCALWY probes reveal high levels of free Zn2+. *ACS chemical biology* **9**, 2111-2120 (2014).
423 Kim, Y. Y. *et al.* AtHMA1 contributes to the detoxification of excess Zn (II) in Arabidopsis. *The Plant Journal* **58**, 737-753 (2009).
424 Gustin, J. L. *et al.* MTP1-dependent Zn sequestration into shoot vacuoles suggests dual roles in Zn tolerance and accumulation in Zn-hyperaccumulating plants. *The Plant Journal* **57**, 1116-1127 (2009).
425 Talke, I. N., Hanikenne, M. & Krämer, U. Zinc-dependent global transcriptional control, transcriptional deregulation, and higher gene copy number for genes in metal homeostasis of the hyperaccumulator Arabidopsis halleri. *Plant Physiol.* **142**, 148-167 (2006).
426 Wu, J. *et al.* Identification and functional analysis of two ZIP metal transporters of the hyperaccumulator Thlaspi caerulescens. *Plant Soil* **325**, 79 (2009). https://doi.org:10.1007/s11104-009-0151-6
427 Khan, M. A. *et al.* Changes in iron availability in Arabidopsis are rapidly sensed in the leaf vasculature and impaired sensing leads to opposite transcriptional programs in leaves and roots. *Plant, Cell Environ.* **41**, 2263-2276 (2018).
428 Sivitz, A. B., Hermand, V., Curie, C. & Vert, G. Arabidopsis bHLH100 and bHLH101 control iron homeostasis via a FIT-independent pathway. *PLoS ONE* **7**, e44843 (2012).
429 Ugartechea-Chirino, Y. *et al.* The AUX1 LAX family of auxin influx carriers is required for the establishment of embryonic root cell organization in Arabidopsis thaliana. *Ann. Bot.* **105**, 277-289 (2009).
430 Yang, H. & Murphy, A. S. Functional expression and characterization of Arabidopsis ABCB, AUX 1 and PIN auxin transporters in Schizosaccharomyces pombe. *The Plant Journal* **59**, 179-191 (2009).
431 Dolan, L. *et al.* Cellular organisation of the Arabidopsis thaliana root. *Development* **119**, 71-84 (1993).
432 Van Den Berg, C., Willemsen, V., Hendriks, G., Weisbeek, P. & Scheres, B. Short-range control of cell differentiation in the Arabidopsis root meristem. *Nature* **390**, 287-289 (1997).
433 Scheres, B. *et al.* Embryonic origin of the Arabidopsis primary root and root meristem initials. *Development* **120**, 2475-2487 (1994).
434 Beemster, G. T. S. & Baskin, T. I. Analysis of Cell Division and Elongation Underlying the Developmental Acceleration of Root Growth in Arabidopsis thaliana. *Plant Physiol.* **116**, 1515-1526 (1998).
435 Brumos, J. *et al.* Local auxin biosynthesis is a key regulator of plant development. *Dev. Cell* **47**, 306-318 (2018).
436 Laxmi, A., Pan, J., Morsy, M. & Chen, R. Light plays an essential role in intracellular distribution of auxin efflux carrier PIN2 in Arabidopsis thaliana. *PloS ONE* **3**, e1510 (2008).
437 Kleine-Vehn, J. *et al.* Gravity-induced PIN transcytosis for polarization of auxin fluxes in gravity-sensing root cells. *Proceedings of the National Academy of Sciences* **107**, 22344-22349 (2010).
438 Band, L. R. *et al.* Systems Analysis of Auxin Transport in the Arabidopsis Root Apex *The Plant Cell* **26**, 862-875 (2014).

439 Barbez, E., Dünser, K., Gaidora, A., Lendl, T. & Busch, W. Auxin steers root cell expansion via apoplastic pH regulation in Arabidopsis thaliana. *Proceedings of the National Academy of Sciences* **114**, E4884-E4893 (2017).
440 Rayle, D. L. Auxin-induced hydrogen-ion secretion in Avena coleoptiles and its implications. *Planta* **114**, 63-73 (1973).
441 Rayle, D. L. & Cleland, R. Enhancement of wall loosening and elongation by acid solutions. *Plant Physiol.* **46**, 250-253 (1970).
442 Hager, A., Menzel, H. & Krauss, A. Experiments and hypothesis concerning the primary action of auxin in elongation growth. *Planta* **100**, 47-75 (1971).
443 Li, L. *et al.* Cell surface and intracellular auxin signalling for H+ fluxes in root growth. *Nature* **599**, 273-277 (2021).
444 Chadwick, A. V. & Burg, S. P. An explanation of the inhibition of root growth caused by indole-3-acetic acid. *Plant Physiol.* **42**, 415-420 (1967).
445 Wilson, J. W. & Wilson, P. M. W. Effects of Auxin Concentration on the Dimensions and Patterns of Tracheary Elements Differentiating in Pith Explants. *Ann. Bot.* **68**, 463-467 (1991).
446 Evans, M. L., Ishikawa, H. & Estelle, M. A. Responses of Arabidopsis roots to auxin studied with high temporal resolution: comparison of wild type and auxin-response mutants. *Planta* **194**, 215-222 (1994).
447 Baskin, T. I. & Bivens, N. J. Stimulation of radial expansion in Arabidopsis roots by inhibitors of actomyosin and vesicle secretion but not by various inhibitors of metabolism. *Planta* **197**, 514-521 (1995).
448 Blancaflor, E. B. Cortical actin filaments potentially interact with cortical microtubules in regulating polarity of cell expansion in primary roots of maize (Zea mays L.). *J. Plant Growth Regul.* **19**, 406 (2000).
449 Thomas, D. d. S., Lager, N. & Manavathu, E. Cytochalasin B: effects on root morphogenesis in Allium cepa. *Canadian Journal of Botany* **51**, 2269-2273 (1973).
450 Collings, D. A., Lill, A. W., Himmelspach, R. & Wasteneys, G. O. Hypersensitivity to cytoskeletal antagonists demonstrates microtubule–microfilament cross-talk in the control of root elongation in Arabidopsis thaliana. *New Phytol.* **170**, 275-290 (2006).
451 Baluska, F., Vitha, S., Barlow, P. & Volkmann, D. Rearrangements of F-actin arrays in growing cells of intact maize root apex tissues: a major developmental switch occurs in the postmitotic transition region. *Eur. J. Cell Biol.* **72**, 113-121 (1997).
452 Schindelman, G. *et al.* COBRA encodes a putative GPI-anchored protein, which is polarly localized and necessary for oriented cell expansion in Arabidopsis. *Genes Dev.* **15**, 1115-1127 (2001).
453 Dünser, K. *et al.* Extracellular matrix sensing by FERONIA and Leucine-Rich Repeat Extensins controls vacuolar expansion during cellular elongation in Arabidopsis thaliana. *The EMBO journal* **38**, e100353 (2019).
454 Sergeeva, L. I. *et al.* Vacuolar invertase regulates elongation of Arabidopsis thaliana roots as revealed by QTL and mutant analysis. *Proceedings of the National Academy of Sciences* **103**, 2994-2999 (2006).
455 Malamy, J. E. & Benfey, P. N. Organization and cell differentiation in lateral roots of Arabidopsis thaliana. *Development* **124**, 33-44 (1997).
456 Laskowski, M. *et al.* Root system architecture from coupling cell shape to auxin transport. *PLoS Biol.* **6**, e307 (2008).
457 Ditengou, F. A. *et al.* Mechanical induction of lateral root initiation in Arabidopsis thaliana. *Proceedings of the National Academy of Sciences* **105**, 18818-18823 (2008).

458 De Rybel, B. *et al.* A role for the root cap in root branching revealed by the non-auxin probe naxillin. *Nat. Chem. Biol.* **8**, 798-805 (2012).
459 Xuan, W. *et al.* Root cap-derived auxin pre-patterns the longitudinal axis of the Arabidopsis root. *Curr. Biol.* **25**, 1381-1388 (2015).
460 Xuan, W. *et al.* Cyclic programmed cell death stimulates hormone signaling and root development in Arabidopsis. *Science* **351**, 384-387 (2016).
461 Dubrovsky, J. G. *et al.* Auxin acts as a local morphogenetic trigger to specify lateral root founder cells. *Proceedings of the National Academy of Sciences* **105**, 8790-8794 (2008).
462 Reed, R. C., Brady, S. R. & Muday, G. K. Inhibition of auxin movement from the shoot into the root inhibits lateral root development in Arabidopsis. *Plant Physiol.* **118**, 1369-1378 (1998).
463 Bhalerao, R. P. *et al.* Shoot-derived auxin is essential for early lateral root emergence in Arabidopsis seedlings. *The Plant Journal* **29**, 325-332 (2002).
464 Meier, M., Liu, Y., Lay-Pruitt, K. S., Takahashi, H. & von Wirén, N. Auxin-mediated root branching is determined by the form of available nitrogen. *Nature Plants* **6**, 1136-1145 (2020).
465 Tang, L. P. *et al.* FUSCA 3 interacting with LEAFY COTYLEDON 2 controls lateral root formation through regulating YUCCA 4 gene expression in Arabidopsis thaliana. *New Phytol.* **213**, 1740-1754 (2017).
466 Casimiro, I. *et al.* Auxin transport promotes Arabidopsis lateral root initiation. *The Plant Cell* **13**, 843-852 (2001).
467 Marhavý, P. *et al.* Auxin reflux between the endodermis and pericycle promotes lateral root initiation. *The EMBO Journal* **32**, 149-158 (2013).
468 Marchant, A. *et al.* AUX1 promotes lateral root formation by facilitating indole-3-acetic acid distribution between sink and source tissues in the Arabidopsis seedling. *The Plant Cell* **14**, 589-597 (2002).
469 De Rybel, B. *et al.* A novel aux/IAA28 signaling cascade activates GATA23-dependent specification of lateral root founder cell identity. *Curr. Biol.* **20**, 1697-1706 (2010).
470 Péret, B. *et al.* Sequential induction of auxin efflux and influx carriers regulates lateral root emergence. *Mol. Syst. Biol.* **9**, 699 (2013).
471 Gendreau, E. *et al.* Cellular basis of hypocotyl growth in Arabidopsis thaliana. *Plant Physiol.* **114**, 295-305 (1997).
472 Blakeslee, J. J., Bandyopadhyay, A., Peer, W. A., Makam, S. N. & Murphy, A. S. Relocalization of the PIN1 auxin efflux facilitator plays a role in phototropic responses. *Plant Physiol.* **134**, 28-31 (2004).
473 Romano, C. P., Robson, P. R., Smith, H., Estelle, M. & Klee, H. Transgene-mediated auxin overproduction in Arabidopsis: hypocotyl elongation phenotype and interactions with the hy6-1 hypocotyl elongation and axr1 auxin-resistant mutants. *Plant Mol. Biol.* **27**, 1071-1083 (1995).
474 Goeschl, J. D., Pratt, H. K. & Bonner, B. A. An effect of light on the production of ethylene and the growth of the plumular portion of etiolated pea seedlings. *Plant Physiol.* **42**, 1077-1080 (1967).
475 Smalle, J., Haegman, M., Kurepa, J., Van Montagu, M. & Straeten, D. V. D. Ethylene can stimulate Arabidopsis hypocotyl elongation in the light. *Proceedings of the National Academy of Sciences* **94**, 2756-2761 (1997).
476 Cowling, R. J. & Harberd, N. P. Gibberellins control Arabidopsis hypocotyl growth via regulation of cellular elongation. *J. Exp. Bot.* **50**, 1351-1357 (1999).
477 Rizza, A., Walia, A., Lanquar, V., Frommer, W. B. & Jones, A. M. In vivo gibberellin gradients visualized in rapidly elongating tissues. *Nature Plants* **3**, 803-813 (2017).

478 Collett, C. E., Harberd, N. P. & Leyser, O. Hormonal interactions in the control of Arabidopsis hypocotyl elongation. *Plant Physiol.* **124**, 553-562 (2000).
479 Nicol, F. *et al.* A plasma membrane-bound putative endo-1, 4-β-D-glucanase is required for normal wall assembly and cell elongation in Arabidopsis. *The EMBO journal* **17**, 5563-5576 (1998).
480 Fagard, M. *et al.* PROCUSTE1 encodes a cellulose synthase required for normal cell elongation specifically in roots and dark-grown hypocotyls of Arabidopsis. *The plant cell* **12**, 2409-2423 (2000).
481 Nakajima, K., Furutani, I., Tachimoto, H., Matsubara, H. & Hashimoto, T. SPIRAL1 encodes a plant-specific microtubule-localized protein required for directional control of rapidly expanding Arabidopsis cells. *The Plant Cell* **16**, 1178-1190 (2004).
482 Morillon, R., Catterou, M., Sangwan, R. S., Sangwan, B. S. & Lassalles, J.-P. Brassinolide may control aquaporin activities in Arabidopsis thaliana. *Planta* **212**, 199-204 (2001).
483 Elumalai, R. P., Nagpal, P. & Reed, J. W. A mutation in the Arabidopsis KT2/KUP2 potassium transporter gene affects shoot cell expansion. *The Plant Cell* **14**, 119-131 (2002).
484 Philippar, K. *et al.* Auxin activates KAT1 and KAT2, two K+-channel genes expressed in seedlings of Arabidopsis thaliana. *The Plant Journal* **37**, 815-827 (2004).
485 Gendreau, E., Orbovic, V., Höfte, H. & Traas, J. Gibberellin and ethylene control endoreduplication levels in the Arabidopsis thaliana hypocotyl. *Planta* **209**, 513-516 (1999).
486 Saibo, N. J., Vriezen, W. H., Beemster, G. T. & Van Der Straeten, D. Growth and stomata development of Arabidopsis hypocotyls are controlled by gibberellins and modulated by ethylene and auxins. *The Plant Journal* **33**, 989-1000 (2003).
487 Jensen, P. J., Hangarter, R. P. & Estelle, M. Auxin transport is required for hypocotyl elongation in light-grown but not dark-grown Arabidopsis. *Plant Physiol.* **116**, 455-462 (1998).
488 McQueen-Mason, S., Durachko, D. M. & Cosgrove, D. J. Two endogenous proteins that induce cell wall extension in plants. *The Plant Cell* **4**, 1425-1433 (1992).
489 Takahashi, K., Hayashi, K.-i. & Kinoshita, T. Auxin activates the plasma membrane H+-ATPase by phosphorylation during hypocotyl elongation in Arabidopsis. *Plant Physiol.* **159**, 632-641 (2012).
490 Lin, W. *et al.* TMK-based cell-surface auxin signalling activates cell-wall acidification. *Nature* **599**, 278-282 (2021).
491 Fendrych, M., Leung, J. & Friml, J. TIR1/AFB-Aux/IAA auxin perception mediates rapid cell wall acidification and growth of Arabidopsis hypocotyls. *elife* **5**, e19048 (2016).
492 Uchida, N. *et al.* Chemical hijacking of auxin signaling with an engineered auxin–TIR1 pair. *Nat. Chem. Biol.* **14**, 299-305 (2018).
493 Spartz, A. K. *et al.* Constitutive expression of Arabidopsis SMALL AUXIN UP RNA19 (SAUR19) in tomato confers auxin-independent hypocotyl elongation. *Plant Physiol.* **173**, 1453-1462 (2017).
494 Spartz, A. K. *et al.* SAUR inhibition of PP2C-D phosphatases activates plasma membrane H+-ATPases to promote cell expansion in Arabidopsis. *The Plant Cell* **26**, 2129-2142 (2014).
495 Du, M. *et al.* Biphasic control of cell expansion by auxin coordinates etiolated seedling development. *Science advances* **8**, eabj1570 (2022).

496 Daher, F. B. *et al.* Anisotropic growth is achieved through the additive mechanical effect of material anisotropy and elastic asymmetry. *Elife* **7** (2018).
497 Schwark, A. & Schierle, J. Interaction of ethylene and auxin in the regulation of hook growth I the role of auxin in different growing regions of the hypocotyl hook of Phaseolus vulgaris. *J. Plant Physiol.* **140**, 562-570 (1992).
498 Schwark, A. & Bopp, M. Interaction of ethylene and auxin in the regulation of hook growth II. The role for ethylene in different growing regions of the hypocotyl hook of Phaseolus vulgaris. *J. Plant Physiol.* **142**, 585-592 (1993).
499 Li, H., Johnson, P., Stepanova, A., Alonso, J. M. & Ecker, J. R. Convergence of signaling pathways in the control of differential cell growth in Arabidopsis. *Dev. Cell* **7**, 193-204 (2004).
500 Raz, V. & Ecker, J. R. Regulation of differential growth in the apical hook of Arabidopsis. *Development* **126**, 3661-3668 (1999).
501 Žádníková, P. *et al.* Role of PIN-mediated auxin efflux in apical hook development of Arabidopsis thaliana. *Development* **137**, 607-617 (2010).
502 Vandenbussche, F. *et al.* The auxin influx carriers AUX1 and LAX3 are involved in auxin-ethylene interactions during apical hook development in Arabidopsis thaliana seedlings. *Development* **137**, 597-606 (2010).
503 Gallagher, S., Short, T. W., Ray, P. M., Pratt, L. H. & Briggs, W. R. Light-mediated changes in two proteins found associated with plasma membrane fractions from pea stem sections. *Proceedings of the National Academy of Sciences* **85**, 8003-8007 (1988).
504 Sharrock, R. A. & Quail, P. H. Novel phytochrome sequences in Arabidopsis thaliana: structure, evolution, and differential expression of a plant regulatory photoreceptor family. *Genes Dev.* **3**, 1745-1757 (1989).
505 Lin, C. *et al.* Association of flavin adenine dinucleotide with the Arabidopsis blue light receptor CRY1. *Science* **269**, 968-970 (1995).
506 Rizzini, L. *et al.* Perception of UV-B by the Arabidopsis UVR8 protein. *Science* **332**, 103-106 (2011).
507 Christie, J. M. *et al.* Plant UVR8 photoreceptor senses UV-B by tryptophan-mediated disruption of cross-dimer salt bridges. *Science* **335**, 1492-1496 (2012).
508 Ma, L. *et al.* Light control of Arabidopsis development entails coordinated regulation of genome expression and cellular pathways. *The Plant Cell* **13**, 2589-2607 (2001).
509 Ahmad, M. & Cashmore, A. R. HY4 gene of A. thaliana encodes a protein with characteristics of a blue-light photoreceptor. *Nature* **366**, 162-166 (1993).
510 Somers, D. E., Sharrock, R. A., Tepperman, J. M. & Quail, P. H. The hy3 long hypocotyl mutant of Arabidopsis is deficient in phytochrome B. *The Plant Cell* **3**, 1263-1274 (1991).
511 Ni, M., Tepperman, J. M. & Quail, P. H. PIF3, a phytochrome-interacting factor necessary for normal photoinduced signal transduction, is a novel basic helix-loop-helix protein. *Cell* **95**, 657-667 (1998).
512 Huq, E. & Quail, P. H. PIF4, a phytochrome-interacting bHLH factor, functions as a negative regulator of phytochrome B signaling in Arabidopsis. *The EMBO journal* **21**, 2441-2450 (2002).
513 Shen, H., Moon, J. & Huq, E. PIF1 is regulated by light-mediated degradation through the ubiquitin-26S proteasome pathway to optimize photomorphogenesis of seedlings in Arabidopsis. *The Plant Journal* **44**, 1023-1035 (2005).
514 Shen, Y., Khanna, R., Carle, C. M. & Quail, P. H. Phytochrome induces rapid PIF5 phosphorylation and degradation in response to red-light activation. *Plant Physiol.* **145**, 1043-1051 (2007).

515 Al-Sady, B., Ni, W., Kircher, S., Schäfer, E. & Quail, P. H. Photoactivated phytochrome induces rapid PIF3 phosphorylation prior to proteasome-mediated degradation. *Mol. Cell* **23**, 439-446 (2006).
516 Sun, J., Qi, L., Li, Y., Zhai, Q. & Li, C. PIF4 and PIF5 transcription factors link blue light and auxin to regulate the phototropic response in Arabidopsis. *The Plant Cell* **25**, 2102-2114 (2013).
517 Tavridou, E., Pireyre, M. & Ulm, R. Degradation of the transcription factors PIF4 and PIF5 under UV-B promotes UVR8-mediated inhibition of hypocotyl growth in Arabidopsis. *The Plant Journal* **101**, 507-517 (2020).
518 Shi, H. *et al.* Seedlings transduce the depth and mechanical pressure of covering soil using COP1 and ethylene to regulate EBF1/EBF2 for soil emergence. *Curr. Biol.* **26**, 139-149 (2016).
519 Zhong, S. *et al.* Ethylene-orchestrated circuitry coordinates a seedling's response to soil cover and etiolated growth. *Proceedings of the National Academy of Sciences* **111**, 3913-3920 (2014).
520 Shen, X., Li, Y., Pan, Y. & Zhong, S. Activation of HLS1 by mechanical stress via ethylene-stabilized EIN3 is crucial for seedling soil emergence. *Frontiers in Plant Science* **7**, 1571 (2016).
521 Ang, L.-H. *et al.* Molecular interaction between COP1 and HY5 defines a regulatory switch for light control of Arabidopsis development. *Mol. Cell* **1**, 213-222 (1998).
522 Holm, M., Ma, L.-G., Qu, L.-J. & Deng, X.-W. Two interacting bZIP proteins are direct targets of COP1-mediated control of light-dependent gene expression in Arabidopsis. *Genes Dev.* **16**, 1247-1259 (2002).
523 Sibout, R. *et al.* Opposite root growth phenotypes of hy5 versus hy5 hyh mutants correlate with increased constitutive auxin signaling. *PLoS Genet.* **2**, e202 (2006).
524 Cluis, C. P., Mouchel, C. F. & Hardtke, C. S. The Arabidopsis transcription factor HY5 integrates light and hormone signaling pathways. *The Plant Journal* **38**, 332-347 (2004).
525 Hamon-Josse, M. *et al.* KAI2 regulates seedling development by mediating light-induced remodelling of auxin transport. *New Phytol.* **235**, 126-140 (2022).
526 Villaécija-Aguilar, J. A. *et al.* KAI2 promotes Arabidopsis root hair elongation at low external phosphate by controlling local accumulation of AUX1 and PIN2. *Curr. Biol.* **32**, 228-236 (2021).
527 Sassi, M. *et al.* COP1 mediates the coordination of root and shoot growth by light through modulation of PIN1-and PIN2-dependent auxin transport in Arabidopsis. *Development* **139**, 3402-3412 (2012).
528 Duan, X. *et al.* Periodic root branching is influenced by light through an HY1-HY5-auxin pathway. *Curr. Biol.* **31**, 3834-3847. e3835 (2021).
529 Gray, W. M., Östin, A., Sandberg, G., Romano, C. P. & Estelle, M. High temperature promotes auxin-mediated hypocotyl elongation in Arabidopsis. *Proceedings of the National Academy of Sciences* **95**, 7197-7202 (1998).
530 Sun, J., Qi, L., Li, Y., Chu, J. & Li, C. PIF4–mediated activation of YUCCA8 expression integrates temperature into the auxin pathway in regulating Arabidopsis hypocotyl growth. *PLoS Genet.* **8**, e1002594 (2012).
531 Peng, M. *et al.* Linking PHYTOCHROME-INTERACTING FACTOR to Histone Modification in Plant Shade Avoidance *Plant Physiol.* **176**, 1341-1351 (2017).
532 Tao, Y. *et al.* Rapid synthesis of auxin via a new tryptophan-dependent pathway is required for shade avoidance in plants. *Cell* **133**, 164-176 (2008).
533 Keuskamp, D. H., Pollmann, S., Voesenek, L. A., Peeters, A. J. & Pierik, R. Auxin transport through PIN-FORMED 3 (PIN3) controls shade avoidance and fitness

during competition. *Proceedings of the National Academy of Sciences* **107**, 22740-22744 (2010).
534 Dai, N., Wang, W., Patterson, S. E. & Bleecker, A. B. The TMK subfamily of receptor-like kinases in Arabidopsis display an essential role in growth and a reduced sensitivity to auxin. *PloS one* **8**, e60990 (2013).
535 Huang, R. *et al.* Noncanonical auxin signaling regulates cell division pattern during lateral root development. *Proceedings of the National Academy of Sciences* **116**, 21285-21290 (2019).
536 Marques-Bueno, M. M. *et al.* Auxin-regulated reversible inhibition of TMK1 signaling by MAKR2 modulates the dynamics of root gravitropism. *Curr. Biol.* **31**, 228-237. e210 (2021).
537 Zhao, Y. *et al.* A role for flavin monooxygenase-like enzymes in auxin biosynthesis. *Science* **291**, 306-309 (2001).
538 Delarue, M., Prinsen, E., Va, H., Caboche, M. & Bellini, C. Sur2 mutations of Arabidopsis thaliana define a new locus involved in the control of auxin homeostasis. *The Plant Journal* **14**, 603-611 (1998).
539 Mikkelsen, M. D., Naur, P. & Halkier, B. A. Arabidopsis mutants in the C–S lyase of glucosinolate biosynthesis establish a critical role for indole-3-acetaldoxime in auxin homeostasis. *The Plant Journal* **37**, 770-777 (2004).
540 Nakazawa, M. *et al.* DFL1, an auxin-responsive GH3 gene homologue, negatively regulates shoot cell elongation and lateral root formation, and positively regulates the light response of hypocotyl length. *The Plant Journal* **25**, 213-221 (2001).
541 Niu, Y. *et al.* Phosphorus and magnesium interactively modulate the elongation and directional growth of primary roots in Arabidopsis thaliana (L.) Heynh. *J. Exp. Bot.* **66**, 3841-3854 (2015). https://doi.org:10.1093/jxb/erv181
542 Ivanchenko, M. G., Napsucialy-Mendivil, S. & Dubrovsky, J. G. Auxin-induced inhibition of lateral root initiation contributes to root system shaping in Arabidopsis thaliana. *The Plant Journal* **64**, 740-752 (2010).
543 Stührwohldt, N., Dahlke, R. I., Steffens, B., Johnson, A. & Sauter, M. Phytosulfokine-α controls hypocotyl length and cell expansion in Arabidopsis thaliana through phytosulfokine receptor 1. *PLoS One* **6**, e21054 (2011).
544 Cakmak, I., Marschner, H. & Bangerth, F. Effect of Zinc Nutritional Status on Growth, Protein Metabolism and Levels of Indole-3-acetic Acid and other Phytohormones in Bean (Phaseolus vulgaris L.). *J. Exp. Bot.* **40**, 405-412 (1989).
545 Kitagishi, K. & Obata, H. Effects of zinc deficiency on the nitrogen metabolism of meristematic tissues of rice plants with reference to protein synthesis. *Soil Sci. Plant Nutr.* **32**, 397-405 (1986).
546 Obata, H. & Umebayashi, M. Effect of zinc deficiency on protein synthesis in cultured tobacco plant cells. *Soil Sci. Plant Nutr.* **34**, 351-357 (1988).
547 Aghajanzadeh, T. A., Prajapati, D. H. & Burow, M. Differential partitioning of thiols and glucosinolates between shoot and root in Chinese cabbage upon excess zinc exposure. *J. Plant Physiol.* **244**, 153088 (2020).
548 Kusznierewicz, B. *et al.* The dose-dependent influence of zinc and cadmium contamination of soil on their uptake and glucosinolate content in white cabbage (Brassica oleracea var. capitata f. alba). *Environ. Toxicol. Chem.* **31**, 2482-2489 (2012).
549 Liebminger, E. *et al.* β-N-acetylhexosaminidases HEXO1 and HEXO3 are responsible for the formation of paucimannosidic N-glycans in Arabidopsis thaliana. *J. Biol. Chem.* **286**, 10793-10802 (2011).
550 Velasquez, S. M. *et al.* O-glycosylated cell wall proteins are essential in root hair growth. *Science* **332**, 1401-1403 (2011).

551 Egelund, J. *et al.* Molecular characterization of two Arabidopsis thaliana glycosyltransferase mutants, rra1 and rra2, which have a reduced residual arabinose content in a polymer tightly associated with the cellulosic wall residue. *Plant Mol. Biol.* **64**, 439-451 (2007).
552 Gille, S., Hänsel, U., Ziemann, M. & Pauly, M. Identification of plant cell wall mutants by means of a forward chemical genetic approach using hydrolases. *Proceedings of the National Academy of Sciences* **106**, 14699-14704 (2009).
553 Zielinska, D. F., Gnad, F., Schropp, K., Wiśniewski, J. R. & Mann, M. Mapping N-glycosylation sites across seven evolutionarily distant species reveals a divergent substrate proteome despite a common core machinery. *Mol. Cell* **46**, 542-548 (2012).
554 Fritz, T. A., Hurley, J. H., Trinh, L.-B., Shiloach, J. & Tabak, L. A. The beginnings of mucin biosynthesis: The crystal structure of UDP-GalNAc: polypeptide α-N-acetylgalactosaminyltransferase-T1. *Proceedings of the National Academy of Sciences* **101**, 15307-15312 (2004).
555 Wiggins, C. A. & Munro, S. Activity of the yeast MNN1 α-1, 3-mannosyltransferase requires a motif conserved in many other families of glycosyltransferases. *Proceedings of the National Academy of Sciences* **95**, 7945-7950 (1998).
556 Palma, A. S., Morais, V. A., Coelho, A. V. & Costa, J. Effect of the manganese ion on human α3/4 fucosyltransferase III activity. *BioMetals* **17**, 35-43 (2004).
557 Obayashi, T., Hibara, H., Kagaya, Y., Aoki, Y. & Kinoshita, K. ATTED-II v11: a plant gene coexpression database using a sample balancing technique by subagging of principal components. *Plant and Cell Physiology* **63**, 869–881 (2022).
558 Hong, Z. *et al.* Evolutionarily conserved glycan signal to degrade aberrant brassinosteroid receptors in Arabidopsis. *Proceedings of the National Academy of Sciences* **109**, 11437-11442 (2012).
559 Yuan, Y. *et al.* Mutations of Arabidopsis TBL32 and TBL33 affect xylan acetylation and secondary wall deposition. *PLoS One* **11**, e0146460 (2016).
560 Wang, Y. *et al.* Golgi-localized cation/proton exchangers regulate ionic homeostasis and skotomorphogenesis in Arabidopsis. *Plant, Cell Environ.* **42**, 673-687 (2019).
561 Sinclair, S. A., Gille, S., Pauly, M. & Krämer, U. Regulation of acetylation of plant cell wall components is complex and responds to external stimuli. *Plant signaling & behavior* **15**, 1687185 (2020).
562 Sterling, J. D., Quigley, H. F., Orellana, A. & Mohnen, D. The catalytic site of the pectin biosynthetic enzyme α-1, 4-galacturonosyltransferase is located in the lumen of the Golgi. *Plant Physiol.* **127**, 360-371 (2001).
563 Northcote, D. & Pickett-Heaps, J. A function of the Golgi apparatus in polysaccharide synthesis and transport in the root-cap cells of wheat. *Biochemical Journal* **98**, 159 (1966).
564 Harris, P. & Northcote, D. Polysaccharide formation in plant Golgi bodies. *Biochimica et Biophysica Acta (BBA)-General Subjects* **237**, 56-64 (1971).
565 Zhang, G. F. & Staehelin, L. A. Functional compartmentation of the Golgi apparatus of plant cells: immunocytochemical analysis of high-pressure frozen- and freeze-substituted sycamore maple suspension culture cells. *Plant Physiol.* **99**, 1070-1083 (1992).
566 Huq, E. *et al.* Phytochrome-interacting factor 1 is a critical bHLH regulator of chlorophyll biosynthesis. *science* **305**, 1937-1941 (2004).
567 Stephenson, P. G., Fankhauser, C. & Terry, M. J. PIF3 is a repressor of chloroplast development. *Proceedings of the National Academy of Sciences* **106**, 7654-7659 (2009).

568 Liu, X. *et al.* EIN3 and PIF3 form an interdependent module that represses chloroplast development in buried seedlings. *The Plant Cell* **29**, 3051-3067 (2017).
569 Oh, S. & Montgomery, B. L. Phytochrome-dependent coordinate control of distinct aspects of nuclear and plastid gene expression during anterograde signaling and photomorphogenesis. *Frontiers in plant science* **5**, 171 (2014).
570 Park, S.-C., Kwon, H.-B. & Shih, M.-C. Cis-acting elements essential for light regulation of the nuclear gene encoding the A subunit of chloroplast glyceraldehyde 3-phosphate dehydrogenase in Arabidopsis thaliana. *Plant Physiol.* **112**, 1563-1571 (1996).
571 Jeong, M.-J. & Shih, M.-C. Interaction of a GATA factor with cis-acting elements involved in light regulation of nuclear genes encoding chloroplast glyceraldehyde-3-phosphate dehydrogenase in Arabidopsis. *Biochem. Biophys. Res. Commun.* **300**, 555-562 (2003).
572 Donald, R. & Cashmore, A. R. Mutation of either G box or I box sequences profoundly affects expression from the Arabidopsis rbcS-1A promoter. *The EMBO Journal* **9**, 1717-1726 (1990).
573 Hartmann, U. *et al.* Identification of UV/blue light-response elements in the Arabidopsis thaliana chalcone synthase promoter using a homologous protoplast transient expression system. *Plant Mol. Biol.* **36**, 741-754 (1998).
574 Liu, B. *et al.* A HY5-COL3-COL13 regulatory chain for controlling hypocotyl elongation in Arabidopsis. *Plant, Cell Environ.* **44**, 130-142 (2021).
575 Wan, J. *et al.* Comparative physiological and transcriptomic analyses reveal the toxic effects of ZnO nanoparticles on plant growth. *Environ. Sci. Technol.* **53**, 4235-4244 (2019).
576 Paciorek, T. *et al.* Auxin inhibits endocytosis and promotes its own efflux from cells. *Nature* **435**, 1251-1256 (2005).
577 Narasimhan, M. *et al.* Systematic analysis of specific and nonspecific auxin effects on endocytosis and trafficking. *Plant Physiol.* **186**, 1122-1142 (2021).
578 Naramoto, S. *et al.* Insights into the localization and function of the membrane trafficking regulator GNOM ARF-GEF at the Golgi apparatus in Arabidopsis. *The Plant Cell* **26**, 3062-3076 (2014).
579 Peng, Y. *et al.* Control of root meristem size by DA1-RELATED PROTEIN2 in Arabidopsis. *Plant Physiol.* **161**, 1542-1556 (2013).
580 Lucocq, J. M. & Warren, G. Fragmentation and partitioning of the Golgi apparatus during mitosis in HeLa cells. *The EMBO journal* **6**, 3239-3246 (1987).
581 McCullough, S. & Lucocq, J. Endoplasmic reticulum positioning and partitioning in mitotic HeLa cells. *J. Anat.* **206**, 415-425 (2005).
582 Maret, W. Analyzing free zinc(ii) ion concentrations in cell biology with fluorescent chelating molecules. *Metallomics* **7**, 202-211 (2014).
583 Martinière, A. *et al.* In Vivo Intracellular pH Measurements in Tobacco and Arabidopsis Reveal an Unexpected pH Gradient in the Endomembrane System. *The Plant Cell* **25**, 4028-4043 (2013).
584 Gaither, L. A. & Eide, D. J. Functional expression of the human hZIP2 zinc transporter. *J. Biol. Chem.* **275**, 5560-5564 (2000).
585 Liu, Z. *et al.* Cd2+ versus Zn2+ uptake by the ZIP8 HCO3--dependent symporter: kinetics, electrogenicity and trafficking. *Biochem. Biophys. Res. Commun.* **365**, 814-820 (2008).
586 Nebert, D. W. *et al.* ZIP14 and ZIP8 zinc/bicarbonate symporters in Xenopus oocytes: characterization of metal uptake and inhibition. *Metallomics* **4**, 1218-1225 (2012).